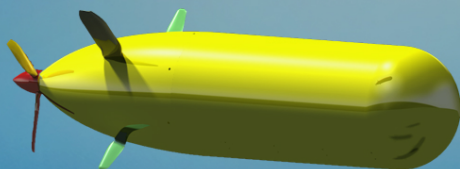


Underwater Locator Beacon

Final Report

Group 19



Underwater Locator Beacon

Final Report

Group 19

Jasper van Beers	-	4479068
Justine De Keyser	-	4288432
Noortje Elbers	-	4364198
Sietske Imming	-	4269497
Charlotte Iványi	-	4466942
Klemens Köstler	-	4437586
Marjolein van Lierop	-	4360087
Armando Poelman	-	4475283
Julia Radius	-	4381416
Braulio Vargas Alvarez	-	4432495

Tutor	-	Paul Roling
Coaches	-	Dirk Van Baelen
	-	Ines Uriol Balbin
AE3200	-	Design Synthesis Exercise

Due Date: 27th of June 2018
Draft

List of Symbols and Abbreviations

Abbreviations

<i>AUV</i>	Autonomous Underwater Vehicle
<i>BEA</i>	Le Bureau d'Enquêtes et d'Analyses
<i>BER</i>	Bit Error Rate
<i>C&DH</i>	Command & Data Handling
<i>CAD</i>	Computer-Aided Design
<i>CARP</i>	Computed Air Release Point
<i>CEO</i>	Chief Executive Officer
<i>CFRP</i>	Carbon Fiber Reinforced Polymer
<i>COLREG</i>	Convention on the International Regulations for Preventing Collisions
<i>CPAS</i>	Crew Exploration Vehicle Parachute Assembly System
<i>CVR</i>	Cockpit Voice Recorder
<i>D&R</i>	Deployment & Retrieval
<i>DATCOM</i>	Data Compendium (US Airforce)
<i>DC</i>	Direct Current
<i>DMC</i>	Digital Magnetic Compass
<i>DOF</i>	Degrees of Freedom
<i>DOT</i>	Design Option Tree
<i>DSE</i>	Design Synthesis Exercise
<i>EOM</i>	Equation of Motion
<i>FBD</i>	Free Body Diagram
<i>FDR</i>	Flight Data Recorder
<i>GB</i>	Distance between center of gravity and buoyancy
<i>GPS</i>	Global Positioning System
<i>HiPAP</i>	High Precision Acoustic Positioning
<i>IMU</i>	Inertial Measurement Unit
<i>INS</i>	Inertial Navigation System
<i>INU</i>	Inertial Navigation Unit
<i>ISI</i>	Intersymbol Interference
<i>MARLIN</i>	Missing Aircraft Reconnaissance Locator In Nautical-Environment
<i>MG</i>	Metacentric height
<i>MRU</i>	Motion Reference Unit
<i>NASA</i>	National Aeronautics and Space Administration
<i>NCA</i>	Nickel Cobalt Aluminium
<i>NM</i>	Nautical Miles
<i>NMC</i>	Nickel Manganese Cobalt
<i>NOAA</i>	National Oceanic and Atmosphere Administration
<i>PEMEX</i>	Petróleos Mexicanos
<i>PEMFC</i>	Proton Exchange Membrane Fuel Cell
<i>PEST</i>	Political-legal, Economic, Socio-cultural and Technological factors
<i>PID</i>	Proportional Integral Derivative
<i>R&D</i>	Research and Development
<i>RAMS</i>	Reliability Availability Maintainability Safety
<i>ROI</i>	Return on Investment
<i>ROV</i>	Remotely Operated Vehicles
<i>SBM</i>	Sustainable Business Model
<i>TAS</i>	Towed Acoustic Sonar
<i>UAV</i>	Unmanned Aerial Vehicle
<i>ULB</i>	Underwater Locator Beacon
<i>VBS</i>	Variable Ballast System

Symbols

α	Angle of attack	[rad]
β	Angle of side slip	[rad]
β_s^j	New desired heading of submarine	[rad]
$\dot{\theta}_r$	Rotational acceleration around y-axis	[rad/s ²]
$\dot{\phi}$	Roll rate	[rad/s]
$\dot{\theta}$	Pitch rate	[rad/s]
$\dot{\theta}_r$	Rotational velocity around y-axis	[rad/s]
\dot{p}	Rolling acceleration	[m/s ²]
\dot{q}	Pitching acceleration	[m/s ²]
\dot{r}	Yawing acceleration	[m/s ²]
\dot{u}	Acceleration of flow along x-axis	[m/s ²]
\dot{v}	Acceleration of flow along y-axis	[m/s ²]
\dot{w}	Acceleration of flow along z-axis	[m/s ²]
\dot{X}	The rate of change of the aerodynamic force vector in body frame along x-axis	[N/s]
\dot{Y}	The rate of change of the aerodynamic force vector in body frame along y-axis	[N/s]
\dot{Z}	The rate of change of the aerodynamic force vector in body frame along z-axis	[N/s]
$\dot{\psi}$	Yaw rate	[rad/s]
\dot{V}	Flow rate	[m ³ /s]
\dot{V}_{inlet}	Flow rate through the VBS inlet	[m ³ /s]
ℓ	Length of tether	[m]
ϵ	Residual error	[m]
η_{engine}	Engine efficiency	[-]
η_{prop}	Propeller efficiency	[-]
η_{pump}	Efficiency of the ballast pump	[-]
γ	Flight path angle	[rad]
\mathbf{v}_c	Speed of submarine	[m/s]
\mathbf{v}_s^j	Simulated submarine speed	[m/s]
\mathbf{x}_a^j	Actual submarine location	[m]
\mathbf{x}_s^j	Simulated submarine location	[m]
\mathbf{v}_i^j	Initial speed of submarine	[m/s]
\mathbf{x}_i^j	Initial position of submarine	[m]
μ	Mean value	[m]
ν	Poisson's ratio	[-]
ω	Rotational velocity	[rad/s]
ω_{IB}	Angular velocity relative to inertial space	[rad/s]
ϕ	Roll angle	[rad]
ψ	Yaw angle	[rad]
ψ_{retr}	Retrieval arm angle	[rad]
ψ_{sub}	Submarine slenderness ratio	[-]
ρ_a	Density of air	[kg/m ³]
ρ_w	Density of sea water	[kg/m ³]
ρ	Density of sea water depending on depth	[kg/m ³]
ρ_0	Density of sea water at sea level	[kg/m ³]
ρ_{sub}	Density of submarine	[kg/m ³]
ρ_{water}	Density of water	[kg/m ³]
$\rho_{z_{max}}$	Density at maximum depth	[m ³]
σ^2	Variance	[m ²]
σ_{circ}	Circular stress	[Pa]
σ_{long}	Longitudinal stress	[Pa]
σ_{vm}	Von Mises stress	[Pa]
σ_{yield}	Yield stress	[Pa]
τ	Shear stress	[MPa]
τ_c	Time constant of capacitor	[s]
B	Center of buoyancy	[m]
M	Metacenter	[m]
θ	Pitch angle	[rad]
θ_i^j	Heading of submarine	[rad]
θ_r	Angle of rotation	[rad]

a	Mean radius of cylindrical shell	$[m]$
A_a	Cross-sectional area above water	$[m^2]$
a_n	Normal acceleration	$[\frac{m}{s^2}]$
A_s	Frontal area of submarine	$[m^2]$
a_t	Tangential acceleration	$[m/s^2]$
A_w	Cross-sectional area in water	$[m^2]$
a_{base}	Base radius of spherical cap	$[m]$
A_f	Cross-sectional area of frame	$[m^2]$
a_f	Radius of centroid of frame	$[m]$
A_{inlet}	Area of the VBS inlet	$[m^2]$
AR	Aspect ratio	$[-]$
B	Buoyancy	$[N]$
b	Span	$[m]$
B'	New center of buoyancy	$[m]$
b_f	Width of shell in direct contact with frame's web	$[m]$
C	Capacity of the capacitor	$[F]$
c_b	Damping constant	$[Ns/m]$
C_D	Drag coefficient	$[-]$
C_f	Friction drag coefficient	$[-]$
C_L	Lift coefficient	$[-]$
C_r	Root chord	$[m]$
C_s	Compressibility coefficient of submarine	$[-]$
C_t	Tip chord	$[m]$
C_w	Compressibility coefficient of water	$[-]$
C_{d0}	Drag coefficient at zero lift	$[-]$
D	Drag	$[N]$
d	Distance between fins	$[m]$
D_a	Drag due to airflow	$[N]$
d_b	Undeformed length	$[m]$
D_f	Friction drag	$[N]$
d_m	Diameter of mother buoy	$[m]$
d_p	Distance between parallel tracks	$[m]$
D_t	Tangential drag	$[N]$
D_{proj}	Impact depth	$[m]$
d_{sub}	Shell diameter	$[m]$
E	Young's modulus	$[Pa]$
e	Oswald efficiency factor	$[-]$
F	Faraday constant	$[sA/mol]$
F_n	Froude number	$[-]$
F_T	Tensile force on tether	$[N]$
F_t	Total tangential forces	$[N]$
F_z	Stabilized force	$[N]$
F_B	Buoyant force	$[N]$
F_{dist}	Disturbance force	$[N]$
f_{IB}	Specific force of the body relative to inertial space	$[N]$
F_{impact}	Impact force	$[N]$
F_x	Force in x-direction	$[N]$
F_y	Force in y-direction	$[N]$
F_z	Force in z-direction	$[N]$
F_{tot_n}	Total normal forces	$[N]$
G	Center of gravity	$[m]$
g	Gravitational acceleration	$[m/s^2]$
h	Search height above the ocean floor	$[m]$
h_a	Aircraft altitude during retrieval	$[m]$
$h_{depth_{max}}$	Maximum operating depth	$[m]$
h_s	Height of the segment in water	$[m]$
I	Current	$[A]$
I_p	Moment of Inertia around a pivot point	$[kgm^2]$
I_{fuel}	Fuel cell stack current	$[A]$

I_{xx}	Second moment of area around the x-axis	$[m^4]$
I_{xz}	Second moment of area around the xz-axis	$[m^4]$
I_{yy}	Second moment of area around the y-axis	$[m^4]$
I_{zz}	Second moment of area around the z-axis	$[m^4]$
k_b	Spring constant	$[N/m]$
KE	Kinetic energy	$[J]$
L	Rolling moment in body frame	$[Nm]$
l	Length of tether	$[m]$
l_b	Load that needs to be lifted	$[N]$
l_{cyl}	Effective cylinder length	$[m]$
l_{sub}	Submarine length	$[m]$
L_{tot}	Total length of submarine or mother buoy	$[m]$
M	Pitching moment in body frame	$[Nm]$
m	Mass of a search unit	$[kg]$
m_b	Mass of main ballast	$[kg]$
m_s	Mass of submarine	$[kg]$
M_{air}	Molar mass of air	$[g/mol]$
m_{buoy}	Mass of mother buoy	$[kg]$
m_{eb}	Mass of the emergency ballast	$[kg]$
M_{H_2}	Molar mass of hydrogen	$[g/mol]$
M_{O_2}	Molar mass of oxygen	$[g/mol]$
m_{total}	Total mass of the submarine	$[kg]$
M_x	Moment in x-direction	$[Nm]$
M_y	Moment in y-direction	$[Nm]$
M_z	Moment in z-direction	$[Nm]$
N	Yawing moment in body frame	$[Nm]$
n	Number of lobes	$[-]$
n_c	Number of fuel cells	$[-]$
P	Power	$[W]$
p	Rolling velocity	$[m/s]$
P_{0atm}	Atmospheric pressure at sea level	$[Pa]$
P_{cr}	Buckling pressure	$[Pa]$
P_{depth}	Pressure at 4,500 m depth	$[Pa]$
P_{FC}	Fuel cell power	$[W]$
P_{impact}	Impact pressure	$[Pa]$
P_{max}	Maximum pressure	$[Pa]$
p_{tank}	Pressure inside the ballast tanks	$[Pa]$
Q	First moment of area	$[m^3]$
q	Pitching velocity	$[m/s]$
Q_{en}	Engine torque	$[Nm]$
R	Radius of spherical cap	$[m]$
r	Yawing velocity	$[m/s]$
R_c	Resistance of resistor	$[\Omega]$
r_i	Inner radius of tank	$[m]$
R_m	Motor Resistance	$[\Omega]$
R_n	Reynolds number	$[-]$
r_o	Outer radius of submarine	$[m]$
r_s	Radius of search system	$[m]$
R_h	Horizontal position	$[m]$
S	Wetted surface area	$[m^2]$
s_x	Horizontal position of search system with respect to aircraft	$[m]$
s_z	Vertical position of search system	$[m]$
T	Thrust	$[N]$
t	Time	$[s]$
T_F	Tension force	$[N]$
T_m	Time difference	$[s]$
T_w	Time to travel	$[s]$
t_{sub}	Wall thickness	$[m]$
U	Voltage	$[V]$
u	Speed of flow along x-axis	$[m/s]$

u_0	Velocity	[m/s]
V	Shear force	[N]
v	Speed of flow along y-axis	[m/s]
V_b	Volume of hydrogen	[m ³]
V_e	External volume of the submarine	[m ³]
v_m	Speed of mother buoy	[m/s]
V_s	Submerged volume submarine	[m ³]
v_s	Nominal speed of submarine	[m/s]
V_t	Linear tangential velocity	[m/s]
v_a	Aircraft retrieval velocity	[m/s]
$V_{b,min}$	Minimum required ballast volume	[m ³]
V_c	Cell voltage	[V]
v_{disp}	Displaced volume	[m ³]
$V_{e,0}$	External submarine volume at sea level	[m ³]
v_{sub}	Velocity of submarine	[m/s]
v_{sW_x}	Submarine speed vector in horizontal direction	[m/s]
v_{sW_y}	Submarine speed vector in vertical direction	[m/s]
V_{tank}	Volume of tank	[m ³]
$V_{z,max}$	Volume of the submarine at maximum depth	[m ³]
W	Weight	[N]
w	Speed of flow along z-axis	[m/s]
w_d	Radial deflection (positive inwards)	[m]
W_{drone}	Weight of drone	[N]
X	Aerodynamic force vector in body frame along x-axis	[N]
Y	Aerodynamic force vector in body frame along y-axis	[N]
Z	Aerodynamic force vector in body frame along z-axis	[N]
z	Depth height	[m]
Z_B	Center of buoyancy distance	[m]
Z_G	Center of gravity distance	[m]
Z_M	Metacenter distance	[m]

Executive Overview

The mission

Despite the growing safety of travelling by plane, accidents in modern aviation still occur. In some cases, such accidents lead to aircraft crashing into water, of which Malaysian Airlines flight 370 is a noticeable case. Even with extensive search missions and costs exceeding €100 million, nothing has been found until today - except some components of the aircraft that washed up on shores around eastern Africa. Locating crashed aircraft is of primary importance as it allows investigators to determine what went wrong; thereby, increasing the safety of future air transport. Furthermore, obtaining answers provides closure to the affected families.

Aircraft are fitted with underwater locator beacons (ULB) that transmit an acoustic signal to enable investigators to locate the recorders. However, these are built to last about 30 days only (or 90 days for aircraft built after 2014) and have limited range under water. Considering this limited range, finding the aircraft is a difficult task - especially when combined with the depth an aircraft can sink into the ocean, the uncertainty in the crash location and the short battery life of a ULB. Therefore, this design synthesis exercise (DSE) project aimed at designing a new system to locate an aircraft lost in deep water within the 30-day window and a search area with a radius of 100km.

Mission Statement: Scan a predetermined ocean region in order to locate an aircraft which has crashed in deep water within 30 days.

Objective Statement: Design an airborne system, within 10 weeks with 10 people, that can reach any location on Earth within 48 hours and is capable to locate the ULB signal of the missing aircraft in deep water.

Design Options

During a brainstorm session with the entire group, ideas were explored in three different categories; the airborne system, the search system and the deployment & retrieval system. All ideas were then sorted into sub-categories and put into a design option tree (DOT). Subsequently, all non-feasible options (based on the requirements) were eliminated. The remaining options were grouped into five mostly independent categories; the airborne system, deployment, retrieval, the search system and relocation. Further research was done before a tradeoff was performed for each category and options that were clearly not feasible were eliminated.

Requirements

User requirements specify requirements of primary importance to the customer and were set by the project. Important user requirements are to be deployable to any location on Earth within 48 hours, to have independent operation of buoys for 2 weeks, that the system shall be reusable for other applications and the total cost does not exceed €50 million. Airborne requirements included the ability to communicate with the base station and with the search system. Furthermore, minimum values were set for minimum payload, speed at maximum payload and range at maximum payload. Search system requirements included that each search system was expected to self-stabilize, determine its location on Earth using a global positioning system (GPS) or another system and communicate with the base station. Furthermore, the search system shall be able to detect a signal when the ULB is located up to 5 km below the surface of the water. For the deployment and retrieval systems, a maximum weight of 3125 kg has been given to each. They should both fit in, but not create any hazard to the aircraft. Furthermore, both systems should not pollute the marine ecosystem nor compromise the safety of the operators and ships.

Tradeoff

In order to eliminate concepts and come to a final design, tradeoffs were performed for the deployment system, the search system, the relocation method of the search system, the retrieval system and the airborne system.

Deployment System Tradeoff For the deployment tradeoff, the feasible concepts included the free fall, a parachute airdrop and deployment from a tether. The associated tradeoff criteria included mass, volume, ease of use, sustainability, impact velocity, reliability, availability, maintainability and safety. The free fall is the simplest method of deployment, where the impact velocity is the biggest concern. The two other concepts are derivatives of free fall that aim to reduce these impact loads, if required. However, parachutes are unsustainable as they contribute to ocean pollution if left in the water - potentially also causing harm to marine life. From the tradeoff of the three options, the free fall option resulted in being the best option, due to its ease of use and sustainability. There is little maintenance required and the estimated impact forces show that the impact loads are not the driving design loads for the structure.

Search System Tradeoff The search system looked at three options, buoys, submarines and gliders. The tradeoff criteria for the search system included risk (by means of communication failure), accuracy, minimum communication interval, complexity, sustainability, power required and mass. The mass and dimensions of the buoys were estimated based on existing scientific buoys. In order to determine the structure and material, extreme loads were calculated, including the impact force, pressure at maximum depth and the retrieval force. For the buoy and the submarine, the mass of the hull was computed, as well as the failure modes for both semi-spherical shapes and cylindrical shapes. For the semi-spherical shape, constant thickness along the circumference, no material imperfections, a diameter much greater than thickness and zero shear stresses were assumed. For the cylindrical shape, constant thickness along its length, no material imperfections, a diameter much greater than thickness, a length much greater than the diameter and small bending and twisting moments due to external pressure were assumed. Furthermore, for the cylindrical shape, uniform compression in the circumferential direction, symmetrical buckling with respect to the diameter and zero shear stresses were assumed.

The buoy concept would have a connected tether which extends down into the ocean, with a submerged hydrophone attached to the end. The mass and material were determined based on yield strength and tension in the tether. For this design, the floating buoy itself would communicate with the satellite. Since the hydrophone is likely not to hang directly below the buoy due to external forces, pressure sensors could be used to determine the depth of the hydrophone. A second option could be to use an underwater GPS system with a submerged receiver sending position data through the cable. The submarine concept would have to communicate underwater with a mother buoy using an acoustic link. This increases the communication risk, such as reflection of signals due to noise in the ocean. The glider concept involved communication via satellites. However, communication is only feasible once the glider is on the water surface. Both the submarine and glider would use inertial navigation system, which made the location data less accurate than for the buoy. The power for the buoy would be generated using solar energy while the submarine and glider would have a charged battery to last the entire mission. When propulsion for autonomous relocation is considered, the buoy concept needed too much power. This made the batteries too heavy and the solar array too large. This eliminated the buoy as an option for the search system. The glider needed less power than the submarine, making the glider the winner of the tradeoff for the search system.

Relocation Method Tradeoff The relocation method considered two options, including autonomous relocation and airborne relocation. The tradeoff criteria considered included relocation velocity, ability to search while relocating, number of systems needed, production cost, operating cost, emission during operations and technology readiness level. For autonomous relocation, three different systems were considered, namely a submarine, buoy and underwater glider. The submarine would need the least number of units as it has the fastest relocation velocity. The submarine also has the lowest production cost. Using the airborne relocation method, almost 5900 unique search system locations would be required if the detection volumes were to be simplified into cubes as to not miss out any part of the search area. Cubes were chosen as the best shape for now, considering their simple 3D shape. Relocation velocity with the airborne system is significantly faster than for autonomous relocation. However, the aircraft would probably require refuelling as to stay in the search area and perform its tasks efficiently. Furthermore, the search system can continue searching with autonomous relocation during the relocation procedure itself, as it is continuously moving and searching. For airborne relocation, this is not the case. For this reason, in combination with other advantages, the autonomous relocation system is the best option from the tradeoff.

Retrieval System For the retrieval system, four different concepts were considered. The first concept presented is the balloon concept shown in fig. 1, which uses a balloon to lift a cable attached to the search system. An aircraft then flies into this cable with a v-hook attached to its nose to capture the cable, as shown in fig. 1.

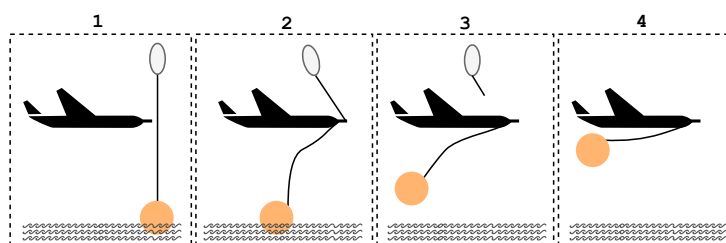


Figure 1: Retrieval of the search system using the balloon concept.

The second concept concerns a fish-out system, where the search system is retrieved from the water using a grapple hook attached to a cable, which is fixed to the aircraft. This is shown in fig. 2.

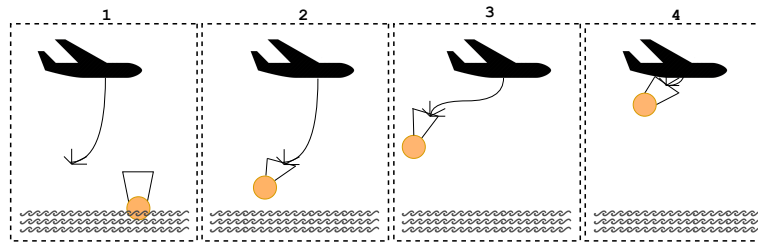


Figure 2: Retrieval of the search system using the fish-out concept.

The third concept is a harpoon system, where a projectile is shot from an aircraft, catching/penetrating the search system. The concept can be found in fig. 3.

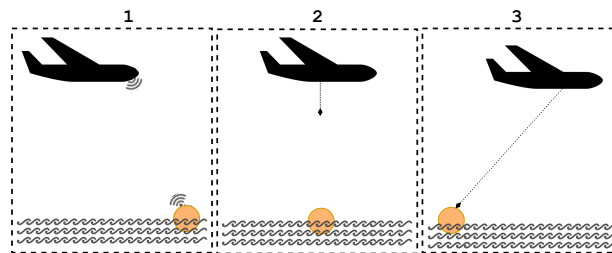


Figure 3: Retrieval of the search system using the harpoon concept.

The last concept is a drone on tether, wherein an autonomous drone is attached to the tip of a tether. This drone is used to adjust the position of the tether to reliably retrieve the search system. This concept is shown in fig. 4.

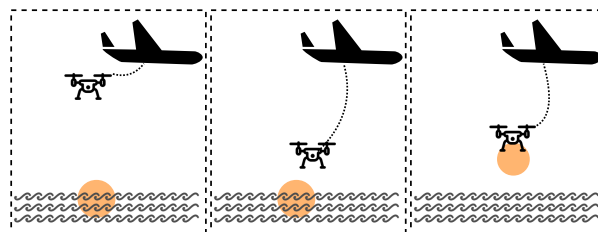


Figure 4: Retrieval of the search system using the drone-on-tether concept.

The criteria used for the tradeoff included accuracy, reliability, safety, ease of use, sustainability, availability, mass, maintainability and volume. The masses and volumes of each concept were calculated by first analyzing the forces induced by retrieval on the search system. These forces were calculated by modelling the retrieval process as a pendulum system. From the tradeoff, the drone on tether came out as the strongest concept, in terms of accuracy, safety, ease of use, sustainability and availability.

Airborne System Tradeoff Various types of airborne vehicles have been looked at and have been traded off using the criteria cargo volume, system integration, payload, cruise speed, reliability, range, sustainability, safety, maintainability and availability. The considered airborne vehicles included the C-130 Hercules and the Airbus A400M (military aircraft), the Airbus A319 (civil aircraft) and the Global Hawk (UAV). The Airbus A400M scored best in the tradeoff, with sustainability (based on fuel consumption) being the only disadvantage of the aircraft. Based on future decisions of the design process, the aircraft used might be changed, as it is one of the last choices in the process. It is assumed that the aircraft can be provided by the military, which will be selected and approached depending on the details of the search mission. The Airbus A400M is an aircraft owned by the military in countries including Germany, France, Spain and Malaysia.

Tradeoff Result Even though each system has their respective tradeoff winner, they must also be compatible with each other for the search mission for a missing aircraft. Therefore, an overall tradeoff is performed on the entire ULB Finder System including the winning and runner up of each system. The tradeoff was assessed using the RAMS characteristics, which stands for reliability, availability, maintainability and safety. The results are presented in table 1.

Table 1: Tradeoff summary presenting the winner concepts and the runner ups.

System	Deployment		Search System		Relocation		Retrieval		Airborne	
Approved concepts	Free fall	Parachute	Glider	Submarine	Submarine	Autonomous Buoy	Drone on tether	Fish-out	Airbus A400M	C-130 Hercules
Score (out of 4)	3.60	2.80	3.41	2.82	3.72	2.94	3.42	2.67	3.68	3.27
In final design	✓	-	-	✓	✓	-	✓	-	✓	-

The final design will use the submarine as a search system and as the relocation method. The submarine will be deployed using free fall and retrieved with a drone on tether. The deployment and retrieval system will utilize the Airbus A400m as the airborne system.

Final Concept

Figure 2.1 gives a schematic description of the final concept. The ULB Project is split into two categories: external elements and the ULB Finder System. The external elements are indicated by circular boxes and represent interactions with the environment (i.e. ULB beacon signal of missing aircraft) and infrastructure (i.e. satellite constellation and ULB ground station). The ULB Finder System encompasses all segments that are designed in order to locate the beacon signal; This includes the search systems, the deployment system, the airborne system and the retrieval system. In order to effectively locate the ULB signal, the search systems will navigate a predefined search area with a radius of 100 km. A search system consists of a submarine and mother buoy. The submarines can submerge and travel above the seabed where it is within reach of the ULB signal. The real-time position of each submarine will be tracked by a mother buoy, which communicates and moves with the submarine. To satisfy the 48-hour deployment window, the search systems will be dropped from an aircraft (i.e. the airborne system). The deployment requires a dropping platform for ease of operations and to minimize damage to the search systems. After the mission, or after the 30-day ULB signal window is over, the search systems will be retrieved via the retrieval system. A flying wing is suspended via tether from the airborne system and proceeds to pick up the submarine or the mother buoy. Once the submarine or the mother buoys is picked up, the pair are reeled in via the tether. The airborne system used is the A400M but it is important to note that the deployment and retrieval system will be designed such that it is compatible with the C-130.

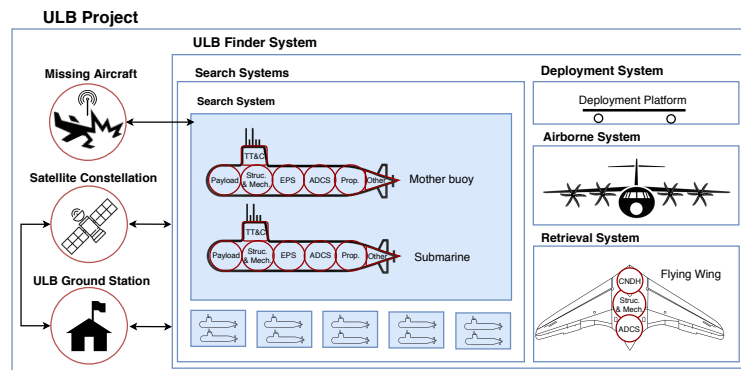


Figure 5: Overview of the systems within the ULB Project.

Operations It is assumed that the exact location and shape of the search area is given prior to the search mission, by an external organization. The coverage path within this search area will then be planned accordingly and is also dependent on factors such as weather and current. For now, a circular search area with a radius of 100 km has been assumed and the range of the ULB is assumed to be 2 km. The coverage path will consist of parallel paths connected with turning points outside the search area as it was found that the Inertial Navigation System implemented within the submarines are most accurate when the submarines travel in straight lines. In order to be well within range of the ULB signal and decrease the total coverage path, the submarines search at 500 m above the bottom of the ocean. This results in a total distance of 9400 km for the coverage path. To confidently cover the search area and locate the ULB signal, the search system will take 20 days to cover the entire search area. This is known as search phase one. Each search system will look for the signal individually and together they will cover the total coverage distance. By combining the distance with the submarine velocity, 1 m/s, and a search time of 20 days, the total number of submarines was determined to be 6. Once one of these search systems receives the ULB signal, an approximate location of the aircraft, in the order of 1km, can be determined. Therefore, the total search area can be reduced. The reduction of the search area initiates the second search phase where all search system will relocate to the smaller search and a new search is started. However in the second search phase, the aircraft position will be determined with a minimum of three submarine - ensuring an accurate aircraft location via triangulation. The relocation of the search systems and coverage of the second search phase will take 10

days. Factors that could create a risk for the operation of the search mission include current, variation of ocean depth, obstacles in the ocean and deep-sea search. A system of equations has been set up that can make up for the deviation due to lost current, by redirecting and slightly speeding up the submarines if necessary. Large obstacles, including small islands, in the search islands can be mapped and therefore taken into consideration when planning the coverage path. The submarines will not be equipped with any obstacle-avoidance equipment, but considering their low speeds, impact with any obstacle is not considered problematic. However, it might pose a risk for marine life. Furthermore, the chance of finding obstacles at a depth of multiple kilometres is very small. The risk of deep-sea search is that the pressure might affect the equipment of the search system. However, this has been taken into account for the design of the search system. Moreover, it was found that it only takes 1148 s to get to the maximum search depth of 4500 m. Thus, depth change is not an issue for the search mission.

Deployment System To design the deployment system, the main aim was to reduce the impact force to a minimum, by decreasing impact velocity and/or surface area. Free fall was analyzed under unsteady, non-straight and symmetric flight conditions and modelled using non-linear differential equations. The outputs of this included a velocity vector, a position vector and an orientation of the submarine during free fall. Two control surfaces on the aft spherical end of the submarine were designed accordingly, in order to control the deployment and to ensure that the submarine lands as to create minimum impact force.

Search system For navigation of the submarine, an Inertial Navigation System is used for up-to-date position updates while moving underwater. It integrates acceleration into velocity and displacement in order to determine its position, requiring force and angular rate in three dimensions, provided by accelerometers and gyroscopes. One problem of the Inertial Navigation System is that it has growing error. One way to compensate for this error is by using the Kalman filter, which improves the accuracy of the state vector and thus of the navigation. Furthermore, depth sensors and a compass are used to aid the measurements for navigation. The mother buoy is connected to the submarine by GPS and will send a GPS update every 5 minutes. For communication, a low frequency must be used to minimize and sound absorption. An acoustic modem including a transducer will be used. Furthermore, a satellite modem and antenna will be present on board of the submarine, so that when it loses communication with the mother buoy, it can come up to the surface and send its location to the base station.

In order to control the depth of the submarine, a buoyancy control system is needed. The submarines will be equipped with a variable ballast system (VBS) to alter the mass of the submarine and control the pitch. To empty the tanks when desired, a pump is used that can overcome the high ambient pressure. Furthermore, an emergency ballast is included into the design in case the submarine sinks due to failure of buoyancy control. A propeller is mounted on the rear end of the submarine to provide the necessary 18.4 N of thrust. For stability of the submarine, it is assumed that the submarine is naturally stable in pitch and yaw. This is due to its torpedo shape, where any rotation is counteracted by an opposite rotation due to the drag on the aft of the hull. The submarine will be controlled in yaw by a rudder mounted on the aft of the hull. Pitch is controlled by horizontal control surfaces on the aft of the hull and the center of gravity, that can be changed by the ballast tanks.

For power, both a battery and a hybrid system were considered. Both systems have the risk of ignition, however the batteries also lack sustainability and recyclability. Furthermore, batteries are much more expensive and would result in a bigger volume than a hybrid system. For these reasons, a hybrid system using a 50 W fuel cell system will be used, supported by a small lithium-ion battery.

To design the structure of the submarine, different load cases were analyzed. The first one included the impact on water, followed by pressure at maximum depth and the retrieval force. Pressure at maximum depths appeared to result in the largest force acting on the submarine structure. Stiffeners were designed to decrease buckling force. This resulted in a reduction of mass, however increases susceptibility to yielding. From the above calculations, the dimensions of the stiffeners used in the submarines were iterated, including a 20% safety factor. The resulting length of the submarine is 2.5 m, with a diameter of 0.5 m. The shell will be made out of 0.0098 m thick CFRP, where 8 stiffeners are used for reinforcement. The total mass of one submarine is 393 kg.

Mother Buoy The mother buoys include a lantern powered by its own solar cells and a battery to prevent collisions with sea traffic. It will use the same communication equipment as the submarines. Furthermore, the mother buoys will follow the submarines by receiving GPS locations from the submarines. In order to move at the same velocity as the submarine, the mother buoys might need to travel slightly faster in order to compensate for stronger currents on the surface of the ocean. However, no structural design changes will be made, as this is not necessary. The total mass of one mother buoy is 414 kg.

Retrieval System For the retrieval, a drone-on-tether system is used. The tether is fixed to a winch, which reels the system once the search system is hooked. The drone keeps the tether taut by manipulating its drag through airbrakes. A small robot arm, on the bottom of the flying wing, will fine-tune the position to ensure successful retrieval. On the search system itself, a hydrogen balloon is deployed, which rises to an altitude of 6 m and is picked up by a hook, attached to the military aircraft by the retrieval arm.

Verification and Validation Verification and validation has taken place at various stages throughout the project, as well as for each subsystem individually. For the validation of results, the aim was to ensure that they were verifiable, achievable, logical, integral and definitive. Potential validation methods have been presented and a variety of experts, from inside and outside the faculty, have been contacted in order to check methods and results. Furthermore, all numerical and computer models were verified, including the Python programs to calculate values relevant for the different concepts. This was done through zero-value tests, limit tests, known example tests and analytic solution tests.

Non-technical aspects

For the market analysis, the external macro-environment was assessed using a generic environment PEST analysis based on four parts: political-legal, economic, and socio-cultural and technological parts. These include factors that can identify the external variables that could affect a business's performance. Furthermore, specific environment was analyzed using Porter's 5 forces.

For the sustainable development strategy, an active agenda was implemented that identifies and pursues value creating activity on sustainability. Concepts central to sustainable development strategy include knowledge driven and dynamic processes and understanding the value creation that the strategy aims for. After this, business processes should be integrated to support the sustainability initiatives. Due to the relatively little use of the design (predicted use is once every 4 years) the impact on the environment is minimal. Furthermore, energy sources are mostly renewable and the system is retrieved as not to pollute the ocean. Due to the secondary purpose of the design, as much value as possible while maintaining sustainability, is created for economical sustainability. If the aircraft is found using the system, social sustainability is achieved through valuable information of the crash, possibly improving safety of air transportation and preventing specific types of crashes in the future. To numerically measure sustainability, indicators used included fuel used, material type and amount used, the production process and the end-of-life assessment.

There are various risks associated with the technical aspects of the ULB finder system, including damage, unavailability of components of the search system, errors in the communicated signals and unfavourable weather conditions. Furthermore, there are risks specifically related individual systems. For instance, power shortages or internal/external damages to the submarine induced by deployment, operation, or retrieval are all possible. To reduce risks, several mitigation strategies are proposed, such as having multiple deployment and retrieval devices and/or airborne vehicles and operating at a higher altitude.

Conclusion & Recommendations

The designed subsystems of the search operation provide a solution that satisfies the mission statement and objective statement of the project. Furthermore, the entire cost of the ULB project have been estimated by taking into consideration the production, development and operational costs. Including a contingency of 25% for inflation and uncertainties lead to a total cost of € 48 million, which is lower than the set budget. The ULB Project is achievable by using the search systems, consisting of the sized and equipped submarines and the mother buoys, for which a deployment method and a retrieval method have been designed extensively. The final design of the submarine can be seen in fig. 6 and fig. 7.

However, due to the variety of subsystems and scope of the project, there are many different possible sources of error, which could be accounted for in further research. Recommendations for further development of the project include further investigation into noise in deep water environments, interaction between a buoyancy control system and propulsion system, as well as more research on the use of PID controllers for control surfaces. This is the most common control algorithm used. Furthermore, vertical displacement of the submarine during search could be considered, both to account for deviations due to current, as well as for planned deviations along with ocean depth variation. For the structural determination, a Finite Element Analysis could be used to obtain a more accurate estimation of stresses. This way, varying thicknesses could be used to reduce weight. For the retrieval process, proposed validation experiments could be executed to determine the feasibility of the concept. Furthermore, the simulation could be expanded by coupling aircraft dynamics to retrieval dynamics. Flight maneuvers to make the retrieval process more efficient could also be further looked into.

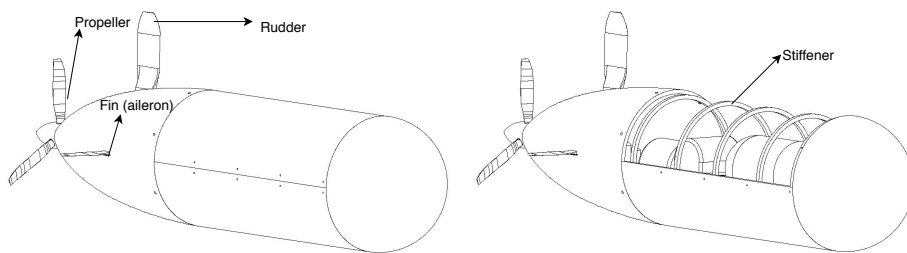


Figure 6: Isometric view of the submarine structure and the elements it houses.

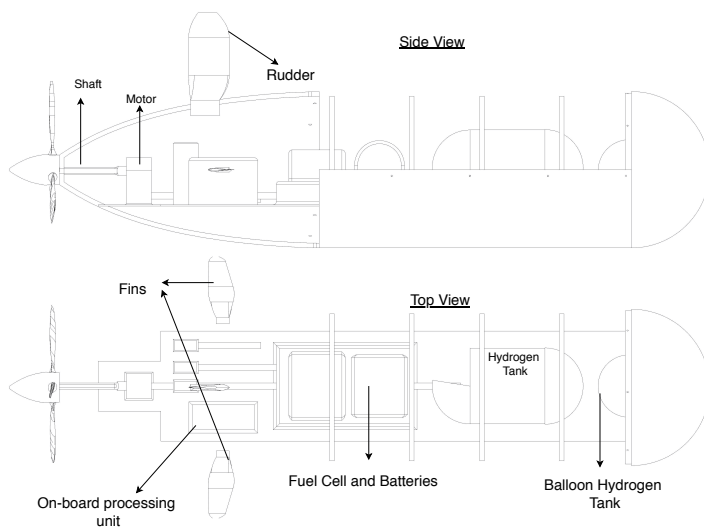


Figure 7: Top and side view of the submarine structure and the elements it houses.

Contents

Executive Overview	vi
1 Introduction	1
2 Overview of the ULB Project	2
2.1 Project Objectives	2
2.2 System Description of the ULB Project	2
2.3 Functional Analysis	3
2.4 Requirements Analysis	3
2.4.1 User Requirements	3
2.4.2 System Requirements	3
2.4.3 Killer Requirements	4
2.4.4 Driving Requirements	4
3 Market Analysis	5
3.1 Generic Environmental Analysis	5
3.1.1 Political-Legal Factors	5
3.1.2 Economic Factors	5
3.1.3 Socio-Cultural Factors	6
3.1.4 Technological Factors	6
3.2 Specific Environmental Analysis	6
3.2.1 Barriers of Entry	6
3.2.2 Substitutes	6
3.2.3 Relationship with Suppliers	6
3.2.4 Relationship with Customers	7
3.2.5 Rivalry within the Industry	7
3.2.6 Barriers of Exit	7
4 Sustainable Development Strategy	8
4.1 Active Agenda for Sustainability	8
4.2 Integration of Sustainability in Business Processes	9
4.3 Capturing Value of Sustainability Initiatives	9
5 Operations	11
5.1 Search Strategy	11
5.1.1 Input Parameters	11
5.1.2 Coverage Path Planning	11
5.1.3 Code Verification	13
5.2 Operational Risks	14
5.2.1 Ocean Currents	14
5.2.2 Depth Variation	16
5.2.3 Obstacles in the Ocean	16
5.2.4 Deep Sea Search	16
5.3 Operations and Logistic Concept Description	16
5.3.1 Operations and Logistics Concept Diagram	16
5.3.2 Military Corporation	17
5.4 Airborne System for Operations	17
5.4.1 Aircraft Characteristics	18
5.4.2 Deployment and Retrieval System Integration	18
6 Deployment System	19
6.1 Overview of the Design Process for the Deployment System	19
6.2 Simulation of the Trajectory	19
6.3 Results and Verification of the Simulation	23
6.3.1 Results of the Simulation	23
6.3.2 Verification of Free Fall Model	24
6.4 Validation of Deployment Simulation	27
6.4.1 Experiment 1: Wind Tunnel Testing with Miniature Model	27
6.4.2 Experiment 2: Wind Tunnel Testing with Real-Size Model	27
6.4.3 Experiment 3: Flight Test of the search system	28
7 Submarine	29
7.1 Payload & Instrumentation	29
7.2 Navigation	29
7.3 Communication	32
7.3.1 Communication Channel Characteristics	33
7.3.2 Equipment	34
7.3.3 Data Handling and Communication Link	34
7.4 Buoyancy Control	35
7.4.1 System Architecture	35
7.4.2 Buoyancy Control Sizing	36
7.4.3 VBS Performance	37
7.4.4 Verification & Validation	39
7.5 Propulsion	40
7.6 Stability & Control of the Submarine	41
7.6.1 Stability	41
7.6.2 Control	41
7.7 Power	41
7.7.1 Batteries	42
7.7.2 Hybrid System	43
7.7.3 Tradeoff	45
7.8 Structure Design of Submarine	47
7.8.1 Load Case Scenarios	47
7.8.2 Design Approach	48
7.8.3 Failure Mode: Yield	49
7.8.4 Failure Mode: Buckling	50
7.8.5 Verification & Validation	55

7.9 Budget Breakdown	57
7.10 Software Diagram	58
7.11 Summary	58
8 Mother Buoy	60
8.1 Payload	60
8.2 Communication	60
8.3 Navigation	60
8.4 Propulsion	61
8.5 Power	61
8.6 Stability in water	62
8.7 Budget Breakdown	63
8.8 Summary	63
9 Retrieval System	64
9.1 Overview of the Retrieval Concept	64
9.2 Simulation of the Retrieval Dynamics	65
9.2.1 Modelling the Retrieval Dynamics	65
9.2.2 Results of the Retrieval Simulation	70
9.2.3 Simulation Verification	73
9.3 Simulation of Aircraft Response	78
9.3.1 Aircraft Equations of Motion	78
9.3.2 Aircraft Model	79
9.3.3 Verification	82
9.4 Drone Sizing	83
9.4.1 Retrieval Arm Sizing	83
9.4.2 Flying Wing Sizing	87
9.5 Hydrogen Balloon with Net	90
9.6 Moving Forward: Possible Validation Experiments	91
9.7 Power	94
9.7.1 Power Requirements of Components Attached to Aircraft	94
9.7.2 Power Requirements of Components Attached to Search System	94
10 Final Concept of the ULB Project	95
10.1 Concept Overview of the ULB Project	95
10.2 Hardware Diagram of the ULB Project	96
11 Risk Assessment	98
11.1 Risk Identification	98
11.2 Risk Mitigation Strategies	101
12 Product Evaluation	104
12.1 Requirement Compliance	104
12.2 Sensitivity Analysis	104
12.2.1 Sensitivity Analysis 1 - Different Shell Material	104
12.2.2 Sensitivity Analysis 2 - Larger search area	105
12.2.3 Sensitivity Analysis 3 - Additional Payload	106
12.2.4 Sensitivity Analysis 4 - New ULB Signal	107
12.3 Reliability, Availability, Maintainability and Safety Characteristics	107
12.3.1 Reliability	107
12.3.2 Availability	107
12.3.3 Maintainability	108
12.3.4 Safety	108
12.4 Safety Functions & Redundancy Philosophy	109
13 Project Development and Manufacturing Plan	110
13.1 Project Development Planning	110
13.2 Gantt Chart	110
13.3 Integration and Manufacturing Plan	112
13.3.1 Production Strategy	112
13.3.2 System Production Plan	112
14 Financial Analysis	117
14.1 Cost Breakdown	117
14.2 Return on Investment	118
14.2.1 Break-even	120
15 Conclusion & Recommendations	121
Bibliography	123
A Functional Flow and Breakdown Diagrams	130
A.1 Functional flow	130
A.2 Functional breakdown structure	132
B Cost distribution	135

Introduction

Despite the growing safety of travelling by plane, accidents in modern aviation still occur. In some cases, such accidents lead to aircraft crashing into water, of which Malaysian Airlines flight 370 is a noticeable case. Even with extensive search missions and costs exceeding €100 million, nothing has been found until today - except some components of the aircraft that washed up on shores around eastern Africa. Locating crashed aircraft is of primary importance as it allows investigators to determine what went wrong; Thereby, increasing the safety of future air transport. Furthermore, obtaining answers provides closure to the affected families.

The mission of the ULB Project is to scan a predetermined ocean region in order to locate an aircraft which has crashed in deep water within 30 days. The project objective is to design an airborne system, within 10 weeks with 10 people, that can reach any location on Earth within 48 hours and is capable to locate the ULB signal of the missing aircraft in deep water. User requirements were set by the project. Important user requirements are to be deployable to any location on Earth within 48 hours, to have independent operation for 2 weeks, that the total cost does not exceed €50 million and that the system shall be reusable.

The main purpose of this report is to determine the feasibility of the ULB Project. The project is evaluated by analyzing each segment of the ULB finder system by MARLIN (This is the company name of the design synthesis group that is undertaking the project underwater locator beacon.) The main segment is the search system which will locate the missing aircraft. The challenges for the search system are how will it detect the ULB signal, how can it keep track of its location and how will it relocate itself. Additional segments are based on the operational aspects of the project. An airborne system is needed to bring the search system to the search area. Furthermore, a deployment and retrieval system is required to bring the search system into the water and to redeploy it.

The report starts with presenting a higher-level system description and the requirements of the ULB Project in chapter 2. Then, a market analysis is performed to identify the competitive advantages of the ULB Project in chapter 3. After the market analysis, the sustainable development strategy for the project is outlined in chapter 4. In order to obtain an idea of how the signal can be located, the operational aspect such as the search strategy and the airborne system are presented in chapter 5. Assuming that an aircraft has crashed in deep water and the airborne system has been deployed, then the search system will have to be placed into the water by the deployment system as discussed in chapter 6. The search system will consists of a submarine and a mother buoy which are designed and shown in chapter 7 and chapter 8 respectively. Once the 30 days of the ULB signal are over, the retrieval system picks up the search system as described in chapter 9. The final concept is then presented in chapter 10. As the ULB finder system is new concept, risks need to be considered in the design process and operations. The risk assessment is covered in chapter 11. The project is then evaluated by performing a sensitive analysis and evaluating the reliability, availability, maintainability and safety characteristics in chapter 12. Once the project has been evaluated, it will developed to show how it can be implemented in the future in chapter 13. Then, all the financial costs for the entire project are summed up in chapter 14. The report ends with the conclusion and recommendations in chapter 15.

Overview of the ULB Project

This chapter provides an overview of the ULB project. Section 2.1 presents the objectives of the ULB project. A system description of the ULB project is discussed in section 2.2. The requirements are presented in section 2.4 along with an analysis on killer and driving requirements.

2.1. Project Objectives

Mission Statement: Scan a predetermined ocean region in order to locate an aircraft which has crashed in deep water within 30 days.

Objective Statement: Design an airborne system, within 10 weeks with 10 people, that can reach any location on Earth within 48 hours and is capable to locate the ULB signal of the missing aircraft in deep water.

2.2. System Description of the the ULB Project

Figure 2.1 gives a schematic description of the ULB Project. The ULB Project is split into two categories: external elements and the ULB Finder System. The external elements are indicated by circular boxes and represent interactions with the environment (i.e. ULB beacon signal of missing aircraft) and infrastructure (i.e. satellite constellation and ULB ground station). The ULB Finder System encompasses all segments that are designed in order to locate the beacon signal; This includes the search systems, the deployment system, the airborne system and the retrieval system.

In order to effectively locate the ULB signal, the search systems will navigate a predefined search area with a radius of 100 km. A search system consists of a submarine and mother buoy. The submarines can submerge and travel above the seabed where it is within reach of the ULB signal. The real-time position of each submarine will be tracked by a mother buoy, which communicates and moves with the submarine.

To satisfy the 48-hour deployment window, the search systems will be dropped from an aircraft (i.e. the airborne system). The deployment requires a dropping platform for ease of operations and to minimize damage to the search systems. After the mission, or after the 30-day ULB signal window is over, the search systems will be retrieved via the retrieval system. A flying wing is suspended via tether from the airborne system and proceeds to pick up the submarine or the mother buoys. Once the submarine or the mother buoys is picked up, the pair are reeled in via the tether.

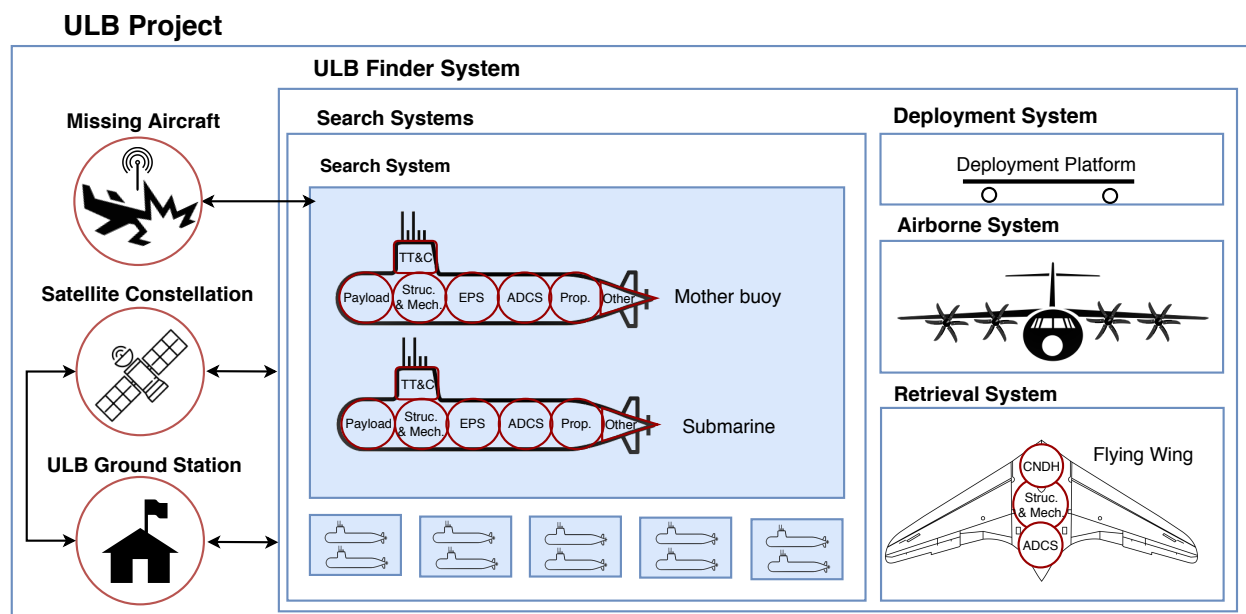


Figure 2.1: System Description of the ULB Project.

2.3. Functional Analysis

A full overview of the functions of the ULB finder system is given in appendix A. The most critical functions are:

- 5.3.1 Communicate signal to data handling center - This is explained in section 7.3.
- 5.3.4 Determine whether signal comes from ULB - More on this is discussed in section 7.3.3.
- 7.3.2.4 Ensure search system is out of water - This is modelled in section 6.2.

2.4. Requirements Analysis

In this section the requirements of the ULB finder system are analyzed. The user requirements are listed in section 2.4.1, followed by the system requirements in section 2.4.2. The section ends with the killer requirements given in section 2.4.3 and the driving requirements in section 2.4.4.

2.4.1. User Requirements

The user requirements are key requirements as these are of primary importance to the customer.

- ULB-USER-01** The ULB finder system must be deployable to any location on Earth within 48 hours.
- ULB-USER-02** The search systems must be able to operate independently for at least 2 weeks.
- ULB-USER-03** Total system cost shall be less than €50 million.
- ULB-USER-04** The ULB finder system shall be able to search an area within a body of water with a radius of 100 km in 30 days.
- ULB-USER-05** The airborne system shall be able to retrieve all buoys.
- ULB-USER-06** The search systems shall be reusable and redeployable.
- ULB-USER-07** The airborne system shall be able to reach any location on a body of water, with full payload.
- ULB-USER-08** The search systems shall be visible for sea traffic.
- ULB-USER-09** The system shall be usable for other applications.
- ULB-USER-10** The search systems shall be able to send instant messages to a base station.

2.4.2. System Requirements

The system requirements are additional requirements necessary for the design. A division is made between airborne, search system (submarines and mother buoys) and deployment & retrieval requirements.

Airborne Requirements (incl. airport network & operations and airborne vehicle)

- ULB-SYS-AIR-01** The airborne system shall be able to communicate with the base station.
- ULB-SYS-AIR-02** The airborne system shall be able to communicate with the search systems.
- ULB-SYS-AIR-03** The airborne system shall comply with airworthiness regulations.
- ULB-SYS-AIR-04** The airborne system shall be able to take-off from all stations in the selected network.
- ULB-SYS-AIR-05** The airborne system shall not be compromised by failure of the deployment and retrieval system.
- ULB-SYS-AIR-06** The airborne system shall be able to identify the drop-off zone with an accuracy of 1 km.
- ULB-SYS-AIR-07** The airborne vehicle shall be able to carry 6 search systems.
- ULB-SYS-AIR-08** The airborne vehicle shall periodically update its location to the base station once every 10 minutes.
- ULB-SYS-AIR-09** The range of the airborne system at full payload weight shall be at least 6850 km.
- ULB-SYS-AIR-10** The airborne vehicle at maximum payload shall have a cruise speed of 700 m/s.
- ULB-SYS-AIR-11** The airborne vehicle shall be maintainable in all stations within the network.
- ULB-SYS-AIR-12** The command center shall comply with the government regulations of the host country.

Search System (Submarines and Mother Buoys) Requirements

- ULB-SYS-SMB-01** Each search system component shall survive the deployment impact load when dropped at an altitude of 600 ft.
- ULB-SYS-SMB-02** Each mother buoy shall be visible in compliance with the Convention on the International Regulations for Preventing Collisions at Sea (COLREG).
- ULB-SYS-SMB-03** Each search system component shall be capable of self stabilizing.
- ULB-SYS-SMB-04** Each search system shall be able to determine its location on Earth with an accuracy of 5 m using a GPS or similar system.
- ULB-SYS-SMB-05** Each submarine shall be able to determine its attitude.
- ULB-SYS-SMB-06** Each search system component shall be able to identify any issues with the on-board systems.
- ULB-SYS-SMB-07** The search systems shall be able to transmit the health & status of the on-board systems.
- ULB-SYS-SMB-08** The mother buoys shall be able to securely communicate with the command center.
- ULB-SYS-SMB-09** The search system components shall not be a contributing factor to pollution of the marine ecosystem during operation.
- ULB-SYS-SMB-10** The search system components shall be disassemblable.

- ULB-SYS-SMB-11** The search system shall communicate their position to the command centre at least once every 30 minutes.
- ULB-SYS-SMB-12** The submarines shall be able to detect the beacon signal when the beacon is 5 km under sea level.
- ULB-SYS-SMB-13** The search system shall be able to record the detected signal of the beacon.
- ULB-SYS-SMB-14** The buoy shall be able to send the recorded beacon signals to the command centre.
- ULB-SYS-SMB-15** The buoy shall be water resistant.
- ULB-SYS-SMB-16** The search system components shall be able to spend 30 days in sea water without corrosion.
- ULB-SYS-SMB-17** The search system shall be able to close its link budget.
- ULB-SYS-SMB-18** The search system components shall have a mass of at most 3125 kg.
- ULB-SYS-SMB-19** The search system shall have a maximum power of 3254 W.
- ULB-SYS-SMB-20** The attachments of the search system components shall be compatible with the attachments of the deployment & retrieval system.
- ULB-SYS-SMB-21** The communication frequencies shall be approved by the frequency regulators.
- ULB-SYS-SMB-22** The search system shall maintain an operational temperature range from -15°C to +35°C.
- ULB-SYS-SMB-23** The search systems shall be maintainable.
- ULB-SYS-SMB-24** *Deleted* The CO₂ emissions during the manufacturing of the search system should stay below <tbd> kg. *This requirement has been deleted because it is unfeasible to set a realistic emission constraint it at this point in the design process.*

Deployment & Retrieval Requirements:

- ULB-SYS-DNR-01** The deployment system shall be capable of deploying the search systems from the airborne vehicle.
- ULB-SYS-DNR-02** The search systems shall be deployable in the operational limit conditions of the airborne vehicle.
- ULB-SYS-DNR-03** The deployment system shall have a mass of at most 3125 kg.
- ULB-SYS-DNR-04** The retrieval system shall have a mass of at most 3125 kg.
- ULB-SYS-DNR-05** The deployment system shall fit within the usable space of the airborne vehicle.
- ULB-SYS-DNR-06** The retrieval system shall fit within the usable space of the airborne vehicle.
- ULB-SYS-DNR-07** The deployment of all loaded buoys shall occur within 1 hour.
- ULB-SYS-DNR-08** The deployment & retrieval system shall pass airworthiness certifications.
- ULB-SYS-DNR-09** The deployment & retrieval system shall be maintainable.
- ULB-SYS-DNR-10** The deployment & retrieval system shall have the capacity to abort operations, if required.
- ULB-SYS-DNR-11** The deployment system shall update the operator on the progress of deployment.
- ULB-SYS-DNR-12** The deployment and retrieval system shall not pollute the marine ecosystem during operation.
- ULB-SYS-DNR-13** The deployment and retrieval system shall not compromise the safety of the operators during its operation.
- ULB-SYS-DNR-14** The deployment and retrieval system shall not compromise the safety of ships during its operation.
- ULB-SYS-DNR-15** *Deleted* The CO₂ emissions during the manufacturing of the deployment and retrieval system should stay below <tbd> kg. *This requirement has been deleted because it is unfeasible to set a realistic emission constraint it at this point in the design process.*

2.4.3. Killer Requirements

The following requirements have been classified as killer requirements since these drive the design to an unacceptable extent:

- Requirement **ULB-USER-05**: limits the design options to using retrieval via the airborne system and not from water.

2.4.4. Driving Requirements

The following requirements are driving requirements as they influence the design more than average.

- Requirement **ULB-USER-01** limits the deployment vehicles.
- Requirement **ULB-USER-04** limits the availability of airborne vehicles in terms of range, endurance and operating conditions since the vehicle must take off, deploy and return to its origin.
- Requirement **ULB-USER-06** limits the operation since buoys a retrieval system must be added.
- Requirement **ULB-SYS-SMB-15** limits the layout configuration of the structure since this aspect must protect the buoy's internal systems.
- Requirement **ULB-SYS-DNR-01** limits the deployment vehicle to airborne systems.

Market Analysis

This chapter contains the performed market analysis. It starts with the general analysis which is found in section 3.1 after which the specific analysis is performed in section 3.2. The ULB finder system is sold to potential customers who already own suitable aircraft. The system itself can be integrated without too many alterations of the aircraft itself, so called plug and go. Please note that the market analysis is used as a baseline for the Financial Analysis in chapter 14.

3.1. Generic Environmental Analysis

Generic environment analysis monitors the external macro-environment and is usually performed through a PEST analysis. This tool is used to identify the various external variables that affect a business's performance. The PEST analysis stands for Political-legal, Economic, Socio-cultural and Technological factors which can be found in section 3.1.1, section 3.1.2, section 3.1.3 and section 3.1.4 respectively.

3.1.1. Political-Legal Factors

Political-legal policy changes, which may occur in any government, can have serious implications. Furthermore, legal factors vary between countries. Thus, a company has to be familiar with these legalities in order to trade successfully [1]. Political-legal factors that can influence the ULB project are:

- **Taxation regulation;** This affects the production of the search systems. The production volume of the search systems will likely be low, as such several parts may be outsourced. Any outsourcing contracts with oversea companies will be subject to import taxes and regulations. As an example, the delivery of outsourced parts may be delayed due to these regulations/inspections. Therefore, the legal aspects of the transportation of parts need to be considered when selecting companies to outsource to - if at all.
- **Employment laws;** This is directly related to the cost of the staff involved in the project; an increase in wage increases the cost of the operation.
- **Environmental regulations;** The main focus of these regulations is to ensure environmental protection. The regulations have become stricter in the past decades and are at the forefront of government legislation, as demonstrated by the Paris Agreement. An example of a political environmental legislation is carbon footprint targets set by the government. This highlights the importance of the sustainability of the product/company as it is one of their responsibilities to comply with these regulations.
- **Health & safety requirements;** Each country has health and safety regulations, such as working hours and amount of paid leave days, that need to be complied with.
- **International flight and water regulations;** This affects the operation of the ULB finder system as it will operate (internationally) in both air and water. Such regulations are taken into account when selecting transport/search routes. However, due to the nature of search operations, most access should be granted.

3.1.2. Economic Factors

Economic factors play an important role when analyzing the market. The macroeconomic variables are the same for most countries, but the implementation and execution of policies are different for each country [1, 2]. For the ULB finder system, possible economic factors include:

- **Inflation;** When inflation happens, the costs of implementing the ULB finder system will increase and thus have a negative effect on the budget. However, this system is not supposed to make profit (main goal is making search operations cheaper and more effective). Thus, extra operational costs due to inflation will not be critical.
- **Aircraft market;** The aircraft market has established itself as independent and is ever-increasing. A crashed aircraft would deteriorate the image of the aircraft market. Thus, it is crucial to find the lost aircraft to determine the cause of failure and prevent it, making air travel safer.
- **Humanitarian Efforts;** Families will always push the government/airliners to invest money into search operations, or contribute to search efforts themselves. Additionally, aircraft manufacturers want to know the causes of the crash to improve safety. As such, the ethical reason behind this mission implies that there will always be money available for search operations - especially for a system that would improve search efficiency for lower costs.

3.1.3. Socio-Cultural Factors

When performing a market analysis, the impact of the technological system on the social environment and surrounding culture should be considered. For the ULB finder system, these factors depend on the (random) location of the crash. Some examples of socio-cultural factors are:

- **Education;** Only qualified personnel should be operating the ULB finder system.
- **Population distribution;** When operating in deep water, the local marine life population may be considered a threat to the system and the system a threat to them.
- **Hostile environments;** There is a risk that the ULB finder system is deployed in a hostile environment. In this case, hostile environments encompass: pirates who may steal or damage system, heavily trafficked ship routes which may result in collisions, and hostile governments who are reluctant to cooperate.

3.1.4. Technological Factors

The technological factors are variables that relate to the development, availability and existence of technology. The system is to be implemented in the near future. Therefore, incipient and untested technologies are considered unavailable. The efficiency and automation of technologies are all of importance when developing a system [1, 3]. The following list identifies the different types of technologies in the system [3]:

- **Untested Technologies;** The retrieval of an object from the water with an aircraft is the most novel technology used in the ULB finder system as it has yet to be implemented. Thus, determining the feasibility of this system is of primary importance.
- **Proven Technologies;** The constituents of all other systems have been implemented before, but the interfaces between these systems is novel.

3.2. Specific Environmental Analysis

Specific environment represents the environment closest to firms. The analysis is done by evaluating Porter's 5 Forces (barriers of entry, substitutes, relationship with suppliers, relationship with customers and rivalry within the industry) along with the barriers of exit [4]. These tools help understand the business environment. Section 3.2.1, section 3.2.2, section 3.2.3, section 3.2.4 and section 3.2.5 examine the Porter's 5 Forces respectively and section 3.2.6 investigates the barriers of exit.

3.2.1. Barriers of Entry

Barriers of entry are aspects that prevent a company from entering a specific market [4]. Potential factors that can result in a barrier of entry are:

- **Capital requirement;** This relates to the financial resources required for infrastructure, research & development (R&D) and machinery. The submarines and mother buoys will have to be manufactured and a robust communication system needs to be established. Capital requirements can be reduced by using more proven technologies (less R&D expenditures).
- **Access to distribution channels;** The ULB finder system should be stored at a ground station close to an airport (where it can be deployed quickly) when it is not in use.
- **Legal/Regulation policies;** Governments can limit, regulate and quality check industries through licensing requirements. For instance, the retrieval mechanism has to be tested and needs to pass certain safety tests in order to be certified.

3.2.2. Substitutes

The threat of substitutes refers to the likelihood of potential customers finding a different way of doing things (i.e. locating the ULB). As the ULB finder system's purpose is to be cheaper and more effective than current methods, there are no real existing substitutes. Regardless, if costs of current methods decrease, then the search can be done in multiple ways, known as substitutes [4]. The most likely substitute is a search system using autonomous underwater vehicles (AUVs) deployed from boats to search for the lost aircraft. The advantage of this substitute is that it is already used and therefore less risky.

3.2.3. Relationship with Suppliers

For the ULB concept there are suppliers needed for the search system, deployment system, and retrieval system. A good relationship with suppliers allows for better communication and minimizes risks associated with delays and faults. For instance, for the search system, suppliers are needed for the following parts: the payload instruments (such as the hydrophone), communication instruments (such as Inmarsat for mother buoy and base station communications), materials for the structure, navigation system instruments, buoyancy instruments and propulsion systems.

3.2.4. Relationship with Customers

The primary customer market for the ULB project is **Search and Rescue**. Therefore, potential customers for this project are governmental and military institutions (e.g. Dutch Ministry of Defence), private search companies and emergency response teams specializing in search and rescue. Another potential customer are insurance companies. Most aircraft are insured, therefore the insurance company will partly cover the costs of the search and rescue mission of a crashed aircraft. Such companies would like to have some information about the cause of the crash (i.e. technical failure or human error).

Moreover, through changing the payload that is being deployed and retrieved by the airborne system, the ULB Project could also be adapted to other search and rescue operations. For example, inflatable boats could be deployed by the airborne system when a ship is sinking. Furthermore, the payload instruments on the submarine itself can be changed to adapt it to scientific missions. Secondary customer markets for the ULB Project are:

- **Defense and security;** The system has the potential to be used as anti-submarine warfare (i.e. to detect and track live submarine) and surface vessel detection. Thus, the military is a potential customer.
- **Environmental assessment;** Since the system has a large coverage area of the ocean, it can be used to monitor the ocean environment. Specific examples of ocean environment can include oceanography, marine mammal monitoring and tsunami monitoring. Potential customers include marine companies such as Fugro, marine biologists and environmental organizations such as the National Oceanic and Atmosphere Administration (NOAA).
- **Offshore energy;** The system has the potential to explore new offshore sights for the Oil & Gas industry and provide a communication platform for operational offshore sites. Potential customers are offshore companies such as Shell, British Petroleum and PEMEX.

3.2.5. Rivalry within the Industry

If an airplane crashes, the main goal is to locate it as fast as possible in order to find the flight data and cockpit voice recorders. As such, efforts are usually concentrated and there is not much rivalry. From the information stored in the flight data and cockpit voice recorders, knowledge is obtained which can be used to prevent similar future accidents. This is in the benefit of all involved parties. However, other companies and organizations are also designing similar systems which could be potentially implemented as a ULB finder system. Similar projects are the following:

- **Sonobuoy;** A Sonobuoy is a device that can detect and identify moving objects underwater. It accomplishes this through both passive and active detection. This concept was first used during the Cold War to detect (nuclear) submarines and stems from a company called Sonobuoy TechSystems [5].
- **SHARC;** This product is commonly referred to as a wave glider and is a project of Liquid Robotics. It harnesses wave energy and uses it to propel itself forward. It is currently being used to monitor and map the ocean [6].
- **REMUS6000;** This is an AUV which can operate at a depth of 6000 m. It makes use of sonar and was used for the search of the missing Air France flight AF447 [7]. [8]

3.2.6. Barriers of Exit

The barriers of exit are obstructions that hinder a business from exiting a market. It is important to analyze the existence of these barriers because they can determine whether a company should enter the market or not. Potential factors that can result in a barrier of exit are:

- **Investment in specialized equipment;** A local government requires a business to stay in the market, because its goods or services are considered to be for the benefit of the public. For example: assume that the ULB finder system receives subsidies from the Dutch ministry of defense (i.e. less expensive fees to use military bases as ground stations, etc.). They might require that the ULB project continues due to its functional purpose in retrieving lost aircraft even though operational profit is limited. This will likely be the case for this project.
- **High fixed cost;** For example, the investment in a new retrieval system that is capable of retrieving the search systems has a high fixed cost and can be a barrier to leave the market, as the ULB project should be sold at a price which covers the development costs. If the search and rescue market is too concentrated and difficult to establish, the secondary market options should be explored to cover the costs.

Sustainable Development Strategy

In the new global economy, sustainability has become a central factor in short term and long term success [9]. However in past decades, the environmental, economical and social activities have been disconnected from core strategy instead of focusing on their direct impact on business results [10]. Recent trends demonstrate that companies are actively implementing sustainability principles into their business strategy and capturing their value through indicators on growth and return on capital [10–13]. Therefore, in order for MARLIN to be competitive within the industry, a sustainable development strategy must be integrated into its business processes.

The first step in this process is implementing an active agenda that identifies and pursues value creating activity on sustainability, elaborated on in section 4.1. Once these sustainability initiatives are identified, the business processes should be integrated to support them as discussed in section 4.2. The final stage is capturing the value of sustainability initiatives demonstrated in section 4.3.

4.1. Active Agenda for Sustainability

Central to a sustainable development strategy are the concepts of knowledge-driven and dynamic processes aimed at creating value. The system has to be knowledge-driven such that all sustainability initiatives can be recognized. Thus, the entire workforce is required to improve the business towards sustainable development by utilizing the knowledge of each individual. Frontline workers observe the implications of the production which allows them to identify potential improvements to reduce waste. This indicates the crucial role of improving operations and supply-chain management processes [14].

Furthermore, a dynamic process is fundamental to the philosophy of sustainable development, which grows and evolves over time. Identifying and pursuing new sustainable initiatives for value creation is an ongoing process that is able to respond to changing requirements. Applying this methodology helps stimulate continuous improvements.

The last key factor of sustainable development is understanding value creation. In order to create value, it is important to define this term in a sustainable framework. Sustainable value encompasses environmental, economic and social aspects while considering the needs of all stakeholders [13]. Natural environment factors (i.e. environmental, economic and social) are conceptualized as stakeholders as they can affect or are affected by the business. McKinsey research published that the three ways sustainability can create value is through growth, return on capital and risk management [10, 11]. Specific examples of value creation levels are demonstrated in table 4.1 along with their significance in the ULB industry.

Table 4.1: Importance of value creation levers in the ULB industry.

Value creation level		Potential Value
<i>Growth</i>	Committing R&D resources to sustainable products.	3
	Managing portfolio to capture trends in sustainability.	1
	Leveraging sustainability to reach new customers or markets.	1
<i>Return on capital</i>	Achieving higher prices because of sustainable products.	2
	Reducing energy use in operations.	1
	Reducing waste from operations.	1
	Reducing water use in operations.	2
	Reducing emissions from operations.	1
	Managing impact of products throughout the value chain.	2
	Improving employee motivation related to sustainability activities.	2
<i>Risk management</i>	Mitigating operational risk related to climate change.	3
	Managing corporate reputation for sustainability.	1
	Responding to regulatory constraints or opportunities.	3

1 Significant value 2 Modest value 3 Little to no value

The values obtained in table 4.1 are given based on results from transportation industries [10] and applicability of initiatives that can be applied to the ULB Project. Significant values for levers represent easy to apply initiatives that create large values. This is evident in eliminating operational waste because a small reduction results in large value impact due to long lifetime duration of the product. Also, the search system should be retrieved from the water, leaving no man-made objects in the ocean. Another example is leveraging sustainability to reach new markets as missing aircraft only occur once every two years. The ULB Project presents a new sustainable solution to

challenges in marine environment allowing it to enter competitively into new markets such as defense & security, environmental assessment and offshore energy (for more information see chapter 3).

Modest values for levers represent initiatives that create moderate value. For example, the ULB Project can demand higher prices for search and rescue missions as it provides a sustainable solution compared to using ships. However, the entire ULB Project is being sold to a contractor and thus value creation is less than when selling multiple products. In addition, moderate value can be achieved through reducing waste in the value chain. This includes enhancing production processes (or ensuring sustainable partners for outsourcing production) to not compromise the environment or deplete the resources for future generations. The transportation of parts during assembly should be minimized. Lastly, disposal/recycling processes can be improved by ensuring disassemble capabilities of the product and reusable materials.

Lastly, sustainability initiatives that create little to no value often risk management related. For example, reducing the chance of defects and failures leads to a reduction of additional spare parts and maintenance operations. However, the sustainability value of these processes is low and thus have little value creation. Finally, committing R&D resources to sustainable product does not create value because the majority of the ULB Project is designed based on an off-the-shelf system.

4.2. Integration of Sustainability in Business Processes

A primary concern for sustainability initiatives is the lack of support received from the company. Therefore, integration of sustainability in business processes must see a switch in its mission & values and corporate culture; One way to do this is by introducing sustainability as a top-tier item on the CEO's agenda. This will rearrange the companies priorities and decision making processes. Hence, strategic planning should focus on long-term nature of sustainability and should reduce pressure of short-term earning. Furthermore, business units will be more engaged with implementing sustainability initiatives and a new organizational structure is created to support accountability of these initiatives. In addition, this new organizational structure should also focus on holding more employees accountable for sustainability [10].

Another barrier to integrating sustainability into business processes is a low employee engagement. Therefore, sustainability initiatives should be tied to incentives such that employees actively engage with these activities. Once activities have been identified, the company should be ready to mobilize resources to enable these initiatives. One more way to increase employee engagement is through raising awareness of these topics through improving internal communication processes. The communication processes can be improved by embedding sustainability data/initiatives in the communication chain with investors and employees (i.e. weekly emails) or through informal presentation implemented into the company schedules [10].

Lastly, marketing and external communications processes represents another barrier to sustainability initiatives. This is evident because it reduces the value captured by corporate reputation. An example to improve these processes is to publish posts about sustainability initiatives on the corporate web site, issuing sustainability reports and participating in sustainability rankings [10].

At MARLIN, sustainability has been introduced as a top priority in the chairwoman's agenda. This has resulted in factoring sustainability into important decisions for the ULB Project, as demonstrated in power source tradeoff (see section 7.7.3) and design tradeoffs in the midterm report. Additionally, a switch in accountability of the system engineer on sustainability initiatives (partially accountable to equally accountable as sustainability manager) has allowed better integration with technical roles. The switch in priorities has resulted in a higher employment engagement on sustainability initiatives. Furthermore, it has prompted to find innovative sustainable solutions for the design of the ULB Finder System; Specific examples are the fuel used for the retrieval balloon in section 9.5 and the ballast in the mother buoys as can be found in section 8.3.

4.3. Capturing Value of Sustainability Initiatives

Measuring value captures is fundamental to the sustainable business model (SBM) and it gives insight on impacts that sustainability initiatives have. It requires various departments within a business to collect and analyze the data. The metrics have to be measured regularly such that observations can be made over time on the effectiveness of sustainability initiatives. Furthermore, these metrics should be normalized [10, 13]; For example, the energy use per mass/volume/area is more useful than the total amount of energy. Indicators for sustainability initiatives can be found in table 4.2.

Table 4.2: Sustainability indicators.

Indicator	Parameter	Unit
Fuel used	Weight	[tons]
Material type used	Depletion of non-renewable resources	[kg of non-renewable resources]
Material amount used	Mass	[kg]
	Volume	[m ³]
Production process	Embodied energy	[MJ/m ³],[kg CO ₂ /m ³]
End-of-life assessment	Recycled content	[% of total mass]
	Reused content	[% of total mass]

Operations

This chapter concerns the operations of the ULB finder system. The search strategy is covered in section 5.1. Possible risks of operating in the ocean are defined in section 5.2. A full outline of the operations and logistics procedure for the ULB project is presented in section 5.3. The airborne system used for the operations is discussed in section 5.4.

5.1. Search Strategy

The coordinates and shape of the search area for the mission are assumed to be given by an external organization. However, the best way to cover this area is dependent on a variety of factors, which will be explored in this section.

5.1.1. Input Parameters

In order to come up with an efficient coverage path within the search area, a few assumptions are made to simplify the model.

i The search area is circular with a radius of 100km. [15]

Implications: The actual search path might be different, depending on the shape of the search area. In reality, the shape will vary per individual case and be more elliptical due to factors such as the intended flight path and deviations due to weather and current.

ii The ULB inside the aircraft is assumed to have a detection range of 2 km. [16]

Implications: As this assumption is based on a worst case scenario, the probability of finding the aircraft is higher. The ULB can transmit up to 3 or 4 km in good conditions with little to no noise.

iii The submarine is moving in a straight horizontal line.

Implications: This reduces the total distance of the coverage path as change in altitude is not taken into consideration. This assumption is further elaborated upon in section 5.2.2.

To confidently cover the search area, the search systems will cover the entire search area within 20 days. This is known as search phase 1. Each search system will look for the signal individually. Once a search system receives the ULB signal, an approximate location of the aircraft can be determined [17, 18]. Thus, the search area can be reduced - this is when the second phase of the search will start.

In the second phase, all search systems will be relocated to the smaller search area and a new search is started. However, only three submarines are required to accurately determine the aircraft's position via triangulation. The relocation of the submarines and coverage of the reduced search area will take 10 days - ensuring that the beacon signal is located within 30 days as required [15].

5.1.2. Coverage Path Planning

As will be explained in section 7.2, the submarines will keep track of their location using an Inertial Navigation System (INS). This usually consists of a combination of accelerometers and gyroscopes, of which the error in location measurement grows in time. Assuming that the likelihood of finding the aircraft is biggest in the center of the search area, a logical search pattern for this configuration would be to start in the center of the search area, and gradually spiral outwards. However, the image quality when travelling in a straight line is greater than when travelling along a curved path. Furthermore, the location and orientation of the submarines will be measured from rotational velocities and accelerations. The position and attitude errors are bigger in when travelling along curved path, compared to when travelling in a straight line [19]. Therefore, parallel tracks will be used to cover the search path.

The distance between each parallel track depends on the depth of the submarines and on the assumed error margin (based on sensor accuracy, drift off due to current etc.). The relationship between search height above the bottom of the ocean (h) and distance between parallel tracks (d_p) is shown in fig. 5.1. Assuming the pathways run in and out of the page, the distance between them must never lie outside the detection range of 2 km, depicted by the dotted line. By knowing the distance between parallel tracks, the total distance travelled to cover the search area can be calculated.

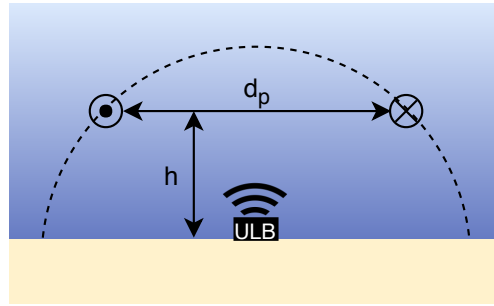


Figure 5.1: Relation between search height and distance between search paths, where X represents the search path going into the page (on the right) and the dot represents it coming out of the page.

In order to determine the optimal search height above the ocean floor, the total search distance and the number of submarines needed are calculated for a range of search heights. The results can be seen in fig. 5.2 and fig. 5.3, respectively. An error margin of 10% is taken for distance between the parallel paths, to account for possible deviations from the coverage path. Furthermore, the minimum distance between pathways always remains higher than 2 km, which is required to avoid acoustical interference [20].

In fig. 5.2, one can find the search height above the ocean floor plotted against the total distance travelled. The total distance is calculated as a function of the search area radius, ULB detection range, search height above ocean floor, error margin, submarine velocity and search mission duration. The general pattern shows an increase of distance travelled as search height increases. For a certain search height, a specific number of parallel paths are required, which are equally distributed along the diameter of the search area. These parallel paths gradually spread out as search height increases, which is why distance first decreases before suddenly increasing. At some point, the distance between them cannot increase any further (due to the ULB range) and one extra parallel path is added. This is depicted by the vertical jumps in the graph. The optimal search height can therefore be found at the bottom of the vertical jumps, where search height is maximum and total distance is minimum. The first vertical jump suggests a search height of 251 m, which is considered too low, taking into account ocean depth variation and the straight path of the submarines. The next optimal point gives a height of 574 m above the bottom of the ocean, depicted by the pink circle.

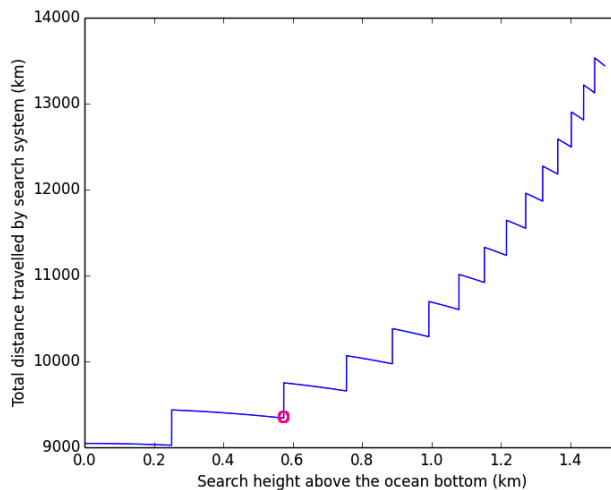


Figure 5.2: Graph showing search height above ocean floor vs distance travelled of a submarine. The ideal search height is circled in pink.

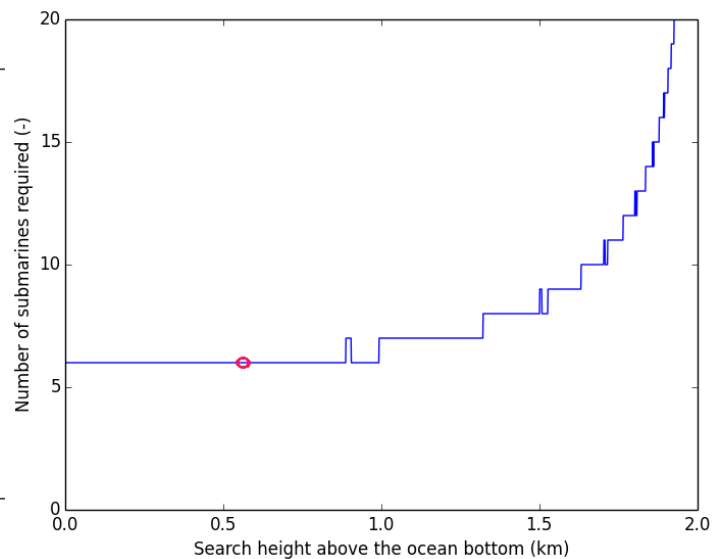


Figure 5.3: Graph showing the search height above the ocean floor versus number of submarines.

Figure 5.3 shows that the number of submarines required does not increase drastically until a search height of approximately 1.7 km is used. For certain heights, the number of submarines drops back down after a jump caused by the addition of an extra parallel search path. When the search paths proceed to spread further apart, total distance travelled decreases, resulting in a temporary decrease of the number of required submarines. From the graph, it can be seen that the optimum altitude to search for based on the submarines needed is just below 1 km, as only 6 submarines are required and the external pressure is less. However, this search height is sensitive to deviations, as slight changes in search height could result in requiring 7 submarines rather than 6.

Taking into account both the total distance travelled and number of submarines needed, it was decided to operate the search at a height of 500 meters. The reason for this is that it is close to the minimum search distance and has a large margin before an extra submarine is needed. Therefore, the total distance covered by the submarines is calculated to be 9369.61 km, which is rounded up to 9400 km to take into account possible deviations and other uncertainties. Using a submarine velocity of 1 m/s as decided in section 7.5, this leads to a necessity of 6 (5.42) submarines. For redundancy, an extra submarine could be manufactured and brought along on the mission, dependent on the total weight carried by the airborne vehicle and the budget of the mission.

To get from one parallel path to the other, the submarines will make the turns outside the search area, in order to avoid increased errors and to get back on track after possible deviations before re-entering the search area. A scaled illustration of the search path of half the search area is shown by fig. 5.4. The top half of the search pattern will be the exact same, mirrored with respect to the green line, which depicts the halfway line.

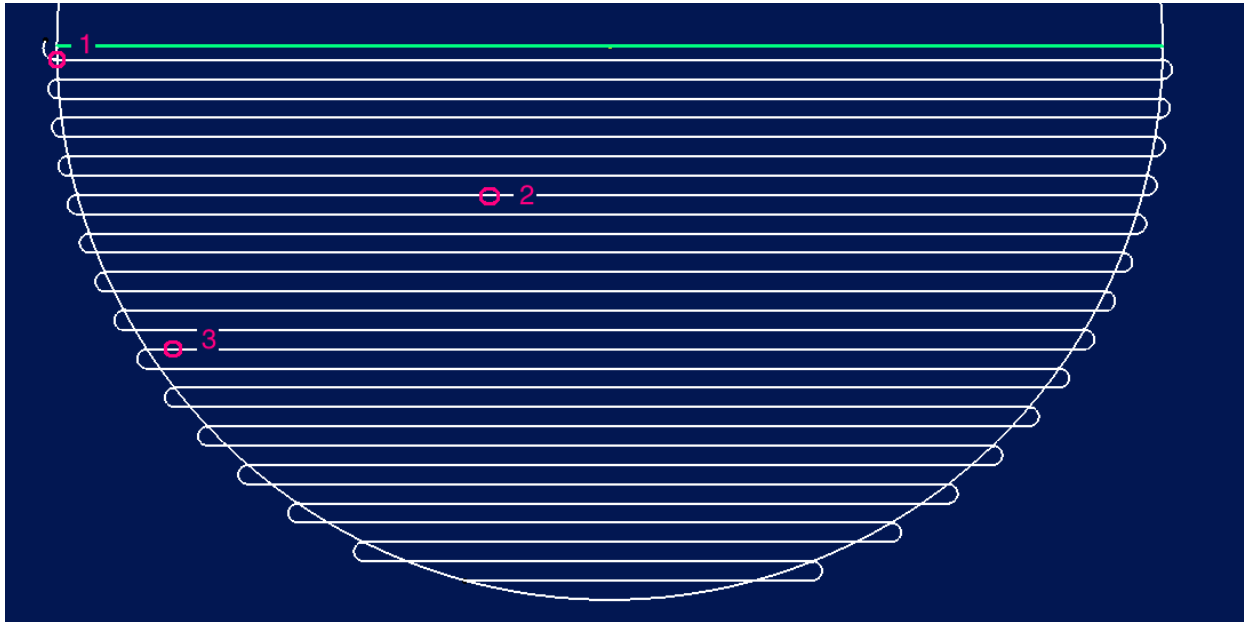


Figure 5.4: Illustration of the coverage path configuration of half the search area.

Three submarines and their corresponding mother buoys will be deployed in each half of the search area. One will be deployed close to the horizontal (green) middle line of the search area, shown by deployment location 1 on fig. 5.4. The second and third submarines and mother buoys will respectively be deployed 1561.15 km and 3122.30 km further along the coverage path. On the other (hidden) half of the search area, the deployment locations will be mirrored with respect to the vertical axis (after the search pattern been mirrored with respect to the horizontal middle line). This is to ensure the search system travels in opposite direction, which minimizes acoustic interference [20]. All submarines and mother buoys shall manoeuvre towards the ends of the search path at the top and bottom of the search area. This deployment configuration is done as to avoid any collision between search systems and to cover the search area in the given time of 20 days.

5.1.3. Code Verification

In order to verify the code used, a variety of tests could be used. A *limit test* is used to check the outcome of the program at limit values. The limit for the search height is 2 km, as shown by fig. 5.1. Above this height, the submarine would travel outside of the range of the ULB, considering it is located on the bottom of the ocean. When plotting distance between parallel paths against search height of the submarine, the maximum distance between paths should be 4 km, in case the error margin is reduced to zero (prior to this, a value of 10% was used). In fig. 5.5, one can see that this is indeed the case.

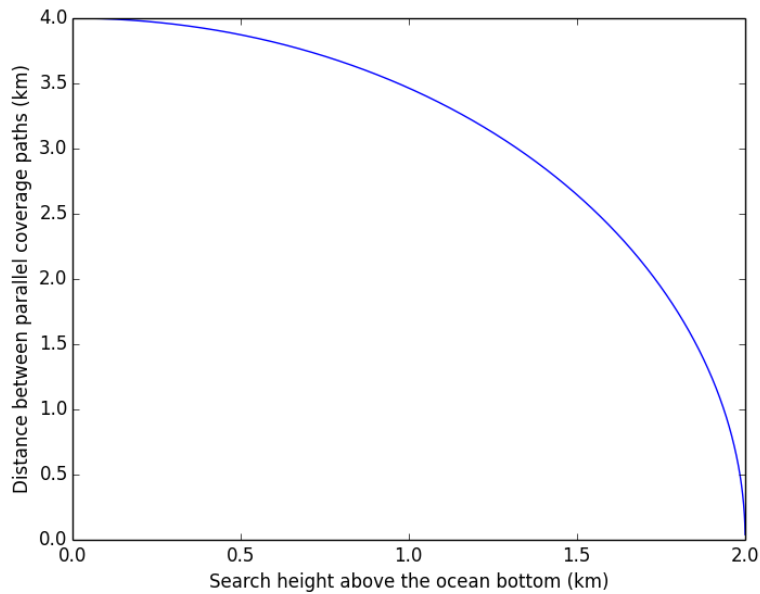


Figure 5.5: Graph used for code verification showing the search height vs distance between parallel covered paths.

Another test that can be used is the *consistency test*. As seen from fig. 5.2, there is no linear relationship between search height and distance between paths. However, variables from the Python program can be changed to analyze their effects on certain outcomes. The radius squared of the search area is proportional the number of parallel paths that must be taken. This in turn corresponds to the number of submarines needed. When halving the radius from 100 km to 50 km, the number of submarines reduces from 6 to 2. This is as expected, according to $0.5^2 * 6 = 1.25 * 6 = 2$ submarines. When the search area is doubled, a total of 22 submarines are needed, which is slightly lower than the expected 24 submarines. This is due to the fact that the relationship between the parameters depends on other factors as well. For a radius of 200 km, the distance between the search paths is likely to be close to maximum value and requiring another search path, which would then result in a 'vertical jump' on fig. 5.2 and an increased number of submarines required. The same pattern is seen for comparing a change in time frame to the number of submarines required. When doubling the time frame for the first phase to 40 days, 3 submarines are needed. This is half of the current number. However, for halving the time frame to 10 days, 11 submarines are needed. This again is likely to be due to the relationship shown in fig. 5.2.

5.2. Operational Risks

The exact configuration of the search mission will depend on various factors, such as the nature of the search area. Things such as current, weather, obstacles (islands, ships) and other (environmental) elements can either simplify or complicate the mission. There are too many possible variations in terms of location to take them all into account for the design process. Therefore, a variety of risks will be analyzed, to ensure they can be dealt with when similar scenarios occur.

5.2.1. Ocean Currents

Seawater has varying densities, that depend on factors including temperature and salinity. These differences in density lead to different pressures. Due to the fact that water flows towards points of lower pressure, currents are generated [21]. There are various types of current that can be found in the ocean, including sea/ocean surface currents, wind currents and tidal stream currents. Wind currents only appear close to shores as this is not applicable for the ULB finder system, this will be ignored. The surface current applies to floating objects and will thus be neglected for the submarines. The second and third type of current apply to a depth over 30 and 100 m respectively and are both considered applicable for a crashed aircraft at the bottom of the ocean. Surface currents can be observed and mapped using high frequency radar systems, but for analyzing deep sea currents, measuring probes can be used. Furthermore, mathematical models can be generated that among current, also forecast salinity, temperature and plankton concentrations. It is assumed that the mathematical model of the search area, with values at the depth of the submarine, will be provided by an external organization. Furthermore, it is assumed that this data is ready for use at the start of the search mission. This data will help to pick a rotation of the search area, as to align the coverage paths with the current to the most efficient extent possible [22]. For local currents, the submarine itself will detect the deviations from the current and adjust its trajectory accordingly.

Due to the relatively low velocity of the submarines, currents can highly influence the navigation of submarines. Tentative way points are created along the coverage path to guide the submarine. These tentative way points $[\mathbf{x}_i^j, \mathbf{x}_{i+1}^j]$ can be obtained from eq. (5.1). The simple predicted trajectory path neglects any external forces.

$$\mathbf{x}_{i+1}^j = \mathbf{x}_i^j + \mathbf{v}_i^j T_w \quad (5.1)$$

$$\mathbf{v}_i^j = v[\cos\theta_i^j, \sin\theta_i^j]^T \quad (5.2)$$

In the above equation, \mathbf{x}_i^j is the initial position of the submarine and \mathbf{v}_i^j is derived from eq. (5.2), which takes into account the heading direction of the submarine θ_i^j and its nominal velocity v . The direction of the submarine is assumed to be affected by current in the side way direction, as well as in the heading direction and against the heading direction. However, it is assumed to be at a stable search height, without being moved up or down by the current. The time planned to travel from one way point to the other is given by T_w .

A more realistic trajectory of a j^{th} submarine between two consecutive way points can be generated by comparing the actual submarine location \mathbf{x}_a^j to the simulated location \mathbf{x}_s^j , which might differ due to local current. A comparison will be made every T_m seconds. When, after this time, the two locations are not the same, a new way point must be simulated to guide the submarine back to the initial desired coverage path. The simulated way point can be calculated by the following equations.

$$\mathbf{x}_{s+1}^j = \mathbf{x}_s^j + \mathbf{v}_s^j T_m \quad (5.3)$$

$$\mathbf{v}_s^j = v_s[\cos\beta_s^j, \sin\beta_s^j]^T \quad (5.4)$$

In eq. (5.3), \mathbf{v}_s^j is based on the required simulated submarine speed v_s and can be derived from eq. (5.4). It takes into account the new desired heading direction of the submarine β_s^j . The local current causing the difference in actual submarine location and simulated submarine location can be calculated using eq. (5.5), in the form of a velocity field. This velocity field can then be added to the nominal speed v_s to generate an improved trajectory to the next simulated way point \mathbf{x}_{s+1}^j , which as a result should lead to the next tentative way point \mathbf{x}_{i+1}^j . In order to maintain a nominal velocity v of 1 m/s and cover the search area in the indicated time frame, the simulated submarine speed v_s might need to increase to make up for the path deviation. With a maximum speed of 2.5 m/s section 7.5, this is not an issue.

$$\mathbf{v}_c = \frac{\mathbf{x}_a^j - \mathbf{x}_s^j}{T_m} \quad (5.5)$$

The new heading direction to navigate to the next way point is given by eq. (5.6). In this equation, v_{sW_x} and v_{sW_y} represent the speed vector of the submarine.

$$\beta_s^j = \tan^{-1}\left(\frac{v_{sW_x}^j - v_{c_x}}{v_{sW_y}^j - v_{c_y}}\right) \quad (5.6)$$

$$\mathbf{v}_{sW}^j = v_s \frac{(\mathbf{x}_i - \mathbf{x}_s)}{\|\mathbf{x}_i - \mathbf{x}_s\|} \quad (5.7)$$

In fig. 5.6, the desired and most efficient coverage pathway is shown in green. The actual submarine locations and pathways are shown in red. The simulated pathway to get back onto the green track is shown in blue. The time to get from one tentative way point X_i^j to the next should always be T_w . The time between the red pathways is T_m , which is when location is determined. At the end of the mission, the sum of the travel time between way points should be equal to the sum of measurement intervals, equal to the mission duration of the first phase. It is assumed the mother buoy follows the submarine autonomously.

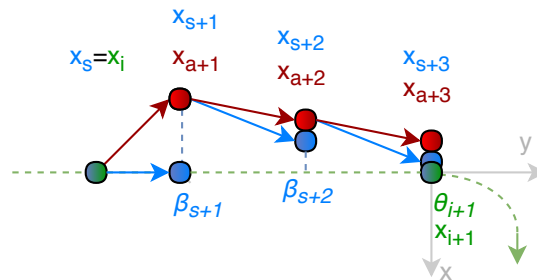


Figure 5.6: Diagram of the planned, simulated and actual pathway of the submarine.

To verify assumptions made, real values for the current could be used to calculate the deviation from the path. Since a maximum error of 10% was chosen for the distance between parallel paths, the submarine is allowed to deviate up to 0.19363 km perpendicular to its direction of motion. Deep sea current was found to flow at a speed of a few centimeters per second [23]. For a direction of current 90° to the submarine motion and a velocity of 0.05 m/s, a total distance of 3.872 km is covered by the submarine before it reaches the limit and skips part of the search area. This would take the submarine 1.08 hour. Using a measuring time T_m , as discussed in section 5.2.1, that is lower than 1.08 hour will result in the submarine staying sufficiently close to the pathway. Considering the submarine is continuously detecting and processing its location, T_m can indeed be much smaller. Therefore, the margin of 10% is considered a verified assumption.

5.2.2. Depth Variation

The ocean floor can be split up into continental margin and deep sea floor. Deep sea floors generally have a low gradient (approximately 0.001°). However, sea mounts exist that can exceed 1 km in height. Nevertheless, these sea mounts can be mapped using various different techniques, including sonar techniques and buoy/satellite altimeters. In order to deal with these obstacles, one solution would be to make the submarine search further from the bottom of the ocean. Travelling at a height of 1 km would result in a search distance of 10689.79 km and would only require one extra submarine, as shown in fig. 5.3. However, a search height of 500 m is maintained whenever geographically possible, to minimize distance travelled and consequently leave more search time for relocation and the second search phase. If the submarine enters a unmapped area, it will increase its search height.

Continental margin consists of continental shelf, continental slope and continental rise. These, on average, have 0.1°, 4° and 1° gradients respectively. For a maximum unidirectional distance of 200 km, this could be problematic. However, the parts with gradients that high usually only occur over a small distance and close to coast. This can therefore quite easily be mapped and accounted for [24].

5.2.3. Obstacles in the Ocean

Obstacles along the coverage path might be present and might or might not be predictable. When the search area contains various islands, a terrain map can be used to adjust the coverage path accordingly. It is assumed this can be done prior to the deployment of the search system, where the search system is programmed to follow the adjusted coverage path. Potentially shallow bits should therefore not create any hazard.

A more dynamic risk of the system is that, especially in water close to land, the search system might come across obstacles such as ships. In deep seas at depths of 4500 m, this is unlikely to be an issue, though in aforementioned environments, one should foresee these issues and prevent them whenever possible. However, with a speed of 1 m/s, any collision is unlikely to create any damage to either the search system or the object it impacted with. An impact might displace the search system, but due to the navigational devices, the search system can easily get back on track. This topic is further elaborated upon in section 7.2.

5.2.4. Deep Sea Search

At the beginning of the project, a deep sea search was seen as a problem in terms of getting the search system close to the bottom of the ocean. However, it has been found that the time for the submarine to go get to the maximum depth of 4500 m is 1148 s and is therefore not a significant problem in terms of search operation. For this reason, this risk is not analyzed to any further extent. Search in deep sea might in fact be advantageous, as it is likely to decrease the chance of coming across obstacles.

5.3. Operations and Logistic Concept Description

This section addresses the operations and logistics of the entire ULB Project. A flow chart of the operational and logistic procedure is given in section 5.3.1. Furthermore, section 5.3.2 discusses the corporation with the military.

5.3.1. Operations and Logistics Concept Diagram

The diagram in this section outlines the required actions to be executed to operate the ULB finder system. The diagram also includes actions that need to be taken by ground support. This is presented in section 5.3.1.

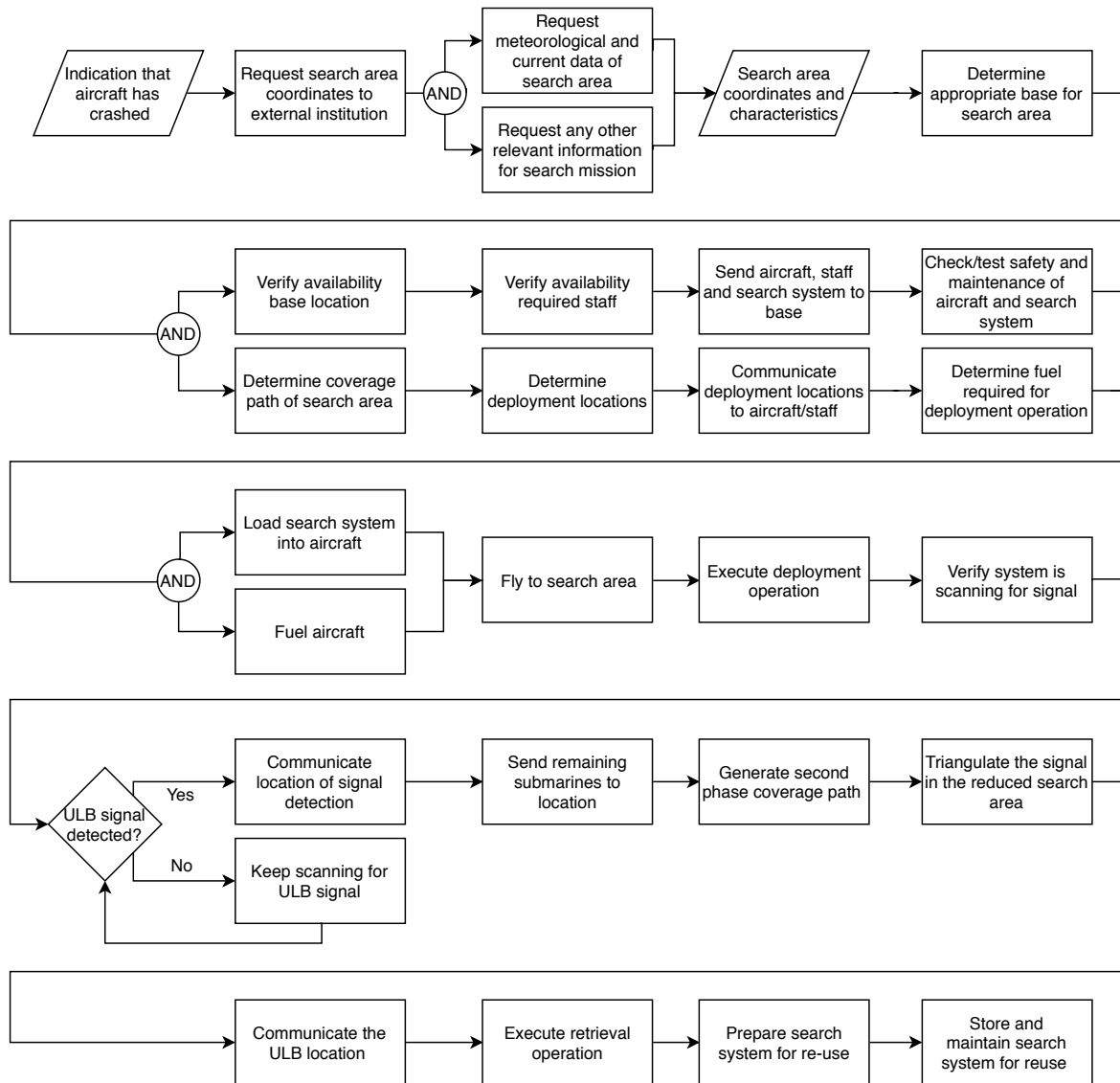


Figure 5.7: Operations and logistics flow diagram of the ULB finder system.

5.3.2. Military Corporation

The aircraft chosen for the deployment and retrieval of the submarines and mother buoys is the Airbus A400M. This is a military cargo aircraft and is widely used for transportation of paratroops or cargo like heavy vehicles. It is currently only used by the German, French, Spanish, British, Turkish and Malaysian air force [25]. The limited locations of the Airbus A400 has resulted in the ULB Finder System being designed such that it is compatible with the C-130 Hercules. Since the aircraft that is being designed for the Airbus A400, the cruise speed is 781 km/h with a range of 8900 km as stated in table 5.1. Thus, it will be able to reach the search area within the 48 hours, as required.

Considering Germany and France own multiple Airbus A400's, both of their militaries are identified as appropriate partners for testing the mechanisms and possibly the full operation. The french military is especially applicable as Air France has a history to missing aircraft operations due to Flight 447. Other potential partners are the Royal Netherlands Airforce as they own several C-130's and have provided information on attachment points of their aircraft for the deployment and retrieval system.

Military aircraft are mostly stationed at their respective bases. This significantly increases the chance of easy access to an aircraft, rather than when using aircraft that are stationed across the globe. Furthermore, the military is generally involved when aircraft have crashed, as an attempt to rescue but also for search missions [26].

5.4. Airborne System for Operations

This section covers the airborne system of the ULB finder system. In section 5.4.1, the characteristics of the aircraft will be elaborated on and section 5.4.2 will cover the system integration of the retrieval and deployment systems into the cargo bay of the aircraft.

5.4.1. Aircraft Characteristics

The characteristics of the A400M are given in table 5.1. The A400M will be used as reference aircraft for the ULB system operations and design.

Table 5.1: Airbus A400M characteristics.

	Airbus A400M [25] [27] [28]	
Speed	Cruise	Stall
	781 km/h	203.7 km/h (110 kt)
Range	Maximum	Ferry ¹
	8900 km	3298 km
Cargo volume	340 m ³	
Payload capacity	Maximum	Airdrop
	37000 kg	25000 kg
Fuel consumption	12000 kg/h	
Power plant	8200 kW (4x)	

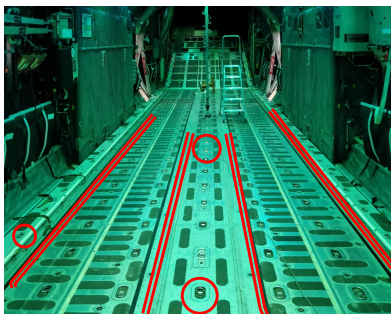
5.4.2. Deployment and Retrieval System Integration

This section covers the integration of the deployment and retrieval system into the aircraft. The cargo volume of the A400M is 340 m³ with a payload capacity for airdrop of 25000 kg [25]. To support diverse payload, there are a lot of mounting points available, therefore integration of the retrieval system should not be a problem. As for the deployment, the submarines and mother buoys will be dropped in free fall from the rear cargo door. Most of the airdrops done from military aircraft do so by sliding the payload along a platform on rails. However, mounting the search system on a platform, and dropping these out of the airplane, will result in a platform in the ocean which is sustainable. The submarines and buoys could roll over the rails without the platform or a treadmill or slide could be mounted in the cargo bay over which they will be dropped. The 12 submarines and mother buoys will fit inside the cargo hold, as well as the winch and control surface needed for retrieval. To reel the search systems in, a crane is mounted inside the cargo bay of the A400M, which can be used for this purpose.

For the operation of the aircraft, three to four crew members are needed [27]. For the deployment and retrieval system, at least two crew members are needed. The A400M has a computed air release point (CARP) which is linked to the automated release system which accurately determines the release point for delivery and includes wind effects [25].

The military airbase in Eindhoven was visited to check whether it is possible for the ULB system to be integrated in a C-130 Hercules, as the Dutch military does not own a A400M. Maj. Brian Zoll provided information regarding the C-130 Hercules as he flown it many times. There are many connection points to secure the deployment system, retrieval system and search systems as can be seen in section 5.4.2. The air drop does need an additional releasing structure to drop the search systems as they will not be connected to a platform or pallet when dropping. A slide or structure similar to what they have at bowling alleys should suffice. A minimum of 5 people can operate the aircraft, this will be a pilot, co-pilot, navigator and two load masters. The load masters are the persons responsible for the cargo and the location of the cargo inside the cargo hold. There is no crane present inside the cargo hold of the C-130 Hercules, this should be integrated just like the winch inside the bay.

It was concluded that the integration of the systems into the C-130 is possible. Furthermore, it was also concluded that system can easily be integrated into A400 as it is a newer version of the cargo aircraft. In the C-130, there is enough space for the 12 search systems, a winch, the control surface and the crane. However, the search systems might be piled up in a structure and need to be manually helped to be dropped from the aircraft by the load masters.



(a) Cargo bay with attachment points along the fuselage length (attachment points shown in red). (b) Back door of the cargo bay of the inspected military cargo aircraft.

Figure 5.8: Cargo bay of the C-130 Hercules used by the Royal Dutch Air Force.

¹The maximum distance that an aircraft can fly without refueling and arrive at the destination with a specified reserve of fuel.

Deployment System

In this chapter, the deployment system from the ULB Project is realized. An overview of the design process can be found in section 6.1. The simulation of the trajectory and its results are described in section 6.2 and section 6.3 respectively. Moreover, the verification of the simulation directly follows the results in section 6.3. Finally validation proposals for the simulation are discussed in section 6.4.

6.1. Overview of the Design Process for the Deployment System

A primary concern for the deployment system is the force upon impact. Therefore, investigating ways to reduce the impact force is of paramount importance. The impact process is complicated by nature due to the water tension and interaction of individual water particles. It has been established that the most effective way to reduce the impact force is by decreasing the impact velocity and impact area. Thus, the aim of this analysis is to size control surfaces of the submarine/mother buoy to help control their pitch. This will ensure that the submarine/mother buoy can enter the water with the minimum impact area - nose first. The impact velocity can be controlled through changing the altitude of the deployment.

The proposed method is to model the trajectory of the submarine assuming unsteady, non-straight and symmetric flight. Aerodynamic properties will be calculated based on the geometry of the submarine with control surfaces and its orientation. Then, a forward integration scheme will be used to discretize the equations of motions and obtain the trajectory. The process is demonstrated in fig. 6.1.

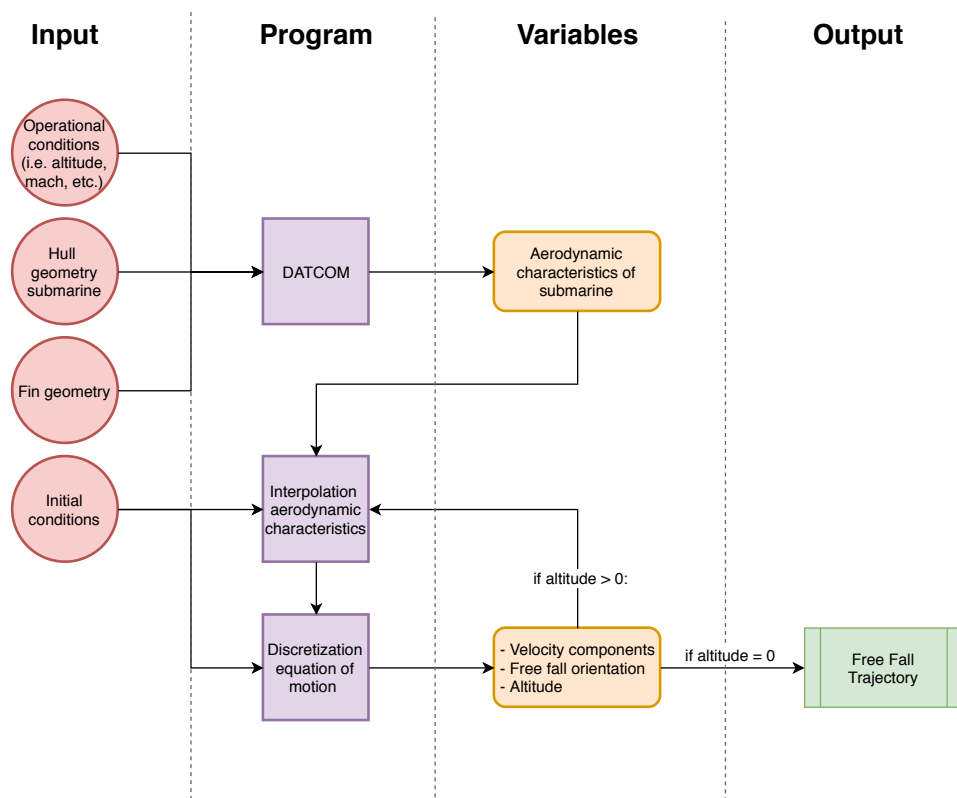


Figure 6.1: Flowchart of the free fall model.

6.2. Simulation of the Trajectory

This section encompasses the entire simulation process of the trajectory. In order to describe the flight path of the submarine or mother buoy¹, a 3DOF model is constructed. The following assumptions are applied to simplify the equations of motions:

¹From now on, the term search system will be used analogously to indicate the object experiencing free fall (i.e. submarine or mother buoy).

i **The Earth is considered to be flat, non-rotating and spherical.**

Implications: A flat earth implies that the radius of the curvature becomes infinity. Thus, the kinematic equations of rotational motion are reduced because the rate change in both latitude and longitude is equal to 0. A non-rotating earth implies that the Coriolis and centrifugal forces do not affect the translation motion. Hence, the dynamic equations are simplified. A spherical earth assumes that earth is a perfect sphere, such that there are no gravity perturbations.

ii **Constant gravity.**

Implications: Altitude variations of gravity are neglected in the model.

iii **The search system is a rigid body.**

Implications: Body parts of the submarine do not move. Therefore, the fins cannot extend or retract.

iv **The search system has a constant mass.**

Implications: The mass is constant over time; Thus, the center of gravity remains in the same position.

v **The search system is non-rotating.**

Implications: The search system does not experience gyroscopic forces.

vi **The search system has a plane of symmetry in X_bZ_b .**

Implications: Mass asymmetries can be neglected ($I_{xy} = I_{yz} = 0$).

vii **Constant wind.**

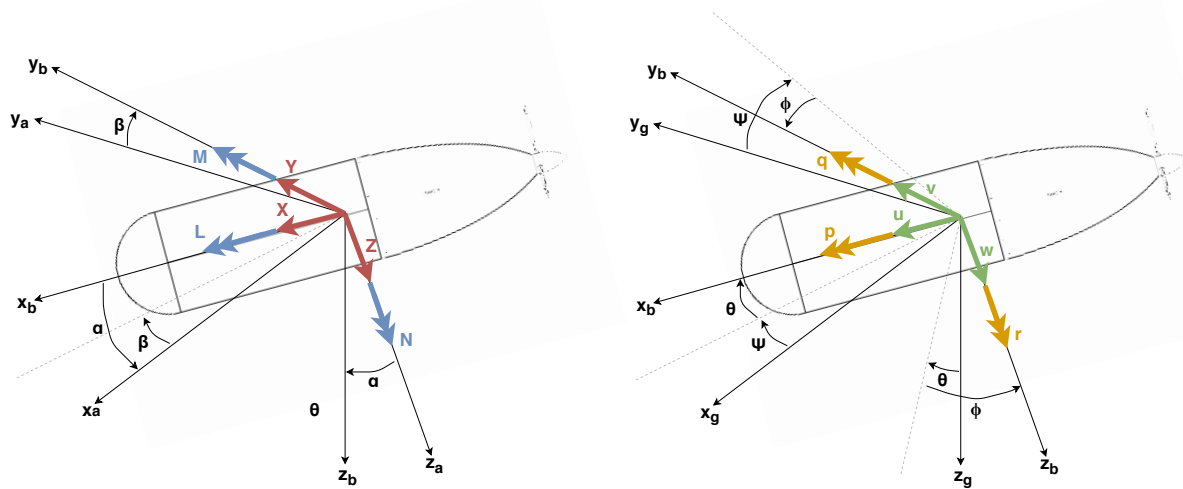
Implications: Turbulence in the search system velocities are neglected.

viii **The non-uniform airflow in the wake of the aircraft is negligible.**

Implications: The trajectory of the search system is not influenced by the aircraft. The justification behind this assumption is that aerodynamic characteristics are independent of the search system after 1-2 seconds of the release.

To formulate the equations of motion, the following coordinate systems are defined. The body-fixed reference frame ($OX_bY_bZ_b$) with origin at the center of gravity. X_b goes through the nose of the search system, the Y_b points to the right and Z_b points downward with an inclination of α to make a right hand coordinate system. The aerodynamic reference frame ($OX_aY_aZ_a$) given with respect to the free stream velocity, including the slide slip of the aircraft out of its symmetry plane. Lastly, the vehicle carried normal earth reference frame ($OX_gY_gZ_g$) is centered around the center of gravity of the aircraft. The X_gY_g plane is tangent to Earth's surface. Thus, Z_g is perpendicular to Earth's surface and pointing downward, X_g is pointing North and Y_g to the left.

The transformation between these coordinate-systems can be seen in fig. 6.2. The vehicle carried normal earth reference frame is related to the body fixed reference frame via the pitch angle (θ), the roll angle (ϕ) and yaw angle (ψ). The body fixed reference frame and the aerodynamic reference frame are related via the angle of attack (α) and the angle of side slip (β) [29, 30].



(a) Free body diagram of the search system during free fall.

(b) Kinetic diagram of the search system during free fall.

Figure 6.2: Equation of motion diagrams of the search system during free fall.

The forces acting on the search system during the free fall are shown in fig. 6.2a. X , Y and Z represent the aerodynamic force vector in the body fixed reference frame as there is no propulsion force vector from the search system. Similarly, L , M and N only represent the aerodynamic moment vector in the body fixed reference frame. Applying Newton's second law of motion, the force and moment equations can be determined and are given by eq. (6.1) [29].

$$\begin{aligned}\Sigma F_x: \quad m(\dot{u} + qw - rv) &= -mg \sin(\theta) + X \\ \Sigma F_y: \quad m(\dot{v} + ru - pw) &= mg \sin(\phi) \cos(\theta) + Y \\ \Sigma F_z: \quad m(\dot{w} + pv - qu) &= mg \cos(\phi) \cos(\theta) + Z\end{aligned}\quad (6.1)$$

$$\begin{aligned}\Sigma M_x: \quad I_{xx}\dot{p} + (I_{zz} - I_{yy})qr - I_{xz}(\dot{r} + pq) &= L \\ \Sigma M_y: \quad I_{yy}\dot{q} + (I_{xx} - I_{zz})rp + I_{xz}(p^2 - r^2) &= M \\ \Sigma M_z: \quad I_{zz}\dot{r} + (I_{yy} - I_{xx})pq - I_{xz}(\dot{p} - rq) &= N\end{aligned}\quad (6.2)$$

The above equations are a set of non-linear differential equations that can be solved for $p(t)$, $q(t)$ and $r(t)$ based on initial conditions. However, the objective of this analysis is to determine the orientation of the search system upon impact. Thus, the pitch angle, yaw angle and roll angle need to be determined. These angles can be determined through the kinematic equations of rotational motion, given by eq. (6.3) [29].

$$\begin{aligned}\Sigma \dot{\phi}: \quad \dot{\phi} &= p + \sin(\phi) \tan(\theta) q + \cos(\phi) \tan(\theta) r \\ \Sigma \dot{\theta}: \quad \dot{\theta} &= \cos(\phi) q - \sin(\phi) r \\ \Sigma \dot{\psi}: \quad \dot{\psi} &= \frac{\sin(\phi)}{\cos(\theta)} r + \frac{\cos(\phi)}{\cos(\theta)} p\end{aligned}\quad (6.3)$$

The equation of motions are simplified by analyzing the free fall of the search system about unsteady, non-straight and symmetric flight conditions. Unsteady flight means that the velocity is changing ($\dot{V} \neq 0$). Non-straight flight means that the flight path angle is changing ($\dot{\gamma} \neq 0$). Symmetric flight means that there is no roll angle and the turn rate is zero (thus, $\beta = 0$). The implications of these flight conditions are given in eq. (6.4).

$$\begin{aligned}u \neq 0 \quad \dot{u} \neq 0 \quad p = 0 \quad \dot{p} = 0 \\ v = 0 \quad \dot{v} = 0 \quad q \neq 0 \quad \dot{q} \neq 0 \\ w \neq 0 \quad \dot{w} \neq 0 \quad r = 0 \quad \dot{r} = 0 \\ \phi = 0 \quad \dot{\phi} = 0 \quad X \neq 0 \quad \dot{X} \neq 0 \\ \theta \neq 0 \quad \dot{\theta} \neq 0 \quad Y = 0 \quad \dot{Y} = 0 \\ \psi = 0 \quad \dot{\psi} = 0 \quad Z \neq 0 \quad \dot{Z} \neq 0\end{aligned}\quad (6.4)$$

Therefore, the equations of motions are reduced to eq. (6.5).

$$\begin{aligned}\Sigma F_x: \quad m(\dot{u} + qw) &= -mg \sin(\theta) + X \\ \Sigma F_z: \quad m(\dot{w} - qu) &= mg \cos(\theta) + Z \\ \Sigma M_y: \quad I_{yy}\dot{q} &= M \\ \Sigma \theta: \quad \dot{\theta} &= q\end{aligned}\quad (6.5)$$

In order to analyze the motion, the above equations are turned into a set of non-linear differential equations. First, X and Y are given in terms of the lift and drag by applying the transformation from the aerodynamic reference to the body fixed reference frame ($X = -D \cos(\alpha) + L \sin(\alpha)$ and $Z = -D \sin(\alpha) - L \cos(\alpha)$). In addition, the rate of change of the angle of attack is defined as the fraction of the vertical velocity rate over the total velocity ($\frac{\dot{w}}{V}$).

The non-linear differential equations for unsteady, non-straight and symmetric flight are given in eq. (6.6).

$$\begin{aligned}\dot{u} &= qw - g \sin(\theta) - \frac{D \cos(\alpha) - L \cos(\alpha)}{m} \\ \dot{w} &= -qu + g \cos(\theta) + \frac{-D \sin(\alpha) - L \cos(\alpha)}{m} \\ \dot{q} &= \frac{M}{I_{yy}} \\ \dot{\theta} &= q \\ \dot{\alpha} &= \frac{\dot{w}}{V}\end{aligned}\quad (6.6)$$

Furthermore, it is important to notice that the drag and lift change with the geometry of the search system and its free-fall conditions (i.e. angle of attack, altitude and velocity). In order to determine these values, the United States Airforce Stability and Control Digital DATCOM [31] is used.

The input for the DATCOM program is the flight case that is being analyzed. A flight case consists of a case identification, flight conditions, body geometry and wing geometries. In the flight conditions, a range of mach numbers, angle of attacks and altitudes can be specified. The output for the DATCOM program are the aerodynamic characteristics and the dynamic derivatives for all possible combinations of flight conditions [31–34].

The non-linear differential equations are solved by applying a 4th order Runge-Kutta forward integration scheme. The total accumulation error is on the order of $O(h^4)$ and its local truncation error is in the order of $O(h^5)$. To demonstrate the implementation of the 4th order Runge-Kutta discretization as applied to the equations of motion during free fall, the horizontal velocity u is used. Equation (6.7) shows the initial value condition.

$$\dot{u} = f(w, \alpha, q, \theta) \quad \text{where} \quad u(t_0) = u_0 \quad (6.7)$$

The discretization of the horizontal velocity is given in eq. (6.8).

$$\begin{aligned} u_{n+1} &= u_n + \frac{1}{6}(k_1 + 2k_2 + 2k_3 + k_4) \\ t_{n+1} &= t_n + dt \end{aligned} \quad (6.8)$$

The estimated slope of the horizontal velocity is presented in eq. (6.9). It is dependent multiple variables (w_n , α_n , q_n and θ_n) and their respective estimated slopes at the current time value. The estimates slopes of the variables are given by the terms l , n , m and n respectively.

$$\begin{aligned} k_1 &= dt \cdot f(w_n, \alpha_n, q_n, \theta_n) \\ k_2 &= dt \cdot f\left(w_n + \frac{l_1}{2}, \alpha_n + \frac{m_1}{2}, q_n + \frac{n_1}{2}, \theta_n + \frac{o_1}{2}\right) \\ k_3 &= dt \cdot f\left(w_n + \frac{l_2}{2}, \alpha_n + \frac{m_2}{2}, q_n + \frac{n_2}{2}, \theta_n + \frac{o_2}{2}\right) \\ k_4 &= dt \cdot f\left(w_n + l_3, \alpha_n + m_3, q_n + n_3, \theta_n + o_3\right) \end{aligned} \quad (6.9)$$

Another aspect that the discretization needs to consider is that, due to its small step size, the flight conditions from the discretization will not match the flight conditions input for the DATCOM. Therefore, the aerodynamic characteristics must be determined through interpolation.

The interpolation is done based on a hierarchical clustering dendrogram. This diagram demonstrates how close the flight conditions during the discretization are with respect to the nearest input flight conditions for the DATCOM. Each of these flight conditions have corresponding aerodynamic characteristics.

The interpolation is given by eq. (6.10). The aerodynamic characteristics for the flight condition at the current time discretization ($c_{L_{discretized}}$) is the sum of aerodynamic characteristics at the nearest input flight condition ($c_{L_{fc}}$) multiplied by their relative closeness (RC_{fc}) to the data point. The term N refers to the amount of nearest input flight conditions there are from DATCOM.

$$c_{L_{discretized}} = \sum_{fc=0}^N c_{L_{fc}} (RC_{fc}) \quad (6.10)$$

The relative closeness is determined by $RC_{fc} = (1 - r_h)(1 - r_M)(1 - r_\alpha)$. The terms r_h , r_M and r_α represent the the ratio of how close the discretized altitude, Mach and angle of attack are with respect to their nearest input flight condition data point. An example of this is illustrated in fig. 6.3 and an example calculation is given by eq. (6.11). In fig. 6.3, the green boxes represent the discretized flight conditions. The yellow boxes represent the nearest input flight conditions for the DATCOM.

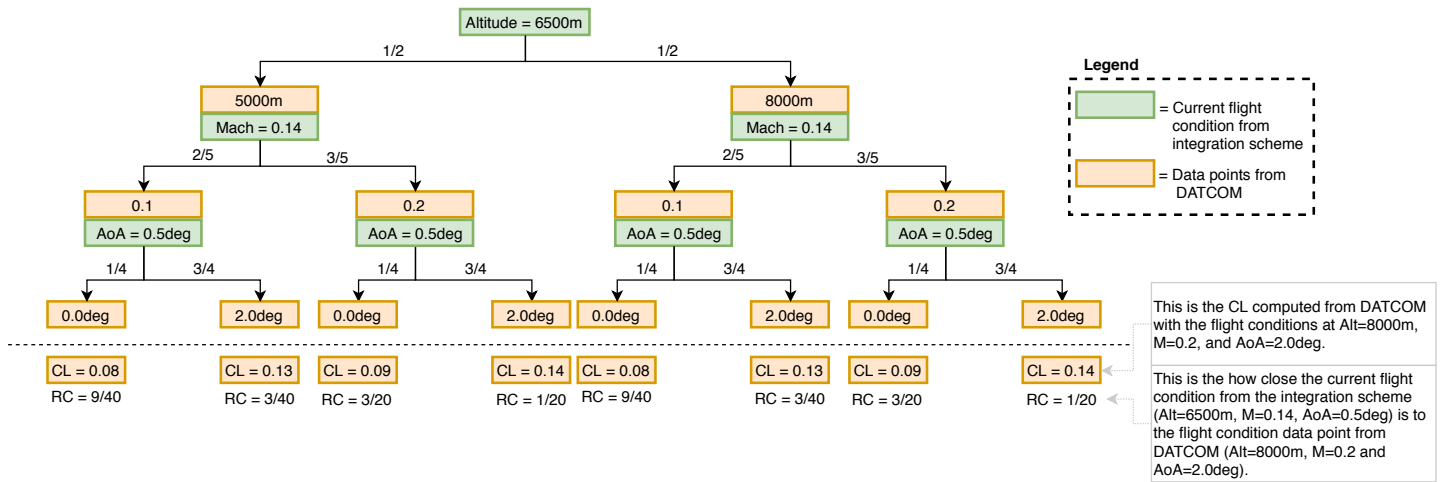


Figure 6.3: Hierarchical clustering dendrogram comparing discretized flight conditions to input flight conditions for the DATCOM.

$$C_{L_{discretized}} = 2 \left[(0.08) \left(\frac{9}{40} \right) + (0.13) \left(\frac{3}{40} \right) + (0.09) \left(\frac{3}{20} \right) + (0.14) \left(\frac{1}{20} \right) \right] = 0.0965 \quad (6.11)$$

By applying the Runge-Kutta forward integration scheme and the interpolation procedure for the aerodynamic characteristics, the free fall of the search system can be modelled until impact. The outputs of the simulation are the velocity vector, position vector and orientation of the search system for the duration of the free fall.

6.3. Results and Verification of the Simulation

This section presents the finalized fin geometry that produces the desired trajectory. These results are presented in section 6.3.1. Following this, in section 6.3.2, the simulation itself is verified.

6.3.1. Results of the Simulation

The main output of the deployment section is the sizing of the fins, namely the two lateral fins. To do this, the geometry of the fins were changed such that the impact angle - calculated by the simulation - is close to 90 degrees. It was assumed that the search system will be dropped at an altitude between 300 feet (91.4meters) and 600 feet (182.8 meters) as this is currently the deployment altitude of the C-130. The dimension of the search system case was based on the final design presented in section 7.8; the total length is 2.5 m and the diameter is 0.5 m. The final results for fin geometry, trajectory and orientation are demonstrated in fig. 6.4 fig. 6.5 and fig. 6.6 respectively.

Each of the horizontal fins has a span of 0.4 meters, a root chord of 0.25 meters and a tip chord of 0.2 meters. The distance between the fins is 0.3 meters which means that each fin enters the spherical cap by 0.1 meters (refer to fig. 6.4).

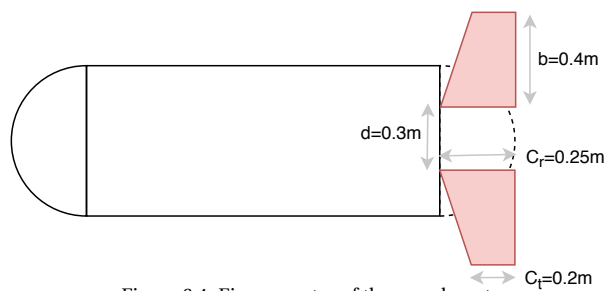
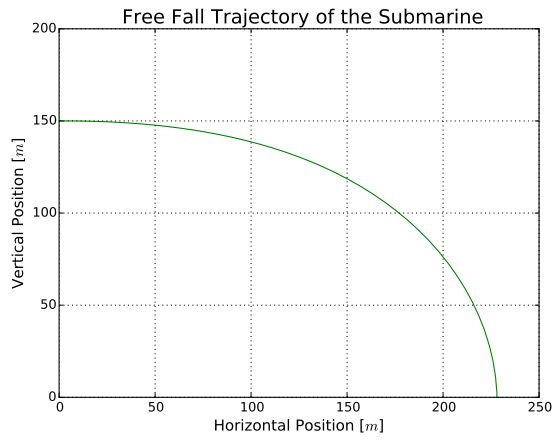
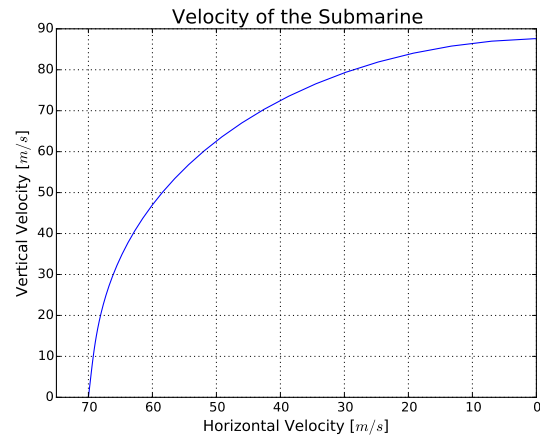


Figure 6.4: Fin geometry of the search system.

Upon impact the search system only experiences a vertical velocity. Thus, the flight path angle is -90 degrees upon impact. Originally, it was proposed to have a pitch angle of -90 degrees upon impact. However, from the results of the simulation, this is actually undesirable as there will be a pitching moment during impact. Assume that the search system hits the water nose down (pitch angle = -90 degrees) and still has a pitching moment; The tail of the search system would continue the pitching moment resulting in a whiplash effect and exposing its backside. Therefore, the final (desired) orientation results yield a pitch angle of -71.4 degrees, an angle of attack of 19.1 degrees and a flight path angle of -90.0 degrees.

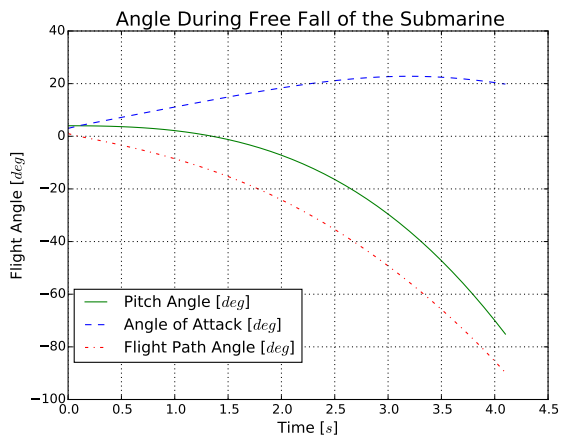


(a) Free fall trajectory of the search system.

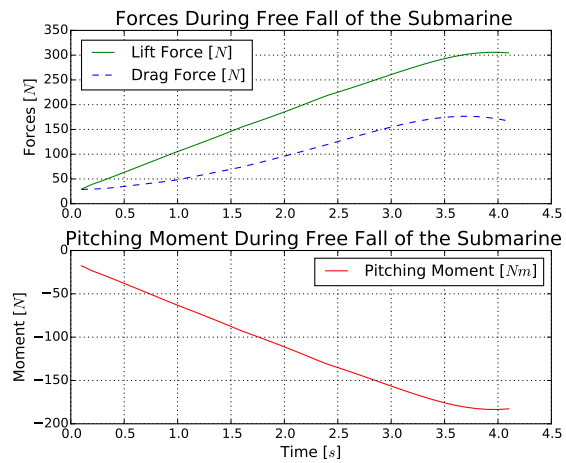


(b) Free fall velocity of the search system.

Figure 6.5: Free fall trajectory and velocity of the search system with time vector travelling to the right.



(a) Angle during free fall of the search system.



(b) Forces and moments during free fall of the search system.

Figure 6.6: Equation of motion diagrams of the search system during free fall.

6.3.2. Verification of Free Fall Model

This subsection discusses the verification procedure for the free fall model. First, continuity tests are performed to see that known parameters behave how they are expected to behave. Next, the aerodynamic characteristics are compared to those of a published simulation for missile trajectory. Finally, simplified model tests are performed.

Continuity Testing

Continuity tests were performed in the program through printing values and observing that they conform to the expected value. Among the values checked are that the relative closeness in the interpolation of the aerodynamic characteristics. It is expected that the sum of all of the relative is always 1. This can be seen from fig. 6.3 in section 6.2 where $2(9/40 + 4/40 + 3/20 + 1/20) = 1$. An example test is demonstrated in table 6.1, where individual flight conditions are checked. As can be seen, the total relative closeness is always equal to 1.

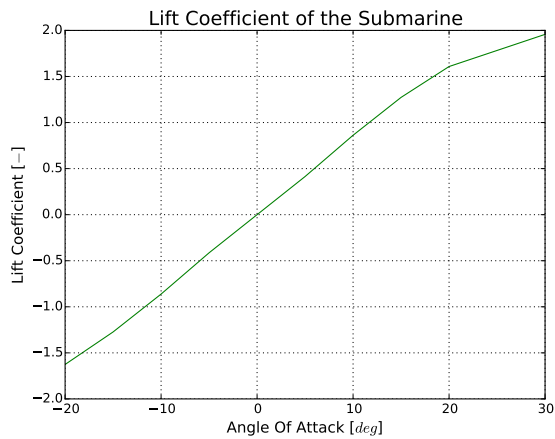
Table 6.1: Total relative closeness continuity test.

Input flight conditions for digital DATCOM					
Altitude Case [m]	0	500	1000	1500	2000
Mach Case [-]	0.1	0.2	0.3	0.4	0.5
Angle of Attack Case [deg]	-2.0	0.0	2.0	4.0	8.0
Continuity test flight conditions					
Altitude [m]	100.0	220.0	1684.1	934.7	452.0
Mach [-]	0.15	0.32	0.27	0.49	0.02
Angle of Attack [deg]	-2.00	4.30	3.81	7.22	0.06
Total Relative Closeness [-]	1.0	1.0	1.0	1.0	1.0

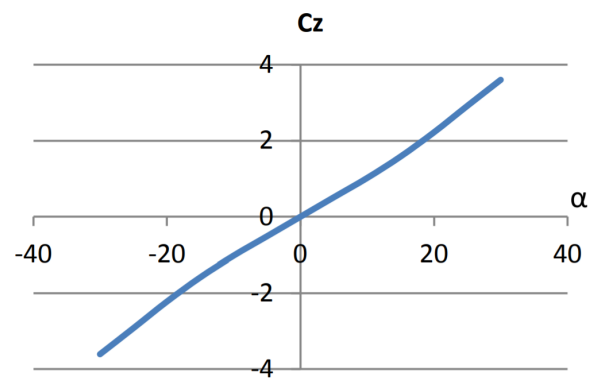
Comparison of Aerodynamic Characteristics with Reference Simulation

In order to check that the input case was defined correctly, the aerodynamic characteristics are compared with a reference simulation [30]. This reference simulation models the trajectory of a missile using a 6DOF system. Although, the paper does not mention the dimensions of its fins its body geometry is similar to that of the search system; the length is 2.3 meters and the diameter is 0.273m. The general shapes of the aerodynamic characteristics was compared visually to verify the results. The coefficients² for lift and drag as a function of angle of attack can be found in fig. 6.7 and fig. 6.8 respectively.

The search system case used in the DATCOM has a length of 2.5m and a diameter of 0.5m. The fin geometry started at the end of cylindrical section and has a root chord of 0.25m, a tip chord of 0.2m and span of 0.4m.



(a) Lift coefficient of the search system.

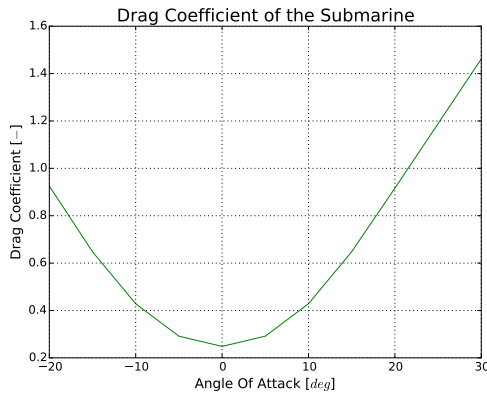


(b) Example lift coefficient of a missile [30]

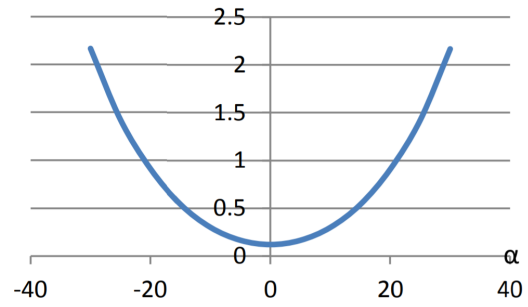
Figure 6.7: Verification of lift coefficient of the search system.

As it can be observed from the diagram, the lift curve of both fig. 6.7a and fig. 6.7b resemble each other and have a linear trend. Furthermore, the lift coefficient of the missile has a steeper slope which is expected due its smaller body fineness ratio [34].

²Note that the moment coefficient was in the reference paper but cannot be reliably compared as the center of gravity of the missile is not known.



(a) Drag coefficient of the search system.



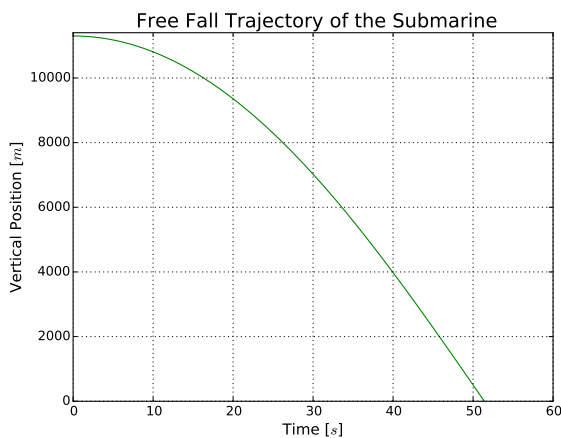
(b) Example drag coefficient of a missile [30].

Figure 6.8: Verification of drag coefficient of the search system.

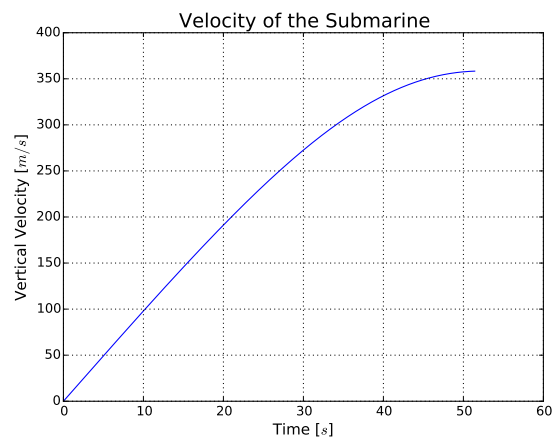
The drag coefficient of both the search system and missile follows a parabolic trend as demonstrated in fig. 6.8a and fig. 6.8b. At angles of attack up to around 20 degrees, the drag of the search system is marginally greater. This is expected due to its spherical end caps which increases the wave drag.

Simplified Model Testing

The first simplified model tests was to observe the velocity and position of the search system when it is dropped from rest. If the altitude is large enough, it is expected that the search system will reach an equilibrium position where the drag is equal to its weight - resulting in the terminal velocity of the search system. This test can be found in fig. 6.9 where the search system is dropped from an altitude of 13000 m nose first.



(a) Free fall trajectory of the search system.



(b) Free fall velocity of the search system.

Figure 6.9: Free fall trajectory and velocity of the search system at rest from an altitude of 13000 m.

As expected, the search system is initially experiencing linear acceleration due to gravity and then starts to dampen quadratically because of the drag term. It reaches a terminal velocity around 360-370 m/s . Furthermore, the trajectory corresponds to area underneath the velocity indicating that the forward integration scheme is working.

Another simplified model test done comes from aircraft dynamics. It is known that the pitch angle is equal to the sum of the angle of attack and flight path angle ($\theta = \alpha + \gamma$). Therefore, another simplified model test is to see that the residual error, $\epsilon = \theta - (\alpha + \gamma)$, is close to zero. This test was done at an altitude of 150meters with the angle of attack, pitch angle and flight path angle all equal to zero. The results can be found in fig. 6.10

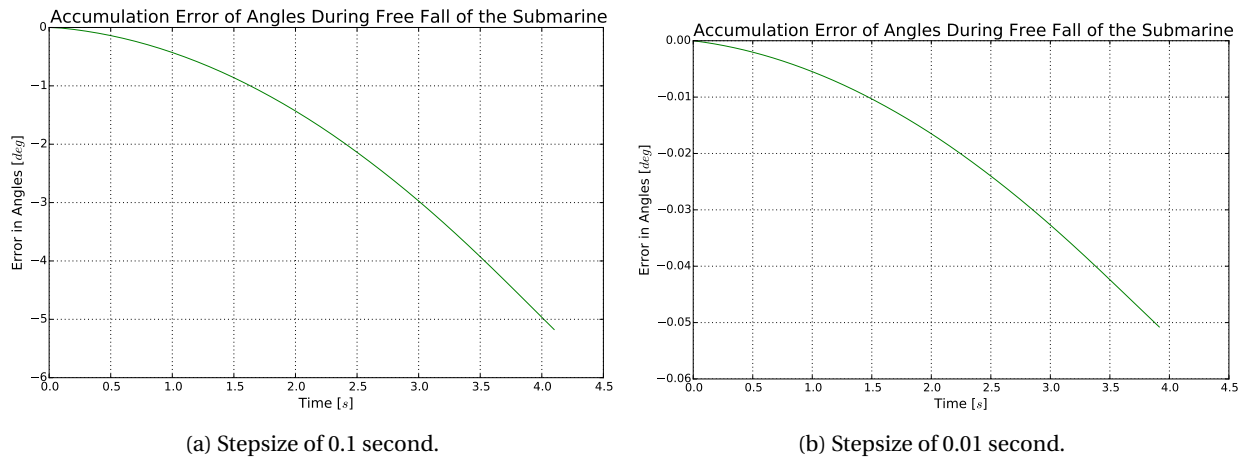


Figure 6.10: Accumulation error of angles during free fall from 150 meters with $\theta = \alpha = \gamma = 0$.

As can be seen in fig. 6.10, the error experiences a quadratic growth. This is expected as the angle of attack is a function of the vertical acceleration (\dot{w}); thus, the total accumulated error was expected to be in the order of $O(h^2)$. In addition, as the step size is increased by a factor of 10 the accumulated error also drops by a factor of 100 as expected.

6.4. Validation of Deployment Simulation

The deployment of the search system has many similarities to a ballistic weapon system. As such, validation proposals are derived from ballistic test programs. Three basic objectives have been outlined based on ballistic test programs [35]:

- i To obtain data on the freestream flight characteristics of the search system.
- ii To obtain data on the separation effects of the search system from the aircraft.
- iii To obtain data on the accuracy of the system.

Section 6.4.1, section 6.4.2 and section 6.4.3 propose validation experiments for the three basic objectives.

6.4.1. Experiment 1: Wind Tunnel Testing with Miniature Model

Experiment Goal: To quantify the aerodynamic characteristics of the search system and to identify possible separation effects of the search system.

Experiment Outline: Experiment 1 will test a miniature model of the search system in the wind tunnel at similar Reynolds Number to the free fall. The model will be mounted on a force balance that can measure the forces and moments. The experiment will involve varying the angle of attack to simulate the free fall of the search system. It is important to note that freestream conditions will be different than during free fall due to the size of the model and keeping the Reynolds Number the same.

Furthermore, a miniature model of the aircraft will also be tested in the wind tunnel at similar Reynolds Number to the free fall. The diagnostic information of the aircraft will be captured through free stream smoke and total pressure rakes.

Experiment Outcome: The miniature model test of the search system will give data on the aerodynamic characteristics. Furthermore, this type of experiment allows multiple prototypes to be manufactured and tested. The results from test can be compared with the interpolated data from DATCOM.

The miniature aircraft model will provide insights of the flow field of the aircraft. From this data, a rough approximation can be made how the freestream drag characteristics of the search system are affected by the non-uniform flow of air.

6.4.2. Experiment 2: Wind Tunnel Testing with Real-Size Model

Experiment Goal: To quantify the aerodynamic characteristics of the search system.

Experiment Outline: Experiment 2 will test a real-size model of the search system in the wind tunnel. Again, the model will be mounted on a force balance that can measure the forces and moments. Furthermore, diagnostic information will be obtained of the search system through surface oil flow. The experiment will vary the angle of attack and free stream conditions to simulate the free fall.

Experiment Outcome: A better representation of the aerodynamic characteristics of the search system can be determined using a real-scale model. Again, these results will be compared with the interpolated data from DAT-COM.

6.4.3. Experiment 3: Flight Test of the search system

Experiment Goal: To quantify the accuracy of the system and the separation effects of the search system from the aircraft.

Experiment Outline: Experiment 3 involves a flight test of the search system. The deployment draws many similarities with the drop test used by NASA for its Orion capsule; Thus, this experiment is modelled based on the CPAS flight testing program [36, 37]. Initially, this experiment can be conducted with a helicopter as it is a relatively inexpensive airborne vehicle to lift and drop vehicles. The CH-47 helicopter can be used as a drop test vehicle and its operational limits are 14 0000 feet.

Finally, a flight test with the C-130 is also required. This experiment would be an exact replica of the proposed deployment for the ULB project. The time-space position data will be collected from release until impact. The aerodynamic characteristics and separation-effect will be evaluated by the trajectory and event times of the hardware and software.

Experiment Outcome: The first flight test experiment (CH 47) will provide feedback on the accuracy of the system as the control surfaces can be tested. Furthermore, the aerodynamic characteristics are re-evaluated as wind tunnel test techniques have some limitations.

The second flight test experiment (C-130) will quantify the separation effects by analyzing the trajectory of the search system. Once separation effects are determined, they can be mathematically modelled and used in the trajectory simulation. Furthermore, the experiment will demonstrate the location and orientation upon impact. This would provide validation for the eventual PID controllers used for the control surfaces.

Submarine

This chapter presents the design approach and the final concept of the submarine. Section 7.1 covers the payload and instrumentation needed for the submarine to complete the mission. In order for this mission to be a success, the submarine must transmit the payload data as well as its location. The navigation and communication are discussed in section 7.2 and section 7.3 respectively. Performance aspects of the submarine such as the buoyancy control, propulsion subsystem and stability control are addressed in section 7.4, section 7.5 and section 7.6 respectively. Then, the power system is sized based on the power requirements of the other subsystems in section 7.7. Concluding the design approach is the structural sizing, in section 7.8 ensuring that all of the instruments fit inside the shell. Finally, a budget breakdown, software diagram and summary of the final concept can be found in section 7.9, section 7.10 and section 7.11, respectively.

It is important to note that the final concept was derived using an iterative process as the subsystems are interlinked with each other. For example, the propulsion subsystem requires the frontal area of the shell (i.e. the structural subsystem) as input parameter and the structural subsystem requires the internal volume it needs to encompass (i.e. propulsion subsystem volume).

7.1. Payload & Instrumentation

To understand why an aircraft crashed, it is important to retrieve the Cockpit Voice Recorder (CVR) and the Flight Data Recorder (FDR). Both of these devices are equipped with an underwater locator beacon that emits an acoustic signal after the crash. Once the beacon is immersed in water, an electrical circuit closes and the beacon emits an acoustic signal of 37.5 kHz.¹

This signal has a range of 2 kilometers in poor conditions, meaning that in deep sea, it might not reach the surface. In order to record the acoustic signal, a hydrophone must be submerged. This is done by using a set of submarines that scan through a search area. Four possible events arise, including the options that there is a detection or not and a beacon nearby or not. The worst that can happen is a false negative, meaning the hydrophone moves nearby or over the beacon but it does not detect it. This is catastrophic for the mission and should therefore be avoided [19].

The search process is divided in two search phases. During the first phase each search system is scanning through its respective search pattern along the search area. Once the ULB signal is detected, the second search phase begins and an approximate location of the aircraft can be determined [17, 18].

In the second phase, the search systems will be relocated to the smaller search area. Omnidirectional hydrophones will be used to receive acoustic signals and an underwater GPS system will be created to determine the position of the submarine. When three acoustic signals are found at different locations, triangulation can determine the location of the beacon.

For the detection of the signal, a hydrophone array is used with four omnidirectional hydrophones. The sounds in the ocean will reach each hydrophone at a different time depending on where the sound is coming from. This time difference can then be turned into a direction, making the hydrophone array a directional hydrophone [39]. The array can filter out the noise coming from different directions and thus focus on the sound from only one direction. In theory, two hydrophones are sufficient to give an approximation of the direction, but usually a minimum of four is used for redundancy and better accuracy. The hydrophones used are the Ocean Sonics icListen High Frequency Smart Hydrophones [40]. They eliminate the need to add pre-amplifiers, filters, analog/digital converters and data storage. Instead of the voltages as output, a binary stream is the output.

7.2. Navigation

Accurate positioning is key in confidently stripping of search area as 'empty', meaning no signal has been detected, as well as for following the planned coverage path. It might occur that the submarines need to deviate from their commanded coverage paths, which would need to be communicated by the base station to prevent overlapping, collision or uncovered search area.

¹After researching the Air France Flight 447 crash in 2009 the BEA recommends to the EASA and ICAO "make it mandatory, as rapidly as possible, for airplanes performing public transport flights over maritime areas to be equipped with an additional ULB capable of transmitting on a frequency (for example between 8.5 kHz and 9.5 kHz) and for a duration adapted to the pre-localization of wreckage". However, this project focuses on finding the 37.5 kHz [38]

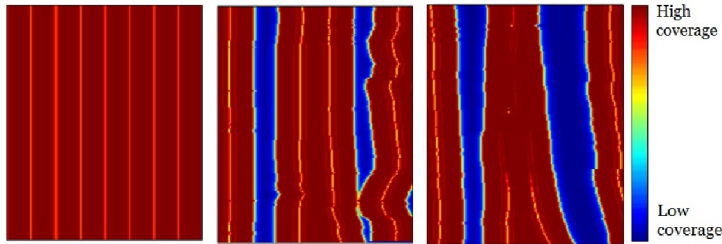


Figure 7.1: Planned coverage path, believed path and actual path from an experiment [43].

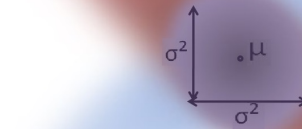


Figure 7.2: A Gaussian distribution of predicted state distribution and the calculated state have an overlap.

In the first phase, the search systems move through the entire search area. Each submarine follows a coverage path and the mother buoys follow the submarine. The submarine needs to know its initial position and up-to-date position, in order to determine whether the coverage path is accurately followed. Besides that, the base stations must be updated on the positions of the submarines.

To provide the submarine with its own up-to-date position while moving underwater, an INS (Inertial Navigation System) is used. The INS integrates the acceleration into velocity and then into displacement, to determine the up-to-date position. This system requires the specific force and angular rate in three dimensions. This is achieved by using an Inertial Measurement Unit (IMU), using three accelerometers and three gyroscopes. The accelerometers measure the acceleration relative to free-fall. To determine the acceleration of the submarine, the gravitational acceleration needs to be subtracted. Next to that, it compensates for centrifugal force (due to rotating of the Earth) and the Coriolis force (due to movement in a rotating frame). The IMU is calibrated to measure zero acceleration when the submarine is not displacing. The gyroscope will measure the angular velocity, which is integrated into attitude. This helps the submarine maintain its orientation. The INS uses navigation equations to calculate the state vector from the IMU measurements. The state vector contains position, velocity, acceleration, orientation, and angular velocity for three dimensions.

An IMU typically operates a 300Hz. The state vector is updated every time the loop finishes. A problem of the INS is the unlimited error. Any slight error of the accelerometer or gyroscope is integrated (twice) and then added to the state vector. Even with a very accurate IMU, the error increases over time². The Honeywell HG9900 [41] is a IMU sensor suitable for deep sea as proven by the HUGIN 6000 [42]. This INS system has a drift of 1.486 km per hour. If the submarine would stay in the same place for an hour, the INS could measure it to have moved 1.486 km. This leads to a difference in believed path and actual path. Additional sensors, such as a depth sensor, can be used to compensate for these errors. They are combined with a Kalman filter.

Kalman Filter

The Kalman filter improves the accuracy of the state vector. It combines the distributions of the estimated state and the measured state. The Kalman filter assumes that the variables are Gaussian distributed. Each variable has a mean value μ and a variance σ^2 . The mean value represents the most likely state and the variance represents the uncertainty. If the old velocity in the x-direction is high, then the new x-position is likely to be further then the old x-position. It uses the old state vector to predict the new state vector. Of course, it cannot precisely predict what the new state vector will be, but it can give a prediction with a mean and a variance. To include uncertainties from external factors, an uncertainty Gaussian distribution is added to every prediction. The best estimate of the new state is then a prediction made from the old state plus a correction for possible noise.

Additional sensors can be added to enable the filter to have some redundancy and facilitates detection of outliers. A compass gives input for the attitude, a positioning system aids the horizontal positioning and a pressure sensor helps with the depth.

The measured state, provided by the accelerometer and gyroscope and the navigation equations, is used to predict the new state. These measurements produced by the sensors contain noise and are Gaussian distributed. The mean value μ is the measured state and the σ^2 is the sensor noise. Some state predictions are more likely than others, for which a covariance matrix can be applied. This covariance of a sensor has a mean equal to that of the

² The errors increase at as a function of time squared for the accelerometer cubed for the gyroscope.

measured state. The Kalman filter compares the Gaussian distributions of the predicted state with the measured state. The two distributions have an overlap; if these two are multiplied a new Gaussian distribution is formed. This new distribution has its own mean and covariance. In fig. 7.2 the overlap is colored purple. The darkest point represents the mean and the variance is the radius of the purple shape. Figure 7.2 is an example of two variables in which the filter creates a matrix with the overlap in prediction and measurement for every variable.

Compass and Depth Sensor

To further aid the IMU system, a depth sensor and a compass are added. A depth sensor uses the change in pressure to measure the depth of the submarine. This gives a redundant input for the position in z-direction. A suitable deep sea compass would be the Leica Digital Magnetic Compass (DMC) compass. It has been used on the HUGIN 6000 [42] and is suitable for deep sea AUV missions. The DMC consists of three magnetic field sensors that measure the response of the device to the Earth's magnetic field. It is important to calibrate this sensor, or else the compass could be distorted by electrical currents running through wires of the submarine.³ The compass provides the orientation of the submarine relative to the magnetic North.

GPS Update

Even though the accuracy of the positioning is quite high, the error will accumulate over time. The mother buoy will follow the submarine and can use GPS. The mother buoy will send a GPS update every 5 minutes. This will reset the IMU position.

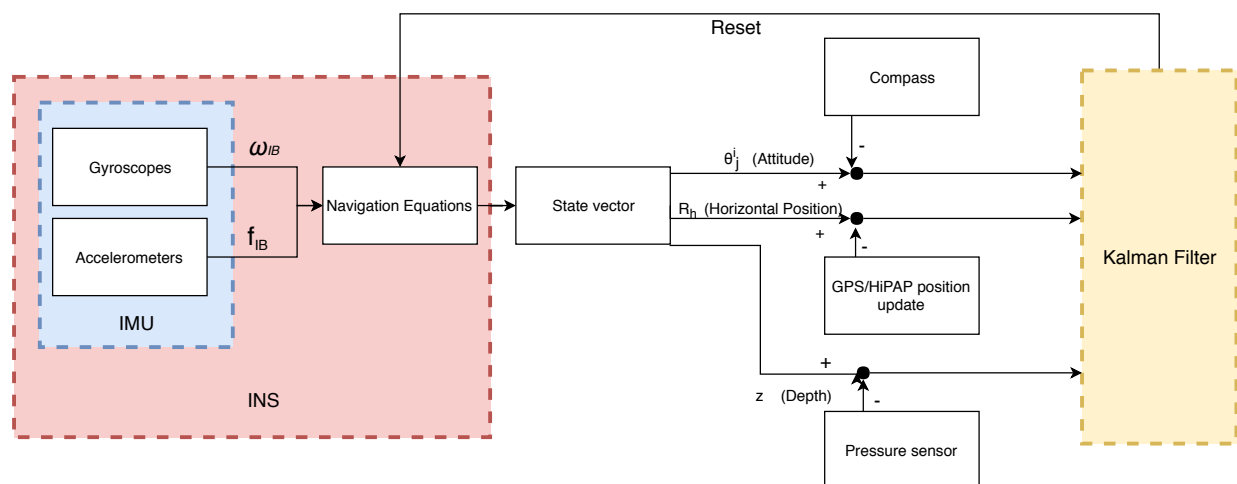


Figure 7.3: Navigation block diagram involving the positioning instruments and Kalman filter.

Second Phase Search Procedure

The first search phase will end when a ULB signal is detected. To triangulate the exact location of the ULB in the second phase, the signal has to be measured from multiple points. Different from phase 1, the required accuracy of the measurement location. To properly triangulate the origin of the ULB signal, the location should be precise in all three directions. The challenging aspect about underwater positioning, is the limited option in signals. Radio electromagnetic do not travel well through conductors like salt water and light travels through water but gets diffracted. However, low frequency acoustic signals travel quite well through water. An underwater locator system that makes use of this is the High Precision Acoustic Positioning system (HiPAP). Just as in search phase 1, the submarine must know its own location. To get a precise location, the submarine determines its distance to (a) point(s) with a constant, known location. Each point has a transponder. When a transponder receives a signal, it immediately emits a signal back.

The submarine puts its transmitter into beacon mode. The submarine then releases a pulse every 12 seconds [44]. This pulse is received by the transponder(s) and immediately sent back. This way, the submarine knows how long the signal travelled to the transponders. Because the speed of sound in the water conditions is known on board, the submarine can calculate its position to the transponders. Three distances to three known points is enough to triangulate its own position. The submarine needs to distinguish the signals from the different transponders. The frequency of the signal response from each transponder could be installed with a slight difference. Else, a known delay in the response of the transponder could help distinguish the responses. The first option requires the submarine to have a broader frequency receiving range, the last option increases the risk of positioning error. Because the submarine updates its position often, the known delays have to be small. The submarine might confuse which set of responses belonged to which position, hence the frequency difference is preferred.

³This could be prevented by using a gyroscopic compass, however the gyroscopic compass has a growing inaccuracy just like the IMU

HiPAP

The HiPAP system will replace the GPS updates from the mother buoy in phase 2. For short distances, one transponder is enough. The submarine can calculate the distance and angle at which the signal was received (Super Short Base Line). However, when the range becomes larger, a small angle deviation can have great consequences for the accuracy of the positioning. A Long Base Line system uses an array of transponders. Four transponders are placed on the seabed and calibrated. The submarine can position itself with the three distances, and use the extra distance to correct deviations.

The Kongsberg HiPAP system has been used a lot for Remotely Operated Vehicles (ROV). The transponders are mounted to the seabed and then calibrated. For this mission the entire search system has to be retrieved by aircraft, thus mounting transponder to the seabed is not possible. Nevertheless, they could be anchored. When the second search area is determined the mother buoys will form the array. The transponders will then be anchored down. The HiPAP transponders have a maximum range of 10000 meter. The array can therefore be 9 by 9 kilometer. The depth of the second search phase could be up to 5000 meter. The HiPAP 102 Ultra Deep Water Positioning transponder is usable up to 7000 meter depth. When the mother buoys are at the corners of the second search phase array, the transponder are anchored. The transponders then sink right below the mother buoys. The transponders might not sink down straight so the system will be calibrated when the transponders are down. The calibration process has three steps.

- i. Initial position of transponder provided by mother buoy GPS
- ii. Baseline measurement with telemetry acoustic communication
- iii. Correction with fifth mother buoy

The position of the mother buoys (determined by GPS) is used as a start position of the transponders [44]. Then all ranges between the transponders are measured by acoustic telemetry communication between the transponders. This provides the first calibration of the HiPAP system. Four mother buoys are required for the array, the fifth or the sixth mother buoy can aid for a second calibration. The fifth mother buoy positions itself in the array. It then its transmitter to send out a pulse to the transponders. Three distances to transponders are enough to triangulate its position. Only three of the four transponders are needed to triangulate the position of the mother buoy. This gives four different options to calculate the mother buoys position. The mother buoy is connected to GPS and can calculate its position independently of the HiPAP system.

The accuracy of the HiPAP system depends on the position of the submarine within the array. The most optimal position is right in the middle, with equal distances to all transponders. Any position error, due to an inaccuracy from the speed of sound calculation, is equal for all transponder distances. The error increases when the submarine moves to the sides of the array. Figure 7.4 shows the error of the distances measured by the submarine to the transponders. If the submarine is at the east bound of the array, the maximal error of the distance to the transponder on the west side is 4 meter. The worst position for the HiPAP is in the corner, right above one of the transponders. The distance error to two of the (furthest) transponders could then be up to 4 meter. This can be seen in fig. 7.4.

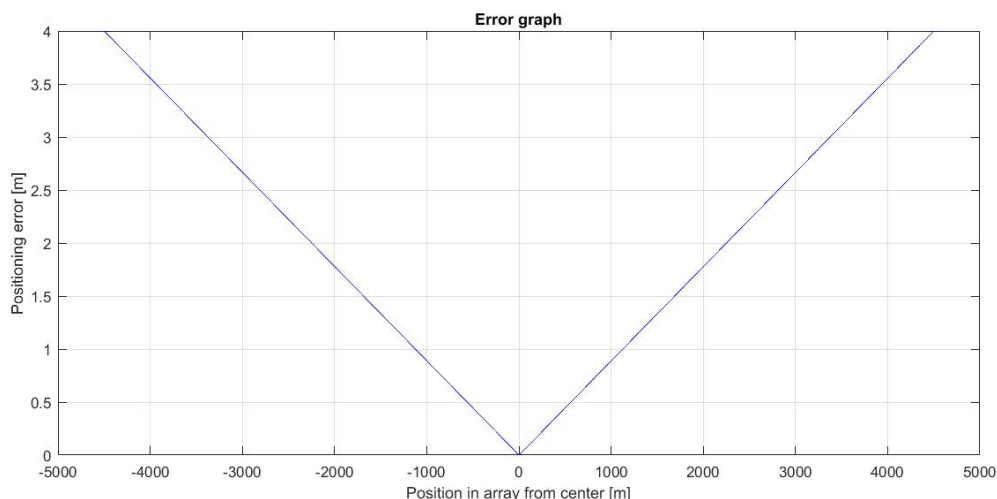


Figure 7.4: Error of the distance to the transponder.

7.3. Communication

When wirelessly transmitting signals underwater, acoustic sound waves are used for a large transmission range. Radio waves only propagate well underwater at a very low frequency and over a short distance, while optical

signals are easily attenuated and do not propagate further than a couple of hundred meters [45].

7.3.1. Communication Channel Characteristics

There are several different parameters affecting the propagation of acoustic signals from the transmitter to the receiver. The main acoustic communication channel characteristics are attenuation and noise, multi-path propagation and time variability.

Signal Attenuation and Noise

Signal attenuation is due to transmission loss which is caused by energy spreading and sound absorption. While energy spreading loss solely depends on the transmission range, sound absorption also depends on the signal frequency. A higher signal frequency results in a higher absorption loss, as shown in fig. 7.5. Therefore, a low frequency has to be used for communication between the submarine and the mother buoy. This frequency is chosen to be 10 kHz.

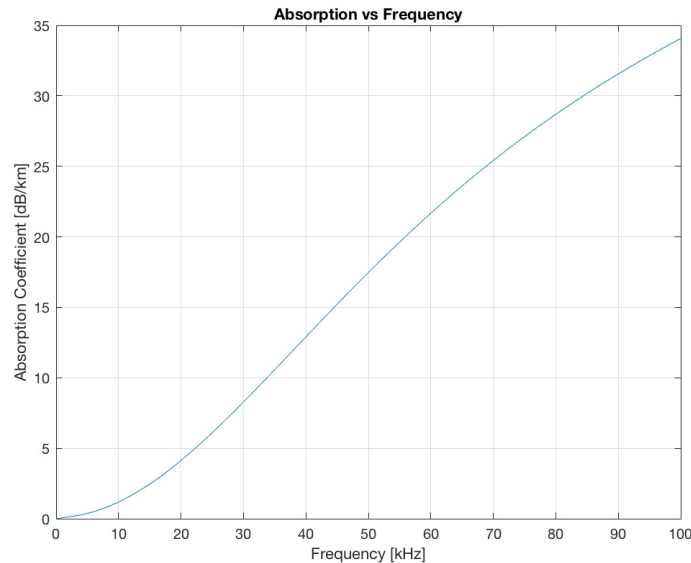


Figure 7.5: Increase of the sound absorption coefficient when the frequency is increased [46].

The two types of noise that can be observed in the ocean are ambient noise and site-specific noise. Ambient noise is present everywhere in the ocean and has four components: turbulence, wind, shipping and thermal noise. On the other hand, site-specific noise is present only in certain areas. As this is difficult to determine, it is not taken into account for this project. The only component of ambient noise influencing either the ULB signal or the transmission signal is wind noise which is dominant in the 100 Hz-100 kHz frequency range [46].

Multipath Propagation

When using a single carrier wave for modulation of the input signal, multipath propagation occurs and will cause intersymbol interference (ISI). There are two main mechanisms for multipath propagation depending on the water depth. For shallow water (depth < 100 m), multipath formation is caused by the reflection of sound waves at the ocean surface, bottom or another object. For deep water, the main cause is refraction of the sound wave due to sound speed variation with depth.

Time Variability

The time variability of the channel has two sources: random changes in the propagation medium resulting in signal fading and relative motion of the submarine and motherbuoy causing frequency shifting (Doppler effect). The Doppler spread will lower when range increases and lower frequencies are used.

Acoustic Modem

Tests have proven that underwater communication over a range of 10 km in deep water and 5 km in shallow water are possible with a low bit error rate (BER) [47]. The modulation technique used by the acoustic modem has a great influence on how much the signal is affected by the previously mentioned parameters. The acoustic modem that will be used is EvoLogics S2CR 7/17 with a BER of less than 10^{-10} [48]. This modem uses the sweep-spread carrier technology, which makes it possible to deliver the acoustic signal in adverse water conditions. This technology is based on a succession of signal sweeps causing permanent rapid variation of the frequency which counteracts the multipath propagation effects.

7.3.2. Equipment

The equipment that is needed for the communication between the submarine and the mother buoy is an acoustic modem including a transducer. This modem was already discussed in section 7.3.1. For safety reasons, a satellite modem and antenna are also present on board the submarine. In case the submarine loses communication with the mother buoy, it can come up to the surface and send its location to the base station for retrieval or repositioning commands. The Iridium satellite network is used for the satellite communications. The chosen satellite modem on board the submarine is the Quake Q9612 modem [49]. The antenna is a dual GPS/Iridium antenna [50].

7.3.3. Data Handling and Communication Link

The acoustic modem of the submarine can send 1.8 Mb up to the mother buoy every 30 minutes. This is not enough to send up all the acoustic data. Therefore, an on board selection should be made to determine which payload sample could be valuable and which one is not. In 30 minutes, four hydrophones have collected 7200 seconds of acoustic data. This data is sampled into samples of 1 second.

The beacon transmits a pulse of 8 ms every second. This signal has a frequency of 37.5 kHz. Or submarine has a notch filter with a range of 35 kHz to 40 kHz. Using Nyquist frequency, the sampling frequency is then 80 kHz. A resolution of 8 bits results in a sample size of 640 kb. In 30 minutes, 7200 samples have been collected, that gives a total of 4608 Mb. However, there is only 1.8 Mb available, therefore the submarine should determine which samples can be discarded.

The challenging part about finding the ULB signal is to distinguish the pulse from noise. The submarine needs to determine if a signal with a frequency of 37.5 kHz is noise or the ULB signal. The difference between noise and a pulse is that noise is instantaneous and the ULB pulse lasts 8 ms. If a sample of 1000 ms contains the ULB signal, then 37.5 kHz is measured for 8ms. The hydrophones of the submarine are not on the exact same location. Therefore, there will be a phase difference in the measurement of the pulse. This phase difference is key in distinguishing the pulse from noise. The concept of cross correlation measures similarity in signals with a phase displacement.

If the submarine is near the ULB, all four hydrophones will measure a pulse of 8ms in the sample of 1 second. The closest hydrophone, now hydrophone 1, will measure the pulse at instant t . The second closest hydrophone, now hydrophone 2, will measure the pulse slightly later, at instant $t+i$.⁴ If the dot product is calculated of the sample of hydrophone 1 and sample of hydrophone 2, non-zero values only appear when the same frequency is measured at the same time. Because the pulse is longer than the time shift i , non-zero values will appear if the beacon signal is recorded by hydrophone 1 and 2. Hydrophone 3 and 4 will also measure the pulse from the ULB. If the cross correlation test gives a positive result for all four samples, a pulse was present. The acoustic sample is then send up to the mother buoy. Data analysts at the base station will then determine if the pulse originates from the beacon.

For the processing of the data, a single board computer is used while all of the data will be stored in a 16 TB hard disk [52, 53]. The data handling diagram is shown in fig. 7.6.

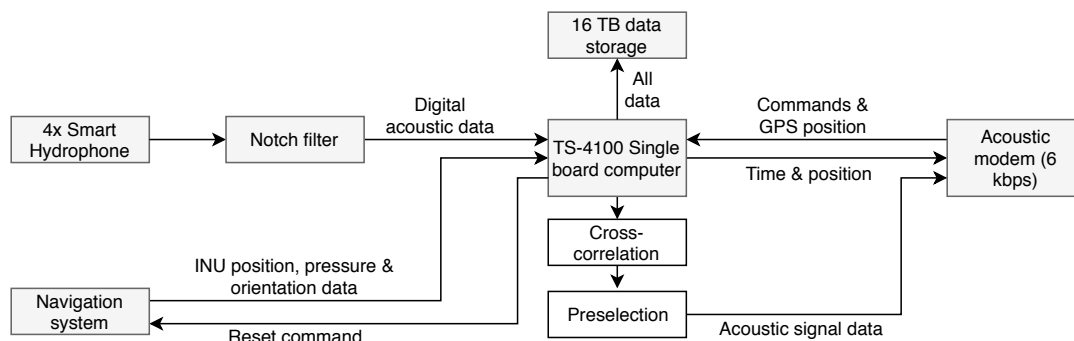


Figure 7.6: Data handling diagram of the submarine.

Communication flow

The communication flows travel through water (red), electrical wires (green) and space (blue).

⁴Speed of sound in water is 1500 m/s. When the hydrophones are placed very close (<1.5 meter) the discretization step (i) of the cross correlation has to be in microseconds. According to [51], microphone array spacing has a minimum of 75mm.

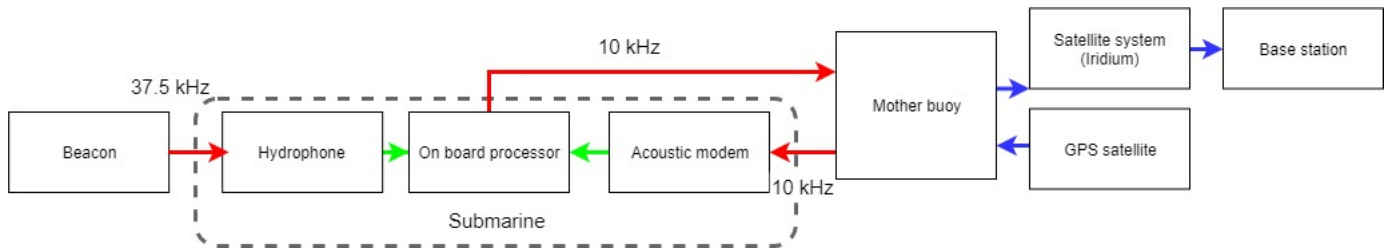


Figure 7.7: Communication flow for phase 1.

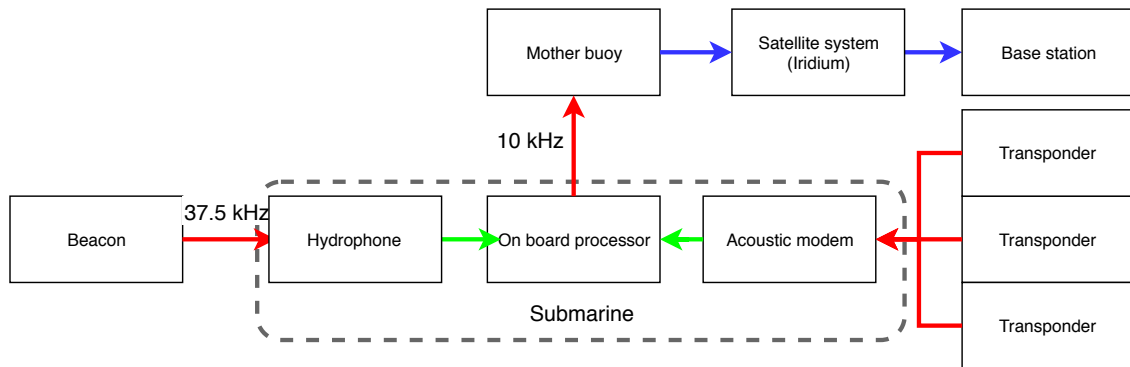


Figure 7.8: Communication flow for phase 2.

7.4. Buoyancy Control

To control the depth of the submarine a buoyancy control system is needed. Firstly, the type of system and the system architecture are determined in section 7.4.1, followed by the system sizing in section 7.4.2. Lastly, the effects of the system are modelled in section 7.4.3

7.4.1. System Architecture

There are three methods of controlling the depth of a submarine; vertical propulsion to counteract any net buoyancy, a variable ballast system (VBS) to alter the mass of the submarine and an external bladder to alter its volume. Using the propulsion system is both faster and less energy intensive than the other methods for significant changes in depth. [54] However, it needs constant power to counteract the net buoyancy of the submarine and stay at a constant depth. Both systems need (near)zero power for this. Furthermore, the external bladder poses an extra risk during the deployment of the submarine, as it could burst under the impact. Also, the VBS can be emptied completely for deployment and retrieval to achieve a lower mass, which is not possible for the bladder. Therefore, the submarines will be equipped with a VBS.

The VBS consists of the following main components: ballast tank(s), ballast pump, valves and sensors. In addition to the VBS, an emergency ballast is needed to enable the submarine to surface in case of power outage or failure of any of the VBS components.

Ballast Tanks

The main purpose of the ballast tanks is to hold the water needed to achieve the desired mass. Since the tanks hold varying mass they can be used to shift the center of gravity and thereby control the pitch of the submarine. To do this two tanks are placed at opposite ends of the submarine to create the maximum moment arm. This also allows for the submarine to float near vertical which is advantageous for retrieval. Since the tanks will be in regular contact with salt water, it is important that they are protected from its corroding effects. Therefore, the tanks will be lined with custom fitted corrosion resistant bladders.

Both tanks will be fitted with solenoid valves to control the in- and outflow of the water, using little power. The tanks will also be connected to differential pressure sensors that measure the difference in pressure between the water and air in the tanks. These measurements can be used to determine the water height in the separate tanks, which are important to control the parameters of the submarine.

Ballast Pump

To empty the tanks at 4500 m depth, a pump is needed that can overcome the high ambient pressure. To enable the system to produce this pressure, an intensifier is used. The intensifier works by using a double plunger with different diameters on either side. Hydraulic oil pressurized by the (positive displacement) pump acts on the large side, thereby creating a higher pressure on the small side to push out the water. Another advantage of this is that

the pump does not come into contact with the salt water, improving its durability. A schematic overview of the pump coupled with the intensifier can be seen in fig. 7.9. A similar system has been proven to work at a pressure of 44.8 MPa [55], which is equivalent to a depth of 4450 m.

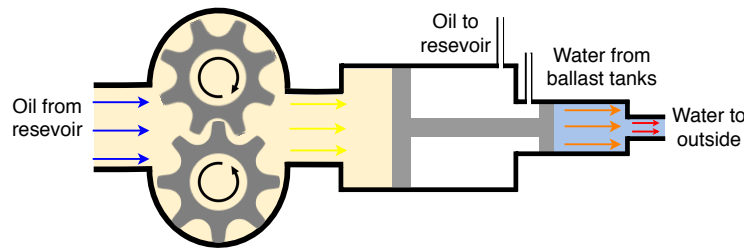


Figure 7.9: Schematic overview of ballast pump with intensifier.

Emergency Ballast

A considerable risk in using submarines is that the submarine sinks due to a failure of the buoyancy control system or a power outage. To mitigate this risk the submarine is equipped with emergency ballast. The emergency ballast is a completely separate system from the VBS, providing a fail-safe alternative for ascent. The emergency ballast is made up by a lead plate with a corrosion resistant coating. The plate is attached on the outside of the submarine to allow easy release. The release mechanism consists of a solenoid bolt, which releases automatically when it loses power. This means the submarine will surface after a power outage, but it can also be used when running low on power or after the ballast pump has failed.

7.4.2. Buoyancy Control Sizing

The buoyancy control sizing is done in three parts. First the size of the ballast tanks is determined. Then an existing pump is selected. Finally, the emergency ballast is sized.

Ballast Tank Sizing

The submarine has to be able to operate at any depth up to 4500 m. This means the submarine needs to be able to be buoyancy neutral in this entire range. The submarine is buoyancy neutral if eq. (7.1) is satisfied.

$$m_{total} = V_e \cdot \rho \quad (7.1)$$

Both the density of the water and the volume of the submarine are affected by the increasing pressure at greater depth. These relations are given in eq. (7.2) and eq. (7.3). [56]

$$\rho = \rho_0 \cdot C_w^{-z} \quad (7.2) \quad V_e = V_{e,0} \cdot C_s^{-z} \quad (7.3)$$

Since the submarine has a higher compressibility than water, the lowest mass is needed at maximum depth, as can be seen in fig. 7.10. In this way, the maximum mass of the submarine at zero ballast is limited by this value. Similarly, the minimum ballast mass is defined by the difference between the mass needed for neutral buoyancy at sea level and the mass of the empty submarine. The minimum ballast volume is given by eq. (7.4).

$$V_{b,min} = \frac{\rho_0 \cdot V_{e,0} - m_s}{\rho_0} \quad (7.4)$$

To minimize the internal volume needed for the submarine, the VBS is designed with this minimum ballast volume. However, it is scaled by a safety factor of 1.1 to account for changes in density due to temperature and salinity, which are in the range of 5 % and allow for a non-zero net buoyancy.[56] Also the volume of the tanks has to be larger than the ballast volume to account for the volume of the structure and the air in the tanks. A comparison of existing AUVs shows that their ballast volume is around 90 % of the total tank volume.

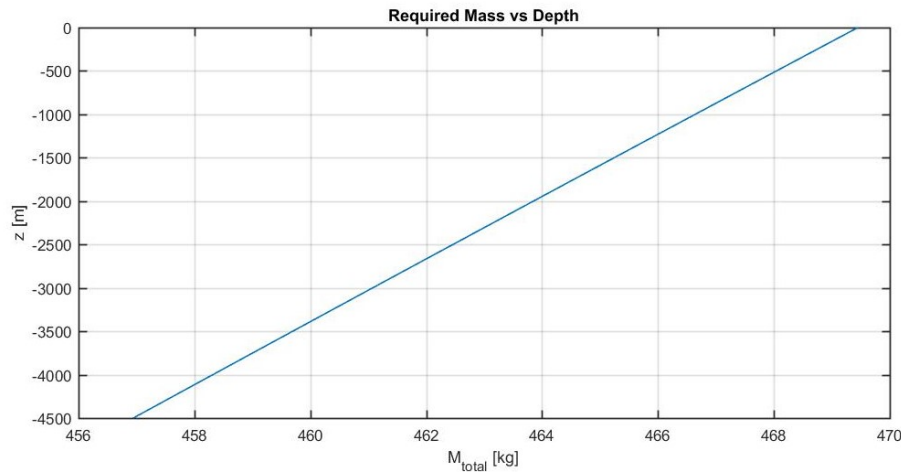


Figure 7.10: Required mass to be buoyancy neutral for a submarine with an uncompressed volume of $0.458 m^3$ and a compressibility coefficient of 1.0001.

For a submarine with a diameter of 0.5 m, this results in a maximum mass of 434 kg. However, using a mass of 393 kg, gives a maximum ballast mass of 102 kg and a tank volume of $0.11 m^3$.

Ballast Pump Selection

Since the submarine will only surface twice during the mission duration, the pump is selected for power and mass conservation rather than speed. The power used by the pump is given by eq. (7.5) where the pressure at a specific depth is given by eq. (7.6).

$$P = \frac{\dot{V} \cdot (p - p_{\text{tank}})}{\eta_{\text{pump}}} \quad (7.5) \quad p = \rho \cdot -z \cdot g \quad (7.6)$$

The pump used by the ROV Tiburon was designed for similar use and will therefore be used as a reference pump. Its specifications can be found in table 7.1.

Table 7.1: Characteristics of the ballast pump [55].

Buoyancy Characteristics	
Mass	56 kg
Volume	$0.00919 m^3$
Flow rate	$0.000146 m^3/s$
Efficiency	0.89

Emergency Ballast Sizing

The sizing requirement for the emergency ballast is that the submarine has to be able to surface from a maximum depth of 4500 m while the ballast tanks are full. This requirement is chosen to enable ascent after total failure of the ballast pump or valves. The mass of the emergency ballast is given by eq. (7.7).

$$m_{eb} = 1.1 \cdot (m_s + m_b - V_{z_{max}} \cdot \rho_{z_{max}}) \quad (7.7)$$

Filling in results in an emergency ballast of 24 kg. The emergency ballast will be shaped as a lead strip along the bottom of the cylindrical part of the submarine hull, with dimensions $2.00 \times 0.053 \times 0.02$ m.

7.4.3. VBS Performance

To evaluate the performance of the VBS, a model was developed simulating the effects of a change in mass on the submarine. The following assumptions were made in this model:

i Salinity and temperature do not change with depth.

Implication: The density of the seawater is only influenced by its compressibility with depth. This assumption was made because the salinity and temperature distributions depend highly on the exact location and time of year.

ii There are no currents.

Implication: The relative velocity of the submarine to the water is the same as velocity relative to the earth.

iii All forces act through the same point.

Implication: There are no moments or rotational velocities.

As shown in fig. 7.11, there are three vertical forces acting on the submarine during ascent and descent; weight, buoyant force and drag. Using Newton's first law and the resultant force, the acceleration can be determined. This acceleration can be integrated twice with respect to time, to determine the velocity and depth.

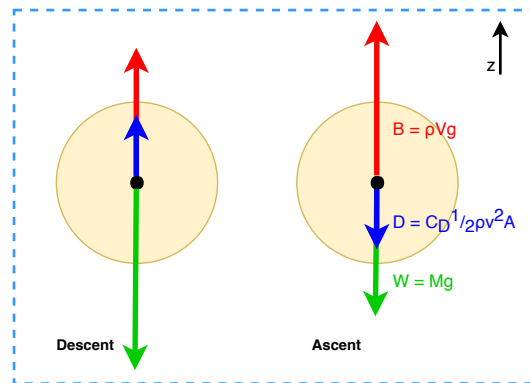


Figure 7.11: Forces on the submarine during ascent and descent.

Descent

Before descending, the ballast tanks are empty ($m_b = 0$). To start descending, the valves of the ballast tanks are opened, causing water to run into the tanks until they are full. According to Torricelli's law, the flow rate of the inlet is determined by the area of the inlet and the depth using eq. (7.8).

$$\dot{V}_{inlet} = A_{inlet} \sqrt{-2 \cdot g \cdot z} \quad (7.8)$$

Using these equations, the trajectory can be determined by iterating over time starting at $z = -1$ m and ending at the desired depth. The model is started at -1 m to ensure that the inlet is underwater, in reality it must be ensured that the inlet is positioned underneath the water level when the ballast tanks are empty. The trajectory can be seen in fig. 7.12. From this figure it can be seen that a full descent takes 1148 seconds.

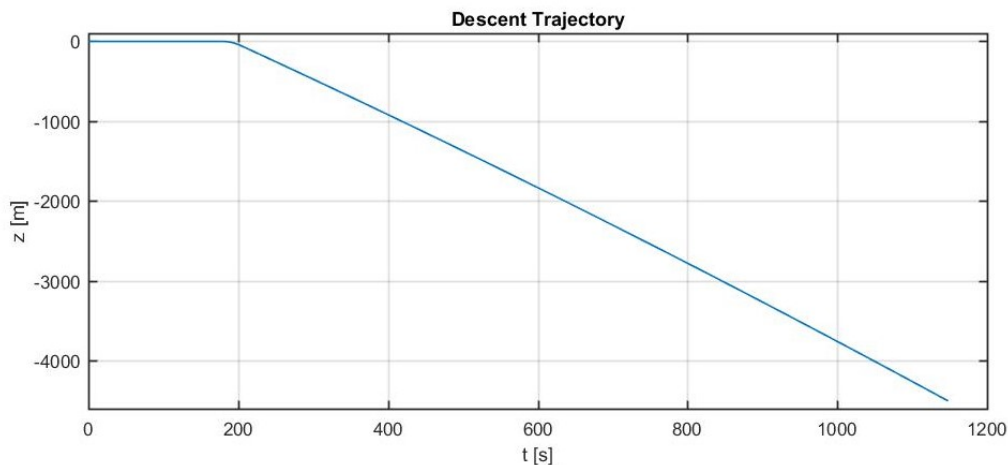


Figure 7.12: Descent trajectory of the submarine.

Ascent

The ascent model starts at an equilibrium position where the weight is equal to the buoyant force and there is no velocity. From this point, water is pumped out of the ballast tanks until they are empty. This happens with a constant flow rate. [55] Similarly to the method used for descent, the ascension path can be determined by iterating over time from the desired depth to $z = 0$ m. This trajectory can be seen in fig. 7.13. In addition to the time taken to ascent, the power needed for the pumps can be approximated by eq. (7.5). This results in an average power of 3097 W over the 1015 seconds taken by the ascent. However, the ballast tanks are full after 344 seconds so no more power is used after this. The power used by the pump over time is displayed in fig. 7.14.

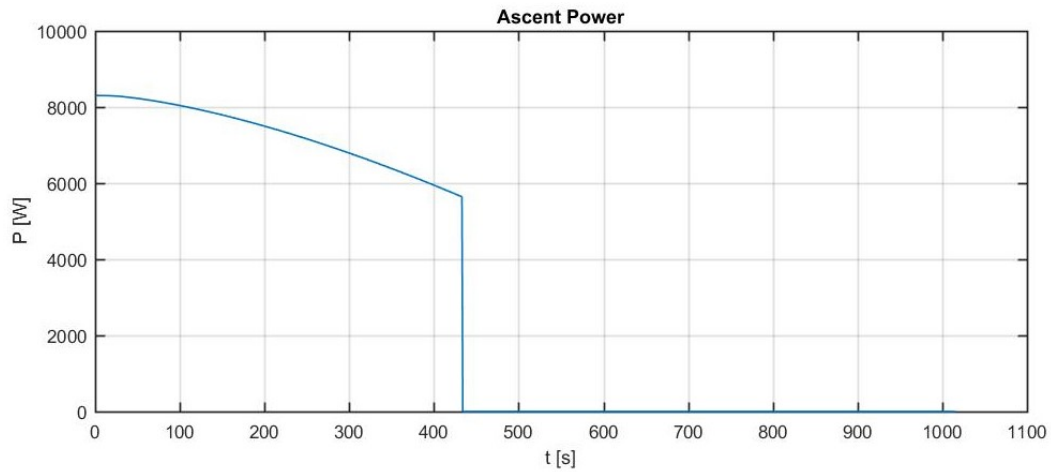


Figure 7.14: Power used by the pump during ascent.

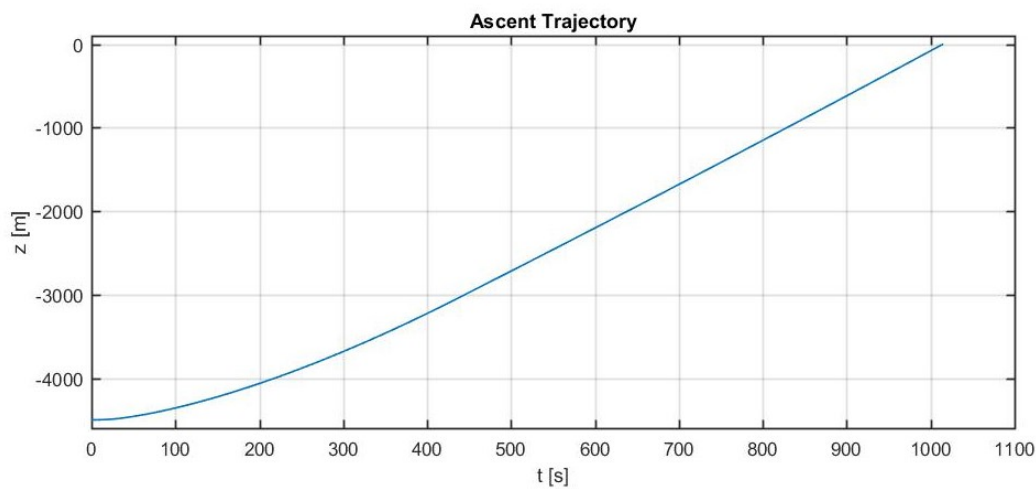


Figure 7.13: Ascent trajectory of the submarine.

7.4.4. Verification & Validation

This section addresses the verification of the scripts used to size the VBS and proposes validation methods for the system.

Verification

To verify the model, first a few simple test are performed. Both the ascent and descent simulations are tested with a *zero test*, where it can be seen that, as expected, the submarine reaches equilibrium after 0 seconds and the simulation is stopped. Also the descent simulation reaches equilibrium immediately when a mass of 1025 kg is used with a volume of 1 m^3 . This is because in this case the submarine has the same density as the water at sea level, so the buoyant force and weight are equal.

The method used to size the ballast tanks is verified by comparing the results with those of other researches. As seen in table 7.2, the difference between the results of the ballast tank sizing script and the research by Tiwari [57] is 10%. This is a considerable difference, however it is the same size as the safety margin used by the script. This margin is used to account for the variations in temperature and salinity with depth. Since the AUV designed by Tiwari only reaches a depth of 400 m, these variations are a lot less severe [56], so less of a safety margin is needed.

Table 7.2: Verification of ballast tank sizing.

Input Values	$V_{ballast}$ Tiwari [57]	$V_{ballast}$ script	Difference
$M_s = 204.7228 \text{ kg}$ $V_0 = 0.2973 \text{ m}^3$ $z_{max} = -400 \text{ m}$	0.0976	0.1073	10%

Validation

Three components of the buoyancy control need to be validated; the tanks, the pump and the emergency ballast. The pump performance can be validated by testing the pump in a pressure vessel [55]. During this test the flow rate and power used by the pump should be monitored at increasing pressure.

The sizing of the tanks and emergency ballast need to be tested in an actual ocean environment to account for the variations in temperature and salinity. However, to reduce cost, preliminary testing can be done in a water basin. Also the volume and mass of the prototype could be scaled down for testing. During these tests, the water level in the ballast tanks should be monitored alongside the depth of the submarine. Also the release mechanism of the emergency ballast should be tested.

7.5. Propulsion

Since the propulsion system is the largest consumer of energy, it is vital to design it with optimal efficiency in mind. The power consumed by the propulsion system is related to the velocity of the submarine through eq. (7.9) and eq. (7.10).

$$D = C_D \cdot \frac{1}{2} \cdot \rho_{z_{max}} v_{sub}^2 \cdot A_s \quad (7.9)$$

$$P = \eta_{prop} \cdot \eta_{engine} v_{sub} \cdot D \quad (7.10)$$

The relation between power and velocity is shown in fig. 7.15. From this graph a velocity of 1 m/s is chosen as this is the point where the power starts to grow drastically with higher velocity. This velocity is also constrained by the maximum velocity of the motherbuoy which is explained in section 8.4.

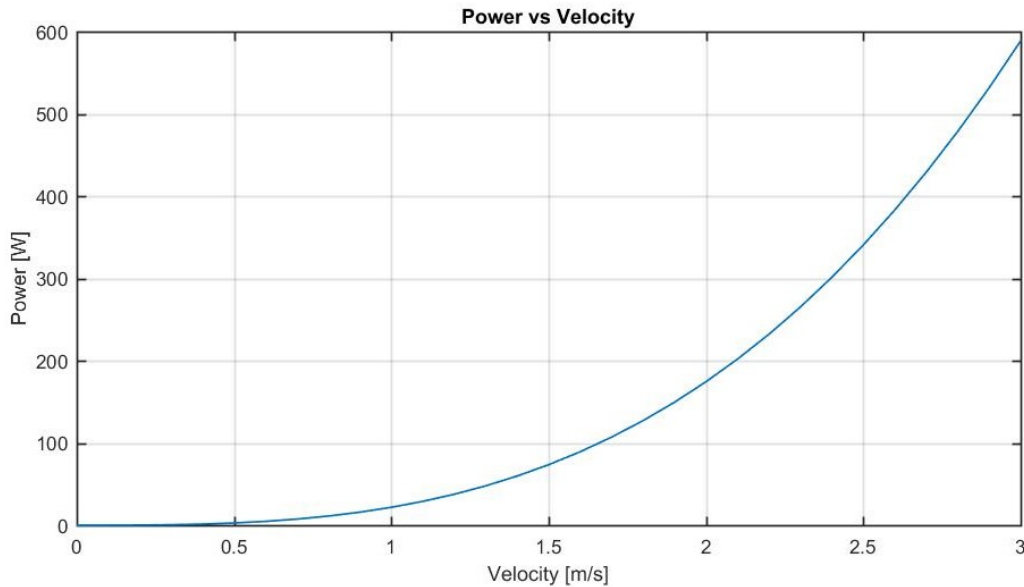


Figure 7.15: The relation between velocity and power.

The drag coefficient of a torpedo shaped object is approximately 0.12 [58]. To also account for the added drag due to the control surfaces, this is scaled by a factor of 1.5 resulting in a drag coefficient of 0.18. This is in line with the drag coefficient found during testing of the Thetys AUV [59]. For a diameter of 0.5 m, this leads to a drag force of 18.4 N. To sustain constant velocity, the thrust generated by the propulsion system must be equal to the determined drag. Since the SPYROS propeller [58] is optimized for the same velocity and drag range, this propeller design will be used. It was found that this propeller has an optimum efficiency of 0.79 at 300 rpm. Using eq. (7.11), it can be found that a torque of 0.75 Nm is needed to provide the required thrust.

$$\eta_{prop} = \frac{T \cdot v}{Q_{en} \cdot \omega} \quad (7.11)$$

To find the best engine to provide this torque, the method described by [58] is used. From this it is found that the BLOV-29-07-12P [60] with a no-load speed of 392 rpm, uses the least power, at 2.43 A at 12 V. Using eq. (7.12), the efficiency of the engine is determined to be 0.82. From this the total power for the propulsion system is given as 28.5 W by eq. (7.10). Using this engine the maximum velocity of the submarine is around 2.5 m/s.

$$\eta_{engine} = \frac{I \cdot U}{I \cdot U + R_m \cdot I^2} \quad (7.12)$$

7.6. Stability & Control of the Submarine

This section discusses the stability and control of the submarine while it is in the water. The stability and control during deployment and retrieval can be found in chapter 6 and chapter 9 respectively.

7.6.1. Stability

Firstly, the stability of the submarine while it is underwater, is discussed. Afterwards, the stability of the submarine while it is waiting on the surface to be retrieved is addressed.

Underwater Stability

Due to the torpedo shape, the submarine is naturally stable in pitch and yaw. When a small rotation is caused by a disturbance force, this rotation is counteracted by an opposite rotation due to the additional drag on the aft of the hull. This is displayed for yaw in fig. 7.16, but the same principle applies for pitch.

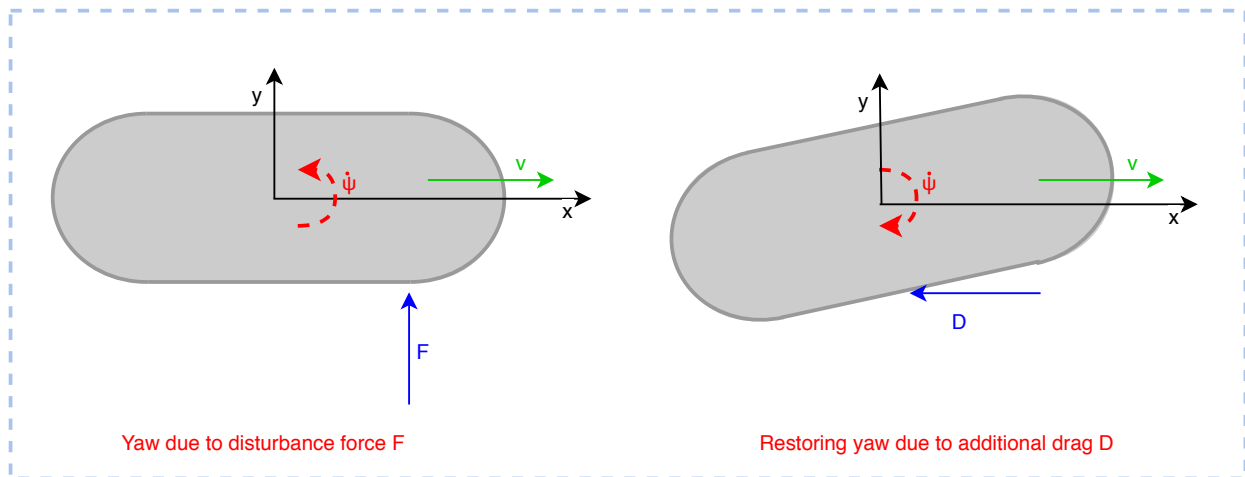


Figure 7.16: Yaw due to disturbance force followed by a restoring yaw due to the additional drag.

The cross-section in the yz -plane is circular so this principle does not apply for roll. However since the weight always acts down, this can be used to stabilize the submarine in roll. By ensuring the center of gravity is located below the middle of the submarine, the moment caused by the weight is a restoring moment after a small disturbance.

As described in section 7.4, the emergency ballast is mounted on the bottom of the submarine, ensuring the center of gravity is located on the bottom half of the submarine.

On Surface Stability

When the submarine comes to the surface to be retrieved, it will be oriented with the x -axis perpendicular to the water surface. To ensure the submarine is stable in this position, the same procedure is used as in fig. 8.1.

In this case the submerged volume of the submarine is given by eq. (7.13), where h is the height of the part of the cylindrical segment of the hull that is submerged as given by eq. (7.14). For a mass of 393 kg (so without any ballast in the tanks) and a diameter of 0.5 m, metacentric height (MG) is 0.05 m defining the submarine stable. Furthermore, 1.9 m of the submarine is submerged.

$$V_s = \frac{2}{3} \cdot \pi \cdot r^3 + \pi \cdot r^2 \cdot h \quad (7.13)$$

$$h = \frac{m_s + m_b}{r h_{O_0} \cdot \pi \cdot r^2} - \frac{2 \cdot r}{3} \quad (7.14)$$

7.6.2. Control

The submarine is controlled in yaw by a rudder mounted on the rear of the hull. There are two systems that control the pitch; the horizontal control surfaces mounted on the rear of the hull and the shifting of center of gravity by pumping different amounts of water into the two ballast tanks. These two systems should be used in tandem to minimize power consumption. For the roll, no active control is necessary since the submarine is stable in this direction as is explained in section 7.6.1. The sizing of the control surfaces is done in section 6.3.

7.7. Power

This section discusses the two remaining options for the power subsystem of the submarine: batteries and a hybrid system using a combination of fuel cells and batteries. The use of a fuel cell system on its own is not considered as it would considerably increase the mass and volume needed for the power subsystem. Both options

are fully designed in this section and at the end, a tradeoff is performed to choose the final power system design. The power subsystem has to last the maximum duration of the mission (i.e. 30 days) since the submarine does not come up to the surface or is retrieved before the end of the mission. The search systems will relocate themselves autonomously to the second phase search area. Thus, there is no option for recharging outside the submarine or replacement of the components.

The total power needed for the equipment with a constant power supply is based on the values in the budget breakdown table in section 7.9. The energy needed for the buoyancy control can be found in section 7.4.3 and for the communication in section 7.3.3.

7.7.1. Batteries

In this section, the battery system is designed and a closer look is taken at the risk, sustainability and cost of this system to do a proper tradeoff in the end.

Design of Battery System

The most important property of the batteries for the mission is the energy density. High energy density is necessary since the batteries have to last for 30 days without recharging. Therefore, lithium-ion batteries are chosen with a specific power of 150-220 Wh/kg [61]. The lithium batteries are rechargeable so they can be reused for the next mission. There are several types of lithium-ion batteries as can be seen in fig. 7.17. Lithium-nickel-manganese-cobalt (NMC) is the only battery scoring (relatively) well on all different properties, making that the best option. Although nickel-cobalt-aluminum (NCA) batteries score higher on energy density and specific power, the safety is considerably lower which is not ideal in order to power the submarine.

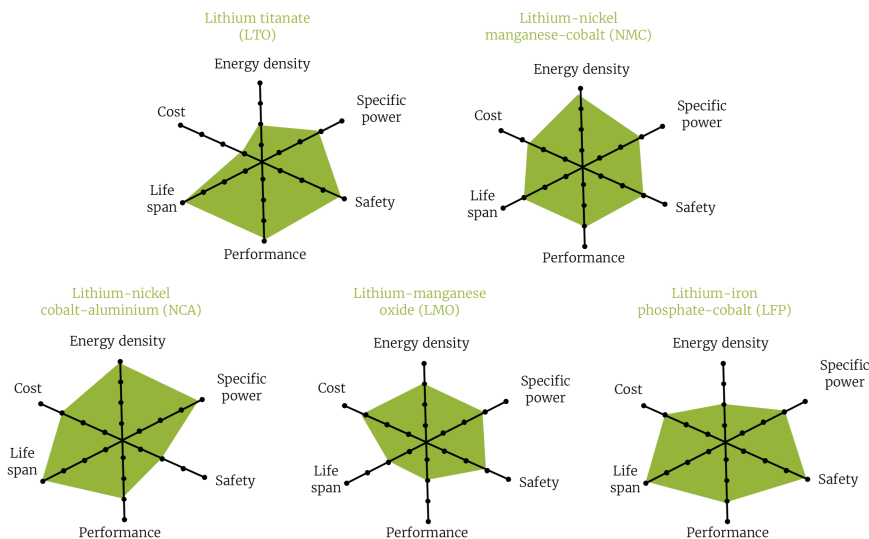


Figure 7.17: Comparison of lithium-ion batteries [62].

Although NMC batteries can have a very high specific energy and power, it cannot have both at the same time. So a lower value of 150 Wh/kg is used for the specific energy and 150 W/kg for the specific power [63]. Furthermore, the batteries have a volumetric energy density of 250 Wh/L [64]. For a total amount of 40.9 kWh energy needed, the battery mass and volume can be found in table 7.3.

Table 7.3: Size of the designed battery for the submarine.

Property	Value
Mass [kg]	274.6
Volume [m ³]	0.164

Risk, Sustainability and Cost

The main risks that come with lithium-ion batteries are thermal instability of the active materials in the battery at elevated temperatures and internal short circuits that may lead to thermal runaway, which in turn may lead to explosions or fires. Also, the heat may propagate to the next cells, making them thermally unstable as well.

Although lithium is less toxic than other common battery materials like lead, improvements can still be made concerning the environmental impact and public health. Some of those impacts include resource depletion, ecological toxicity and global warming. Furthermore, the production of lithium-ion batteries produces 12 kg of CO₂

emission per kg which is more than for other types of batteries. The main materials for the NMC batteries specifically are lithium, cobalt, nickel and manganese. Lithium and cobalt are both scarce products, while nickel is highly toxic in the environment. Manganese, on the other hand, is less of a worry when it comes to scarcity and the environment [65, 66].

When it comes to the recycling of lithium-ion batteries, a complex and expensive process is needed. For this reason, cobalt-based lithium batteries (such as the NMC battery) are rarely recycled, despite their high metal value. Subsidies would be needed to break-even since the retrieved raw material from the recycling barely pays for the labour. Nonetheless, it is possible to recycle the batteries. One of the companies doing so, is American Manganese Inc. [67]. It has a proven process capable of recovering 100% of the lithium, cobalt, manganese and nickel from cathode materials used in lithium-ion batteries. Furthermore, since there is an ever-increasing demand for lithium-ion batteries, their recycling will become more attractive in the future.

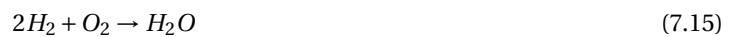
The NMC batteries have a cycle life of 1000 cycles or a calendar life of 15 years [68]. A battery is considered to be beyond its lifetime when it has lost 20% of its initial capacity. The price for 1 kWh of NMC batteries is approximately €362 [61]. This makes the total cost for the battery system €14 806.

7.7.2. Hybrid System

In this section, the hybrid system is designed and a risk, sustainability and cost assessment is done.

Fuel Cell System

A hybrid system is advantageous when the power requirements are variable. The fuel cell system is used to provide constant power to most of the payload on board the submarine. When the necessary power exceeds the provided power by the fuel cell, energy is taken from the batteries. This occurs when data is transmitted from the submarine to the mother buoy or when the submarine ascends to the surface. Fuel cells need hydrogen and oxygen to produce an electric current and only emit water as reactive product as seen in the reaction in eq. (7.15).



The main components needed for a fuel cell system are a fuel cell stack, hydrogen tank, oxygen tank and water storage tank. The latter is used to store the water on board of the submarine instead of pumping it out. This is done to keep the total mass constant and not complicate the buoyancy control subsystem. The amount of hydrogen and oxygen that is needed to provide the necessary amount of power is calculated using eq. (7.16) and eq. (7.17) [69].

$$H_{2usage} = \frac{I_{fuel} \cdot n_c \cdot M_{H_2}}{2 \cdot F} \quad (7.16)$$

$$O_{2usage} = \frac{I_{fuel} \cdot n_c \cdot M_{O_2}}{4 \cdot F} \quad (7.17)$$

There are three ways of storing hydrogen that are considered in table 7.4. It can be stored in liquid form, as a compressed gas or as a solid using metal hydrides. Liquid hydrogen storage is not frequently used, mainly due to the loss of hydrogen through boil-off. Also, it has a low volumetric density (71 kg/m³) which makes it not a suitable option for the submarine. The second option is storage as a compressed gas for which usually less than 2% of the total storage mass is hydrogen. Normally, it is only used for small amounts of hydrogen and it has to be transported with great care. The third option is using reversible metal hydrides where metal reacts with hydrogen and then desorbs the hydrogen under increased temperatures. Since the hydrogen is not stored at elevated pressure, it will not rapidly and dangerously discharge. Also, the decrease in temperature in case of a leak will restrict a large release of hydrogen. Furthermore, since the gravimetric density is similar to compressed gas storage, metal hydrides are chosen for their safety and high volumetric density [69, 70].

Table 7.4: Hydrogen storage options [70].

Hydrogen storage method	Features
Liquid hydrogen	<ul style="list-style-type: none"> - Need for insulating vessel since temperature is -250°C or lower - Practical use on land - Low volumetric density - Boil-off losses and arising pressure must be ventilated - Unsafe when leakage
Compressed gas	<ul style="list-style-type: none"> - Tank mass increases with pressure - Practical use on land - Unsafe when leakage
Metal hydride	<ul style="list-style-type: none"> - High volumetric density - Low gravimetric density and heavy weight - Reversible process - Safer when leakage

The metal hydride can desorb the hydrogen using heat from the fuel cell. This heat is transferred using a heat exchanger [71]. In fig. 7.18, an overview is given of the different components in the fuel cell system. The rate of the water produced is given by eq. (7.18) [69].

$$H_2O_{rate} = 9.34 \cdot 10^{-8} \cdot \frac{P_{FC}}{V_c} \quad (7.18)$$

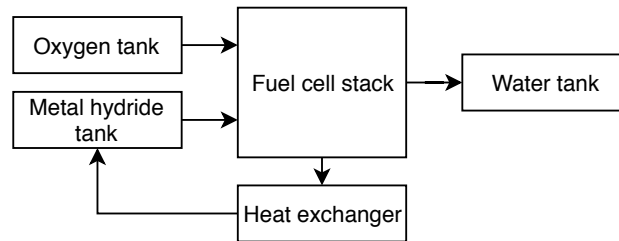


Figure 7.18: Fuel cell system used as a power source for the submarine.

The fuel cell that is used is a 50 W proton exchange membrane fuel cell (PEMFC) [72]. The PEMFC is commonly used as it operates at relatively low temperatures (30-100°C). The slow reaction of these cells is improved by using sophisticated catalysts (i.e. platinum) and electrodes [69]. Although the fuel cell stack has a nominal power of 50 W, it can provide a maximum power up to 67 W. When necessary, this extra amount of power can be used for buoyancy control or propulsion when the submarine has to adjust its path or speed. There fuel cell stack also contains an integrated air blowing fan.

The PEMFC has a stack current of 4.25 A and consists of 20 cells. Using eq. (7.16) and eq. (7.17), a total mass of 2.3 kg hydrogen and 18.3 kg oxygen is needed. The amount of water that is produced is calculated for maximum power and a single fuel cell voltage of 0.6 V using eq. (7.18) which results in 27 L of water produced.

Tank Sizing

The metal hydride will be stored in an aluminum tank at a pressure of 1 bar at room temperature. The metal hydride used has a mass percentage of 2 and volumetric density of 150 kg H₂/m³ [73]. The tank has a spherical shape.

The water tank is also a spherical tank made out of aluminum, more specifically aluminum 6061, with a density of 2720 kg/m³. Both tanks have a thickness of 3 mm for ease of manufacturing. The inner radius is based on the volume of metal hydride and water needed. The volume of both tanks is calculated using eq. (7.19).

$$V_{tank} = \frac{4}{3} \cdot \pi \cdot (r_i + 0.003)^3 \quad (7.19)$$

The oxygen tank is pressurized at 200 bar (density of 279.6 kg/m³) and is sized based on off-the-shelf products with an average empty tank density of 610 kg/m³ and a volumetric density of 969.6 l/m³ [74, 75].

Battery

For the battery component, the same type of batteries is used as mentioned in section 7.7.1. The battery will provide power for the transmission and for the ascent to the surface at the end of the mission. The total amount of energy in the battery is 3.09 kWh, including a 5% safety margin. Since the transmission energy is only a very small part of the total amount, the fuel cell can recharge the battery to restore the energy lost after every transmission. This requires only a very small amount of power from the fuel cell. In table 7.5 the mass and volume values can be found for the different components of the hybrid power subsystem.

Table 7.5: Mass and volume of the hybrid power subsystem.

Component	Mass [kg]	Volume [m ³]
Fuel cell stack	0.9	0.001
Metal hydride tank	117.6	0.016
Oxygen tank	59.4	0.067
Water tank	30.7	0.028
Heat exchanger	3.14	0.002
Battery	20.9	0.012
Total	232.2	0.128

Risk, Sustainability and Cost

The main risk of the fuel cell system would be when there is a leak in the hydrogen tank. Then the hydrogen could be ignited with the ambient air inside the submarine causing a fire. Since metal hydrides are used for the storage of the hydrogen, this risk is close to non-existent.

The PEMFC has an expected lifetime of 10,000 operation hours [76]. If the search system would be continuously used for 30-day primary and secondary missions, the fuel cell would have to be changed every 416 days. The metal alloy used to form the metal hydride can be reused up to 2,000 times [77]. When the fuel cell reaches its end of lifetime, more than 95% of the platinum can be reclaimed during recycling of the membrane electrode assembly. Other components of the fuel cell system such as electronics, valves, pumps can also easily be recycled.

The prices of hydrogen and oxygen per kg are €12 and €2.6, respectively [78, 79]. Fuel cell stacks can be expensive, but since only a 50 W fuel cell stack is used, this price is relatively low. All the prices can be found in table 7.6.

Table 7.6: Cost budget of hybrid system.

Component	Cost [€]
Fuel cell stack [80]	948
Hydrogen	28
Oxygen (incl. tank)	570
Metal alloy (incl. tank) [81]	758
Water tank	15
Heat exchanger	172
Battery	500
Total	2,991

7.7.3. Tradeoff

To compare the two different designs, tradeoff criteria are proposed and a tradeoff is performed. From this, the final power subsystem is chosen.

Tradeoff Criteria

The tradeoff criteria are proposed along with their respective weight in table 7.7. Risk is the most important criterion since if a part of the subsystem fails, it can potentially have catastrophic consequences for the submarine. The second most important criterion is sustainability. Although the ocean polluting options were already discarded, the options left can still be unsustainable when it comes to the production or disposal process. The cost is also an important factor, as the total budget of the mission is fixed and no extremely expensive price can be afforded. Finally, the lesser important criteria are mass and volume. For a certain volume of the submarine, a maximum mass is allowed to avoid sinking to the surface. This is why the mass is more important than the volume. Also, for the retrieval process a lighter submarine is beneficial.

Table 7.7: Tradeoff criteria for power subsystem of the submarine.

Tradeoff criteria	Weight
Safety	5
Sustainability	4
Cost	3
Mass	2
Volume	1

Tradeoff table

When looking at table 7.8, it is clear that the hybrid system wins over the batteries. Both systems have the risk of starting a fire which would destroy the power subsystem. However, for both designs the chances of that happening are minimal.

Table 7.8: Tradeoff summary for the power subsystem.

Criteria	Concept	
	Battery	Hybrid
Risk	Minor chance	Minor chance
Sustainability	Not very sustainable	Recyclable
Cost [€]	14806	2991
Mass [kg]	274.6	232.2
Volume [m³]	0.164	0.128

4 Good
 3 Marginal
 2 Poor
 1 Bad

The batteries are not very sustainable as the production process includes energy extensive and polluting measures. Also, the recycling of the batteries is still not a common procedure but it can be done. For the hybrid system, most of the fuel cell components are recycled but it also includes a smaller battery making it less sustainable.

Although the hybrid system is considerably cheaper, it should be mentioned that for a full lifetime of the batteries, the fuel cell stack has to be replaced (inside the submarine) 13 times making it more expensive over a longer time span. Furthermore, new hydrogen and oxygen have to be bought for every mission.

The mass of both designs is quite large due to the long duration of the mission, but the hybrid system scores slightly better for this criterion.

For the volume, both are quite compact relative to the mass. However, the hybrid system scores better again.

Final Result

The power subsystem of the submarine will be a hybrid system using a fuel cell system supported by a smaller lithium-ion battery. The main components of the fuel cell system are a metal hydride tank, oxygen tank, fuel cell stack, water storage tank and heat exchanger. There is also a power management module to manage the power system [82, 83]. If an instrument develops a fault, the module can shut off the instrument so that no other instruments are affected. In case the power consumption exceeds the power available, the power management module will lower the supply to some of the instruments or shut some down to avoid a blackout.

There is also a DC/DC converter integrated in the subsystem to adapt the voltage to the supply voltage of the specific instruments [84]. Furthermore, a very lightweight capacitor (50 F) is used to provide the 90 W to open and close the electrical valve of the retrieval subsystem [85]. All these components add up to a cost of €3,288. All values for the design can be found in section 7.7.2 and fig. 7.19 shows the electrical diagram of the submarine.

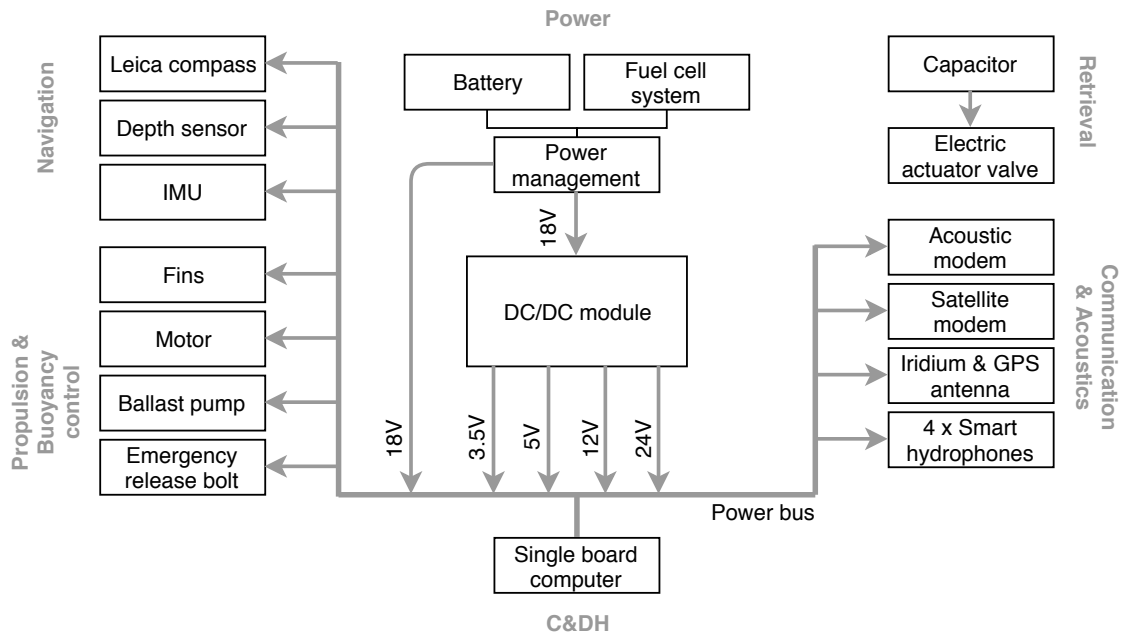


Figure 7.19: Electrical diagram of the submarine.

7.8. Structure Design of Submarine

This section covers the structural design of the submarine. It considers the different load cases and covers the design approach as well as the different failure modes. It ends with the verification and validation of the model made to design the structure.

7.8.1. Load Case Scenarios

In order to determine the optimal dimensions of the submarine structure, the different load cases during operations are considered. The three dominant forces that drive the design of the submarine are: the impact force of the submarine on water, the pressure at the maximum operating depth and the retrieval force.

Impact Force on Water

A high impact force is exerted on the submarine once it hits the water, this is due to the tension of the water surface and the buoyant force working in the opposite direction of movement. Once the submarine hits the water, the impact force is felt as a pressure distribution on the surface of the submarine as shown in fig. 7.20.

An estimate for the the maximum impact force is found by looking at the work performed by the object falling. For this, the displacement of the object and its change in kinetic energy are needed. The displacement is approximated via Newton's equation for the impact depth, see eq. (7.20).

$$D_{proj} \approx l_{sub} \frac{\rho_{sub}}{\rho_{water}} \tag{7.20}$$

This equation is derived by taking into consideration the transfer of momentum of the projectile (submarine) to the medium (water) as it penetrates [86]. Here, l_{sub} is the length of the submarine, ρ_{sub} is the density of the projectile and ρ_{water} is the density of water.

Then, the work performed is determined by calculating the change in kinetic energy. This is done by filling in eq. (7.21) with the mass and corresponding impact velocity from section 6.3.

$$W = \Delta KE = \frac{1}{2} m_s (\Delta v)^2 \tag{7.21} \qquad W = F_{impact} \cdot D_{proj} \tag{7.22}$$

From eq. (7.22) the work done can be interpreted as a force. In order to translate the impact force to a pressure, it is assumed that the force creates a uniform pressure on the impact surface as shown in fig. 7.20.



Figure 7.20: Impact force to impact pressure.

Assuming the submarine has a semi-spherical nose, the equation used to translate the force to an impact pressure is shown in eq. (7.23). To perform this preliminary estimate the drop height is assumed 100 meters, and the mass,

corresponding density and dimensions of a reference AUV are used, e.g. the Remus 6000 [8]. The result of this load case is presented in table 7.9.

$$P_{impact} = \frac{F_{impact}}{A_s} = \frac{F_{impact}}{\pi d_{sub}^2 / 4} \quad (7.23)$$

Pressure at Maximum Depth

The pressure difference between the external and internal pressure of the submarine, plays a driving role in the sizing of the shell structure. For this, the thickness is considered the most determining factor since the submarine operates in deep waters. The pressure at maximum depth is given by eq. (7.24). The seawater density is 1025 kg/m^3 and the atmospheric sea-level pressure is 101325 Pa. Notice the pressure is independent of the mass of the submarine.

$$P_{max} = P_{0_{atm}} + (\rho_{water} \cdot g \cdot h_{depth_{max}}) = 101325 + (1025 \cdot 9.80665 \cdot 4500) = 45.35 \text{ MPa} \quad (7.24)$$

At the maximum operating depth ($h_{depth_{max}}=4,500\text{m}$), the pressure experienced by the submarine is 45.35 MPa, which is significantly higher than the impact pressure. This means that the pressure at maximum depth is *critical for the design of the structure*.

Retrieval Force

The retrieval force represents the maximum force experienced by the search system when it is being picked up by the airborne system. A detailed explanation to determining the force is discussed in section 9.2. The maximum retrieval acceleration experienced by the submarine is 4.9g. Thus, the *retrieval force is not critical* because its magnitude is significantly smaller than the impact load and the depth pressure.

It is important to note that all retrieval options require additional modifications to the structure of the search system such that it can be retrieved. These modifications are not considered part of the load-carrying structure and thus are neglected in the structure design process. The results of the load case analysis is presented in table 7.9. The critical load case to design for is the pressure at operating depth, this is pressure is highlighted in table 7.9.

Table 7.9: Driving forces on the submarine and their influencing parameters.

Parameter	Reference Submarine (REMUS6000 [8])
Mass [kg]	862
Diameter [m]	0.69
Impact Velocity [m/s]	68.98
Impact Depth [m]	1.98
Impact Force [N]	$1 \cdot 10^6$
Impact Pressure [MPa]	2.61
Pressure at 4500 m depth [MPa]	45.35

7.8.2. Design Approach

The ultimate goal of the structure is to have a lightweight, but still positively buoyant body that can fit the payload in its interior.

The design of the submarine structure is an iterative process. Nevertheless, to size the load-carrying shell, preliminary dimensions from reference AUVs are used such as the Remus 6000 [8]. To compute the load case analysis a Python script is used; the analytical method implemented on the program is described in the subsequent subsections. Initially the fixed parameters are the diameter (set to 0.6 m) and the slenderness ratio ψ_{sub} which is defined in eq. (7.25).

$$\psi_{sub} = \frac{l_{sub}}{d_{sub}} \quad (7.25)$$

This ratio is fixed with the value of $\psi_{sub} = 5$ since this value results on a low drag, but stable body for different Reynolds numbers [87]. These parameters (diameter and ψ_{sub}) are then input in the script. An overview of the design process (which is also followed by the Python script) can be found in fig. 7.21.

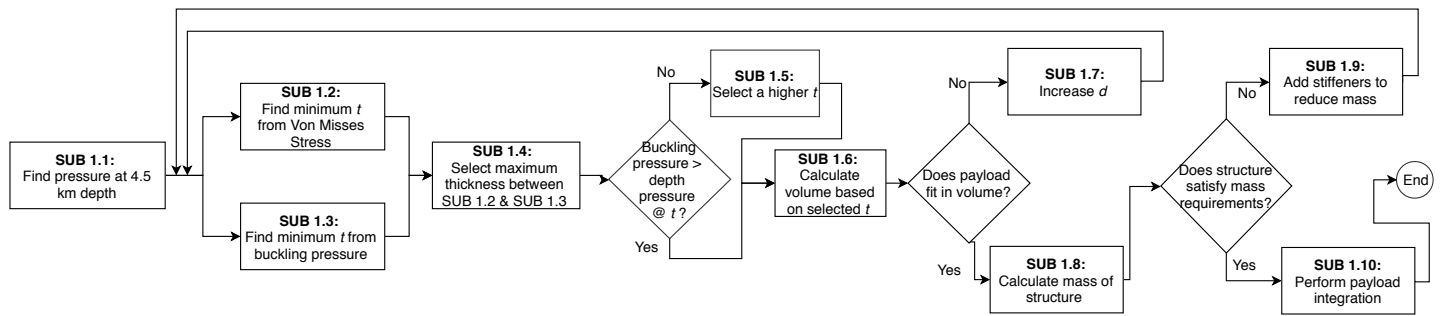


Figure 7.21: Overview of design approach of the submarine structure.

Assumptions Sizing the shell requires the stress analysis of the different sections of the submarine. For the analysis, the submarine was split in two sections: the semi-spherical shells at the ends and the cylindrical shell. The assumptions for computing the failure modes for the cylinder can be found below.

- i The external pressure exerted on the cylinder is the maximum operating pressure of 45.35 MPa (at 4,500 m depth).
- ii The possible failure modes at the load case are yield of material and shell buckling.
- iii The cylindrical shell has the same thickness along its length.
- iv The only load acting on the shell is the external water pressure.
- v The material is assumed to have no imperfections.
- vi External pressure is uniform along the surface of the cylinder.
- vii The diameter is much greater than the thickness. Thus, thin wall assumptions apply for the stress.
- viii The bending and twisting moments created by external pressure are negligibly small when compared to the external pressure. Thus, the normal stresses due to these moments are neglected.
- ix The buckling of the shell is symmetrical with respect to the center of the cylinder.
- x The buckling of the shell creates small deflections of the uniformly compressed hull.
- xi All shear stresses are zero.

Material Properties It is important to consider the type of material used in the structure since this directly affects the weight, the thickness and the manufacturing process of the submarine. Table 7.10 presents commonly used materials for AUVs.

Table 7.10: Properties of pressure hull materials. [88–90]

Material	Density [kg/m^3]	E [GPa]	Poisson Ratio [–]	Compressive Yield Strength [MPa]
Steel HY80	7800	207	0.28	550
Steel HY130	7800	207	0.28	890
Aluminum (L65 Alloy)	2800	70	0.34	390
Titanium (6-4 STOA Alloy)	4500	110	0.33	830
GRP (Epoxy/S-Glass UD)	2100	65	0.23	1200
CFRP (Epoxy/HS Carbon UD)	1700	210	0.3	1200
MMC (Aluminum/SiC Fiber UD)	2700	140	0.17	3000

7.8.3. Failure Mode: Yield

The submarine section is considered to fail in yield when the von Mises stress on the section exceeds the compressive yield strength of the selected material. It is important to note that the only the cylindrical section of the submarine will be pressurized. Thus, the thickness of the spherical caps will not be sized.

A cylindrical vessel has two types of stress in the material: longitudinal stress and cylindrical stress. The longitudinal stress is given in eq. (7.26). The circumferential stress is given in eq. (7.27). [91]

$$\sigma_{long} = \frac{P_{depth} r_o}{2t} \quad (7.26)$$

$$\sigma_{circ} = \frac{P_{depth} r_o}{t} \quad (7.27)$$

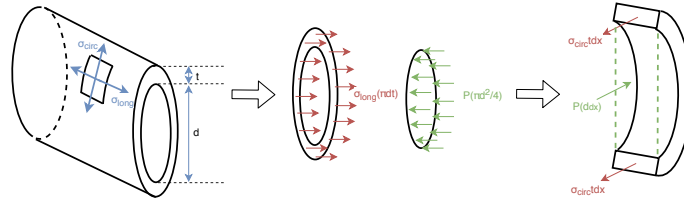


Figure 7.22: Stress forces for cylindrical pressure vessels.

To get the stresses described above, a preliminary diameter is fixed and the pressure at 4,500 m is used with a varying thickness, t_{sub} . Subsequently, with the circular and longitudinal stress known, the resultant stress, i.e. the von Mises stress, can be determined. This is done by filling in eq. (7.28). Since the external pressure is uniform, the shear stresses are assumed to be zero as seen in eq. (7.29).

$$\sigma_{vm} = \sqrt{\frac{1}{2} \left[(\sigma_x - \sigma_y)^2 + (\sigma_y - \sigma_z)^2 + (\sigma_z - \sigma_x)^2 \right] + 3\tau_{yz}^2 + 3\tau_{xy}^2 + 3\tau_{xz}^2} \quad (7.28)$$

$$\sigma_{vm} = \sqrt{\frac{1}{2} \left[(\sigma_{long} - \sigma_{circ})^2 + (\sigma_{circ} - 0)^2 + (0 - \sigma_{long})^2 \right] + 0^2 + 0^2 + 0^2} \quad (7.29)$$

In fig. 7.25, the compressive yield strength and von Mises stress for varying thickness is plotted for the materials from table 7.10. The intersection point determines the minimal thickness required to withstand failure due to yield. As one can see, MMC requires the smallest thickness to withstand yield failure. Nonetheless CFRP is chosen because of its lowest thickness and density combination, see point A in fig. 7.23.

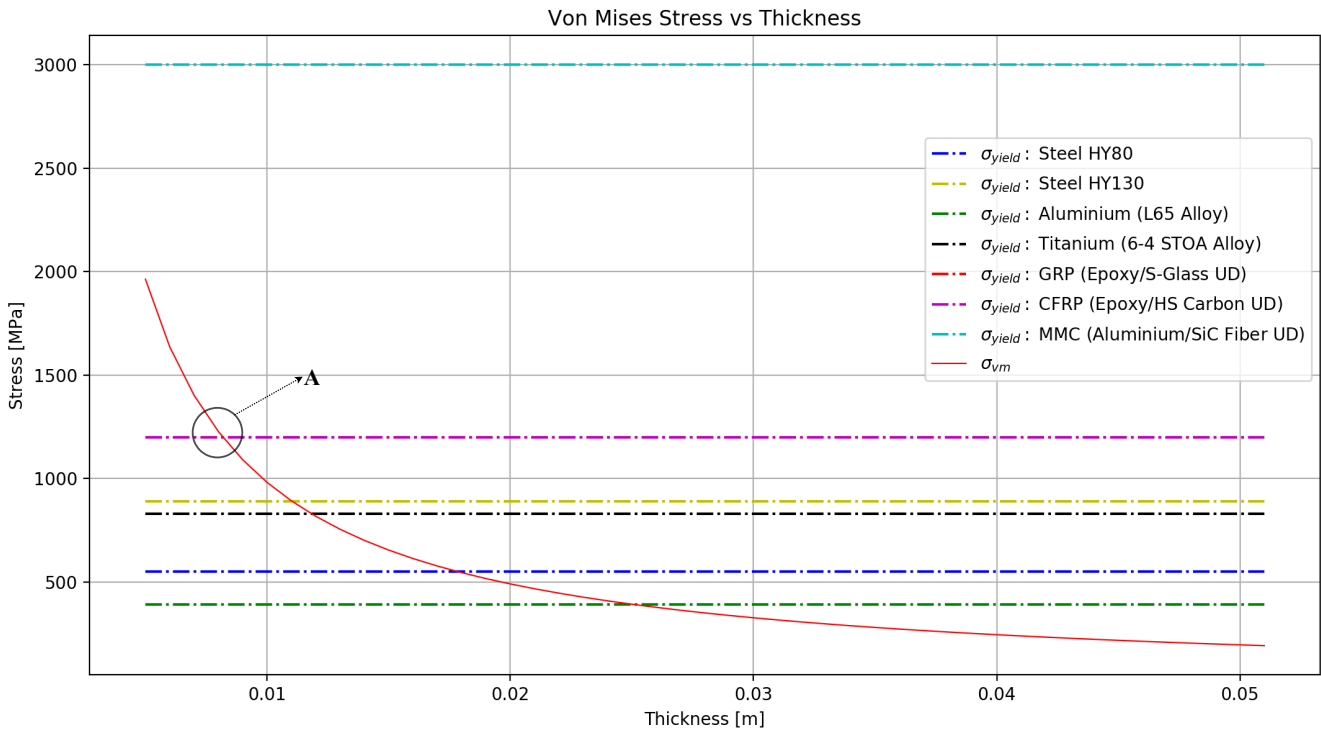


Figure 7.23: Compressive yield strength of discussed materials and von Mises stress versus varying thickness.

7.8.4. Failure Mode: Buckling

(Unstiffened) Buckling Failure After determining the critical thickness to withstand yield failure, the limit for buckling failure must be determined. This is done by looking at the shell instability of the cylindrical vessel under uniform external pressure [92]. First the von Mises equation for elastic instability pressure is used, see eq. (7.30). This equation holds for relatively short tubes firmly supported at their ends subjected to the combination of uniform lateral and axial pressure.

$$P_{crvm} = \frac{E(t/a)}{[n^2 - 1 + 0.5(\pi a/l_{cyl})^2]} \cdot \left\{ \frac{1}{[n^2(l_{cyl}/\pi a)^2 + 1]^2} + \frac{t^2}{12a^2(1-\nu^2)} \left[n^2 - 1 + \left(\frac{\pi a}{l_{cyl}} \right)^2 \right]^2 \right\} \quad (7.30)$$

As one can see, the critical buckling pressure depends on the amount of lobes (n) into which the vessel will buckle. The value of n corresponding to the minimum buckling pressure is called the buckling eigenmode. This is determined by fixing a certain thickness to radius ratio and subsequently plotting the buckling pressure versus the amount of lobes. As seen in fig. 7.24, for a preliminary thickness of 0.03 m and radius of 0.25 m, a minimal buckling pressure is obtained at $n=4$ for all materials discussed in table 7.10. By changing the thickness, the buckling eigenmode varies between $n=3$ & $n=4$. Therefore, it is concluded to use a fixed value of $n=4$ for any thickness used in eq. (7.30).

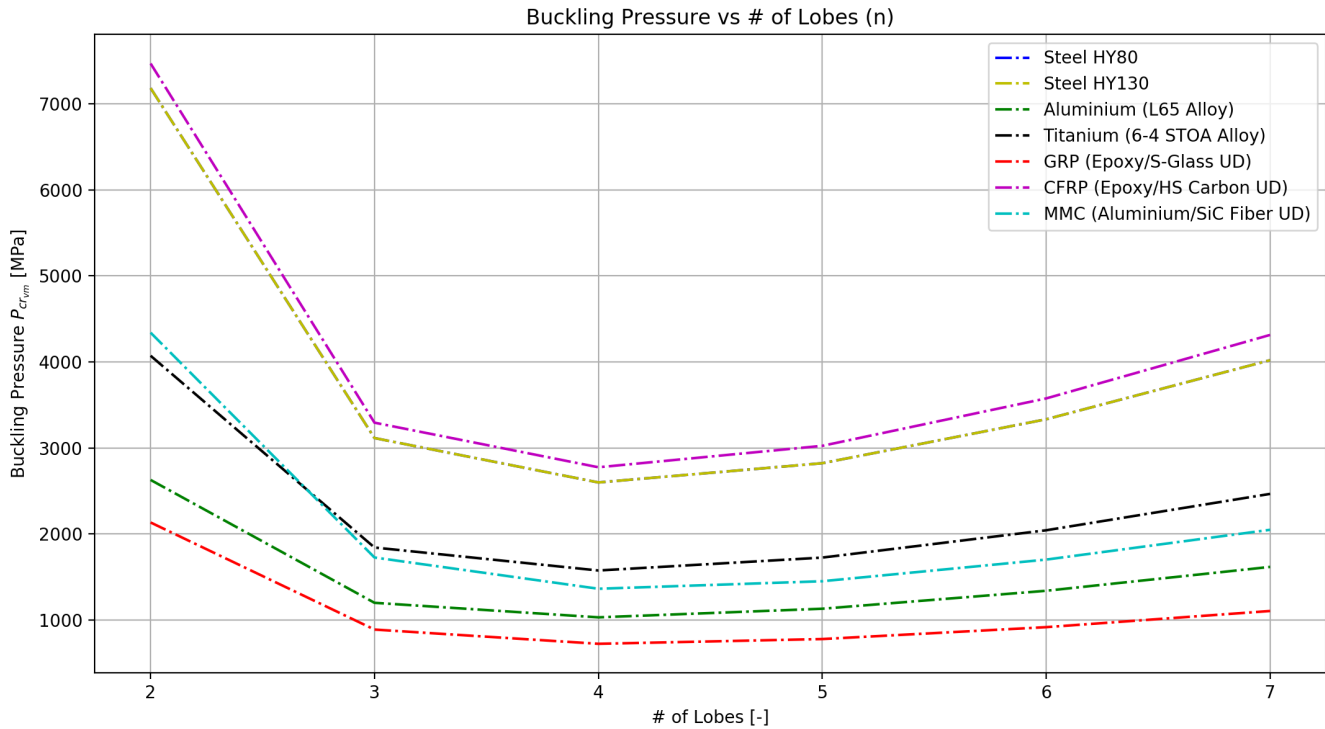


Figure 7.24: Determination buckling eigenmode for discussed materials.

A simpler version of the von Mises buckling equation that predicts a similar buckling pressure, is provided by Windenburg and Trilling [92]; these are presented in eq. (7.31). Now, however, the critical buckling pressure does not depend on the number of lobes. Later on, this equation can be used to determine the buckling pressure for a stiffened cylindrical vessel.

$$P_{cr_{wb}} = \frac{2.42E(t/2a)^{5/2}}{(1-\nu^2)^{0.75}[(l/2a) - 0.447(t/2a)^{1/2}]} \quad (7.31)$$

Lastly, another equation is used for determining the critical buckling pressure, see eq. (7.32). This equation holds for a cylinder with shorter length where the ends are free to expand axially and rotate with the restriction of expanding radially [93]. Note that, similar to eq. (7.30), this equation also depends on the number of lobes into which it will buckle. For consistency, again a fixed value of $n=4$ is used.

$$P_{cr_{chatt}} = \frac{2E}{3(1-\nu^2)} \left(\frac{t}{d_{sub}} \right)^3 \left[(n^2 - 1) + \frac{2n^2 - 1 - \nu}{1 + \frac{4n^2 L^2}{\pi^2 d_{sub}^2}} \right] + \left[2E \left(\frac{t}{d_{sub}} \right) \frac{1}{(n^2 - 1) \left(1 + \frac{4n^2 L^2}{\pi^2 d_{sub}^2} \right)} \right] \quad (7.32)$$

Now, as done for the yield failure, the minimum thickness required to withstand buckling failure is determined. This is done by plotting all three discussed buckling pressure equations for the material CFRP with the buckling pressure on the y-axis and varying thickness on the x-axis. By looking at fig. 7.25, one can see that the higher the thickness, the more the methods diverge. From this, it is concluded that they are comparable for small thicknesses only. Furthermore, the pressure at a depth of 4,500 m is plotted in fig. 7.25. The critical thickness is the point at which the buckling pressure is equal to the pressure at 4,500 m depth. These points are marked with **B**, **C** & **D** for each respective equation.

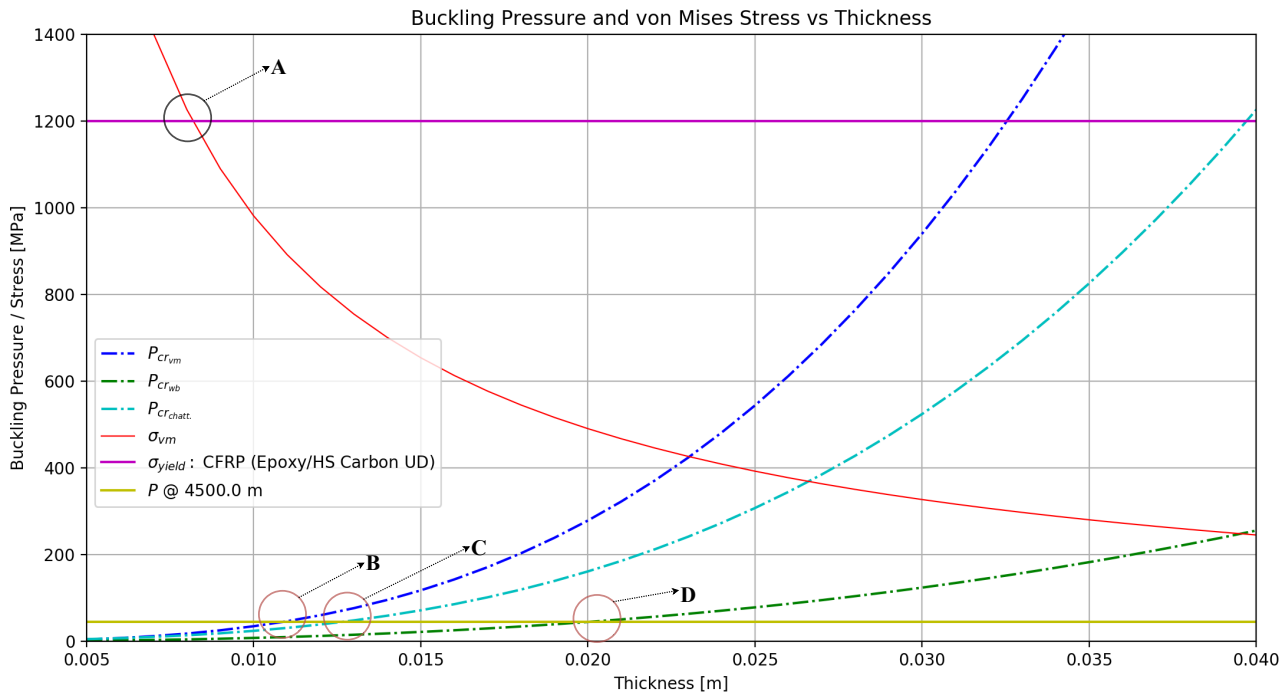


Figure 7.25: Analysis of pressure/stress limits with corresponding thickness for an unstiffened cylindrical vessel.

The buckling pressure and corresponding thickness for every failure mode can be found in table 7.11. Since these are all approximations with no explicit order of accuracy, the one with the highest thickness needed was chosen for the design. The critical thickness due to buckling failure has the highest value and will therefore be used for sizing the hull. Then, with the thickness, density of the material, diameter and length known, the volume and mass of the hull can be determined by filling in eq. (7.33) and eq. (7.34). It is important to note that using different methods to find the critical buckling pressure leads to uncertainties in the correctness thickness. Because of this, eq. (7.31) is used in further calculations since this method is the most conservative of the three used.

$$V = \frac{4}{3}\pi r^3 - \frac{4}{3}\pi(r-t)^3 + (\pi r^2 - \pi(r-t)^2) \cdot l_{sub} \quad (7.33) \quad m = \rho V_s \quad (7.34)$$

Table 7.11: Buckling pressure and corresponding thickness of critical points marked in fig. 7.25.

Variable	Buckling Pressure [MPa]	Thickness [m]
Yield Failure (A)	1200	0.0082
Buckling Failure (B)	45.35	0.011
Buckling Failure (C)	45.35	0.0126
Buckling Failure (D)	45.35	0.0201

(Stiffened) Buckling Failure In order to reduce the total weight of the structure, the thickness must be reduced. This can be done by adding CFRP ring stiffeners to the shell structure and performing a similar buckling and yield failure analysis on the cylindrical shell structure. To determine the optimal amount of ring stiffeners, eq. (7.31) can be used. Note that this equation *does not consider the geometrical aspect of the stiffeners*. The stiffener implementation is merely by a reduction in the effective free length (l_{sub}) of the cylinder. For example, adding three equally spaced ring stiffeners, leads to an effective length of 1/4 of the length of the original cylinder. A schematic view of an internal ring stiffened shell structure with 3 ring stiffeners can be seen in fig. 7.26.

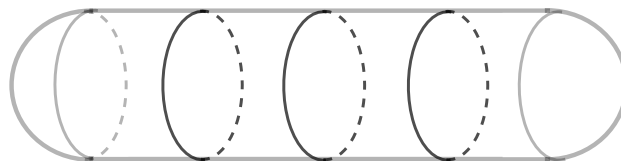


Figure 7.26: Schematic view of an internal ring stiffened shell structure.

Equation (7.31) is used to compute the buckling pressure for varying number of stiffeners as presented in fig. 7.27. From a simple inspection of the graph it can be observed that the curve becomes more steep with the more stiffeners there are. This is as expected since the effective length that would buckle is reduced.

From fig. 7.27 it can be observed that the minimum thickness for the shell to buckle and/or yield at approximately the same pressure is 0.08 m. This is because at this thickness the von Mises stress in the material reaches the yield stress, σ_{yield} . The selected thickness in fig. 7.27 should be outside the red shaded areas; however to maintain the mass at a minimum, the thickness should be as small as possible within the constrained area.

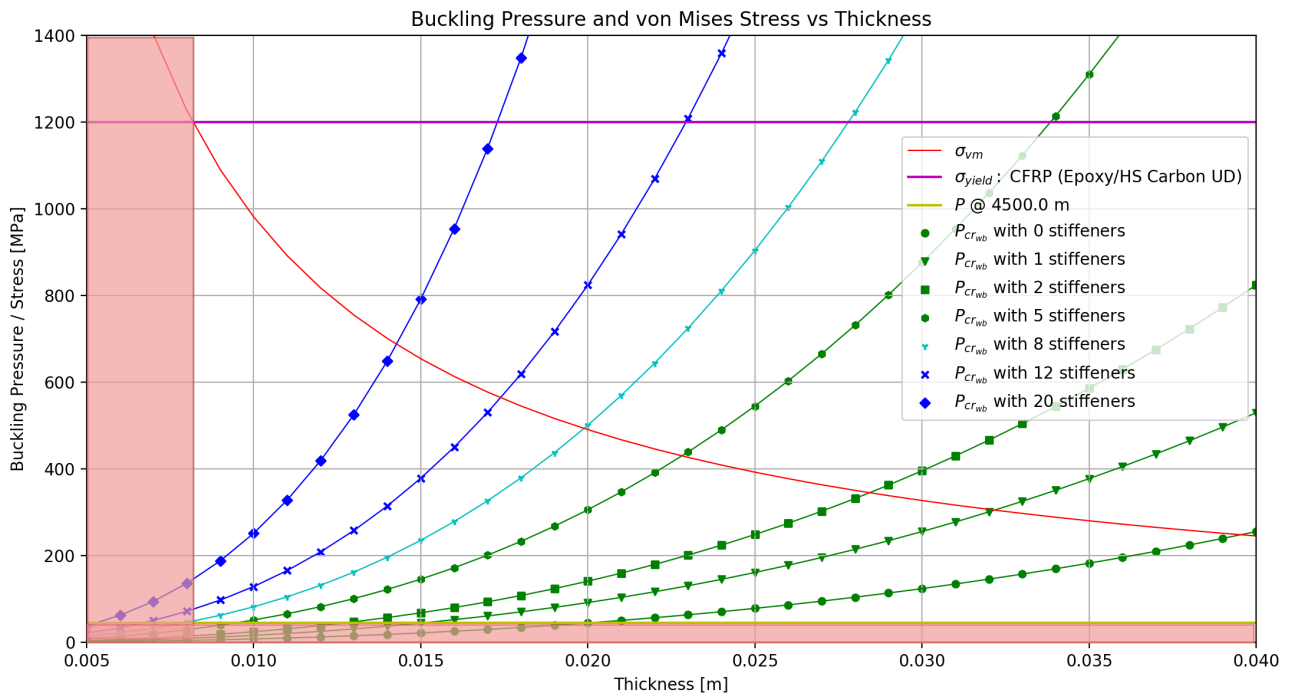


Figure 7.27: Critical thickness for varying number of stiffeners of a cylindrical shell with diameter $d_{sub} = 0.5$ m.

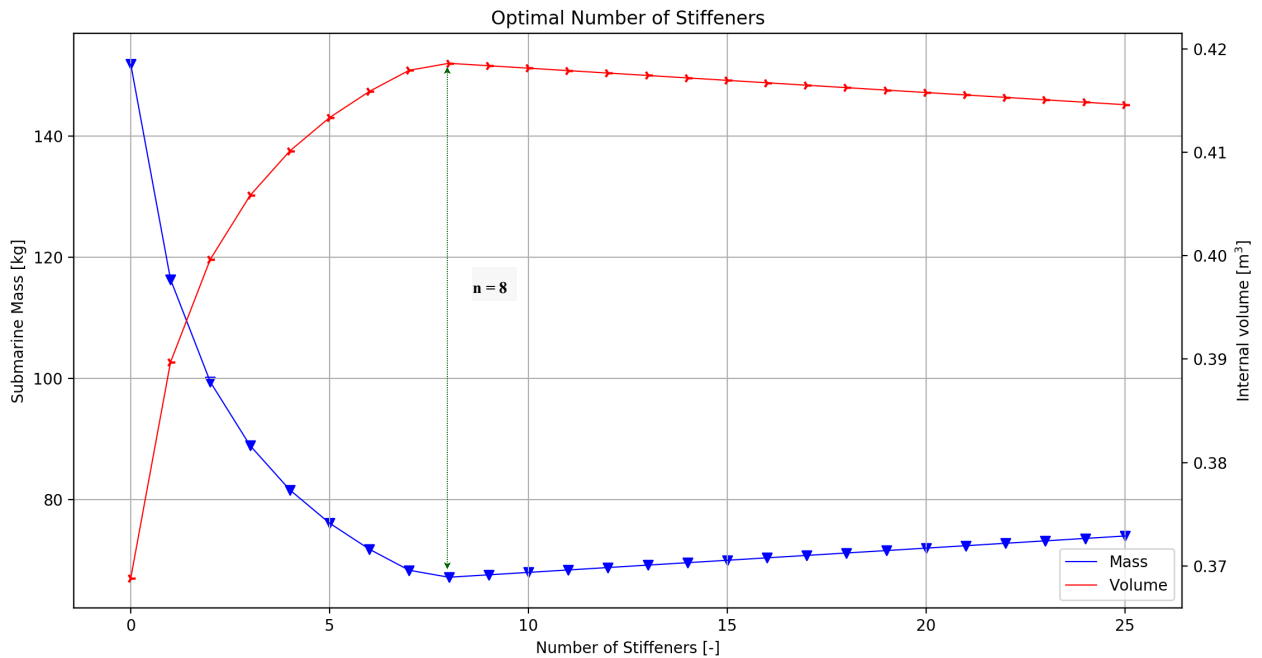


Figure 7.28: Graph showing variation of shell mass and volume as a function of the number of stiffeners. The optimal number of stiffeners is shown with the green arrow.

The optimal thickness and number of stiffeners can then be obtained from fig. 7.28. The optimal point is where

vertical distance between the mass and volume is maximum; in this case for 8 stiffeners as depicted by the green vertical line. Something to consider is that increasing the number of stiffeners also increases the mass since the thickness is kept its critical value. Subsequently, the internal volume goes down since the effective internal volume decreases by adding extra internal ring stiffeners at the same critical thickness.

Axisymmetric deformation When adding stiffeners to reduce the shell thickness, larger stresses will be imposed on the shell (resulting in a von Mises stress) that might exceed the yield criteria of the material. To address this potential problem, the axisymmetric deformation of the ring-stiffened circular cylinder is analyzed. Ross [92] presents the differential equation, given by eq. (7.35), that describes the deformation behaviour of the cylindrical shell due to an external pressure. Ross, also presents the solution to the equation which can be seen in eq. (7.37).

$$\frac{d^4 w_d}{dx^4} + 4\alpha^4 \beta^2 \frac{d^2 w_d}{dx^2} + 4\alpha^4 w_d = \frac{12(1-\nu^2)C_0}{t^2 a^2} \quad (7.35)$$

To solve this, boundary conditions ought to be set. For a symmetrical deformed shell about mid-span, the following boundary conditions assumed by Wilson are:

- i. w_d is symmetrical about $x=0$ (mid-span);
- ii. $\frac{dw_d}{dx} = 0$ at $x=\pm L/2$;
- iii. $\frac{Et^3}{6(1-\nu^2)} \frac{d^3 w_d}{dx^3} = G_1 w - H_1$ at $x=\pm L/2$;

$$G_1 = E(A_f/a_f^2 + b_f t/a^2) \quad (7.36)$$

As seen above, G_1 is a function of the dimensions and positioning of the ring stiffeners. For the stiffened structure, internal ring stiffeners with a rectangular cross-sectional area of 1.5 by 1 cm are used. The solution is given in eq. (7.37) and is only valid for evenly spaced stiffeners.

$$w_d = A_1 \cosh F_1 x \cos F_2 x + A_2 \sinh F_1 x \sin F_2 x + C_0 \quad (7.37)$$

Furthermore, the coefficients in eq. (7.35) are shown in the equations below.

$$\alpha^4 = 3(1-\nu^2)/(a^2 t^2)$$

$$\beta^2 = \frac{pa^3}{2Et} + \frac{t^2 \nu}{12(1-\nu^2)} \quad (7.38)$$

$$C_0 = pa^2(1-\nu/2)/(Et)$$

$$F_1 = \alpha \sqrt{(1-\alpha^2 \beta^2)}$$

$$F_2 = \alpha \sqrt{(1+\alpha^2 \beta^2)} \quad (7.39)$$

The arbitrary constants, A_1 & A_2 , are obtained from boundary conditions i & ii as $A_1 = N_1/D_{12}$ and $A_2 = N_2/D_{12}$. N_1 , N_2 & D_{12} are determined by filling in the following equations;

$$N_1 = -(G_1 C_0 - H_1) \cdot (F_1 \cosh 0.5 F_1 L \sin 0.5 F_2 L + F_2 \sinh 0.5 F_1 L \cos 0.5 F_2 L)$$

$$N_2 = (G_1 C_0 - H_1) \cdot (F_1 \sinh 0.5 F_1 L \cos 0.5 F_2 L - F_2 \cosh 0.5 F_1 L \sin 0.5 F_2 L) \quad (7.40)$$

$$D_{12} = \{Et^3/(12(1-\nu^2))\} \{2F_1 F_2 (F_1^2 + F_2^2) (\cosh F_1 L - \cos F_2 L)\} + 0.5 G_1 (F_1 \sin F_2 L + F_2 \sinh F_1 L)$$

By plotting the deflection along the length, a buckling pattern can be seen. As one can see, the deflection is symmetrical along the effective free length and equals zero at the junction points, i.e. stiffener locations. In fig. 7.29, the deflection along the length of the cylinder is plotted for a shell structure with 3 internal ring stiffeners.

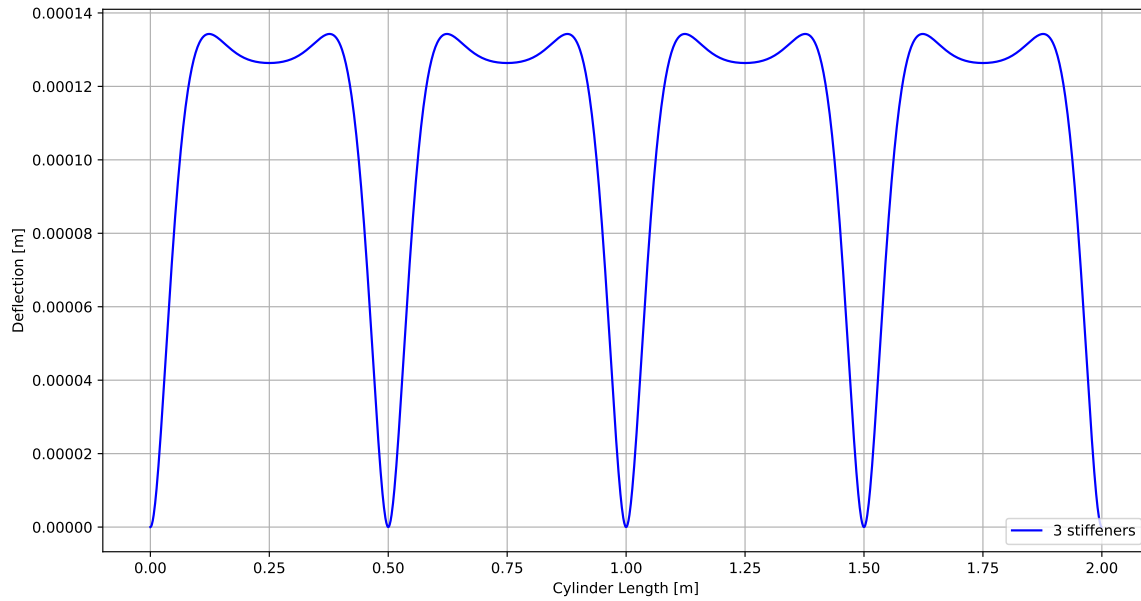


Figure 7.29: Deflection of cylindrical shell structure with 3 internal ring stiffeners.

Lastly, the stress distributions across the bay can be obtained by calculating the circular and longitudinal stress again for every point along the length. This is done by substituting eq. (7.37) and eq. (7.41) in eq. (7.42) & eq. (7.43).

$$\frac{d^2 w_d}{dx^2} = [A_1(F_1^2 - F_2^2) + 2A_2F_1F_2] \cosh F_1 x \cos F_2 x + [A_2(F_1^2 - F_2^2) - 2A_1F_1F_2] \sinh F_1 x \sin F_2 x \quad (7.41)$$

$$\sigma_{circ} = -\frac{Ew_d}{a} - \frac{pav}{2t} \pm \frac{Et}{2(1-\nu^2)} \left(\frac{w_d}{a^2} + \nu \frac{d^2 w_d}{dx^2} \right) \quad (7.42)$$

$$\sigma_{long} = -\frac{pa}{2t} \pm \frac{Et}{2(1-\nu^2)} \left(\frac{\nu w_d}{a^2} + \nu \frac{d^2 w_d}{dx^2} \right) \quad (7.43)$$

If the hoop and longitudinal stresses are known for each point along the length of the load carrying cylindrical shell, the von Mises stress can be computed and compared with the compressive yield stress of the material selected. If the von Mises stress is larger than σ_{yield} of the material, then the shell will yield. For example the largest von Mises stress for the given example above with 3 stiffeners is 745 MPa, which in this case means the material will not yield with three stiffeners.

Results and Dimensions

The results of the performed approach are obtained via an iterative procedure. In the following table, the final dimensions, mass and volume of the submarine design are shown. Furthermore, a safety factor of 20% is taken into account for the thickness. This is done to avoid the structure being on the limit of buckling and also to compensate for inaccuracies.

Table 7.12: Final dimensions of submarine structure with and without safety factor of 20%.

	Length [m]	Diameter [m]	Thickness [m]	Number of Stiffeners [-]	Stiffener Mass [kg]	Total Mass [kg]	Inner Volume [m ³]	Outer Volume [m ³]
Final Design	2.5	0.5	0.0082	8	0.40	56.74	0.43	0.46
Final Design incl. SF	2.5	0.5	0.0098	8	0.40	67.19	0.42	0.46

7.8.5. Verification & Validation

This subsection discusses the verification method of the program created to size the structure of the submarine. A validation method that can be used to validate the design is also proposed in this section.

Verification

To verify the program, a set of tests are performed such as consistency and system tests to find the optimal thickness.

To verify the results obtained to find the critical buckling pressure and corresponding thickness (from eq. (7.31), or the green curve in fig. 7.25), a *system test* was done by comparing the results presented by the original author, Windenburg [94]. The book presents the critical buckling pressure for a set of cylindrical vessels with the given parameters as presented in table 7.13. As it can be seen, the maximum difference between the computed pressures $P_{cr_{wb}}$ is only 0.64% which thereby verifies the Python script. A reason for the minor difference could be because of rounding; Windenburg rounds the value to the closest integer.

Table 7.13: Verification by comparison of the buckling pressure using eq. (7.31).

Input Values	$P_{cr_{wb}}$ Windenburg [94]	$P_{cr_{wb}}$ Python Script	Difference
t = 0.05 in. d = 60 in. $l_{cyl} = 32$ in. E = 32 lb/in. ²	23 [lbs/in. ²]	22.995 [lbs/in. ²]	0.0217%
t = 0.0635 in. d = 16 in. $l_{cyl} = 32$ in. E = 30 lb/in. ²	39 [lbs/in. ²]	39.253 [lbs/in. ²]	0.64%

A *consistency test* was performed to assess if the program changes the value of outputs as expected by changing an input parameter. Two cases were analyzed and compared to observe the output of the program: case 1 consists of a thickness of 0.015 and case 2 is double the thickness. For case 2, it is expected that the mass of the shell will be close to two times the thickness of case 1. This is because the mass is a function of the volume, and doubling the thickness does not necessarily double the volume. The results are presented in table 7.14.

Table 7.14: Results on mass change when thickness is doubled (consistency test).

Consistency Test	Thickness [m]	Mass [kg]	Stiffener Mass [kg]	# of Stiffeners
Case 1: Original Thickness	0.015	97.765	0.4	1
Case 2: Double Thickness	0.03	187.942	0.4	1

For continuity of this consistency test, the deflections are also plotted for case 1 and case 2 in table 7.14. The deflections are shown in fig. 7.30, and as expected, the deflection of case 2 is significantly smaller than the deflection of case 1 since a larger thickness withstands a higher buckling load. Note that the deflection at the position of the

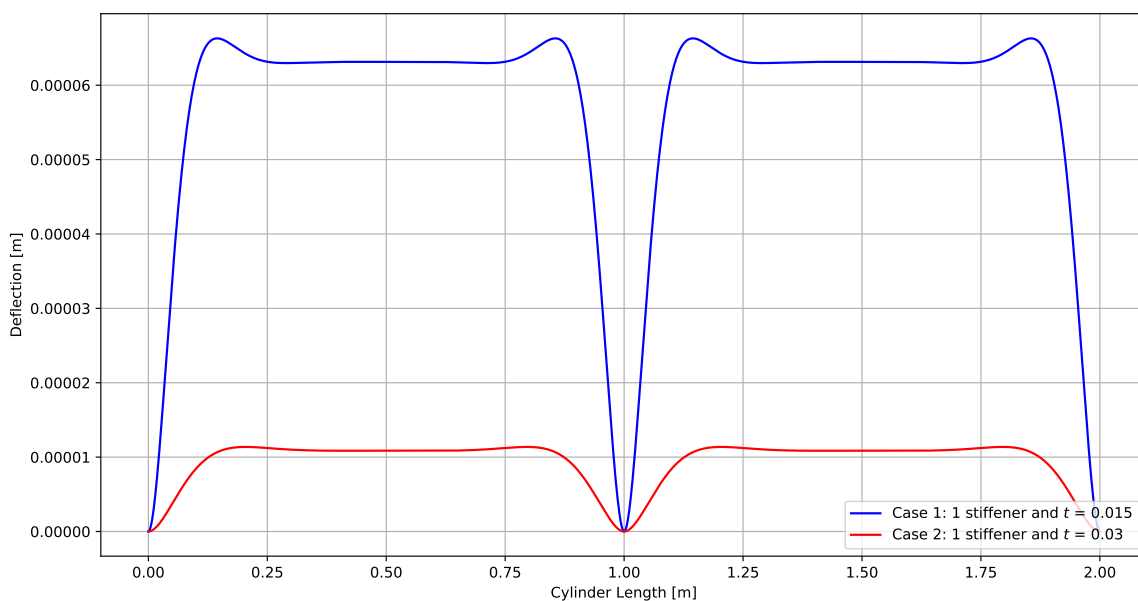


Figure 7.30: Deflection of both case 1 and case 2 from the consistency verification test.

Validation Proposal In order to validate that the submarine structure performs as it is designed to, experimental data is required. Due to the uniqueness of the product and its operating conditions, an experiment is proposed that could potentially be used to validate the design.

Experiment Goal: Quantify the actual external pressure at which the submarine shell fails either in yield or in buckling.

Experiment Outline: A set of different hydro-static pressure tests can be performed to test the shell at a pressure similar to that at 4,500 m depth in the ocean. The fundamental principle is based on pumping a fluid into a pressure chamber. This fluid consequently is compressed as more fluid is pumped in. Different experiments have been proposed that are able to control the volume inside the pressure chamber [95]. A schematic drawing of the test set up is shown in fig. 7.31.

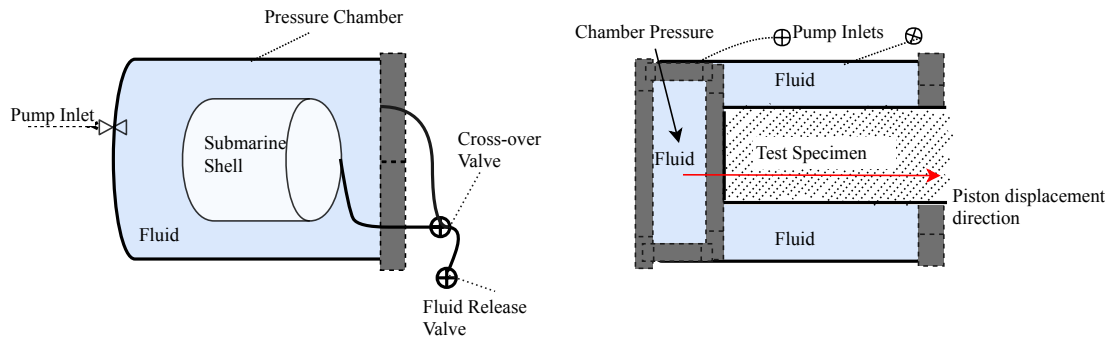


Figure 7.31: Proposed test set up to validate the design of the submarine shell. A close-ended test set up (Left) and a volume-control set up (right) are shown.

The set up on the left side of fig. 7.31 first pre-pressurizes the specimen by pumping fluid through the cross-over valve. Then, by opening the fluid release valve and closing the cross-over valve, external pressure is applied to the test specimen. This type of test is called a volume control test. The right side of fig. 7.31 presents a test set up in which the axial pressure can also be applied to the shell by means of a piston [95].

Additionally, to further investigate the buckling behaviour during the test, strain gauges can be placed at locations where buckling is expected to occur.

Experiment Outcome: The expected outcome of this test is a set of data measured from pressure gauges and strain gauges that can be analyzed to quantify the pressure of failure. In addition this data can be used to improve the design.

7.9. Budget Breakdown

Table 7.15 shows the mass, power and energy budgets for the submarine. In addition to the expected values as computed in the previous sections, contingencies are given to reflect the certainty of the values at this stage in the design. The contingencies were initially taken from [96] and then adjusted to reflect the specifics of the subsystem.

The payload contingencies were adjusted down, because the selected hydrophone has been proven to work during similar missions. The contingency for the navigation has been increased to allow for the potential addition of an extra sensor if the accuracy of the navigation subsystem proves to be insufficient. The power contingency of the communication subsystem was increased significantly to account for uncertainties in the required bit rate and distance between the submarine and mother buoy. Similarly, the power contingency for the buoyancy control system is larger to account for the possible necessity to perform more climbs at large depth.

Table 7.15: Mass, power and energy budget of the submarine.

Subsystem	Mass [kg]	Mass contingency [%]	Power [W]	Power contingency [%]	Energy [kWh]	Energy contingency [%]
Payload	4.0	5	4.8	5	3.5	5
Navigation	5.5	15	15.5	15	11.2	15
Structure	67.0	15	0	-	0	-
Communication	8.1	10	19.5	20	2	20
C&DH	2.5	10	0.3	10	0.2	10
Power	232.2	15	0.3	10	0.2	10
Propulsion	2.0	15	27	15	19.4	15
Buoyancy control	80.0	10	3097	20	0.9	20
Retrieval mechanism	3.4	5	90	5	0.5	5
Total	393	-	-	-	37.9	-

7.10. Software Diagram

The software diagram in fig. 7.32 shows the interactions between the command and data handling subsystem (C&DH) and the other subsystems for which software has to be developed.

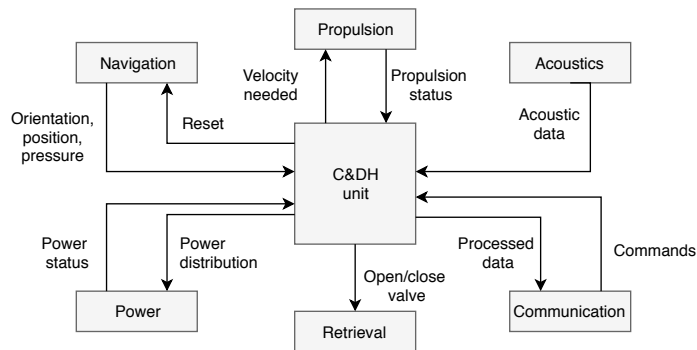


Figure 7.32: Software diagram of the submarine.

7.11. Summary

The submarines are cylindrical in shape with spherical ends on either side. It will have a total length of 2.5 m and a diameter of 0.5 m. The shell will be made out of 0.0098 m thick CFRP reinforced by 8 ring stiffeners. Three control surfaces will be mounted on the aft spherical end; one rudder and two horizontal control surfaces. A single propeller will be mounted on the rear end of the shell to provide the necessary 18.4 N of thrust.

A simple drawing made from a 3-dimensional CAD model shown in fig. 7.33 shows the main structure and layout of the instruments. A visual impression of the submarine showing the inside structure can be seen in fig. 7.34. In addition, a top view and side view of the submarine can be found in fig. 7.35

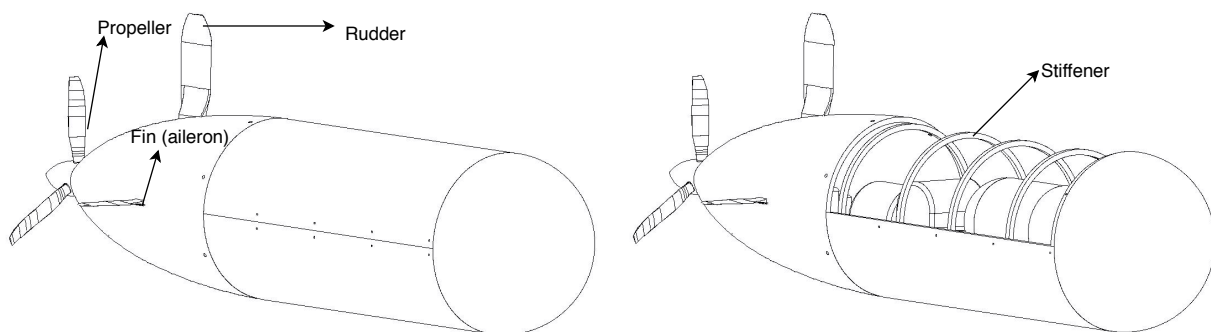


Figure 7.33: Isometric view of the submarine structure and the elements it houses.

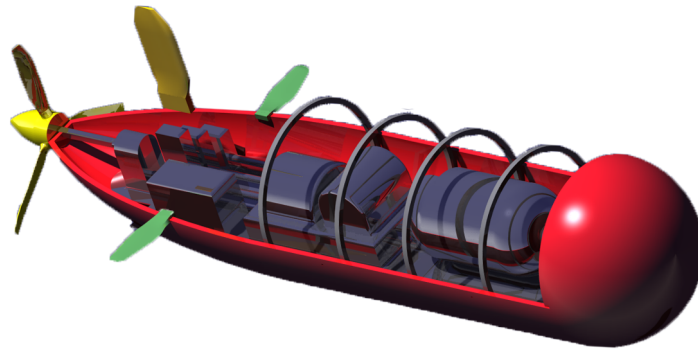


Figure 7.34: Visual impression of submarine structure.

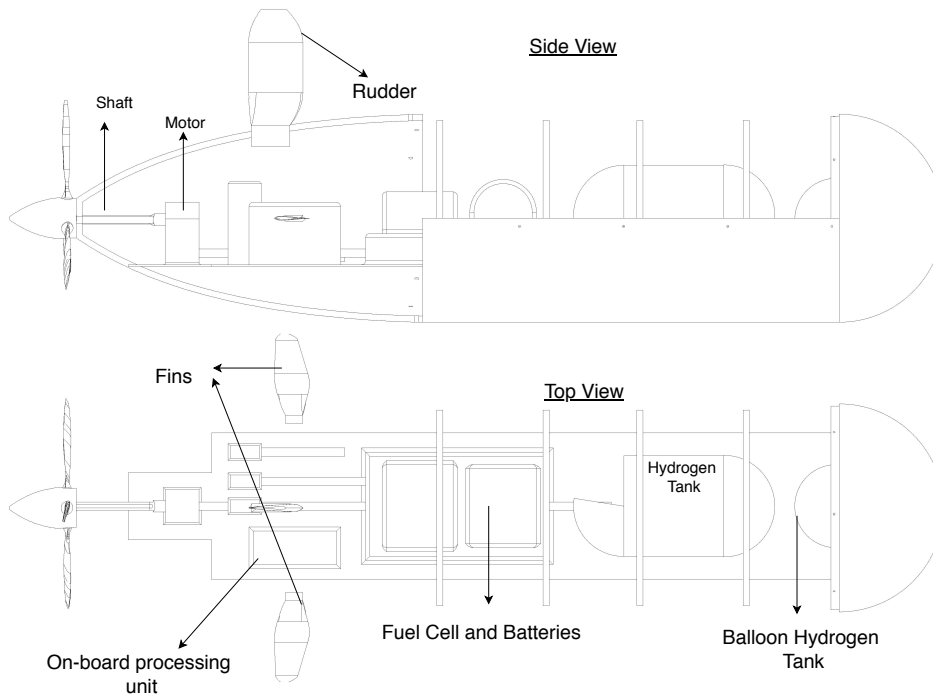


Figure 7.35: Top and side view of the submarine structure and the elements it houses.

The shell houses the rest of the subsystems. The payload consists of an array of four hydrophones to pick up the ULB signal. To determine its position while underwater the submarine uses a leica compass, a depth sensor and an internal navigation unit. In addition to this it has a GPS antenna for use at the water surface. The submarine communicates its payload data and location with the mother buoy via an acoustic modem. It is also equipped with an iridium antenna and satellite modem for communication at the surface.

To control its depth the submarine uses a variable ballast system, consisting of two tanks with a total volume of 0.11 m^3 and a ballast pump. This system is backed up by an emergency ballast mounted on the outside of the shell. For retrieval the submarine houses a balloon and a hydrogen tank to inflate it. Finally all the subsystems are powered by a hybrid power system. This consists of a 50 W fuel cell used for the systems that constantly need power, supplemented with batteries for moments of high power consumption. The total mass of the submarine is 393 kg.

Mother Buoy

This chapter discusses the design of the mother buoys that will accompany the submarines. During the first search phase, each mother buoy will follow one submarine to provide a link for communication and navigation. Before the second search phase, the mother buoys will use HiPAP transponders to create an underwater GPS system. The details of the communication can be found in section 8.2. To simplify the retrieval process and reduce on development cost, the structure of the mother buoys is identical to that of the submarines, as discussed in section 7.8. The propulsion and power system design can be found in section 8.4 and section 8.5 respectively, followed by the stability in section 8.6. Lastly the mass and power budgets of the mother buoy can be found in section 8.7.

8.1. Payload

The mother buoy has an off-the-shelf lantern that is powered by its own solar cells and battery. The lantern is visible over a distance of up to 2 NM (3.7 km) and prevents sea traffic from colliding with the mother buoy [97]. In addition, it carries the HiPAP transponder, which it lowered to the ocean floor during the second search phase. The workings of the transponder are discussed in section 7.2.

8.2. Communication

The mother buoy communicates both with the submarine and the base station. It will use exactly the same equipment as the submarine for this. So, more specifically, an acoustic modem, satellite modem and Iridium antenna. The exact products can be found in section 7.3.

The mother buoy sends commands to and receives data from the submarine. It also sends the data to the base station and receives commands from the base station.

8.3. Navigation

The mother buoy follows the submarine. It receives the payload, sends commands and updates the submarine with a GPS location. The GPS update of the mother buoy resets the INU of the submarine.

GPS and MRU

The GPS position that the mother buoy sends to the submarine should be accurate. This means that possible deviations due to roll and pitch of the mother buoy should be corrected. Furthermore, the mother buoy has to stay above the submarine. It should monitor its own drift due to currents and correct for it.

The mother buoy cannot lie perfectly still in the ocean. Pitch, yaw, heave and roll movements cause the GPS antenna to move while the location of the mother buoy stays the same. This needs to be corrected. A Motion Reference Unit (MRU) [98] calculates the motion of the mother buoy with gyroscopes and accelerometers.

Drift

Strong currents can cause the mother buoy to drift. In order to use the propulsion system to correct for the motion caused by drift, the drift should be measured. The mother buoy is in constant connection with GPS satellites and gets a position update every second [99]. If it is drifting, the GPS locations will show the irregularity in the path of the mother buoy. If the submarine is drifting, then the mother buoy should change its path to follow the submarine.

HiPAP

At the start of the second search phase, four mother buoys release their transponder through an opening at the bottom of the mother buoy. The transponder then sinks to the bottom of the seabed. The bottom part of the transponder has a ballast weight. This helps the transponder to sink with the bottom down. Once sunk, the transponder remains at the seabed for the entire second phase. The transponder system is only calibrated at the beginning of the second phase, therefore the transponders should not move once they are sunk. The cable connecting the transponders to the mother buoy has a length of 6 kilometers. This gives a redundancy in case the mother buoy drifts off, or if currents drag the cable. To retrieve the transponder, the ballast is detached. Provided by Kongsberg, the MPT 316 transponder has a range up to 10000 meter [100].

The transponder weighs 96 kg in total. The transponder itself weighs 30 kg, and the ballast is 66 kg. The transponder has a buoyant force of 10 kg. The collar of the transponder has a buoyant force of 20 kg. After releasing the ballast weight, the transponder becomes neutrally buoyant, which makes it easier to retrieve. The ballast is made of a non nature damaging material, such as basalt.

8.4. Propulsion

Since the mother buoy needs to keep up with the submarine it should also have a velocity of 1 m/s. However since the currents are stronger at the surface than at depth, this needs to be accounted for. In the worst case the currents have a velocity of 2 m/s [101].

The drag of a vessel on the surface consists of two main parts friction drag and wave drag. The friction drag can be accurately estimated based on the Reynolds number using eq. (8.1) and eq. (8.2) [102].

$$C_f = \frac{0.075}{(\log_{10} R_n - 2)^2} \quad (8.1) \quad D_f = C_f \cdot \frac{1}{2} \cdot \rho_0 \cdot v_m^2 \cdot S \quad (8.2)$$

Wave drag is usually calculated using Michell's theory, however more recent research has found that this theory is not accurate for Froude numbers in the range of 0.2 to 0.35 [103]. The Froude number is calculated using eq. (8.3). For the nominal velocity of 1 m/s the Froude number is 0.2, therefore Michell's theory cannot be used.

$$F_n = \frac{v_m}{\sqrt{g \cdot L_{tot}}} \quad (8.3)$$

To obtain an accurate value for the drag a towing tank test needs to be performed. However a statistical method is used to find an initial estimate. Papanikolaou [104] gives a relation between the displacement of the vessel and the total drag it experiences. For velocities of 1 m/s and 2 m/s this results in a drag of 13 N and 117 N respectively. Since the drag changes this drastically with velocity, the mother buoy is not designed to go any faster than this. In case the currents get to more than 1 m/s in the opposite direction to the coverage path, the mother buoy will tell the submarine to reduce velocity.

Using the same efficiency found in section 7.5, it is found that the power needed for 1 m/s and 2 m/s are 21.8 W and 392.7 W respectively.

8.5. Power

For the power subsystem of the mother buoy, a fuel cell system is used with the same layout as in fig. 7.18. Solar power is not used to power the equipment (except the off-the-shelf lantern) since on cloudy days, the power demand might exceed the power provided. This could lead to the mother buoy falling behind on the submarine and losing communication.

The fuel cell stack has a nominal power of 50 W and a maximum power of 67 W. In case the mother buoy needs a velocity of 2 m/s, 393 W is needed as was determined in section 8.4. To keep the mass to a minimum, capacitors are used that are recharged. A total of 11 parallel 3000 F capacitors with a mass of 0.573 kg each can provide the power needed for a velocity of 2 m/s for a duration of 5 minutes [85]. Once the capacitors are empty, they can be recharged up to 100% of their voltage using power from the fuel cell. This recharging takes 5 times the time constant of the capacitor.

$$\tau_c = R_c \cdot C \quad (8.4)$$

Using a 2mΩ resistor, the 11 capacitors can be recharged in 5 minutes and 30 seconds [105].

Furthermore, an additional capacitor, power management module and DC/DC converter module are added to the power subsystem as mentioned in section 7.7.2.

Table 8.1: Mass and volume of the hybrid power subsystem for the mother buoy.

Component	Mass [kg]	Volume [m ³]
Fuel cell stack	0.9	0.0002
Metal hydride tank	117.6	0.016
Oxygen tank	59.4	0.067
Water tank	30.7	0.028
Heat exchanger	3.14	0.002
Power management module	0.3	0.009
DC/DC converter	0.06	3.7 · 10 ⁻⁵
Capacitors	6.3	0.004
Total	218	0.119

8.6. Stability in water

The mother buoy is floating in water and will be considered stable when it returns to the equilibrium position if displaced. For a floating body, the gravity will act through the center of gravity and the buoyancy force acts through the center of buoyancy. These are points G and B respectively in fig. 8.1. When the body is tilted, the buoyancy center relocates due to the fact that the shape of the displaced volume changed, this is point B'. A new point is established called the metacenter (point M) which is the point where the line of symmetry of the body intersects the vertical line drawn upwards from the new centre of buoyancy [106].

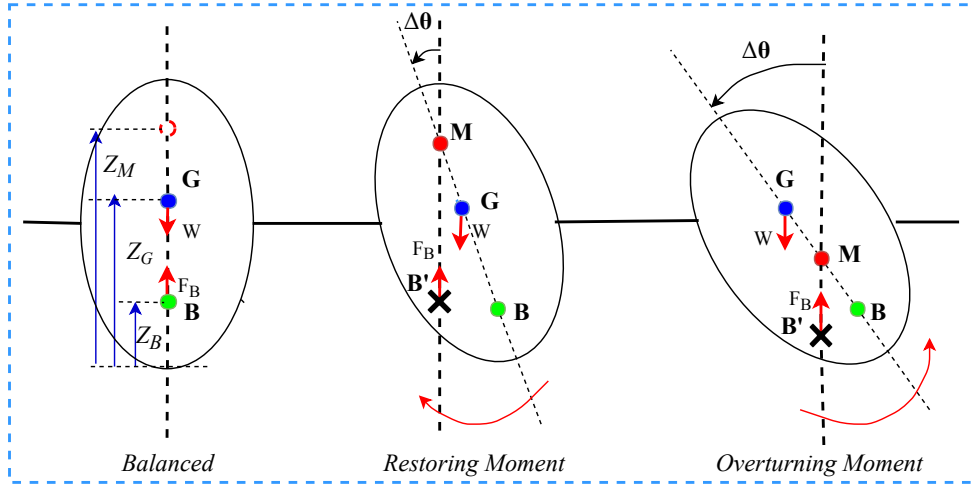


Figure 8.1: Stability diagram for finding the metacenter.

From fig. 8.1 one can see that a metacenter higher than the center of gravity results in a restoring moment, while a metacenter lower than the center of gravity results in an overturning moment. It can be concluded that a floating body with a metacenter located higher than the point of gravity is stable for small disturbances. In other words, the metacentric height (MG) should be positive. ($MG = Z_M - Z_G$) (See fig. 8.1 for definitions) The metacentric height can be calculated using eq. (8.5) [106].

$$MG = \frac{I_{xx}}{V_s} - GB \quad (8.5)$$

I_{xx} is the second moment of area of the solid plane surface of the body when you cut it horizontally at the water surface, V_s is the submerged volume and GB is the distance between the centre of gravity and the centre of buoyancy ($GB = Z_G - Z_B$).

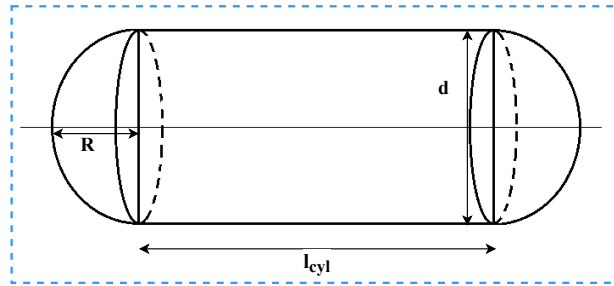


Figure 8.2: The shape of the mother buoy, which consists of a cylinder and two hemispheres at the end.

In fig. 8.2, the shape of the mother buoy is shown. From this the 2nd moment of area, I_{xx} , and the submerged volume, V_s , can be calculated by using eq. (8.6) [107] and eq. (8.7) [108] [109]. The parameters needed for these equations can be seen in fig. 8.3. The a is the base radius and can be determined by eq. (8.8).

$$I_{xx} = \frac{\pi}{64} d_{sub}^4 + \frac{l_{cyl} d_{sub}^3}{12} \quad (8.6)$$

$$V_s = \frac{1}{6} \pi h_s (3a_{base}^2 + h_s^2) + L(R^2 \arccos(\frac{R-h_s}{R}) - (R-h_s) \sqrt{2Rh_s - h_s^2}) \quad (8.7)$$

$$a_{base} = \sqrt{h_s(2R - h_s)} \quad (8.8)$$

d is the diameter of the submarine, h_s and a_{base} are the height and the base radius of the spherical segment in water, R is the radius and l_{cyl} is the length of the cylindrical part of the mother buoy.

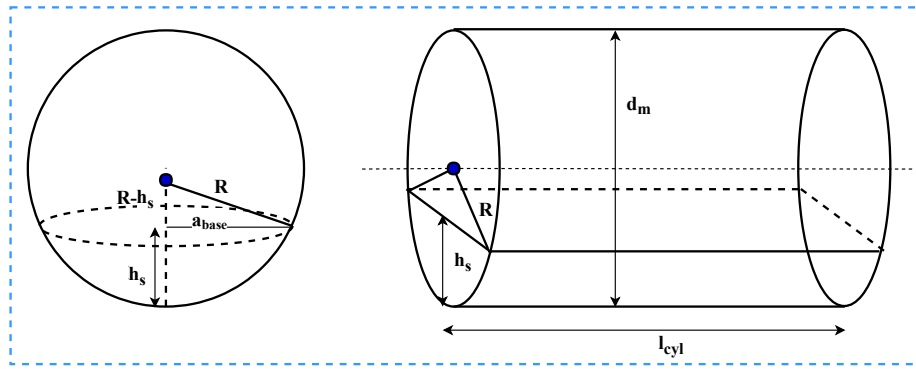


Figure 8.3: The parameters definition to calculate the submerged volume of the mother buoy.

To determine the stability of the mother buoy, it is needed to know the height of the part of the spherical buoy that is submerged in water. The h was determined by setting the weight of fluid displaced equal to the weight of body, as the buoy will be in equilibrium. This is shown in eq. (8.9).

$$V_s \rho g = m_{buoy} g \quad (8.9)$$

The ρ is the density of sea water, which is between $1020 - 1029 \text{ kg/m}^3$ and dependent on the temperature and salinity of the water, g is the gravitational acceleration, which cancels out and V_s is the submerged volume. Substituting eq. (8.8) into eq. (8.7) and substituting that equation into eq. (8.9) and rewriting it, gives the three degrees polynomial given in eq. (8.10).

$$\frac{1}{3} \pi h_s^2 (3R - h_s) + l_{cyl} (R^2 a \cos(\frac{R - h_s}{R}) - (R - h_s) \sqrt{2Rh_s - h_s^2}) = \frac{m_{buoy}}{\rho} \quad (8.10)$$

From this the h is calculated from which the metacentric height can be calculated. For the mother buoy design which has a mass of 414 kg , a diameter of 0.5 m and a length of 2.5 m (including spherical end caps) the h is 0.409 m which lead to a MG of 0.788 m for a density of 1025 kg/m^3 . The MG is positive meaning that the buoy is stable.

8.7. Budget Breakdown

Table 8.2 shows the mass, power and energy budgets for the mother buoy. The contingencies used are the same as those determined for the submarine in section 7.9.

Table 8.2: Mass, power and energy budget of the mother buoy.

Subsystem	Mass [kg]	Mass contingency [%]	Power [W]	Power contingency [%]	Energy [kWh]	Energy contingency [%]
Payload	96.5	5	5.8	5	4.1	5
Navigation	3.5	15	5.5	15	4	15
Structure	67.0	15	0	-	0	-
Communication	8.1	10	19.5	20	1.84	20
C&DH	0.1	10	0.3	10	0.2	10
Power	218	15	0.3	10	0.2	10
Propulsion	2.0	15	21.8	15	15.7	15
Retrieval mechanism	3.4	5	90.0	5	0.05	5
Total	414	13	-	-	-	-

8.8. Summary

The mother buoy has the same 2.5 m long 0.5 m diameter shell as the submarine. It is powered by a single propeller, providing a nominal thrust of 13 N . A light is mounted on the shell for visibility by other vessels. Inside the shell are the same acoustic modem, satellite modem and Iridium antenna used by the submarine for communication. For navigation the mother buoy uses a gyrocompass, GPS receiver and MRU. It also contains a HiPAP transponder which is sunk to the ocean floor during the second search phase. For retrieval the mother buoy houses a balloon and a hydrogen tank to inflate it. The mother buoy is powered by a hydrogen fuel cell. Each mother buoy has a total mass of 414 kg .

Retrieval System

After the search has been performed, the search systems need to be retrieved. This chapter discusses the retrieval process, from the dynamics to the sizing of individual components. First, in section 9.1, an overview of the retrieval process will be given. The main goal of the retrieval chapter is to show that the aircraft is able to withstand the retrieval process. To do this, the retrieval dynamics need to be evaluated, this is done through a simulation in section 9.2. These dynamics are then inputted into a model of the aircraft in section 9.3. Subsequently, some of the retrieval components, such as the flying wing (drone) and hydrogen balloon on the search system, are sized in section 9.4 and section 9.5. Following this, some potential validation experiments for the retrieval process are proposed in section 9.6. Finally, the power requirements (section 9.7) of the system are presented.

9.1. Overview of the Retrieval Concept

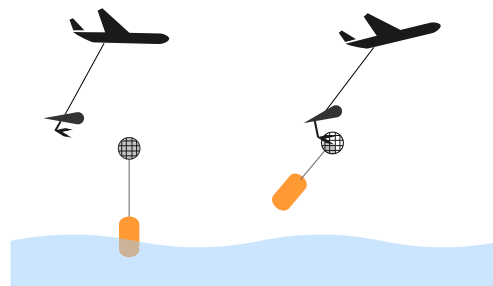


Figure 9.1: Sketch of retrieval concept.

The drone-on-tether concept is comparable to aerial refueling and aerial banner pick-ups. This is because the drone-on-tether takes the controllable aspect of aerial refueling and fuses it with the process of aerial banner pick-ups. In the drone-on-tether system, the controllable drone is attached to a tether. This tether is fixed to a winch, which reels in the entire system once the search system is hooked. Figure 9.1 gives an illustration of this concept. The search system's position will be determined using visual servoing techniques (accuracy in the order of mm [110]), where two stereo cameras will be placed on the exterior of the aircraft¹.

The term "drone" is not used in the colloquial sense (i.e. synonymous with a quadcopter) but rather is a flying wing. This drone would be attached to a tether, at its center of gravity. Therefore, in order to be controllable, the flying wing should keep the tether taut. This can be done by manipulating the aerodynamic forces acting on the flying wing, because the resultant force determines the flying wing's position. Originally, the flying wing would control its vertical position by changing its lift. However, as increasing lift also increases drag, its position would not change much. Therefore, the drone controls its vertical position by manipulating its drag through airbrakes. Its lateral position is adjusted through the rudder on a vertical tail.

However, despite being able to control its position, the accuracy and speed to which the drone can be positioned is insufficient for the purposes of retrieval. Therefore, a small robot arm will be attached to the bottom of the flying wing. While the flying wing autonomously maneuvers to the approximate location of the search system, the retrieval arm will fine-tune its position to ensure successful retrieval. Moreover, this arm is located slightly aft of the flying wing c.g. such that when the search system is caught, the additional weight causes the flying wing to pitch up. Thereby creating lift and drag to more effectively bring the system out of water.

On the search system itself, a hydrogen balloon will be deployed for the retrieval. This balloon will exit the nose fairing of the submarine and rise to an altitude of 6 meters. This balloon acts as a target for the hook, which will pierce it and get caught in the external netting of the balloon. Through this, the search system will be attached to the retrieval arm and be pulled out of the water. Note that the use of a balloon is similar to Project Fulton, which is

¹two are placed on the exterior of the aircraft to ensure that they are sufficiently far apart, a third camera is placed on the drone to improve accuracy

a proven retrieval method. The main reasons for choosing the drone-on-tether concept over Project Fulton were that: 1) No exterior modifications to the aircraft are needed, making it more attractive to the target customers; 2) Less material needs to be stored on the search system (e.g. shorter rope), making it lighter; 3) The autonomous drone negates the pilot error of Project Fulton; and 4) The current option is slightly more sustainable than Project Fulton as the balloon itself is still retrieved².

Once the search system reaches equilibrium in the air, the winch will begin reeling in the tether until the system arrives inside the aircraft. From here, the search system will be secured in the aircraft cargo hold.

9.2. Simulation of the Retrieval Dynamics

The dynamics involved in the proposed retrieval process are an important consideration due to the novelty of the concept. In order to operate safely, the aircraft should be able to counteract the forces induced by the initial pick-up and movement of the search system in the air.

9.2.1. Modelling the Retrieval Dynamics

The main forces involved in this process are; the weight of the search system, w_s , drag, D , tension in the flexible tether, T , and, when in water, the buoyancy force, B . As the search system "swings" behind the aircraft, a non-linear, quadratically damped, pendulum system may be used to model the longitudinal dynamics involved in the retrieval process. Such an equation is given by eq. (9.1), and it may be used to simulate the retrieval process.

$$I_p \ddot{\theta}_r = -\alpha \dot{\theta}_r^2 - \beta \sin(\theta_r) \quad (9.1)$$

In eq. (9.1), $\ddot{\theta}_r$ gives the angular acceleration of the search system, I_p denotes the moment of inertia about the rotational axis, $\dot{\theta}_r$ represents the angular velocity and θ_r gives the angle measured with respect to the downward vertical. Both α and β are constants. However, eq. (9.1) only describes the dynamics in two dimensions. As such, only the longitudinal dynamics will be considered. The reason for this is that the forces acting on the search system primarily influence the longitudinal stability of the aircraft. Furthermore, if the attachment point of the tether to the aircraft is in-line with the y-position of the center of gravity, then any lateral forces induced by perturbations (e.g. by gusts or waves) may be neglected. Other assumptions used for the simulation include:

i The aircraft is perfectly controllable

Implications: This implies that the aircraft is maintaining its altitude and velocity during the retrieval process. This is analogous to the tether being attached to a fixed surface. Consequently, the calculations of dynamics are made assuming that the aircraft can handle the search system oscillations. Afterwards, these forces are applied to the aircraft to evaluate whether it can actually handle the oscillations. This assumption will no longer hold if the aircraft performs maneuvers with large accelerations as these would influence the movement of the search system below.

ii The initial acceleration acts purely in the horizontal direction

Implications: This acceleration needs to be decomposed into the tangential and radial directions before being inputted into the differential equation similar to eq. (9.1).

iii The search system is approximated as an "equivalent" sphere

Implications: This is done to simplify the modelling of the change in area and volume in the water. A sphere was chosen as the rotation of the search system will not affect these values. Modelling the actual shape and its potential rotations is out of the scope of this project. However, to account for this, the "equivalent" sphere will have a cross-sectional area³ larger than that of the actual search system.

iv The search system is initially half submerged

Implications: This is another simplification to ease the calculations needed for the modelling. This assumption is not entirely realistic as the buoyancy of the search system cannot achieve this, from section 7.6.1 around a third of the system will be above water at best. However, as the system is approximated by an equivalent sphere, the equivalent area will be larger⁴ than the submerged area (due to a larger true density of the submarine).

v The tether is tense at the instant of retrieval

Implications: This means that the length of the tether inputted into the simulation is actually its stretched length. Moreover, the force exerted by the aircraft on the search system is almost instantaneous.

²Some parts of the balloon may be lost due to the piercing of the retrieval arm, but the majority will be retrieved. This is not the most sustainable option, but is better than Project Fulton.

³The cross-sectional area was chosen over the volume as the cross-sectional area influences the drag of the system in water, which is a more dominant force than the buoyancy.

⁴From section 7.6.1, the lowest possible submerged area of search system is around $A_1 = 1.9 \cdot 0.5 = 0.95m^2$ while the area of the equivalent sphere is $A_2 = \pi \cdot 0.585^2 = 1.075m^2$. As such $A_1 < A_2$ so the drag is not under-represented.

vi **The movement of the aircraft can be modelled as an incoming airflow**

Implications: This means that there will be an additional drag term which acts only in the horizontal direction, coinciding with the direction of the wind.

vii **The influence of waves is neglected**

Implications: Waves are unpredictable and thus their influence cannot be accurately modelled. This is a significant simplification as waves are always present. However, to account for waves, a factor may be applied to the calculated forces.

viii **The mass of the tether is negligible**

Implications: This simplifies the calculation of the moment of inertia about the pivot point of the pendulum. In reality, the tether will affect this slightly. However, the mass of the tether is much less than that of the search system.

ix **The search system's mass is concentrated at the center of the sphere**

Implications: Rotations due to the center of mass being off set from the center are ignored.

To properly simulate the retrieval process, values for α and β from eq. (9.1) need to be determined. To do this, a Free Body Diagram (FBD) of the search system may be constructed. This FBD is illustrated by fig. 9.2.

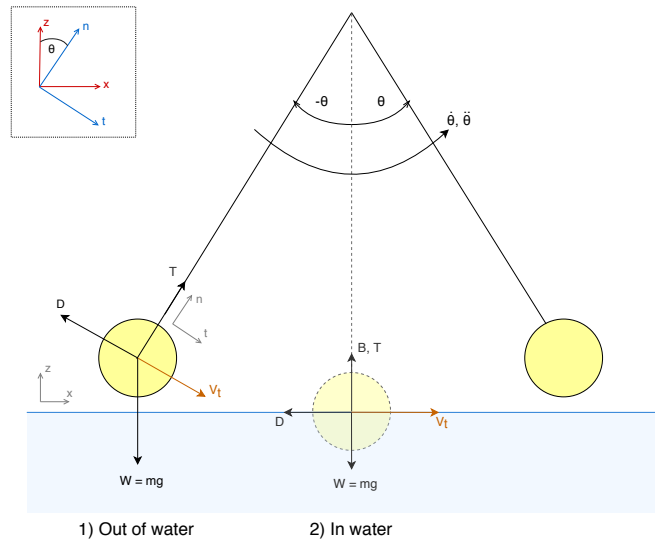


Figure 9.2: FBD of the retrieval process, at different instances of retrieval. Positive rotation is defined as shown.

Taking the sum of forces in the tangential and normal directions yields eqs. (9.2) and (9.3) respectively. Where D_t gives the tangential drag, B denotes the buoyancy force, mg represents the weight of the search system, D_a gives the drag due to the incoming airflow and T_F is the tension in the tether. The positive directions are as indicated in fig. 9.2.

$$\sum F_t : ma_t = -D_t + (B - mg) \cdot \sin(\theta_r) + D_a \cdot \cos(\theta_r) \quad (9.2)$$

$$\sum F_{totn} : ma_n = T_F - (mg - B) \cdot \cos(\theta_r) - D_a \cdot \sin(\theta_r) \quad (9.3)$$

The pendulum moves due to the moment produced by the tangential force. If l is the length of the tether, the motion causing moment is given by eq. (9.4). Where I gives the moment of inertia around the pivot point. In this case, $I = m\ell^2$. Positive rotation is indicated by the arrow in fig. 9.2.

$$I\ddot{\theta} = \ell [-D_t + (B - mg) \cdot \sin(\theta_r) + D_a \cdot \cos(\theta_r)] \quad (9.4)$$

D_t can be expressed through eq. (9.5), where, C_D gives the drag coefficient of the search system, V_t denotes the tangential velocity, ρ_w and ρ_a represent the densities of water and air respectively. Similarly, A_w and A_a give the respective cross-sectional areas (represented by eq. (9.6) and eq. (9.7) respectively).

$$D_t = C_D \frac{1}{2} V_t^2 (\rho_a A_a + \rho_w A_w) \quad (9.5)$$

As it stands, eq. (9.4) is dependent on linear components. For instance, A_w and A_a are a function of the vertical position of the search system from its equilibrium state, s_z . To properly evaluate eq. (9.4), all terms need to be expressed with respect to the angular variables $\dot{\theta}_r$ and θ_r .

$$A_w = \frac{1}{2} \pi r (r - s_z) \quad (9.6)$$

$$A_a = \pi r^2 - A_w \tag{9.7}$$

The vertical position, s_z , of the search system can be found by subtracting the length of the tether by its projection on the vertical axis. As such, s_z is related to θ_r through eq. (9.8). This relation can also be seen through fig. 9.3. From this figure, s_x may be defined as given by eq. (9.9)

$$s_z = \ell [1 - \cos(\theta_r)] \tag{9.8}$$

$$s_x = \ell \sin(\theta_r) \tag{9.9}$$

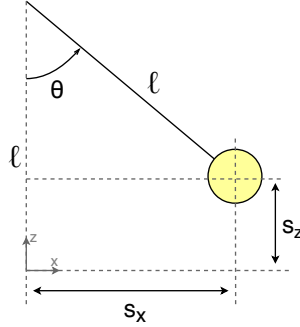


Figure 9.3: Image depicting the relation between θ_r , s_x and s_z .

To completely express D_t in angular terms, V_t^2 needs to be written in terms of $\dot{\theta}_r$. This can be done through eq. (9.10). Here, $\dot{\theta}_r^2$ is expressed as shown to indicate that the direction of velocity needs to be kept. This is because the drag always acts opposite to the tangential velocity.

$$V_t^2 = \ell^2 \dot{\theta}_r | \dot{\theta}_r | \tag{9.10}$$

Now, only B and D_a need to be expressed in the angular frame. D_a is actually a constant (given by the incoming airflow) and is related to the angular frame through $\cos(\theta_r)$ (i.e. the projection of D_a in the tangential direction). As such, it is already appropriately expressed. Hence, only B needs to be transformed. B is defined in linear terms by eq. (9.11).

$$B = \rho_w g v_{disp} \tag{9.11}$$

In eq. (9.12), v_{disp} represents the volume of water displaced by the search system. v_{disp} is related to s_z through eq. (9.12). Consequently, eq. (9.4) can now be completely defined in angular terms.

$$v_{disp} = \frac{1}{3} \pi (r - s_z)^2 (2r + s_z) \tag{9.12}$$

However, solving eq. (9.4) analytically will prove challenging, as such it will be solved numerically. MATLAB's Simulink may be used to solve this non-linear differential equation. For this, a 4th order Runge-Kutta numerical integration scheme will be employed, with a fixed time-step of 0.01 s. Figure 9.4 gives an overview of the diagram created to simulate the retrieval process.

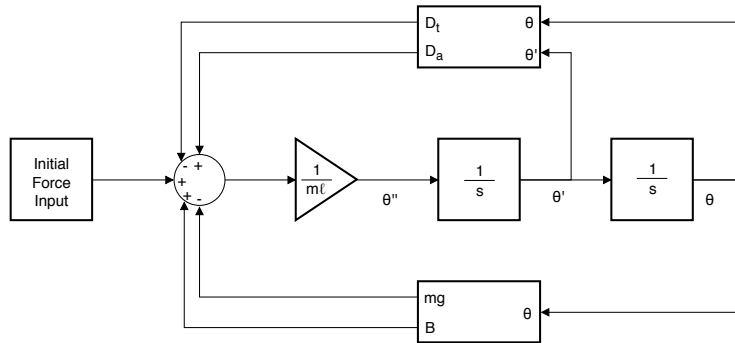


Figure 9.4: Overview of the diagram of the simulation, as implemented in MATLAB's Simulink.

Figure 9.4 shows that the simulation requires an "Initial Force Input". This is because, the pendulum system is subject to an instantaneous pulling force by the aircraft. In the simulation, this force is applied at a time of 1 second, and stops after one time step (i.e. 0.01 s). As the system is modelled as a pendulum, the initial force

exerted on the search system can be represented by eq. (9.13). Here, $a_{t_{initial}}$ gives the initial tangential acceleration that the aircraft exerts, v_a denotes the velocity of the aircraft and h_a represents the altitude of the aircraft.

$$a_{t_{initial}} = \frac{v_a^2}{h_a} \quad (9.13)$$

For the purposes of retrieval, $h_a = 100 \text{ m}$ and $v_a = 70 \frac{\text{m}}{\text{s}}$. This velocity was chosen as it is above the stall speed of the aircraft ($54 \frac{\text{m}}{\text{s}}$), providing some margin for error [28]. The same logic applies to the altitude, ideally this would be higher for safety, but increasing this altitude increases the length of the tether - which has negative consequences for retrieval. One such consequence is the force exerted by the aircraft: as the altitude increases, the force decreases. At first, this seems beneficial, but if the force is too low then the search system takes longer to leave the water - if at all. This is undesirable. Furthermore, a stronger force will pull the search system up high, and thus away from waves. The initial tangential acceleration corresponding to $h_a = 100 \text{ m}$ and $v_a = 70 \frac{\text{m}}{\text{s}}$ is $49 \frac{\text{m}}{\text{s}^2}$. For a tether length, ℓ , of 100 m , the equivalent initial angular acceleration is $0.49 \frac{\text{rad}}{\text{s}^2}$.

The simulation diagram (fig. 9.4) was not built in one go, but rather in steps of increasing complexity. This was done to be able to verify parts of the simulation as it is built. These verification tests are described in detail in section 9.2.3. Another reason for building the simulation this way was that, in the event that the full dynamics could not be simulated, a more simplified - working - model could be presented instead. Some conclusions may be drawn from this model, bearing in mind the assumptions associated with it.

The simulation was built up in the following steps:

Sim_01: Only the tangential drag and gravity are modelled.

Sim_02: A transformation from angular terms to their equivalent Cartesian values is implemented.⁵

Sim_03: Buoyancy is implemented into the simulation.

Sim_04: The difference in drag due to water and air is modelled.

Sim_05: The velocity of the aircraft is implemented as an incoming airflow.

Sim_06: Incorporated calculations for the forces in the radial directions.

Sim_07: Added the option to incorporate drone dynamics (lift and drag) into the equations of motion.

It should be noted that **Sim_07** was not planned, but is an outcome of the results of the previous simulations. Regarding **Sim_07**, it was noticed that, due to the dynamics of the retrieval process, the search system would periodically bounce along the surface of the water. To counter this, either the drag of the search system needs to be increased in the air (e.g. via airbrakes) or the aircraft can begin a slow climb. However, assumption i only holds provided that this climb is not sudden. Consequently, the drone dynamics were included in the simulation.

Despite this change, the search system would still periodically bounce along the surface, but would eventually come to oscillate in the air. This is a more favorable response. However, after consulting with ir. Hans Mulder - a research pilot at the Faculty of Aerospace Engineering at TU Delft in the Netherlands - it was concluded that the poorly damped oscillations would be problematic for the pilot. This phenomenon was initially observed in **Sim_01**. In an attempt to isolate the problem, the drag term was simplified to a linear relationship with the same conditions. Plotting this showed that the oscillations eventually damp out, in fact, they damp out faster than the quadratic oscillations (refer to the top and middle plots in fig. 9.5).

⁵This transformation is done before modelling the effects of water because the vertical distance, s_z , is required for these calculations.

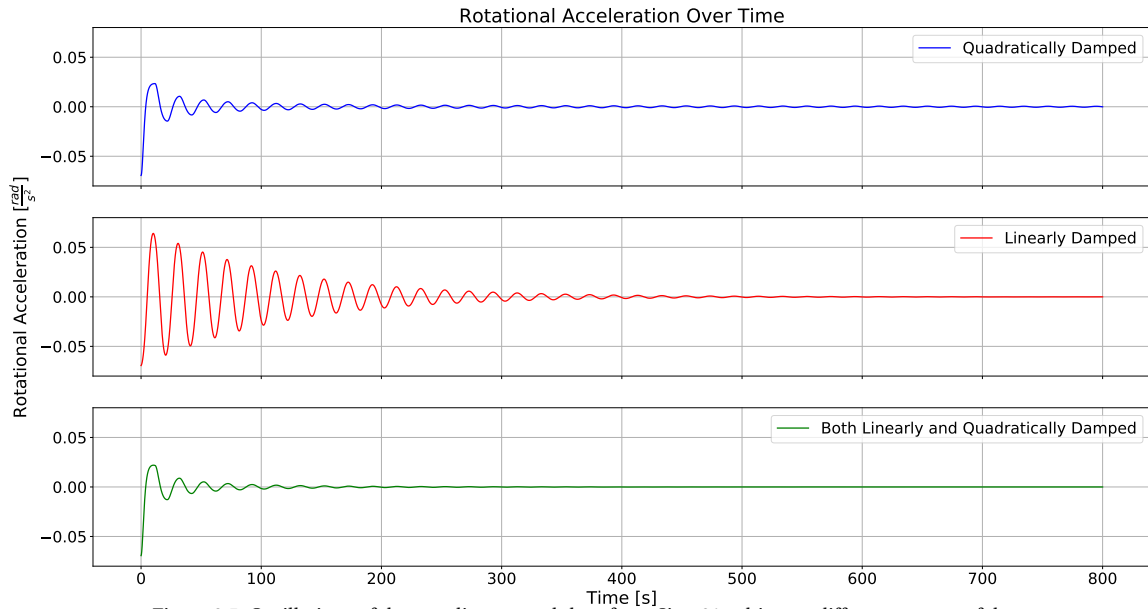


Figure 9.5: Oscillations of the non-linear pendulum from Sim_01 subject to different powers of drag.

J. M. T. Thompson et al. suggest that this oscillatory behavior is expected for quadratically damped pendulums [111]. Thompson indicates that the amplitude of the quadratically damped pendulum decays more vigorously than the linearly damped pendulum for high amplitudes. The opposite is true for low amplitudes [111]. This phenomenon can be seen in fig. 9.5. As such, to fully describe the effects of drag, a linear term needs to be implemented in the EOM [111]. This result is supported by experiments conducted by Patrick T. Spuire [112]. Moreover, Rafael M. Digilov et al. have incorporated a linear damping term to describe their pendulum model, which is also based on experimental data [113]. The bottom graph in fig. 9.5 shows the result of compound damping (i.e. quadratic and linear). This plot gives the more intuitive response.

Physically, the linear damping term would come in the form of frictional forces and other energy dissipating effects. In the context of the simulation, the linear term can be accounted for through a product of the angular velocity, $\dot{\theta}_r$, and a coefficient b . Consequently, eq. (9.14) gives the adjusted differential equation.

$$\ddot{\theta}_r + \alpha \dot{\theta}_r + b \theta_r + \beta \sin \theta_r = 0 \tag{9.14}$$

As α and β have already been defined, only the coefficient b needs to be determined. Unfortunately, the conducted research did not yield any conclusive results for how to calculate this value. Therefore, to best estimate b , the trajectory of Project Fulton will be used as a reference. It is important to note that the direction in which the initial forces act for Project Fulton is different than for the proposed retrieval process. As such, the initial trajectories will inherently be different. However, for the same flight velocities and payload mass, the final stages of the trajectory should be similar. Figure 9.6 illustrates the actual trajectory of a retrieval operation conducted by Project Fulton, as captured by a motion picture of the pickup [114].

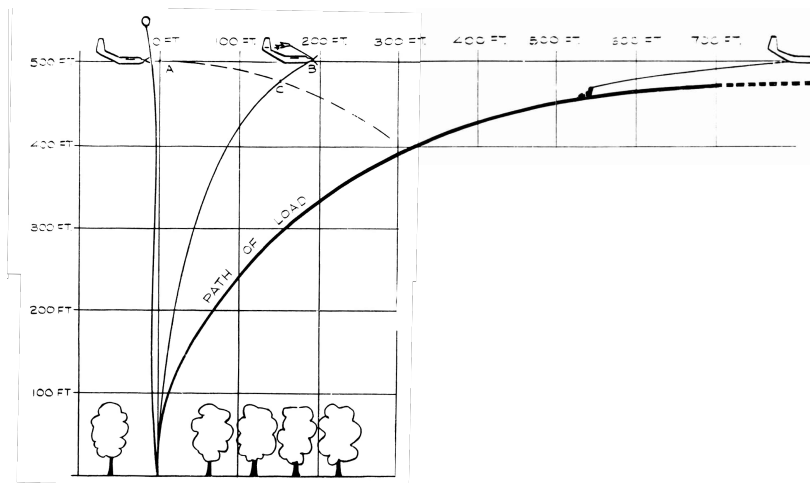


Figure 9.6: Trajectory map of the retrieval of a person with Project Fulton. This map was obtained from a video of the actual retrieval process [114].

The coefficient for b was found through trial and error, until the final phases of the simulated trajectory resemble that of Project Fulton in fig. 9.6. The trajectory of fig. 9.6 was obtained with the aircraft travelling at $65 \frac{m}{s}$ at an altitude of 150 m [114]. Using these parameters, along with a search system mass of 90 kg - to represent the weight of a person including some equipment - the tuned value of b was found to be $10000 \frac{kg \cdot m}{s}$. The resulting trajectory is given by fig. 9.7. The difference in trajectory due to the direction of the initial forces can easily be seen. This is especially evident in the initial horizontal distance travelled. Despite these differences, the final trajectories of both figs. 9.6 and 9.7 appear to be quite similar. This value of b was appended to **all simulations** for continuity.

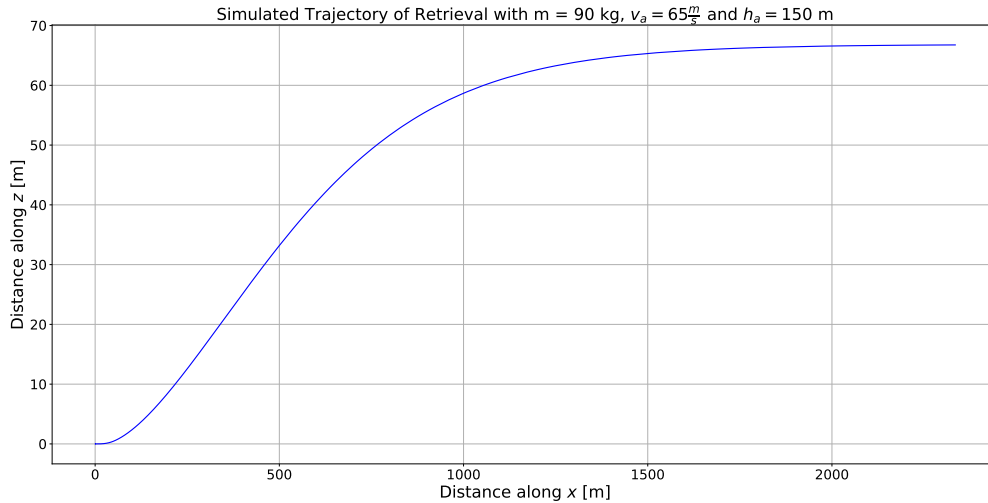


Figure 9.7: Trajectory of the retrieval process as predicted by the simulation with the input parameters of the Project Fulton retrieval operation.

As all the variables for the retrieval process are defined, the actual search system parameters may be inputted into the simulation to determine the retrieval dynamics. Note that the mother buoy's characteristics are used instead of the submarine's, simply because the mother buoy is heavier - and is thus the more critical system for retrieval.

9.2.2. Results of the Retrieval Simulation

In this section, the retrieval process as predicted by **Sim_07** will be presented. The results in this section do not include the final lift and drag of the drone. This is because the drone dynamics affect the overall retrieval dynamics. The design of the drone is therefore an iterative process, and is sized in section 9.4. Once these values are finalized, the complete retrieval dynamics will be given in that same section. However, an example simulation which includes arbitrary values for drone lift and drag will be given in this section to demonstrate their effect on the overall retrieval dynamics.

Table 9.1 presents all the input parameters used in **Sim_07**. A mother buoy mass of 414 kg is used as this was determined to be the final mass in section 8.7. However, in the simulation a mass of 430 kg is used to account for the mass of the drone. Note that if the drone sized in section 9.4 exceeds this 16 kg margin, then the simulations should be adjusted accordingly.

Table 9.1: Table which presents the input parameters used in **Sim_07** to simulate the retrieval process.

Parameter	Input Values (L=0, D=0)	Units
Mass	430	kg
Length Tether	100	m
Equivalent Search System Radius	0.585	m
Spherical Drag Coefficient	0.5	-
Damping Coefficient	10000	$\frac{kg \cdot m}{s}$
Aircraft Velocity	70	$\frac{m}{s}$
Aircraft Altitude	100	m
Density Water	1025	$\frac{kg}{m^3}$
Density Air	1.225	$\frac{kg}{m^3}$
Gravity	9.81	$\frac{m}{s^2}$
Lift of Drone	0	N
Drag of Drone	0	N

To present the dynamics in a more intuitive manner, the angular components are decomposed into their Cartesian equivalents. Figure 9.8 illustrates this, showing the displacements, velocities and accelerations in both the x and z (i.e. horizontal and vertical) directions. It should be noted that the response in fig. 9.8 is plotted relative to the aircraft. The total displacements are a sum of the aircraft displacement and the relative displacements.

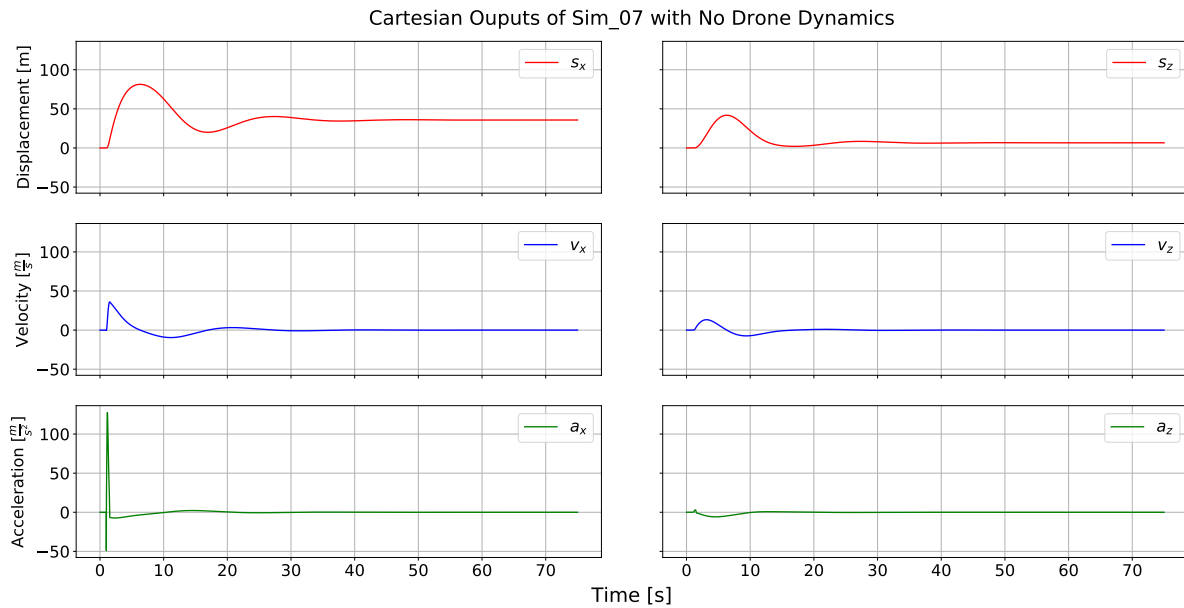


Figure 9.8: The Cartesian equivalents of the retrieval response, as simulated by **Sim_07**. These values are *relative* to the aircraft.

From fig. 9.8, the simulation predicts that the majority of the kinematics occur in the x (horizontal) direction. This is expected as the initial acceleration is applied in the tangential direction. The initial x accelerations are quite high, while those in the z (vertical) direction are not as extreme. Moreover, the accelerations acting on the mother buoy appear to reach zero in around 20 seconds. The same observation can be made about the velocities and relative displacements, which reach zero at around 25 and 30 seconds, respectively. This means that the mother buoy actually reaches equilibrium in approximately 30 seconds. However, the movements after 20 seconds are small and gradual. As the equilibrium values for displacement are hard to extract from fig. 9.8, plotting the trajectory of the search system in the air will give a better indication of these. The blue line (see "Trajectory without Drone Dynamics") in fig. 9.9 plots this trajectory using the total displacements in x and z.

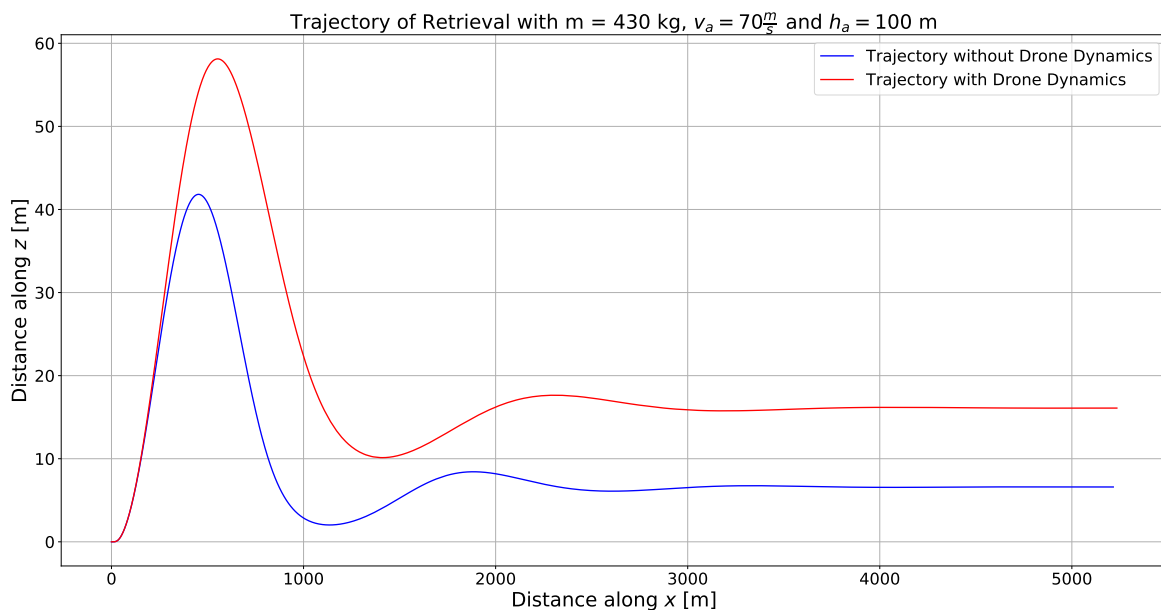


Figure 9.9: Comparison of the trajectory of the retrieval process with and without drone dynamics, as predicted by **Sim_07**. For the trajectory with drone dynamics, drone lift = 1500 N and drone drag = 150 N.

Figure 9.9 shows that, without drone dynamics, the mother buoy reaches equilibrium at a height of 6.5 meters. However, in extreme scenarios, wave heights can reach over 8 meters [115]. Furthermore, the lowest point the mother buoy reaches after leaving water for the first time is 2 meters above sea level, which could be problematic with waves. For these reasons, it would be beneficial to have a drone which generates extra lift and drag to extend the mother buoy's altitude over water. Using an arbitrary drone lift and drag of 1500 and 150 N respectively produces the trajectory given in red (see "Trajectory with Drone Dynamics"). Here, the drone's influence can clearly be seen: the mother buoy reaches equilibrium at an altitude of around 16.2 m, with a lowest dip after leaving the water of around 10 m. This shows that the drone can bring the mother buoy to a safe distance above the waves.

Although the kinematics of the **Sim_07** produce desirable outcomes, the main purpose of the simulation is to determine the forces that the search system exerts on the aircraft. The force that the aircraft feels comes from tension in the tether. As such, the radial forces on the buoy need to be determined. As the dynamics of the buoy are known, the tensile force can easily be found through eq. (9.3). For convenience, this equation is reiterated below:

$$\sum F_{tot_n} : ma_n = T_F - (mg - B) \cdot \cos(\theta_r) - D_a \cdot \sin(\theta_r)$$

As the search system does not move in the radial direction, the right hand side of the equation is equal to zero. Hence, at each instant in time, the tensile force may be evaluated. In the perspective of the aircraft, this tensile force can be decomposed into the x and z coordinates of the aircraft body frame. However, as this tensile force varies with θ_r , and since θ_r varies with time, the projection of the tensile force on the x direction may vary. Consequently, the simulation decomposes the tensile force into its equivalents in the aircraft body frame. These forces will be used to simulate the aircraft's response to the retrieval in section 9.3. Figure 9.10 illustrates these forces with and without drone dynamics, as computed by the simulation. For the drone dynamics, the same lift and drag values were used as before to create fig. 9.9.

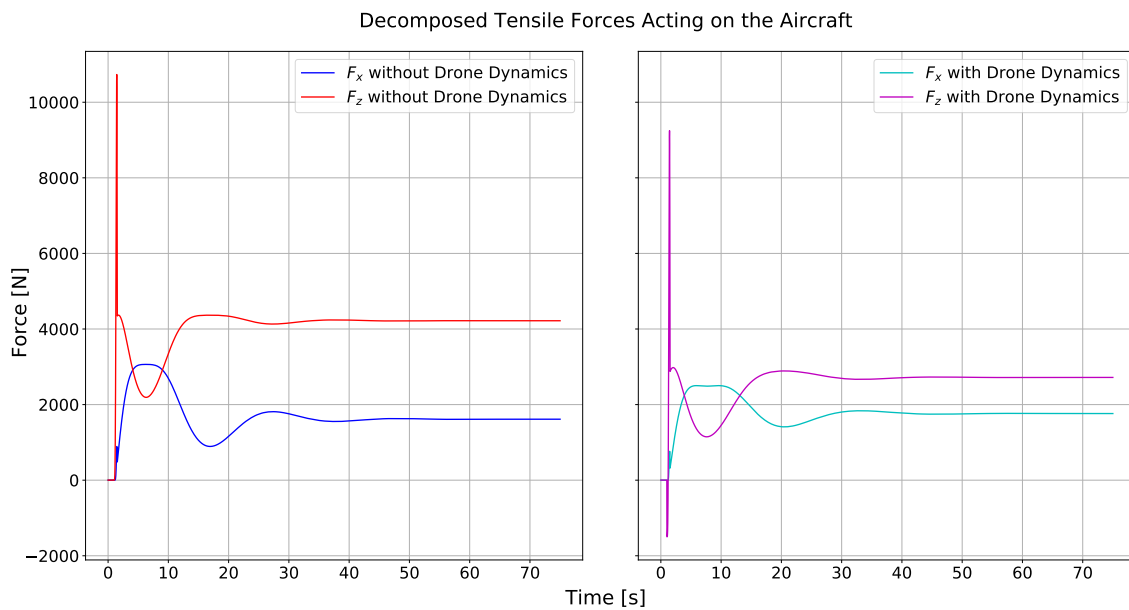


Figure 9.10: Graph illustrating the forces acting in the aircraft body frame with and without drone dynamics over a period of 75 seconds. For the forces with drone dynamics, the lift of the drone is set to 1500 N and the drag to 150 N.

Looking at the forces without the drone dynamics in fig. 9.10 shows that the peak in F_z occurs at around 10750 N, and for F_x the peak occurs at around 3060 N. However, these peaks do not occur at the same time. The sharp peak in F_z occurs at 1.43 s, at this time, the mother buoy is still in the water ($s_z = 0.281 < r = 0.585$). Consequently, this sharp peak corresponds to the large drag of water. Moreover, the instant at which the search system leaves the water can be seen through the kinks in both the F_z and F_x forces. These occur at 1.53 seconds, at this instant $s_z = 0.613 > r = 0.585$. The fluctuations in forces occur due to the movement of the mother buoy in the air. These eventually reach a constant value, implying that the tension at equilibrium is constant. This outcome is expected.

Similar conclusions can be drawn about the forces of retrieval when the drone dynamics are involved. The magnitude of the forces are lower than those without the drone dynamics. This shows that the influence of the drone is not only advantageous for the final equilibrium position of the submarine, but also beneficial in reducing the forces acting on the aircraft. However, there is one notable difference between the plots: when modelling the drone dynamics, there appears to be a negative peak of -1500 N before the large positive peak. This actually rep-

resents the lift of the drone, as initially, the forces in the z direction are in equilibrium (i.e. $B = mg$). In reality, this would mean zero tension in the tether. Consequently, when simulating the aircraft's response in section 9.3, this negative peak should be replaced with $F_z = 0$.

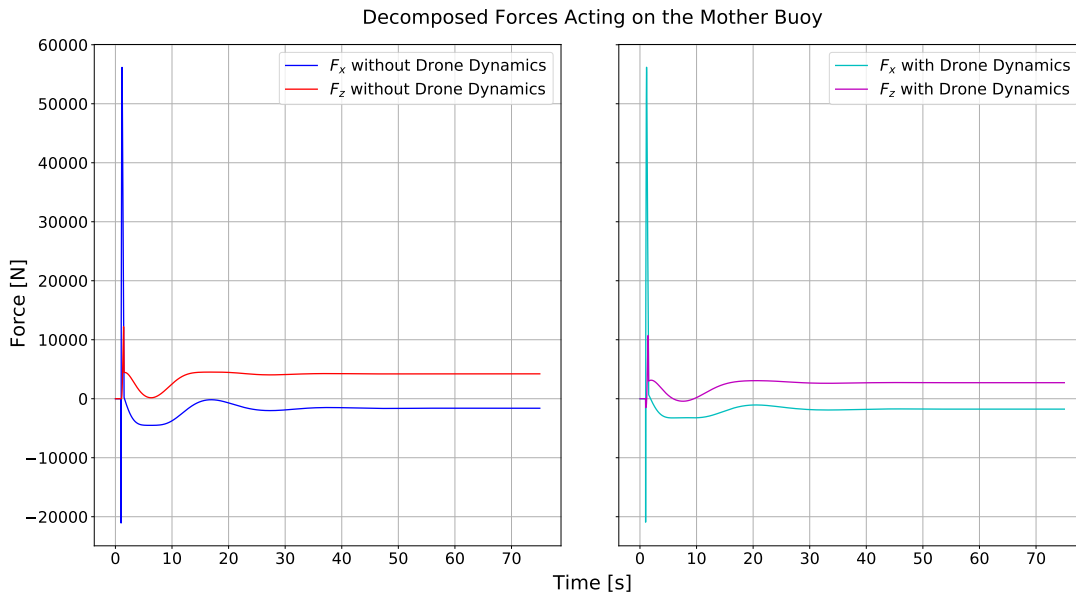


Figure 9.11: Graph illustrating the forces acting on the mother buoy with and without drone dynamics over a period of 75 seconds. For the forces with drone dynamics, the lift of the drone is set to 1500 N and the drag to 150 N.

An outcome which may not be immediately apparent in fig. 9.10 is that F_z is the more dominant force, while the initial force exerted on the search system is in the tangential (primarily x at the instant of retrieval) direction. The reason that F_z is larger than F_x is because these forces are based on the tension of the tether, which is calculated in the radial direction and not the tangential direction. In fact, the forces in the tangential direction represent what the search system itself feels during retrieval. These forces, for both retrieval with and without drone dynamics, is given by fig. 9.11.

In fig. 9.11, this initial tugging force induced by the aircraft on the mother buoy can be seen by a sharp negative peak of -21000 N in the x direction. This is almost immediately followed by a large positive peak of 56000 N, representing the drag of the search system in the water. A similar observation can be made about the forces in the z direction. Like in fig. 9.10, the instant in which the search system leaves the water is marked by a kink in the plots of fig. 9.11. Furthermore, the equilibrium F_x force actually acts in the negative direction. This is due to the definition of the axis system; the final force of F_x is in the same direction as the initial tugging force of the aircraft - which is expected. The only differences between the forces with and without drone dynamics is that the equilibrium forces with drone dynamics are slightly lower in magnitude. Again, these lower forces are beneficial for the retrieval overall.

The main conclusions that can be drawn from the simulation are that the retrieval dynamics, with the tuned linear damping coefficient b , produce responses which only oscillate a few times. This is favorable for the aircraft. Furthermore, it is advised that the drone used during retrieval produces some lift and drag to reduce the magnitudes of forces acting on the aircraft. The added lift and drag will also allow the mother buoy to reach equilibrium at a higher altitude, well above any waves. The outputs of this simulation will be used in section 9.3 and section 9.4 to simulate the response of the aircraft, and size the flying wing (drone) to minimize the effects of this response.

A possible recommendation to improve the results of **Sim_07** would be to use experimental data to compute the actual value of the linear damping coefficient, b . Doing so will improve the accuracy of the simulation.

9.2.3. Simulation Verification

This section will discuss the procedures and methods used to verify the simulation created to model the retrieval process. Note that not every verification test done for each of the simulation variants (i.e. **Sim_01** to **Sim_07**) will be given. However, at least one example will be shown for each simulation which models an additional physical term (e.g. buoyancy, drag, airflow).

Comparison with Reference Simulation

Although this method may seem more closely related to validation rather than verification, the way it is used in this section makes it a verification test. Some of the simulations created can be compared to existing, published, simulations to check if the fundamental equations are implemented correctly. As this does not check if the physical model itself accurately represents reality, it is a form of verification.

Sim_01 models a traditional non-linear, quadratically damped pendulum. Consequently, it may be compared to other simulations - when subject to the same conditions - to see if the outputs match. Similar results would imply that the model is implemented correctly in the simulation. This, of course, assumes that the simulation to which **Sim_01** is compared, is verified itself.

As a comparison, the simulation from "Nonlinear Dynamics and Chaos" by J. M. T. Thompson is used as a reference [111]. The governing equation of Thompson's model is:

$$\ddot{x} + 0.03\dot{x}|\dot{x}| + 4\pi^2 \cdot \sin(x) = 0$$

This is of the same form as the equation of **Sim_01**, if $b = 0$ (i.e. if the linear damping term is ignored). The initial condition that Thompson implemented was $x = 3.054$. Inputting these parameters into the simulation results in a response illustrated by fig. 9.12. The response as found by Thompson is given in fig. 9.13

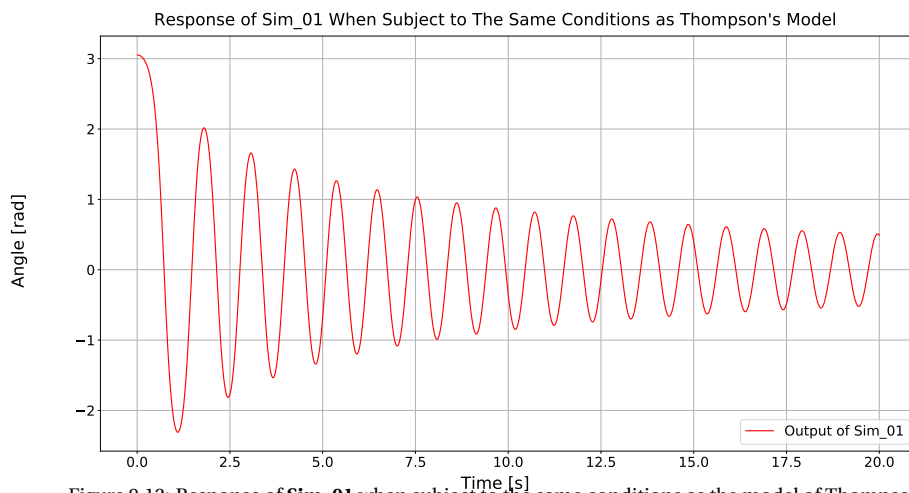


Figure 9.12: Response of **Sim_01** when subject to the same conditions as the model of Thompson.

The responses of figs. 9.12 and 9.13 seem to be quite similar: both simulations start at the correct initial condition of 3.054; the second positive peak occurs at an angle of 2 rad; at $t=18$, both simulations predict a positive peak; and finally, both simulations have 16 minimums. These observations show that **Sim_01** closely matches the simulation of Thompson. Consequently, the differential equation in **Sim_01** seems to be implemented correctly.

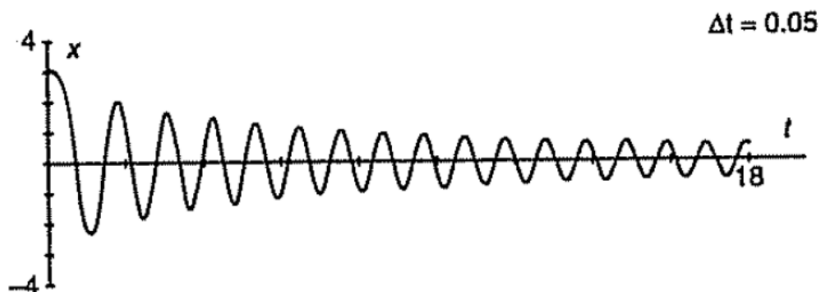


Figure 9.13: Simulation output of Thompson, showing the angle response as a function of time [111].

Simplified Model Testing

This type of testing was conducted per simulation and through a comparison between consecutive simulations (e.g. **Sim_03** and **Sim_04**). In this section, simulations will be subjected to an arbitrary initial condition. An initial condition is used instead of the actual retrieval forces because the dynamics behind these are easier to predict. Consequently, the dynamics can be verified with greater confidence. First, a top level comparison between the

models will be presented. Any significant differences will be identified and verified further.

Figure 9.14 shows the difference between simulations of increasing complexity when subject to an initial condition of $\theta_r = \frac{\pi}{3}$ rad. As described before, the difference between **Sim_01** and **Sim_03** is the effect of buoyancy. The buoyancy appears to have almost no effect on the rotational acceleration of the search system, as can be seen from fig. 9.14. This is expected because the buoyancy term is only active when the search system is in the water, which happens at $\theta_r \approx 0$. Consequently, the tangential component of the buoyancy (i.e. $B \sin \theta_r$) is always approximately zero.

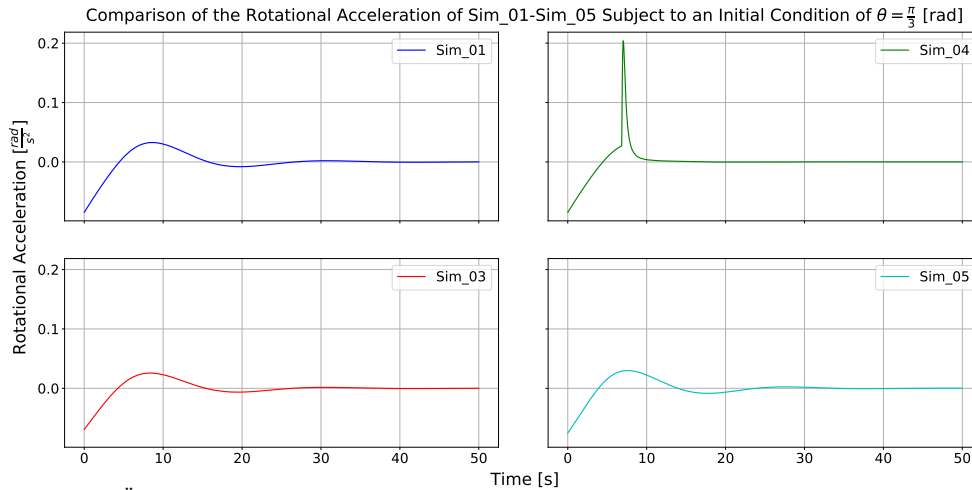


Figure 9.14: Comparison of $\ddot{\theta}$ between the simulations of increasing complexity, where **Sim_05** models the complete dynamics of the system. The simulations were subject to an initial condition of $\theta = \frac{\pi}{3}$ to show their responses.

The first visible difference occurs in **Sim_04**, where the drag due to water is modelled. A spike in acceleration can be seen. It is expected that the search system strikes the water at this time, due to the sudden increase in drag due to the density of water. After this, the acceleration rapidly approaches zero as the search system comes to rest in the water.

However, to verify if this really corresponds to the instant in which the search system hits the water, the moment of impact was analyzed. Figure 9.15 shows the response of the system when dropped from an angle of $\theta_r = \frac{\pi}{3}$. In fig. 9.15, both the dynamics with and without the influence of water are modelled to emphasize any difference.

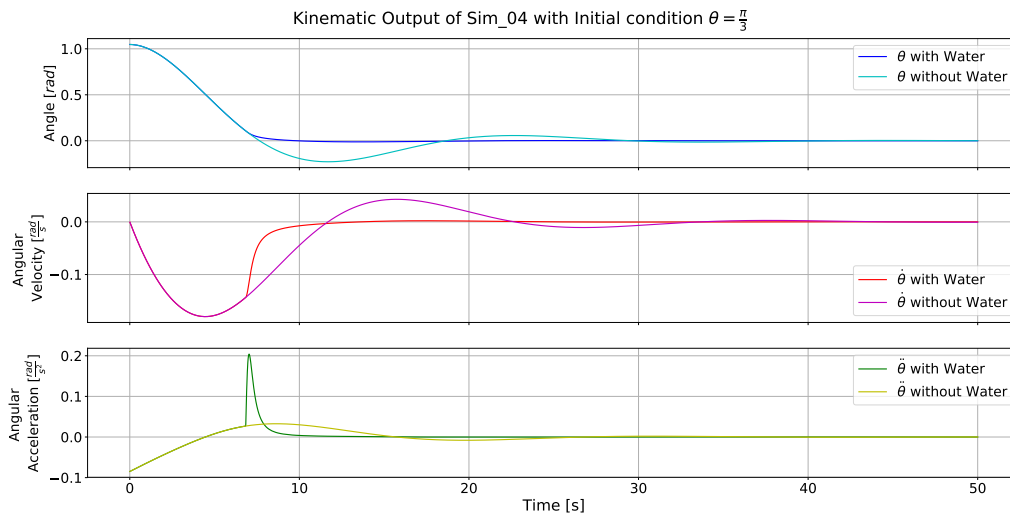


Figure 9.15: Kinematic Output of **Sim_04** with and without water, when subject to an initial condition of $\theta_r = \frac{\pi}{3}$.

Referring to fig. 9.15, when released from $\theta_r = \frac{\pi}{3}$, the same peak can be seen in the acceleration at $t = 6.8$ s. The angle, θ_r at this instant is 0.1066 rad. Using the relation between s_z and θ_r , eq. (9.8), the height, s_z , of the search system is found to be equal to 0.568 m⁶. This is just below the radius of the search system, which was set to $r_s =$

⁶The conditions used for the pendulum for this test in **Sim_04** were: $\ell = 100m$, $m = 400kg$, and $r = 0.571$.

0.571 m. Therefore, this is indeed where the search system strikes the water.

Referring back to fig. 9.14, it appears as though there is no difference between **Sim_05** and **Sim_01** or **Sim_03**. **Sim_05** incorporates the velocity of the aircraft into the model. This can be interpreted as a tugging force by the aircraft. Consequently, this result is unexpected. However, in terms of acceleration this result is indeed correct. The differences can be seen in the final angles of the simulations. From fig. 9.16, it can be seen that in **Sim_05** the search system actually reaches equilibrium in the air. As such, it never hits the water - and the large spike in acceleration is not seen. Physically, the search system would reach equilibrium before hitting the water because it is being pulled along by the aircraft. The equilibrium point of the tension on the tether with the drag due to the flight velocity is somewhere in the air. This shows that the incoming airflow definitely has an effect on the results of **Sim_05**. Moreover, a small difference can be seen in the magnitudes of **Sim_03** compared to **Sim_01** in that the former experiences smaller angles. This corresponds to the effects of the buoyancy.

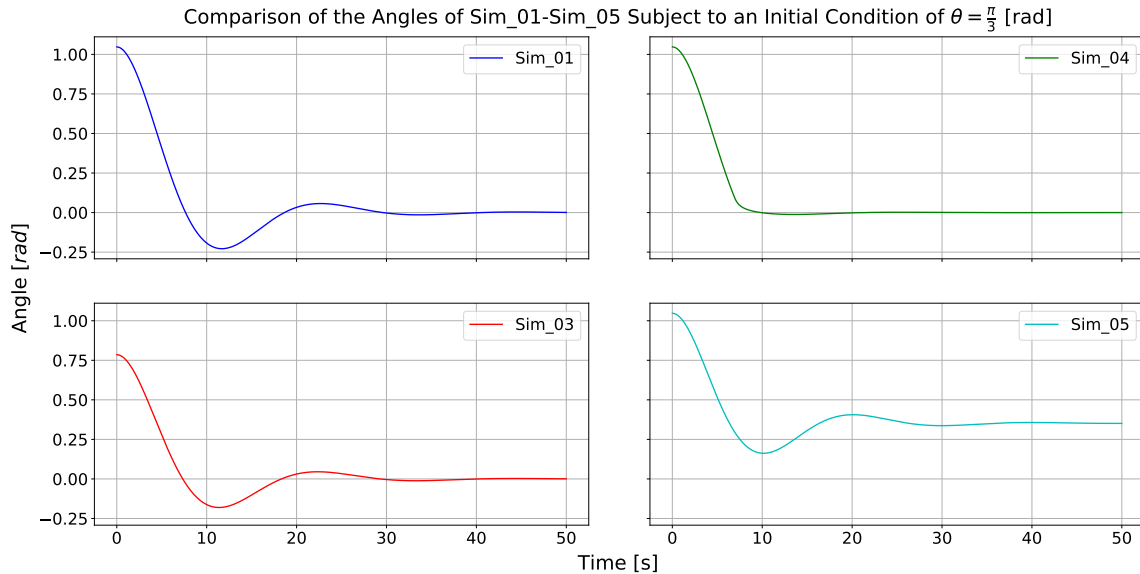


Figure 9.16: Comparison of θ_r between the simulations of increasing complexity, where **Sim_05** models the complete dynamics of the system. The simulations were subject to an initial condition of $\theta_r = \frac{\pi}{3}$ to show their responses.

To compare **Sim_05** with **Sim_07**, some arbitrary values for the drone dynamics need to be selected. This is because the only difference between these simulations is the drone dynamics. For the comparison, 1500 N will be used for the lift and 150 N for the drag. Moreover, the initial retrieval force will also be used instead of the initial condition such that the implementation of this force can also be verified. This initial retrieval acceleration was calculated in section 9.2 to be $0.49 \frac{rad}{s^2}$. Using this, the retrieval dynamics of **Sim_05** and **Sim_07** can be compared. This is illustrated through fig. 9.17.

In both simulations, the initial retrieval can be seen in the angular acceleration plot. This value is indeed of the correct magnitude and acting in the correct direction. Furthermore, the overall shape of both simulations is similar: the peaks in acceleration appear to be the same, but afterwards, the acceleration of **Sim_07** is shallower than that of **Sim_05**. The same observation can be made about the velocity. The reason for this is because of the lift that the drone produces. The extra lift relieves some of the weight of the search system, effectively making it "lighter". Consequently, the magnitude of the total force is reduced. Therefore, these observations suggest that the drone dynamics are implemented correctly.

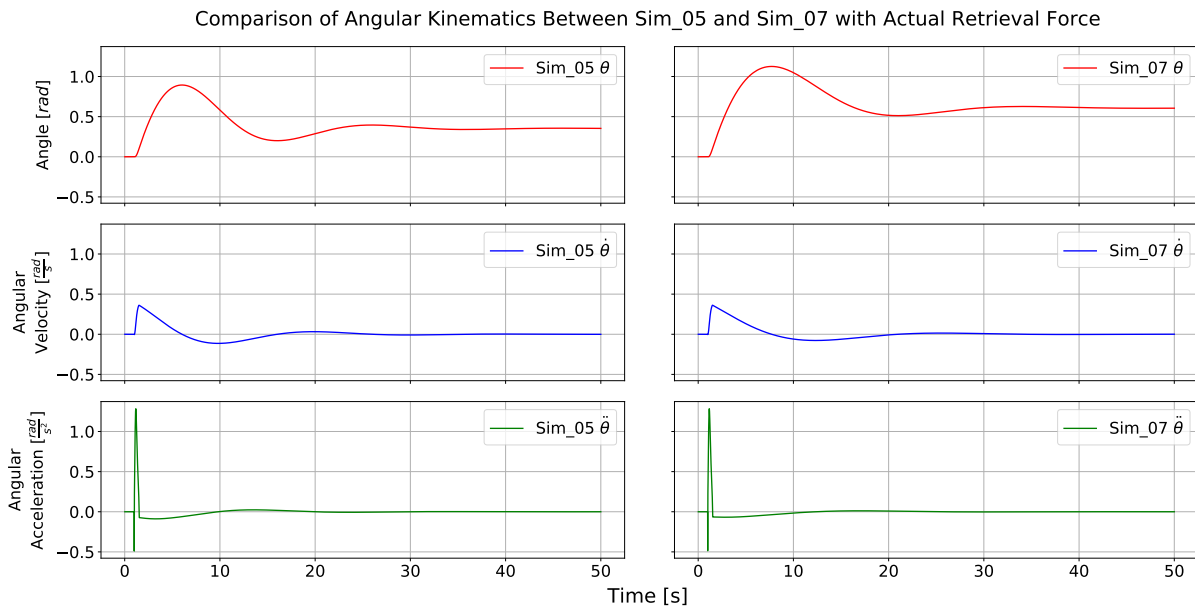


Figure 9.17: Comparison of the retrieval dynamics as predicted by **Sim_05** and **Sim_07** when subjected to the initial retrieval force.

In fig. 9.17, the most notable difference between the two simulations is the plot of the angle. The equilibrium angle corresponding to **Sim_07** is larger than that of **Sim_05**. This means that the search system in **Sim_07** reaches equilibrium at a higher altitude than in **Sim_05**. The reason for this is again due to fact the extra lift produced by the drone relieves some of the weight of the mother buoy. This allows it to reach a higher equilibrium position. This observation is confirmed by the trajectories of Project Fulton [114]. As such, the physical equations seem to be implemented correctly in **Sim_07**.

Continuity Testing

Generally, continuity testing involves changing the input parameters slightly to see the effect on the outputs. For most systems, these small changes in inputs should lead to small changes in outputs. This test will be done for **Sim_07** as it is the most complex form of all the other simulations.

To test the continuity of **Sim_07**, both a slight increase and decrease in an elected parameter will be performed. Two variables will be changed for a more robust test; first only the mass will be changed and second only the aircraft velocity will be changed. Figure 9.18 depicts the change in angle over time, for different search system masses (left) and aircraft velocities (right).

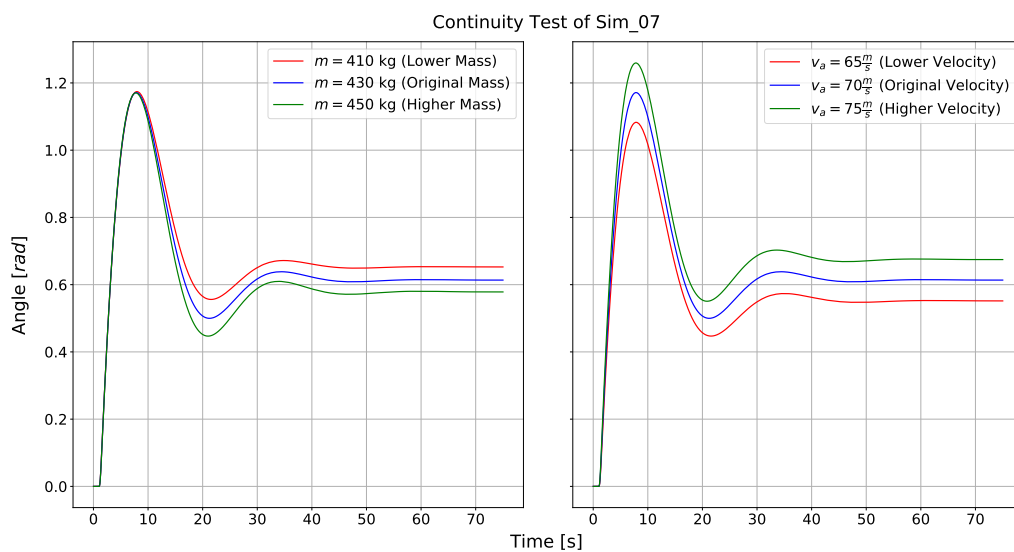


Figure 9.18: Graphs illustrating the continuity tests performed on **Sim_07** by changing the mass (left) and flight velocity (right).

Figure 9.18, shows that the angles over time of the retrieval process do not change significantly if either the mass or velocity is changed. Moreover, the overall shape of the trajectory is the same. This is a good sign as it implies

that the simulation is continuous. For the changes in mass, it is observed that an increase in mass leads to a lower altitude equilibrium position. This is expected as for higher masses the weight term is more dominant. Similarly, a lower aircraft velocity also leads to a lower altitude equilibrium position. In this case, the drag term becomes less influential. Consequently, the weight term becomes more dominant. Therefore, the results of **Sim_07** show that the simulation is continuous, with changes reflecting what is expected physically.

9.3. Simulation of Aircraft Response

In this section, the response of the aircraft to the force obtained in section 9.2.2 is modelled. The model will use the aircraft's EOM to obtain the response as a change in velocity, angle of attack and pitch. With this information, it can be evaluated whether the aircraft can withstand the force T_F .

9.3.1. Aircraft Equations of Motion

The first step in describing the dynamics of the aircraft is the derivation of the EOM. For this, several assumptions are made. These assumptions and their impact are listed below [29]:

- i **The aircraft is a rigid body of constant mass.** This implies no fuel consumption and no vehicle elastic modes. If this is true then the matrix of inertia will be constant.
- ii **The Earth is flat and non-rotating.** The result of this assumption is that the influence of the Earth's curvature is negligible as well as the coriolis acceleration and centripetal acceleration.
- iii **The gravity field is constant.** The magnitude of this field is equal to $g = 9.81 \text{ m/s}^2$.
- iv **The aircraft has a plane of symmetry.** The body-fixed reference frame can thus be aligned with the principle axis of the aircraft, making I_{xy} and I_{yz} equal to zero.
- v **The effects of rotating masses are neglected.**
- vi **The resultant thrust vector lies in the symmetry plane.** Thus, it only affects the aerodynamic forces X, Z and the aerodynamic moment M.

The EOM are based on Newton's laws. Since these laws are only valid when the motion is described in a inertial reference frame, the EOM are first set up in the Earth centered inertial reference frame F_I , as in this frame the Earth's rotational speed can be neglected. Newton's second law, saying the force acting on the body is equal to the time derivative of the momentum (i.e. the product of mass and velocity of the body), is used to set up the translational EOM. For the rotational EOM the Euler equations are used, relating the angular acceleration to the angular velocity, external moments and inertia.

The equations set up in the F_I reference frame can be related to the vehicle carried Earth reference frame F_E by transformation. This transformation is given by three angles, the Euler angles. These angles are defined as follows: ϕ = roll angle, θ = pitch angle, ψ = yaw angle. [116]

The equations obtained with the above described process can be found in eq. (9.15) [29]. Only the longitudinal motion equations are listed, as only the longitudinal stability of the aircraft is examined by the model.

The forces acting on the aircraft can be found in fig. 9.19. As shown, the forces F_{T_x} and F_{T_z} act under an angle θ . However, as this angle is small, it was neglected in the EOM.

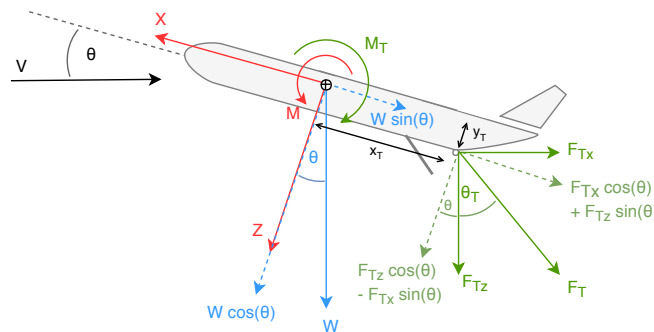


Figure 9.19: Free body diagram of aircraft during retrieval.

$$\begin{aligned}
 \mathbf{F}_x: & \quad -W \sin(\theta) + X - F_{T_x} = m(\dot{u} + qw - rv) \\
 \mathbf{F}_z: & \quad W \cdot \cos(\theta) \cos(\phi) + Z + F_{T_z} = m(\dot{w} + pv - qu) \\
 \mathbf{M}_y: & \quad M - F_{T_z} x_T + F_{T_x} z_T = I_{yy} \dot{q} + (I_{xx} - I_{zz}) r p + I_{xz} (p^2 - r^2) \\
 \mathbf{Kin.}: & \quad \dot{\theta} = q \cdot \cos(\phi) - r \cdot \sin(\phi)
 \end{aligned} \tag{9.15}$$

The equations in eq. (9.15) are non-linear. In order to obtain a set of linear differential equations, the EOM are linearized. These equations will lead to less accurate results, but can still be used to get a good indication of the reaction of the aircraft [29]. The advantage is that linearizing the EOM makes it possible to use stability and control derivatives for the Airbus A400M. The results of linearization of the EOM about the initial state (denoted with a subscript 0) can be found in eq. (9.16).

To simplify the rather lengthy linearized EOM, during linearization, the analysis of the aircraft dynamics will be performed using steady, straight, symmetric flight conditions. This in principle means that the state of the aircraft remains constant, i.e., all derivatives and the angular velocities are zero. Further more, it can be assumed that small asymmetric deviations and disturbances have no influence on the symmetric forces X and Z or on the symmetric moment M [29]. Also, the initial force T_F is equal to zero. The simplified linearized EOM can be found in eq. (9.17).

$$\begin{aligned}
\mathbf{F}_x: \quad & m(\dot{u}_0 + q_0 w_0 - r_0 v_0) + m(\Delta \dot{u} + \Delta q w_0 + q_0 \Delta w - \Delta r v_0 - r_0 \Delta v) = \\
& -W \sin(\theta_0) + X_0 - F_{T_{x0}} - W \cos(\theta_0) \Delta \theta - \Delta F_{T_x} + X_u \Delta u + X_w \Delta w + X_q \Delta q + X_{\delta_e} \Delta \delta_e \\
\mathbf{F}_z: \quad & m(\dot{w}_0 + v_0 p_0 - u_0 q_0) + m(\Delta \dot{w} + \Delta v p_0 + v_0 \Delta p - \Delta u q_0 - u_0 \Delta q) = \\
& W \cos(\theta_0) \cos(\phi_0) + Z_0 + F_{T_{z0}} - W \sin(\theta_0) \cos(\phi_0) \Delta \theta - W \cos(\theta_0) \sin(\phi_0) \Delta \phi + \\
& \Delta F_{T_z} + Z_u \Delta u + Z_w \Delta w + Z_{\dot{w}} \Delta \dot{w} + Z_q \Delta q + Z_{\delta_e} \Delta \delta_e \\
\mathbf{M}_y: \quad & I_{yy} \dot{q}_0 + (I_{xx} - I_{zz}) p_0 r_0 + I_{xz} (p_0^2 - r_0^2) + I_{yy} \Delta \dot{q} + [(I_{xx} - I_{zz}) r_0 + I_{xz} p_0] \Delta p + [(I_{xx} - I_{zz}) p_0 + I_{xz} r_0] \Delta r = \\
& M_0 + F_{T_{x0}} z_T - F_{T_{z0}} x_T + \Delta F_{T_x} z_T - \Delta F_{T_z} x_T + M_u \Delta u + M_w \Delta w + M_{\dot{w}} \Delta \dot{w} + M_q \Delta q + M_{\delta_e} \Delta \delta_e \\
\mathbf{Kin.}: \quad & \dot{\theta}_0 + \Delta \dot{\theta} = q_0 \cdot \cos(\phi_0) - r_0 \cdot \sin(\phi_0) + \cos(\phi_0) \Delta q - q_0 \sin(\phi_0) \Delta \phi - \sin(\phi_0) \Delta r - r_0 \cos(\phi_0) \Delta \phi
\end{aligned} \tag{9.16}$$

$$\begin{aligned}
\mathbf{F}_x: \quad & m(\dot{u} + w_0 q) = -W \cos(\theta_0) \theta - F_{T_x} + X_u u + X_w w + X_q q + X_{\delta_e} \delta_e \\
\mathbf{F}_z: \quad & m(\dot{w} - u_0 q) = -W \sin(\theta_0) \theta + F_{T_z} + Z_u u + Z_w w + Z_{\dot{w}} \dot{w} + Z_q q + Z_{\delta_e} \delta_e \\
\mathbf{M}_y: \quad & I_{yy} \dot{q} = F_{T_x} z_T - F_{T_z} x_T + F_{T_x} z_T + M_u u + M_w w + M_{\dot{w}} \dot{w} + M_q q + M_{\delta_e} \delta_e \\
\mathbf{Kin.}: \quad & \dot{\theta} = q
\end{aligned} \tag{9.17}$$

The linearized EOM are finally rewritten into state-space form, as shown in eq. (9.18). The stability and control derivatives are defined as follows: for a scalar force vector component F the variable $F'_i = \frac{1}{m} F_i = \frac{1}{m} \frac{\partial F}{\partial i}$. Similarly, for a moment vector M , $M'_i = \frac{1}{I_{yy}} M_i = \frac{1}{I_{yy}} \frac{\partial M}{\partial i}$ [116]. The values of these derivatives can be found in table 9.2, together with general characteristics of the aircraft used in table 9.3.

$$\begin{bmatrix} \dot{u} \\ \dot{w} \\ \dot{q} \\ \dot{\theta} \end{bmatrix} = \begin{bmatrix} X'_u & X'_w & -w_0 & -g \cdot \cos(\theta_0) \\ Z'_u & Z'_w & u_0 & -g \cdot \sin(\theta_0) \\ M'_u + M'_{\dot{w}} Z'_u & M'_w + M'_{\dot{w}} Z'_w & M'_q + M'_{\dot{w}} u_0 & -M'_{\dot{w}} g \cdot \sin(\theta_0) \\ 0 & 0 & 1 & 0 \end{bmatrix} \cdot \begin{bmatrix} u \\ w \\ q \\ \theta \end{bmatrix} + \begin{bmatrix} \frac{1}{m} & 0 \\ 0 & -\frac{1}{m} \\ -\frac{z_T}{I_{yy}} & \frac{x_T}{I_{yy}} \\ 0 & 0 \end{bmatrix} \cdot \begin{bmatrix} F_{T_x} \\ F_{T_z} \end{bmatrix} \tag{9.18}$$

Table 9.2: Stability and control derivatives of the Airbus A400M [116].

Parameter	X'_u	X'_w	X'_{δ_e}	Z'_u	Z'_w	Z'_q	Z'_{δ_e}	M'_u	M'_w	$M'_{\dot{w}}$	M'_q	M'_{δ_e}
Value	-0.133,	0.0609,	0	-0.1389	-0.9069	-3.3658	22.933	0	-0.0634	0.0119	-2.2674	-3.577

Table 9.3: General aircraft parameters [116].

Parameter	Value	Unit
Altitude (h)	100	[m]
Velocity ($u_0 = V$)	70	[m/s]
Angle of attack (α_0)	0.0125	[deg]
Pitch angle (θ_0)	0	[rad]
Gravitational acceleration (g)	9.81	[m/s ²]
Mass (m)	111377	[kg]
Moment of inertia (I_{yy})	4655576	[kg · m ²]
Moment arm along x-axis (x_T)	25	[m]
Moment arm along z-axis (z_T)	1	[m]

9.3.2. Aircraft Model

With the state-space equation and input forces F_{T_x} and F_{T_z} , the aircraft dynamics can be modelled. The model was made using the programs MATLAB and Simulink. The output results can be found in fig. 9.20. To obtain a value for the angle of attack α , the approximation of $w_0 \approx u_0 \alpha_0$ is made.

The results show a decreasing velocity and increasing pitch and angle of attack. This is what is expected. By hanging a weight on the aircraft, the drag increases slowing down the aircraft. Furthermore, a nose up moment is generated as the weight is attached to the back of the aircraft behind the centre of gravity. This increases the pitch and angle of attack, and further decreases the velocity as the aircraft climbs. This is also supported by the fact that the velocity is out of phase with pitch and angle of attack in the plots. When θ and α increase V decreases, and vice versa.

The magnitude of the change in parameters is acceptable for the aircraft. The velocity changes within a range of about 5 m/s, with a minimum velocity of 65.5 m/s which is still above the stall speed of 54 m/s [28]. A higher initial velocity can be chosen to increase the safety margin. This would however induce difficulties for the attachment to the search system, as it needs to be successful at higher speed. Test flights should be performed to find a good tradeoff between speed of flight and the risk of missing the search system.

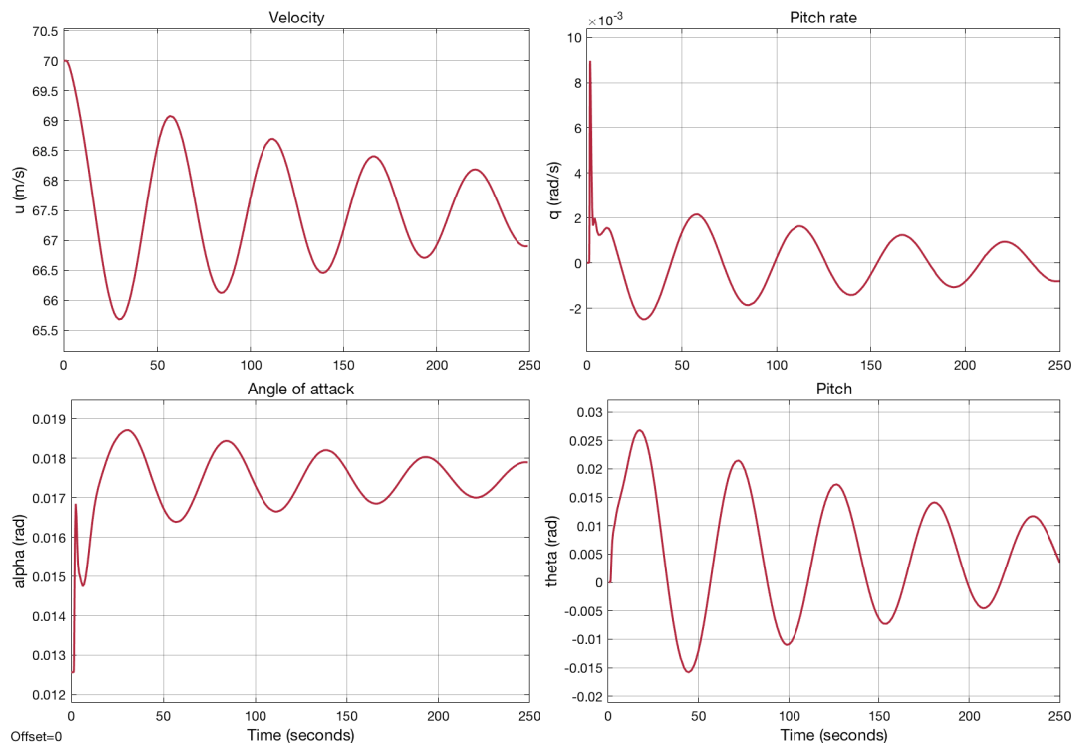


Figure 9.20: Output values as a reaction to the input force T_F , examined over a time span of 250 seconds.

Improvements on Aircraft Response

To even further decrease the loads on the aircraft, and to increase the equilibrium altitude of the attached search system as shown in fig. 9.9, a drone able to generate up- and downward lift will be used. In section 9.4 the sizing of this drone will be explained, and final maximum up- and downward force values will be found. To be able to determine the effects on the aircraft, $F_{max} = 1720$ N and $F_{min} = -2200$ N will be used in this section, where positive values are upward. These values already take into account the weight of the drone itself.

The drone is released with a negative force of 2200 N pulling downwards. When the payload is attached, a positive force of 1720 N is generated. By this the difference in force acting on the aircraft during retrieval is decreased, and the change in parameters will decrease as well.

In the model, the drone is released and given 500 seconds to stabilize. After this the search system is attached and the results are examined for another 500 seconds. These results are shown in fig. 9.21.

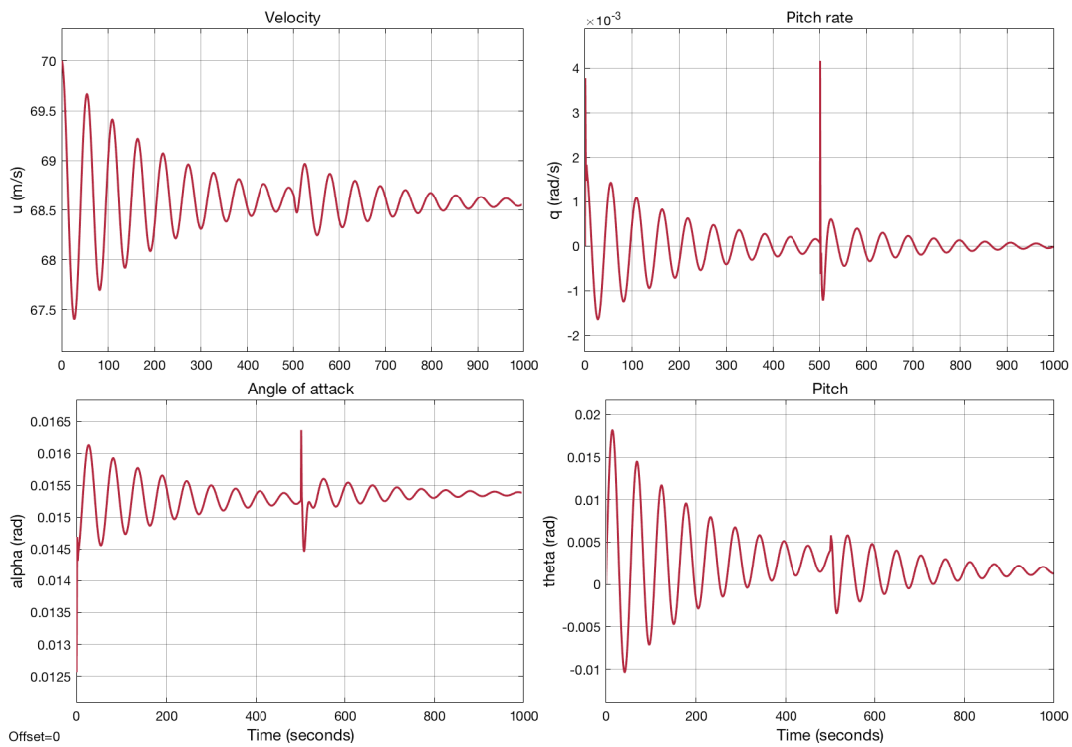


Figure 9.21: Reaction of aircraft to drone release at $t = 0$ and to submarine retrieval at $t = 500$.

It can be observed that the reaction to the drone release is more extreme than to the submarine retrieval itself. This could be caused by the fact this was modeled as a single impulse. To make the drone release more smooth, it was modeled as a ramp reaching the final force over a time span of 100 seconds. The results of this simulation can be found in fig. 9.22.

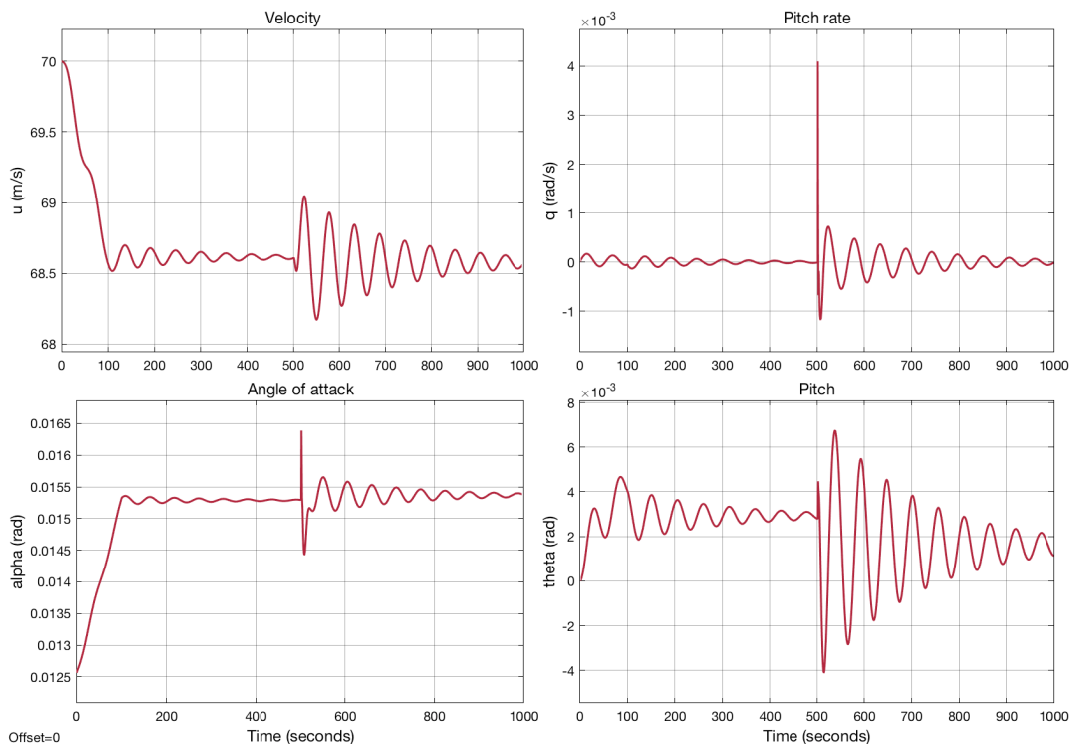


Figure 9.22: Reaction of aircraft to continuous drone release over the first 100 seconds and to submarine retrieval at 500 seconds.

Tests of a model in a wind tunnel test could further help designing an optimal drone release procedure. From the simulations it can be concluded a more smooth release is beneficial both to the aircraft and the drone itself.

9.3.3. Verification

To verify the results, several tests have been done, explained in the sections below. Additionally, a test pilot from the TU Delft, Hans Mulder, was consulted about the expected results. These were compared with the outputs of the simulation, and found to match almost perfectly.

Comparison to Example from Literature

The set of equations can be verified by comparison to theory. The example of the short period and phugoid motion of the Cessna Ce500 'Citation' from [29] is used for this. The input of this motion is the elevator deflection δ_E . This changes the state-space system to eq. (9.19). To initiate this motion, the elevator deflection is set to -0.005 rad.

The code is verified by keeping the parameters and stability and control derivatives of the A400M with the elevator input. The resulting outputs of this simulation can be found in fig. 9.23. The shape and magnitude of the values in the plots can be compared to the literature examples. In general, they match very well, with the only difference being the period of the motion. However, as differences in the results are expected due to the different parameters and eigenvalues of the A400M and the Cessna Ce500 'Citation', it can be concluded that this verification test is successful.

$$\begin{bmatrix} \dot{u} \\ \dot{\alpha} \\ \dot{q} \\ \dot{\theta} \end{bmatrix} = \begin{bmatrix} X_u & X_w & -w_0 & -g \cdot \cos(\theta_0) \\ Z_u & Z_w & u_0 & -g \cdot \sin(\theta_0) \\ M_u + M_{\dot{w}}Z_u & M_w + M_{\dot{w}}Z_w & M_q + M_{\dot{w}}u_0 & -M_{\dot{w}}g \cdot \sin(\theta_0) \\ 0 & 0 & 1 & 0 \end{bmatrix} \cdot \begin{bmatrix} u \\ \alpha \\ q \\ \theta \end{bmatrix} + \begin{bmatrix} X_{\delta_E} \\ Z_{\delta_E} \\ M_{\delta_E} + M_{\dot{w}}Z_{\delta_e} \\ 0 \end{bmatrix} \cdot \delta_E \quad (9.19)$$

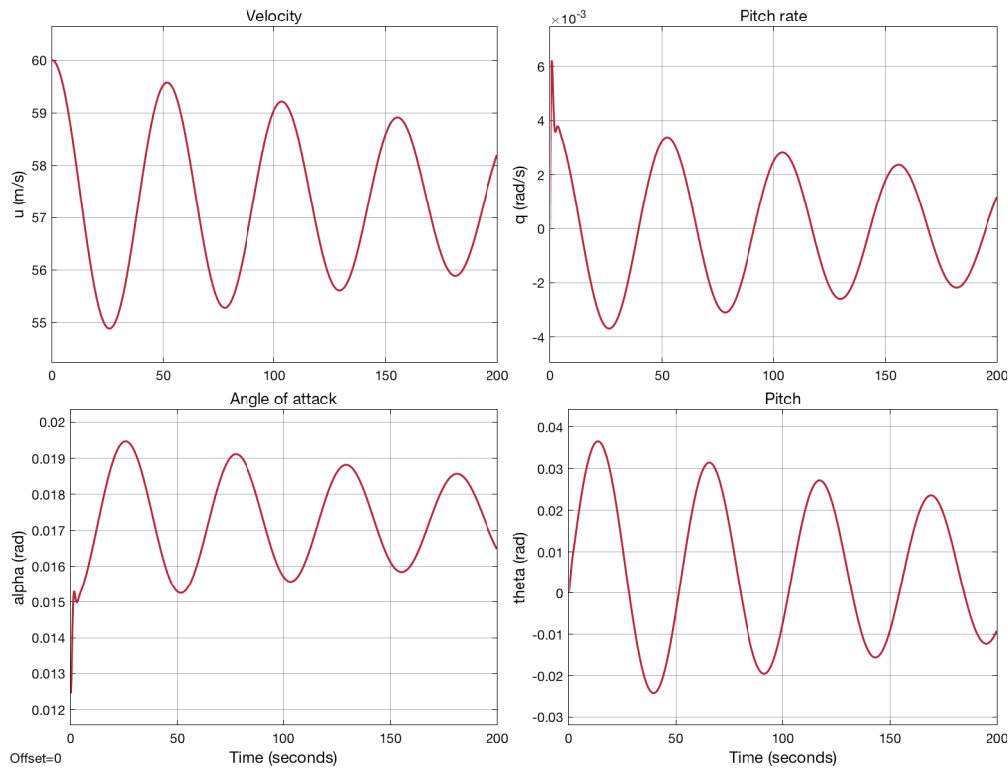


Figure 9.23: Output values as a reaction to an elevator deflection $\delta_e = -0.005$ rad, examined over a time span of 250 seconds.

Continuity Test

For this test the value of the input force is changed. For an increased force the response is expected to be more extreme. Similarly for a lower force the output is more moderate. The force input is multiplied by a gain of 2 and a gain of 0.5. When applying these changes to the model, the expected outputs are obtained, as shown in fig. 9.24. This means this verification test is successful.

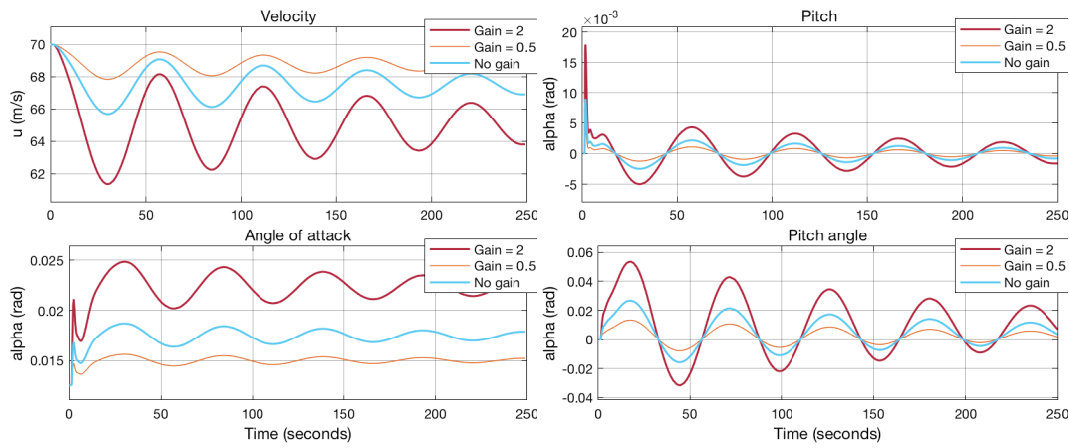


Figure 9.24: Model outputs for input forces multiplied by different gains.

9.4. Drone Sizing

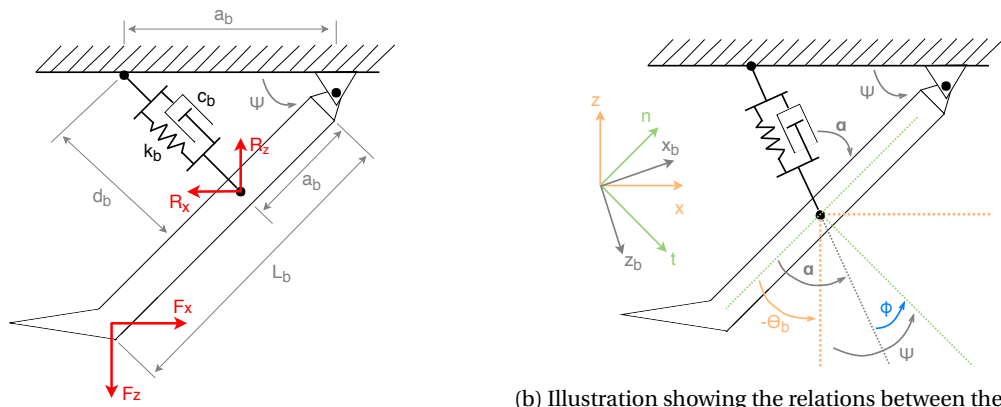
In this section the design and sizing of the aforementioned drone is explained. The functions the drone has to be able to fulfill are listed below:

- The drone has to fit in the aircraft, meaning the span has to be smaller than the width of the cargo compartment including safety margins.
- The drone has to be able to generate both positive and negative lift.
- The change in lift generated by the drone has to be as close as possible to the tensile force F_{T_z} caused by retrieval.
- The drone has to be able to adjust its position with a precision of ≈ 0.5 m, in order to align with the search system to be picked up.
- The drone has to have a robotic arm able to adjust its position with a precision of 1 cm, in order to attach to the search system.
- The drone has to carry a camera, in order to allow the operator to react to changes caused by outer factors (wind, waves, etc.) as quick as possible.

In order to size the drone, the masses of the additional components need to be known. Therefore, the setup of this section is as follows: first, the robotic arm is designed in section 9.4.1. After the dimensions and weight of the arm is defined, the flying wing surface can be sized. This is done in section 9.4.2.

9.4.1. Retrieval Arm Sizing

Before the flying wing can be sized, the masses of the attached components need to be determined. The heaviest mass attached to the flying wing is the retrieval arm, and its surrounding structure. A retrieval arm is needed because the accuracy that can be achieved through the actuators on the drone itself are insufficient; some mechanism is needed to fine-tune the final position of the hook. This retrieval arm should not only be actuated, but should also be able to resist the forces of retrieval. In fact, the majority of the loads from retrieval will pass through this structure.



(a) The retrieval arm depicting the relevant forces acting on the system and the dimensional parameters involved.

(b) Illustration showing the relations between the various angles of the retrieval arm.

Figure 9.25: Illustration showing retrieval arm parameters used for its design.

The retrieval arm can be represented by a beam and spring-damper system, which is depicted in fig. 9.25a. The spring-damper is required to allow actuation and to ensure that the beam can absorb the tangential forces induced by the pick-up. The tangential forces are considered as these are the forces that the retrieval arm needs to resist. Moreover, as the hydrogen balloon should not hit the drone, the height (in fig. 9.25a, height = $L_b \cos \psi_{retr}$) of the retrieval arm should at least be equal to the balloon's diameter. In section 9.5, the diameter of the hydrogen balloon is calculated to be 0.4 meters. To reduce mass, this height should be minimized. Therefore, the height will be set to 0.4 m. The length, L_b of the retrieval arm is related to the height through the angle, ψ_{retr} , which is unknown.

Ideally, $\psi_{retr} = 90$ degrees as this corresponds to the smallest length of L_b . However, this limits the achievable heights of the robot arm (smaller range in which it can adjust). Therefore, an angle less than 90 degrees is preferable. To simplify the problem, it is assumed that $a_b = d_b$ when d_b is undeformed⁷. This results in $\psi_{retr} = 60$ degrees (equilateral triangle). This angle is used instead of $\psi_{retr} = 45$ degrees as a lower mass (directly proportional to smaller L_b) is more important than the additional height. If $\psi_{retr} = 60$ degrees, then the corresponding length, L_b , of the retrieval arm is 0.46 m.

To fully dimension the arm, values for a_b and d_b are needed. Both a_b and d_b can be arbitrarily set to any length less than L_b . Ideally, a_b and d_b should be as small as possible to avoid interference with the retrieval process. This minimum length is dependent on the lengths of the springs and dampers used. Therefore, to size these mechanisms, the response of the retrieval arm to the retrieval forces needs to be determined. This process will be iterative since, to calculate this response, the lengths a_b and d_b need to be defined.

The response of the retrieval arm can be modelled by a pendulum system, with the governing equation defined by eq. (9.20). The variables in eq. (9.20) are defined as seen in figs. 9.25a and 9.25b.

$$\ddot{\theta}_b + c_b \cdot a_b \cos(\phi) \cdot \dot{\theta}_b + k_b \cos(\phi) (d_b^* - d_b) \cdot \theta_b = 0 \quad (9.20)$$

In eq. (9.20), d_b^* represents the deformed length of the spring. This length can be found through the cosine rule, given by eq. (9.21), where ψ_{retr}^* represents the current angle of ψ_{retr} .

$$d_b^* = 2a_b^2 (1 - \cos(\psi_{retr}^*)) \quad (9.21)$$

To evaluate the response of the retrieval arm to the retrieval dynamics, the pendulum system can be drawn as a diagram in MATLAB's simulink. In the simulation, the values for c_b and k_b can be tuned until the desired response is achieved. A favorable response would be heavily damped and as stiff as possible as to not heavily influence the dynamics of the overall retrieval process. Selecting values for c_b and k_b is possible since these are parameters which can be tuned in reality (e.g. the spring constant k can be influenced by changing the spring diameter). Of course, the tuned values of c_b and k_b need to be tuned such that they can be realistically implemented into the drone. To ensure this, the characteristics of off-the-shelf dampers and springs will be used in the simulation, until an acceptable response is attained.

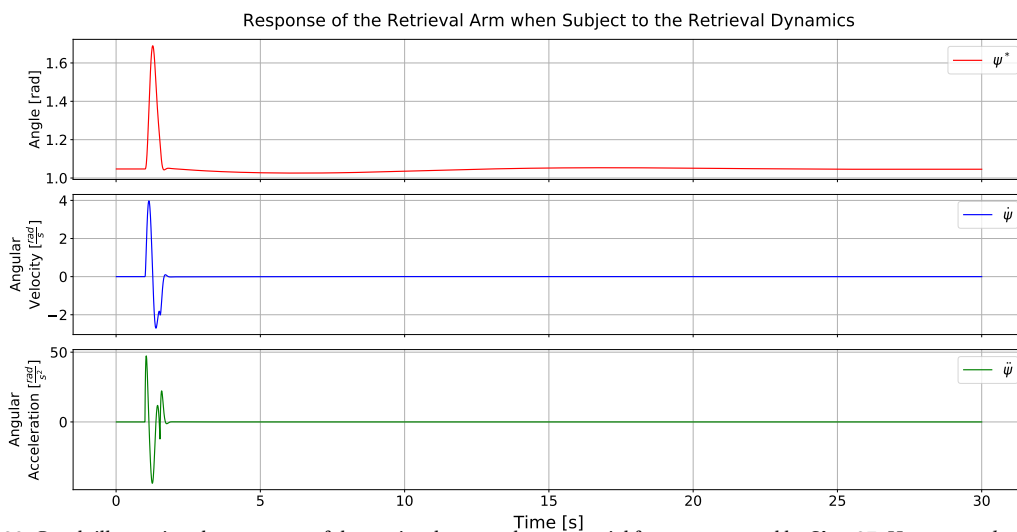


Figure 9.26: Graph illustrating the response of the retrieval arm to the tangential forces outputted by **Sim_07**. Here, $a_b = d_b = 0.24$ m, $c_b = 31000 \frac{Ns}{m}$ and $k_b = 639000 \frac{N}{m}$.

⁷Note that here undeformed is the pre-stretched spring. That is, that the mass of the arm is already accounted for by the spring.

Figure 9.26 depicts the response of the retrieval arm when subject to the tangential forces of the retrieval process, with $a_b = d_b = 0.24 \text{ m}$, $c_b = 31000 \frac{\text{Ns}}{\text{m}}$ and $k_b = 639000 \frac{\text{N}}{\text{m}}$. Table 9.4 gives an overview of the properties of the selected spring [117] and damper [118]. Furthermore, in fig. 9.26, $\dot{\psi}_{retr}$ and $\dot{\psi}_{retr}$ are equivalent to $\dot{\theta}_b$ and $\dot{\theta}_b$, respectively. This is because $\psi_{retr} \equiv \frac{\pi}{2} + \theta_b$, consequently, their rate of change is the same.

Table 9.4: Characteristics of the spring [117] and damper [118] used for the retrieval boom.

Parameter	Unit	Spring	Damper
k_b	$\frac{\text{N}}{\text{m}}$	639000	-
c_b	$\frac{\text{Ns}}{\text{m}}$	-	31000
Diameter	m	0.036	0.040
Length	m	0.150	0.200
Mass	kg	1.86	1.74

In fig. 9.26, it is observed that the response of the retrieval arm lasts for about 1 second, with the angle slowly reaching equilibrium in about 20 seconds. Initially, the angle, ψ_{retr} , increases - this outcome is expected as the retrieval arm will be pushed further aft, thereby increasing ψ_{retr} . In all graphs, the initial reaction is a sharp peak in the positive direction - showing the instant at which the retrieval arm catches the balloon. This is followed by some oscillations in angular velocity and accelerations, which rapidly dampen out. The sharp change in direction at around 1.53 seconds is due to the search system leaving the water, as described in section 9.2.2. At first glance, the accelerations seem quite high peaking at $50 \frac{\text{rad}}{\text{s}^2}$. However, with a length of $L_b = 0.46 \text{ m}$, the linear equivalent of the peak is $23 \frac{\text{m}}{\text{s}^2}$.

To finalize the design of the retrieval arm, the main beam needs to be sized. To reduce the influence of the drone on the retrieval dynamics, the mass of the beam should be minimized. As the pivot point does not support a moment, the main force consideration for the beam is the shear stress acting through it (the tangential force is a shear force in the perspective of the beam). Assuming a thin-walled circular rod, the shear stress acting through the beam is given by eq. (9.22).

$$\tau = \frac{VQ}{It} = \frac{4}{3} \frac{V}{\pi r t} \quad (9.22)$$

To optimize for mass, fig. 9.27 illustrates the relationship between the mass of the retrieval arm boom with its radius. For this plot, Aluminium 6061-T6 was used as a reference material and a safety factor of 1.5 was applied [119]. From fig. 9.27, it can be seen that the lower the radius, the lower the mass. However, the radius cannot be smaller than 0.042 m (i.e. to the left of the red line) as the thin walled assumptions do not hold beyond this point. Therefore, the optimum mass for the boom would be the intersection of these two points. This gives a retrieval arm mass of 1.21 kg. For this boom, the radius is 0.0422 m with a thickness of 3.8 mm. This brings the total mass of the retrieval arm to 4.81 kg.

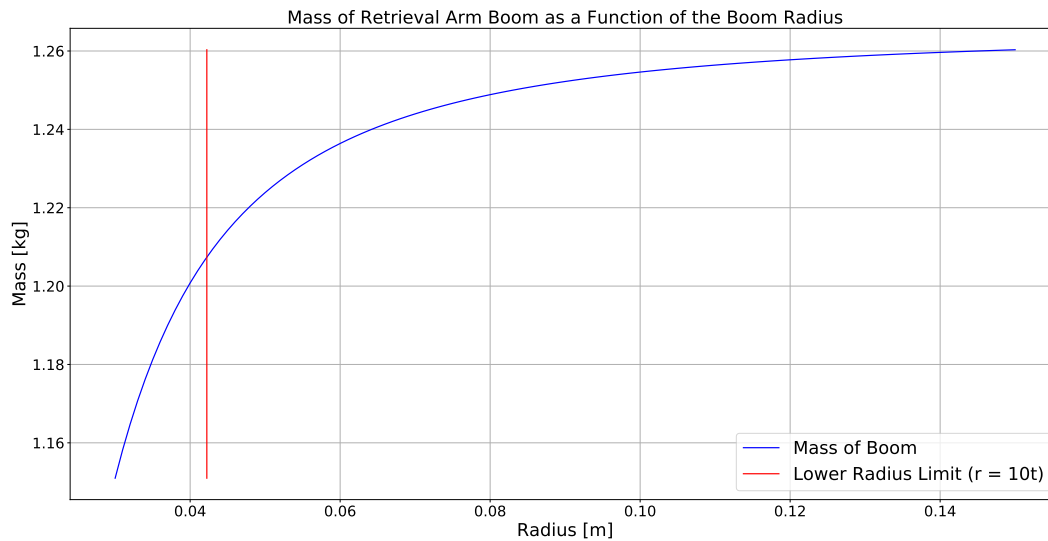


Figure 9.27: Graph depicting the relationship between the mass and radius of the retrieval arm boom.

Simulation Verification

To verify the simulation created to model the retrieval arm's response to the retrieval forces, both a continuity and simplified model test will be performed. For the continuity test, the mass and undeformed length shall be varied.

While for the simplified model test, the simulation will be subject to different initial conditions to see if it behaves as expected.

Continuity Test

For this test, the undeformed length, d_b , will be varied. Moreover, similar to the continuity test done in section 9.2.3, the mass of the search system will be changed. Since the mass also affects the retrieval dynamics, these will be recalculated for each mass tested using **Sim_07**. Figure 9.28 presents the results of the continuity test.

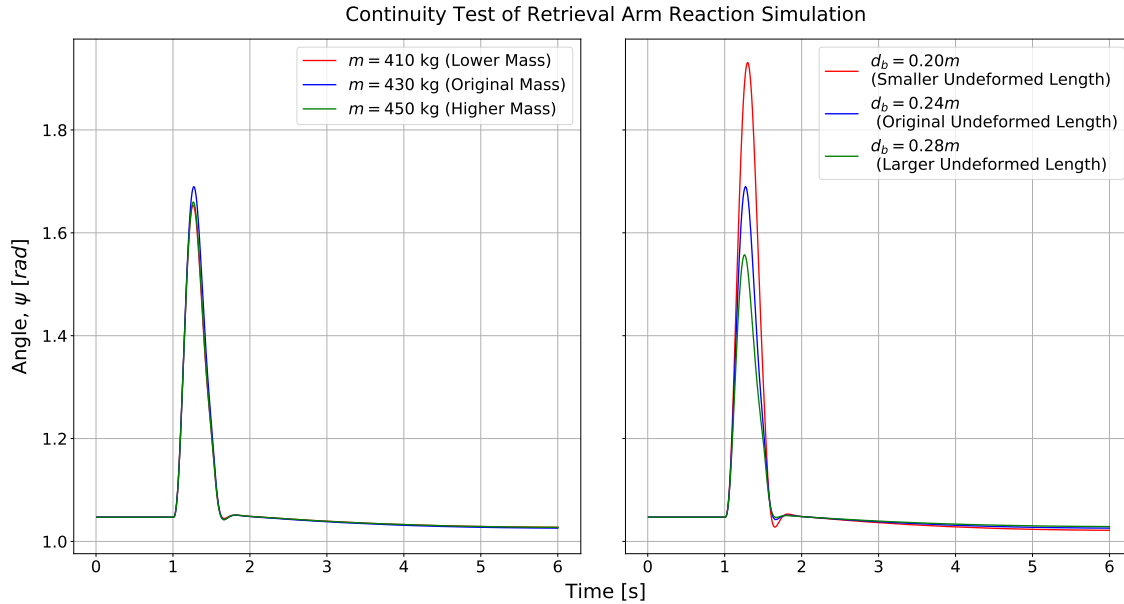


Figure 9.28: Graph presenting the response of the retrieval arm when subject to slight changes in mass (left), and slight changes in undeformed length, d_b (right).

From fig. 9.28, it can be seen that a small change in force/mass produces a smaller change in the angular response when compared to a small change in undeformed length, d_b . Despite this, the responses of the retrieval arm do not change drastically with changes to the inputs; after the initial spike, all reactions seem to coincide with the original response again. Furthermore, the change in inputs produce the expected changes in retrieval arm response. With a higher mass, the angle, ψ_{retr} , is expected to increase due to the stronger forces. Likewise, with a smaller d_b , the angle is also expected to increase as the spring-damper is further away from the point of application of the force. These results show that the simulation is continuous.

Simplified Model Testing

Since $a_b = d_b$ the equilibrium position of the retrieval arm will be where $\psi_{retr} = 60$ deg. To check if this is really the case, the system may be subject to different initial conditions to see if it returns to its equilibrium position. The first initial condition will be $\psi_{retr} = 60$ deg, as this should produce no response. Secondly, the system will be released from $\psi_{retr} = 30$ deg to evaluate the spring-damper under compression. Similarly, the final test will evaluate the system's response to extension by setting $\psi_{retr} = 120$ deg. The response of the retrieval arm can be seen in fig. 9.29. Here, the retrieval arm reacts as expected by starting at the correct initial condition, and returning to its equilibrium position.

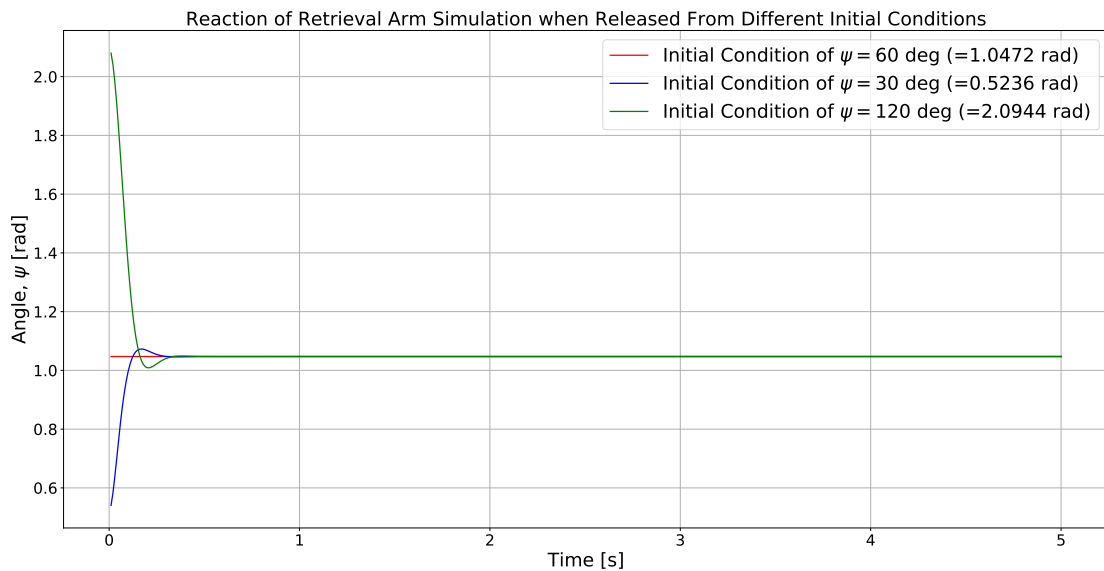


Figure 9.29: Graph illustrating the response of the retrieval arm when released from different angles (initial conditions).

9.4.2. Flying Wing Sizing

As the retrieval arm has been sized, the flying wing may be designed. An illustration of the general layout of the drone is given by fig. 9.30. The drone in this figure has the following control surfaces: a rudder to adjust the lateral position and airbrakes to adjust the longitudinal position by changing the direction of the resultant force on the wing.

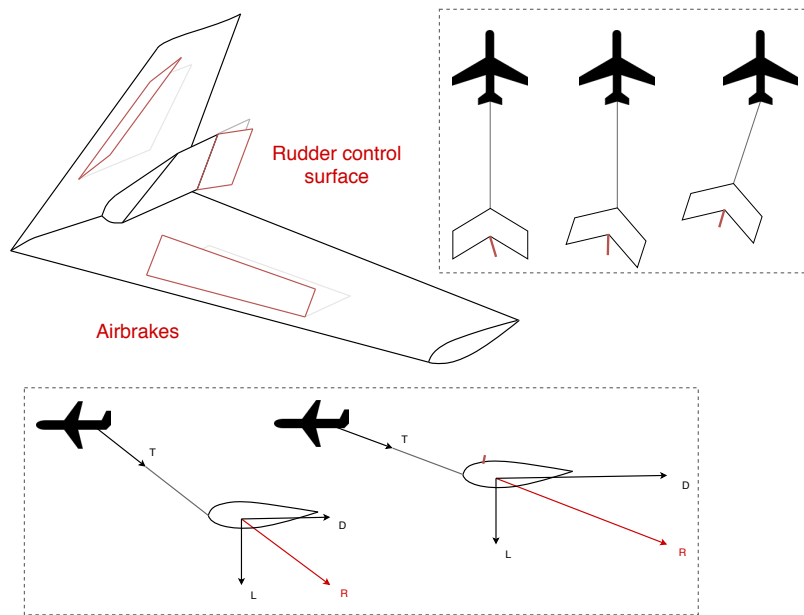


Figure 9.30: Control surfaces used to control the flying wing used for retrieval of the search system.

A symmetric airfoil is selected for the flying wing, as it needs to produce both positive and negative lift. As there are no elevators, the angle of attack of the drone cannot be controlled explicitly. Therefore, to control the angle of attack, the c.g. position with respect to the attachment point of the drone to the tether is changed. Initially, a negative angle of attack is required (to keep tension in the tether). To achieve this, payload on the drone can be used to manipulate the c.g. position. As the camera and retrieval arm are similar in mass (5 [120] and 4.8 kg respectively⁸), they may be placed in-front and aft of the c.g. respectively. The retrieval arm will be placed closer to the c.g. than the camera. This will ensure that a nose down moment occurs as the drone navigates to the search system. However, having a constant pitch down moment would mean that the drone may flip over. To mitigate this, a movable camera may be implemented to actively change the c.g. location. This can also be achieved by moving the retrieval arm with its actuators.

⁸More details about the camera itself can be found in section 9.7

To produce positive lift, the dynamics behind the retrieval process may be exploited to passively increase the angle of attack. As the retrieval arm is located aft of the c.g., once the retrieval arm catches the search system, a nose-up moment will be produced due to the additional mass of the search system. If a cable connects the trailing edge of the drone to the tether, it can be designed such that it becomes tense when the desired angle of attack is reached. This would prevent the drone from flipping over and would ensure an almost instant change in angle of attack, which is favorable.

With the dynamics of the process defined, the best suited symmetric airfoil for the drone should be found. Several NACA airfoils have been researched, more specifically the NACA0008, NACA0015 and NACA0024. XFOIL, an interactive program for the analysis of subsonic isolated airfoils, was used to create $C_l - \alpha$ plots of these airfoils and can be found in fig. 9.31. Only the positive part of the polars are shown, for negative angles of attack the plot would be symmetric around point [0,0]. A Reynold number of 2,200,000 is used, obtained using eq. (9.23), with an airspeed V of 17 m/s and an estimate for the chord length l of 4.5 m. The kinematic viscosity ν is equal to $1.4207 \cdot 10^{-5} \text{ m}^2/\text{s}$ which is the value for air at 10 °C. [121]. It was decided to use the NACA0015 for the design, as its maximum lift coefficient value is highest.

$$R_n = \frac{\rho V l}{\mu} = \frac{V l}{\nu} \tag{9.23}$$

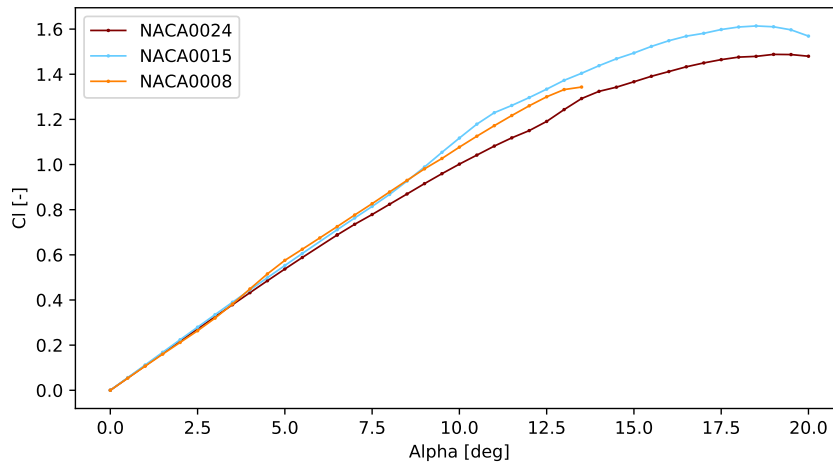


Figure 9.31: Lift coefficient over angle of attack plots for different symmetric airfoils.

The desired lift can be found from eq. (9.24), for which the used forces are shown in fig. 9.32. From section 9.2.2, the force F_z is equal to 3920 N once stable, as can be seen in fig. 9.33. If the sum of forces for both pictures in fig. 9.32 is equal, the aircraft would not experience any change due to the retrieval of the search system. However, as the force F_z varies over time and has a high peak of 0.5 seconds in the beginning, it is impossible to perfectly match the forces. It was decided to find the corresponding lift to the stabilized force F_z .

The weight of the drone including all components is estimated to be $W_{drone} = 15 \text{ kg}$. This includes the robotic arm of 4.8 kg and the camera of 8 kg. The values for L_{max} and L_{min} are equal, as an absolute maximum is desired for both. They will thus be achieved at opposite equal angles of attack. This makes eq. (9.24) an equation with 1 unknown and a lift of $L = \pm 1960 \text{ N}$.

$$F_z + L_{max} + W_{drone} = L_{min} + W_{drone} \tag{9.24}$$

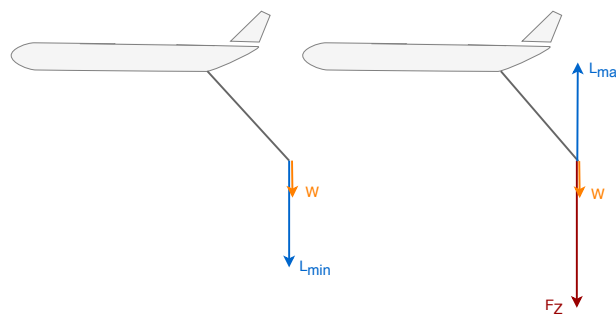


Figure 9.32: Free Body Diagram of retrieval system before and after search system attachment.

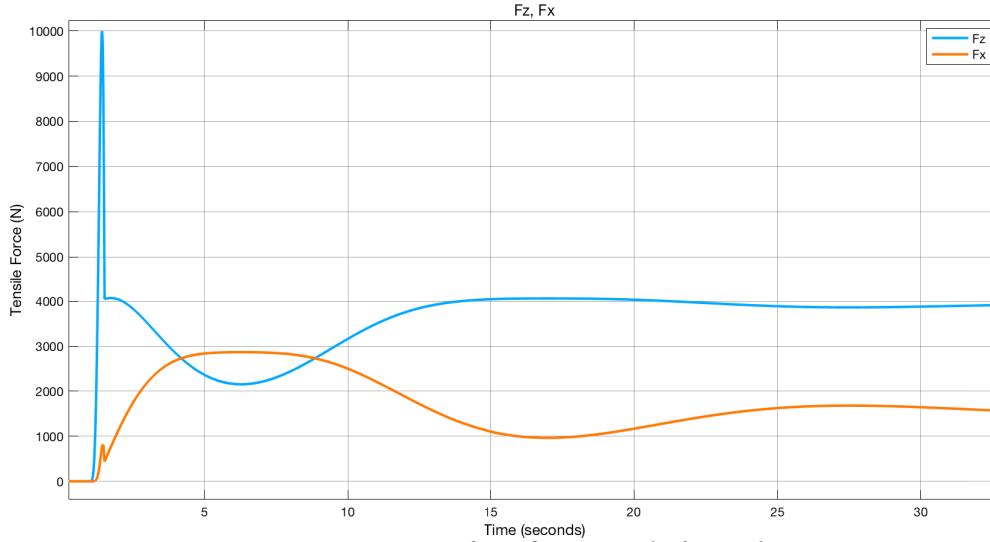


Figure 9.33: Forces acting on aircraft over first 30 seconds of retrieval operation.

To find the needed C_L to generate a lift of 1690 N, the wing aspect ratio, surface and the $C_{L\alpha}$ have to be determined. The slope of the lift curve $C_{L\alpha}$ can be easily found by dividing the change in C_L by the change in α .

To determine the surface and aspect ratio, a preliminary layout has been chosen. However, it is limited by the span. A maximum value of 2 m has been decided on for the span to make it fit into other aircraft as well (e.g. the Lockheed Martin C-130 Hercules).

With the use of an iterative code in Python, different values of C_L and L were calculated for different values of aspect ratio in a range from 3 to 7. The equations used in this code are shown in eq. (9.25), eq. (9.26) and eq. (9.27). With this code, it was found that the lift increases for decreasing aspect ratio and the maximum is achieved when the aspect ratio goes to 0. For an aspect ratio of 3 and a span of 2 m, the lift generated is equal to 2958 N, making the drone over-designed. After making some adjustments, an optimal was found for a span of 1.77 m and aspect ratio of 3.91. The maximum lift for these drone parameters is achieved at an angle of attack of 10° and C_L of 1.1173, as for these values the $C_{L\alpha}$ is highest.

$$L = \frac{1}{2} C_L \rho V^2 S \quad (9.25)$$

$$C_L = \frac{C_{L\alpha} \alpha AR}{AR + 2} \quad (9.26)$$

$$S = \frac{b^2}{AR} \quad (9.27)$$

Drag of Drone

The corresponding drag is found using eq. (9.28) and eq. (9.29). The Oswald efficiency factor e is assumed to be 0.85.

$$D = \frac{1}{2} C_D \rho V^2 S \quad (9.28)$$

$$C_D = C_{d_0} + \frac{C_L^2}{AR\pi e} \quad (9.29)$$

The drag can be further increased using airbrakes. These are placed on the wing and can have a maximum frontal surface of 0.052 m^2 each, when deflected upwards by an angle of 30° . The drag coefficient of a plate is used, equal to 1.28 [122]. The total drag of the wing, when flying at one of the absolute maximum lift value settings, is equal to 167 N. The additional drag caused by the airbrakes is equal to 399 N, resulting in a total drag of 566 N. The final drone parameters can be found in table 9.5. The layout of the drone is shown in fig. 9.34.

Table 9.5: Calculated aerodynamic and geometrical parameters for the flying wing used in the retrieval system.

Parameter	Value	Unit
Span (b)	1.77	[m]
Root chord (c_r)	0.5	[m]
Tip chord (c_t)	0.405	[m]
Sweep (Λ)	30	[°]
Area (S)	0.8012	[m ²]
Aspect ratio (AR)	3.91	[-]
Lift coefficient (C_L)		
- at $\alpha = 10^\circ$	0.815	[-]
- at $\alpha = -10^\circ$	-0.815	[-]
Maximum drag coefficient (C_D)	0.0694	[-]
Drag coefficient at zero lift (C_{d_0})	0.0058	[-]
Oswald efficiency factor (e)	0.85	[-]

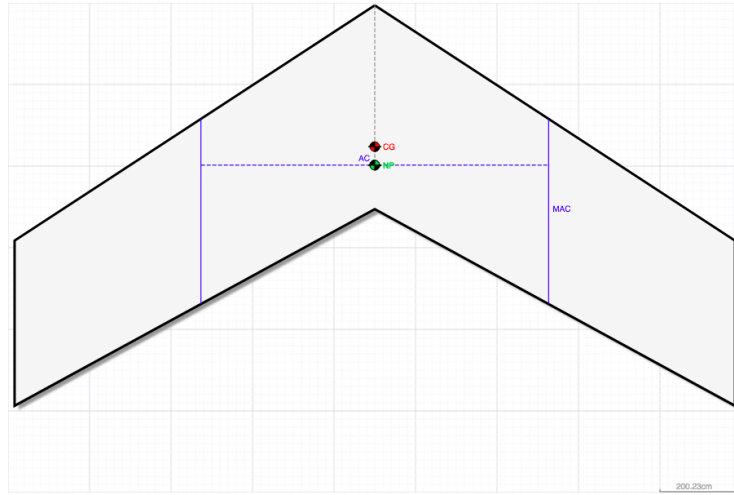


Figure 9.34: Flying wing planform that used in the retrieval system.

When plotting F_z on the aircraft during retrieval, it is found that the resultant force is equal before and after attaching the mother buoy. This verifies that the drone sizing done in this section is correct and achieves the set requirements as displayed in fig. 9.32.

9.5. Hydrogen Balloon with Net

To aid the retrieval process, a hydrogen balloon encased in a net will be released from the search system. This balloon will be inflated from the nose fairing of the search system and these will be connected via a rope. The hydrogen balloon needs to lift the weight of the rope and the net. The rope and net are sized based on the retrieval forces calculated in section 9.2.2. Since the rope will only deal with tension, it will be sized based on the maximum tensile force during retrieval. From **Sim_07**, the predicted maximum tensile force is 56000 N. US Netting sells a rope with a diameter of 0.95 cm and a maximum tensile strength of 17800 lbs (=79200 N) [123], which is strong enough to sustain the retrieval loads. As such, this rope will be used.

$$l_b = \rho_{atm} V_b g \left(1 - \frac{M_{gas}}{M_{air}} \right) \Rightarrow V_b = \frac{L_b}{\rho_{atm} g \left(1 - \frac{M_{gas}}{M_{air}} \right)} \quad (9.30)$$

The volume of hydrogen which is needed to lift the rope is calculated by eq. (9.30) [124]. In the context of the retrieval, the load that needs to be lifted is the rope mass and the mass of the net. To obtain values for the mass, these components need to be sized. For the net, a smaller Kevlar rope diameter may be used (0.64 cm in this case), as the lattice structure of the net allows it to distribute and handle the load better. The hook which is attached to the tether will catch the net structure. The net itself is constructed based on the radius of the hydrogen balloon. The radius is calculated to be 0.72 m for a hydrogen volume of 1.55 m³. The spacing is determined to be 0.05 m, meaning the net is constructed of 29 circumferential ropes in horizontal and vertical directions of length of $2\pi r$. This corresponds to a total rope length of 260.6 m needed to construct the net. With respect to the rope, a length of 6 m was chosen to ensure that there is a clearance of a few meters between the balloon and the waves [115].

The hydrogen, balloon, tether and net need to be stored within the search system. Of these, the hydrogen has the largest volume. Therefore, the hydrogen needs to be compressed such that it fits within the search system dimensions. The tank for the hydrogen is sized based upon an internal pressure of 1000 bar, as this reduces the volume 1000 times. The tank will be a cylinder of length 0.3 m. Using the formula for cylindrical volume and using the pressurized hydrogen volume, the radius was calculated to be 0.0405 m. Using eq. (7.27), and using the yield strength of aluminum 2014-T62, the thickness is determined to be 0.01 m. Aluminum 2014-T62 is used due to its high yield strength and relatively low density [125]. From this, the volume and mass of the cylindrical tank are determined. The materials used and volume and mass of the different components of the on-board retrieval system are summarized in table 9.6.

Table 9.6: Properties and characteristics of the components of the on-board retrieval mechanism.

	Material	Density [$\frac{kg}{m^3}$] [126] [127]	Volume [m^3]	Mass [kg]
Rope	Kevlar	1440	0.00043	0.6156
Net	Kevlar	1440	0.0083	11.88
Hydrogen	-	52	0.00155	0.0804
Tank	Aluminium 2014-T62	2800	0.0024	2.6757
Total	-	-	0.01229	3.5177

9.6. Moving Forward: Possible Validation Experiments

Retrieving payload from land using an aircraft has been demonstrated by the Project Fulton Surface-to-Air Recovery System [114]. Successful retrieval operations have been conducted from water. However, the payload was retrieved from a raft - thereby negating the influence of water drag.

As the proposed retrieval concept will be subject to the effects of water drag, it is important to confirm the feasibility of this concept. Unfortunately, simulations will not suffice to show this. Consequently, a laboratory experiment may be conducted to hopefully show the feasibility of this concept. The goal of this experiment would be to demonstrate a proof-of-concept and to provide data from which the simulation described above may be improved. A few experiments may be conducted which will provide different insights into the dynamics of the retrieval process.

Simply put, the drone-on-tether concept involves the pick-up of a semi-submerged object with a flying vehicle. Consequently, a rudimentary experiment could involve using a conventional quadcopter drone to retrieve a mass floating on water (Experiment 1). If the subsequent results are favorable, then a second - more advanced - experiment may be performed (Experiment 2). This would involve the use of a wind tunnel to match the velocities of the proposed retrieval process. Here, measurements regarding the equilibrium angles and potential retrieval dynamics could be measured. Again, if the results are positive then a third experiment using actual in-flight measurements may be conducted to obtain more accurate data (Experiment 3).

Experiment 1: A Proof-of-Concept

As aforementioned, this experiment would involve the use of a quadcopter to retrieve a semi-submerged object. In this case the quadcopter would act as the aircraft, and the "drone-on-tether" would be a simple hook (e.g. fish hook). Note that this experiment is done before other experiments because it is less time consuming and expensive than the others. As such, if the proposed concept is unfeasible, then resources may be allocated to alternative retrieval methods instead of being spent on further experiments.

Experiment Goal: To show the feasibility of the drone-on-tether retrieval concept on a fundamental level.

Experiment Outline: A small foam (or an equivalent buoyant material) block will be placed in a tub of water. Attached on the top of this foam block will be a hoop/truss which the hook on the drone can catch. Additional mass will be added to this foam block such that it submerges to about half its height. Note that the total mass of the foam block and additional components should be less than 10% of the quadcopter mass.

The quadcopter will fly along a programmed path over the tub of water to retrieve the foam block. High speed cameras may be placed around the tub (at least two in perpendicular directions, with one parallel to the flight path of the quadcopter) to capture the trajectory of retrieval, as well as the change in drone dynamics. A green screen may be used as the backdrop such that a grid backdrop can be easily overlaid. A few practice runs of the flight of the quadcopter with the attached tether can be run such that the equilibrium position of the tether can be determined - this will give an indication of how high the quadcopter can fly when retrieving the foam block. Moreover, the quadcopter can be flown around normally with the foam block attached to see a priori if the foam block severely influences the dynamics of the quadcopter.

If successful, this experiment may be run several times to obtain data to improve the existing simulation of the retrieval process. Furthermore, the mass of the foam block may be slowly increased to see the influence of an increasing mass on the trajectory. A similar change can be done with the volume of the block while holding the mass constant to determine the effect of this variable change. An illustration of the experimental set-up is given by fig. 9.35.

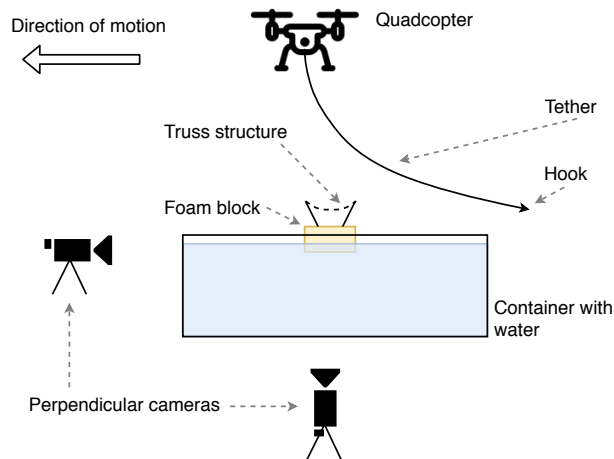


Figure 9.35: Illustration of the set-up of experiment 1.

Experiment Outcomes: There are two main outcomes of this experiment: 1) the drone-on-tether retrieval concept is unfeasible on a fundamental level - in which case, an alternative concept needs to be chosen; 2) this concept is feasible on a fundamental level, and more research can be done with respect to this retrieval option. In case of the latter option, the results of the experiment may be used to improve, and perhaps verify, existing models. Note, however, that the dynamics which occur at this experimental level do not necessarily translate to the real-life situation. As such, more accurate experiments need to be conducted - which leads to Experiment 2.

Experiment 2: Wind Tunnel Measurements

This experiment would involve the use of wind tunnel which can operate at the velocities of the retrieval process. With this, aerodynamics involved in this process are better represented. Two possible tests can be done with the wind tunnel. The first (Experiment 2A) is to investigate the dynamics of the drone itself, and the second (Experiment 2B) is to determine the equilibrium position of a pendulum subject to the velocities of retrieval. The setup of Experiment 2A includes the drone - with deploy-able air-brakes - attached to a rigid⁹ tether. Sensors can be placed to measure the forces induced by the drone. From this, the performance characteristics of the drone, and its influence on the tether, can be measured. Meanwhile, Experiment 2B will involve a scaled model of the search system attached to the end of a flexible tether, if the space in the wind tunnel permits, it would be beneficial to also have a moving water stream to represent the drag in water. As such, the dynamics of drag on the retrieval process can be measured. This would also give an indication of what equilibrium angles can be expected.

Experiment Goal: For Experiment 2A it is to determine the stability and the extent of control of the drone attached to the tether. Meanwhile, for Experiment 2B, it is to establish the influence of air and water drag on a scaled model of the search system when attached to a tether.

Experiment Outline: For both experiments, the test objects¹⁰ will be placed attached to their respective tethers in the wind tunnel section. These test objects will be subject to different air velocities (representing different possible retrieval speeds). First, static measurements of the forces and accelerations acting on the test objects will be taken, along with images/video of the movement of the test object. This will give an indication for the equilibrium position of the tether at the associated flight velocity. See fig. 9.36 for an illustration of the experimental set-up.

For Experiment 2A, the inputs to the control surfaces will be given. The resultant response will be recorded. After this, a mass will be attached to the rear of the drone, representing the moment the search system will induce on the drone. This mass will be "released" to simulate the instantaneous change in moment produced by picking up the search system. Furthermore, if time permits, different profiles and sizes of drones can be tested to obtain relationships between the drone parameters and tether dynamics.

Experiment 2B will also be subject to varying water flow speeds (ideally equal to the air flow velocity) to investigate the effect of water drag on the search system model. Moreover, the mass of the scaled model of the search system will be changed for a given air velocity to investigate the effect of mass on the tether dynamics.

⁹The tether needs to be rigid in this case to limit the angles of the drone such that it does not collide with the boundaries of the wind tunnel. This set-up is not completely unrealistic as the flexible tether will be kept tense.

¹⁰Experiment 2A test objects are the drones. Experiment 2B test object is the scale model of the search system.

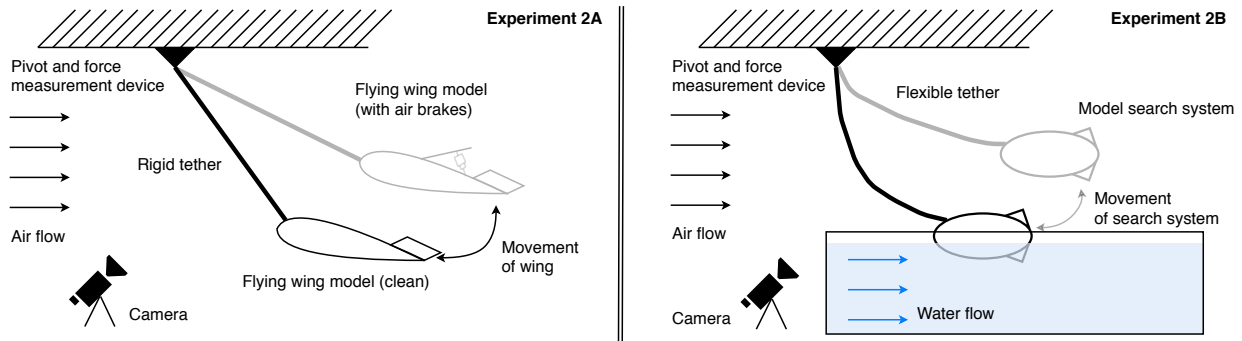


Figure 9.36: Illustration of the set-up of experiment 2A (left) and 2B (right).

Experiment Outcomes: Both experiments will provide insights into the equilibrium positions of the tether, as well as the obtainable range of θ_r . For Experiment 2A, some design changes to the control surfaces/air brakes may be required to obtain better performance. With Experiment 2B, an optimal retrieval velocity may be selected. Both experiments will give relations for the tether dynamics, which can be used to estimate the actual retrieval dynamics. Additionally, the results of this experiment may be used to validate the created simulations.

Experiment 3: In Aircraft, High Altitude Measurements

The prerequisites for this experiment are: a working model drone and an indication of the forces of the retrieval process. With these, an simulation of the retrieval process can be performed by an aircraft at a high altitude. To do this, the drone will produce a artificial forces (e.g. increasing downforce or drag) which mimic the expected retrieval forces. This will be performed at an elevated altitude for safety reasons.

Experiment Goal: Demonstrate the feasibility of the proposed retrieval process in practice.

Experiment Outline: Once at the experiment altitude, the drone will be deployed from the aircraft. From here, the drone will begin simulating the retrieval process by manipulating its drag and down-force. Note that, in order to accurately do this, it may be necessary to use a drone larger than the actual drone of the retrieval process. In the event that this drone is too large to fit in the aircraft, additional mass may be added to the test drone. This, however, is accompanied by added risks and safety hazards. As such, as a countermeasure, the tether will be detachable from the aircraft such that the test can be aborted, should it be necessary. Consequently, this test shall also be performed over water or uninhabited land.

For initial measurements, the pilot will be instructed to not touch the controls such that the aircraft’s natural response can be recorded. Of course, if the response gets out of hand, the pilot may abort the test. This measurement run shall be done several times to obtain more reliable results. After this test, or in the event that it is deemed too unsafe, the pilot can attempt to maintain the aircraft velocity and altitude. This is done to determine if the pilot themselves are capable of controlling the response - or if computer assistance is necessary. An depiction of the experimental set-up is given by fig. 9.37.

Experiment Outcomes: The response of the aircraft to the retrieval process, and if a computer assisted system is needed to maintain control of the aircraft. Moreover, the response of the aircraft will also heavily restrict the velocity and altitude in which the retrieval must occur. Consequently, some design parameters may need to be adjusted to accommodate these restrictions.

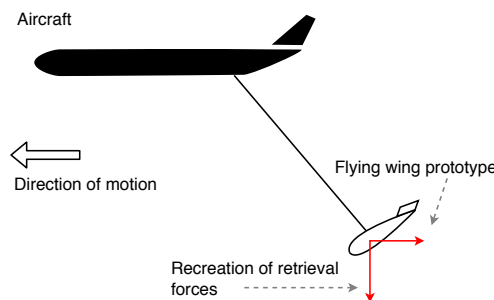


Figure 9.37: Illustration of the set-up of experiment 3.

9.7. Power

As the different aspects of the retrieval process have been established, the power consumed by this system may be estimated. The drone and winch are attached to the aircraft itself. Therefore, the aircraft may supply the power for these components. The only power consuming units which are fixed to the search system are the mechanisms used to inflate and release the balloon. As such, a distinction will be made between the constituents of the retrieval system, depending on where they receive power.

9.7.1. Power Requirements of Components Attached to Aircraft

Some military aircraft have integrated winches, however, if the C-130 is used, then the on-board winch is insufficient as it cannot withstand the retrieval loads. Therefore, a new winch needs to be selected. An off-the-shelf winch may be installed onto the C-130, and its properties are given by table 9.7.

Table 9.7: Specifications of the FA5-24 winch [128].

	FA5-24
Capacity	5000 <i>kg</i>
Mass	849 <i>kg</i>
Volume	1.243 <i>m</i> ³
Power	18642.5 <i>W</i>
Rope length*	166 <i>m</i>

*The rope has a diameter of 22 mm.

From table 9.7, it can be seen that the winch consumes a large amount of power, at 18642.5 *W*. With this winch it is possible to quickly reel in the search system - this can be done in around 20 seconds at maximum capacity. However, lower reel-in speeds are advisable as the retrieval is not time critical.

The additional power requirements for the retrieval subsystem come from the actuators on the drone and the sensors used for retrieval. The sensors on the drone and aircraft are needed to accurately determine the position of the target (i.e. balloon) on the search system. As mentioned in section 9.1, visual seroving will be employed to accomplish this. For this, a minimum of two cameras are needed, but ideally, three cameras should be used [110]. For this two cameras will be put on the aircraft, with one camera on the drone. Additionally, the desired range operational conditions limit the cameras which can be used for this process. For example, the selected camera shall be able to identify the target in fog. A suitable camera is the Opgal Sii FG. This camera has an acquisition rate of 300 frames per second, and is designed to operate in conditions with severely reduced visibility [129]. This camera can also identify objects as far as 10 km, although no visibility condition was specified for this value [129]. An individual camera consumes 45 *W*, corresponding to 90 *W* for two cameras [129]. Only two cameras are used as different, lighter, camera is implemented on the drone, such as Opgal's Sii ML. This camera has a mass of around 5 *kg*, with a power consumption of 60 *W* [120]. However, this comes at the cost of reduced fog visibility.

The power requirements of the actuators used by the control surfaces will be much smaller than that of the cameras. In any case, the aircraft should be able to supply adequate power to these systems. In fact, the APU family used by the A400M is capable of producing 127.6 *kW* of power [130] and can be used for external appliances. This is more than sufficient to meet the power requirements of the winch, drone and sensors.

9.7.2. Power Requirements of Components Attached to Search System

The release mechanisms for the hydrogen balloon are the only components which will consume power from the buoy. These components, however, will use minimal power as they do not run continuously. Despite this, the only power available during retrieval will be the 50 *W* produced by the hydrogen fuel cell selected in section 7.7.2. This is because the batteries will likely be depleted at this point. Recharging is possible, but may delay retrieval. Consequently, the minimum power available will be used.

The release mechanism of the balloon can be designed such that no electrical power is needed. The inflation of the balloon in the nose of the submarine can trigger the opening of the nose fairing, this can be done mechanically. If designed correctly, this opening can be done "one-way" such that the impact from deployment does not open this fairing.

Doing this would mean that only the valve used to inflate the balloon will consume power. An off the shelf electric valve may be used for this purpose. Valworx manufactures a waterproof electric actuator valve suitable for the inflation of the hydrogen balloon [131]. This valve has a nominal power consumption of 30.71 *W* [131] - this can easily be supported by the hydrogen fuel cell, with some power to spare for communications.

Final Concept of the ULB Project

This chapter summarizes the results of the operations, deployment, submarine & mother buoy and retrieval systems. Section 10.1 discusses the design of each of these systems. A hardware diagram of how these system interact with each other can be found in section 10.2.

10.1. Concept Overview of the ULB Project

Operations It is assumed that the exact location and shape of the search area is given prior to the search mission, by an external organisation. The coverage path within this search area will then be planned accordingly and is also dependent on factors such as weather and current. For now, a circular search area with a radius of 100 km has been assumed and the range of the ULB is assumed to be 2 km. The coverage path will consist of parallel paths connected with turning points outside the search area as it was found that the Inertial Navigation System implemented within the submarines are most accurate when the submarines travel in straight lines. In order to be well within range of the ULB signal and decrease the total coverage path, the submarines search at 500 m above the bottom of the ocean. This results in a total distance of 9400 km for the coverage path. To confidently cover the search area and locate the ULB signal, the search system will take 20 days to cover the entire search area. This is known as search phase one. Each search system will look for the signal individually and together they will cover the total coverage distance. By combining the distance with the submarine velocity, 1 m/s, and a search time of 20 days, the total number of submarines was determined to be 6. Once one of these search systems receives the ULB signal, an approximate location of the aircraft, in the order of 1 km, can be determined. Therefore, the total search area can be reduced. The reduction of the search area initiates the second search phase where all search systems will relocate to the smaller search area and a new search is started. However in the second search phase, the aircraft position will be determined with a minimum of three submarines - ensuring an accurate aircraft location via triangulation. The relocation of the search systems and coverage of the second search phase will take 10 days. Factors that could create a risk for the operation of the search mission include current, variation of ocean depth, obstacles in the ocean and deep-sea search. A system of equations has been set up that can make up for the deviation due to lost current, by redirecting and slightly speeding up the submarines if necessary. Large obstacles, including small islands, in the search area can be mapped and therefore taken into consideration when planning the coverage path. The submarines will not be equipped with any obstacle-avoidance equipment, but considering their low speeds, impact with any obstacle is not considered problematic. Furthermore, the chance of finding obstacles at a depth of multiple kilometres is very small. The risk of deep-sea search is that the pressure might affect the equipment of the search system. However, this has been taken into account for the design of the search system. Moreover, it was found that it only takes 1148 s to get to the maximum search depth of 4500 m. Thus, depth change is not an issue for the search mission.

Deployment System To design the deployment system, the main aim was to reduce the impact force to a minimum, by decreasing impact velocity and/or surface area. Free fall was analyzed under unsteady, non-straight and symmetric flight conditions and modelled using non-linear differential equations. The outputs of this included a velocity vector, a position vector and an orientation of the submarine during free fall. Two control surfaces on the aft spherical end of the submarine were designed accordingly, in order to control the deployment and to ensure that the submarine lands as to create minimum impact force.

Submarine For navigation of the submarine, an Inertial Navigation System is used for up-to-date position updates while moving underwater. It integrates acceleration into velocity and displacement in order to determine its position, requiring force and angular rate in three dimensions, provided by accelerometers and gyroscopes. One problem of the Inertial Navigation System is that it has growing error. One way to compensate for this error is by using the Kalman filter, which improves the accuracy of the state vector and thus of the navigation. Furthermore, depth sensors and a compass are used to aid the measurements for navigation. The mother buoy is connected to the submarine by GPS and will send a GPS update every 5 minutes. For communication, a low frequency must be used to minimize sound absorption. An acoustic modem including a transducer will be used. Furthermore, a satellite modem and antenna will be present on board of the submarine, so that when it loses communication with the mother buoy, it can come up to the surface and send its location to the base station.

In order to control the depth of the submarine, a buoyancy control system is needed. The submarines will be equipped with a variable ballast system (VBS) to alter the mass of the submarine and control the pitch. To empty the tanks when desired, a pump is used that can overcome the high ambient pressure. Furthermore, an emergency ballast is included into the design in case the submarine sinks due to failure of buoyancy control. A propeller is mounted on the rear end of the submarine to provide the necessary 18.4 N of thrust. For stability of the submarine, it is assumed that the submarine is naturally stable in pitch and yaw. This is due to its torpedo shape, where any rotation is counteracted by an opposite rotation due to the drag on the aft of the hull. The submarine will be controlled in yaw by a rudder mounted on the aft of the hull. Pitch is controlled by horizontal control surfaces on the aft of the hull and the center of gravity, that can be changed by the ballast tanks.

For power, both a battery and a hybrid system were considered. Both systems have the risk of ignition, however the batteries also lack sustainability and recyclability. Furthermore, batteries are much more expensive and would result in a bigger volume than a hybrid system. For these reasons, a hybrid system using a 50 W fuel cell system will be used, supported by a small lithium-ion battery.

To design the structure of the submarine, different load cases were analyzed. The first one included the impact on water, followed by pressure at maximum depth and the retrieval force. Pressure at maximum depths appeared to result in the largest force acting on the submarine structure. Stiffeners were designed to decrease buckling force. This resulted in a reduction of mass, however increases susceptibility to yielding. From the above calculations, the dimensions of the stiffeners used in the submarines were iterated, including a 20% safety factor. The resulting length of the submarine is 2.5 m, with a diameter of 0.5 m. The shell will be made out of 0.0098 m thick CFRP, where 8 stiffeners are used for reinforcement. The total mass of one submarine is 393 kg.

Mother Buoy The mother buoys include a lantern powered by its own solar cells and a battery to prevent collisions with sea traffic. It will use the same communication equipment as the submarines. Furthermore, the mother buoys will follow the submarines by receiving GPS locations from the submarines. In order to move at the same velocity as the submarine, the mother buoys might need to travel slightly faster in order to compensate for stronger currents on the surface of the ocean. However, no design changes will be made, as this is not necessary. The total mass of one mother buoy is 414 kg. The mother buoy and submarine can be seen together in fig. 10.1.

Retrieval System For the retrieval, a drone-on-tether system is used. The tether is fixed to a winch, which reels the system once the search system is hooked. The drone keeps the tether tense by manipulating its drag through airbrakes. A small robot arm, on the bottom of the flying wing, will fine-tune the position to ensure successful retrieval. On the search system itself, a hydrogen balloon is deployed, which rises to an altitude of 6 m and is picked up by a hook, attached to the military aircraft by the retrieval arm. A render of the retrieval system can be seen in fig. 10.2.

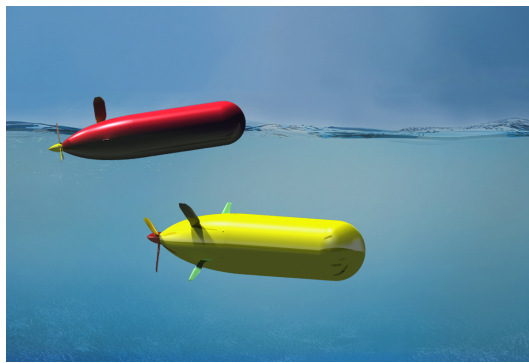


Figure 10.1: Search system render consisting of mother buoy and submarine.



Figure 10.2: Render of retrieval of a submarine using the drone.

10.2. Hardware Diagram of the ULB Project

In fig. 10.3 the hardware components of the different systems and subsystems are illustrated in a block diagram. The hardware components per subsystem of the aircraft, submarine and mother buoy and the relations between these components are shown.

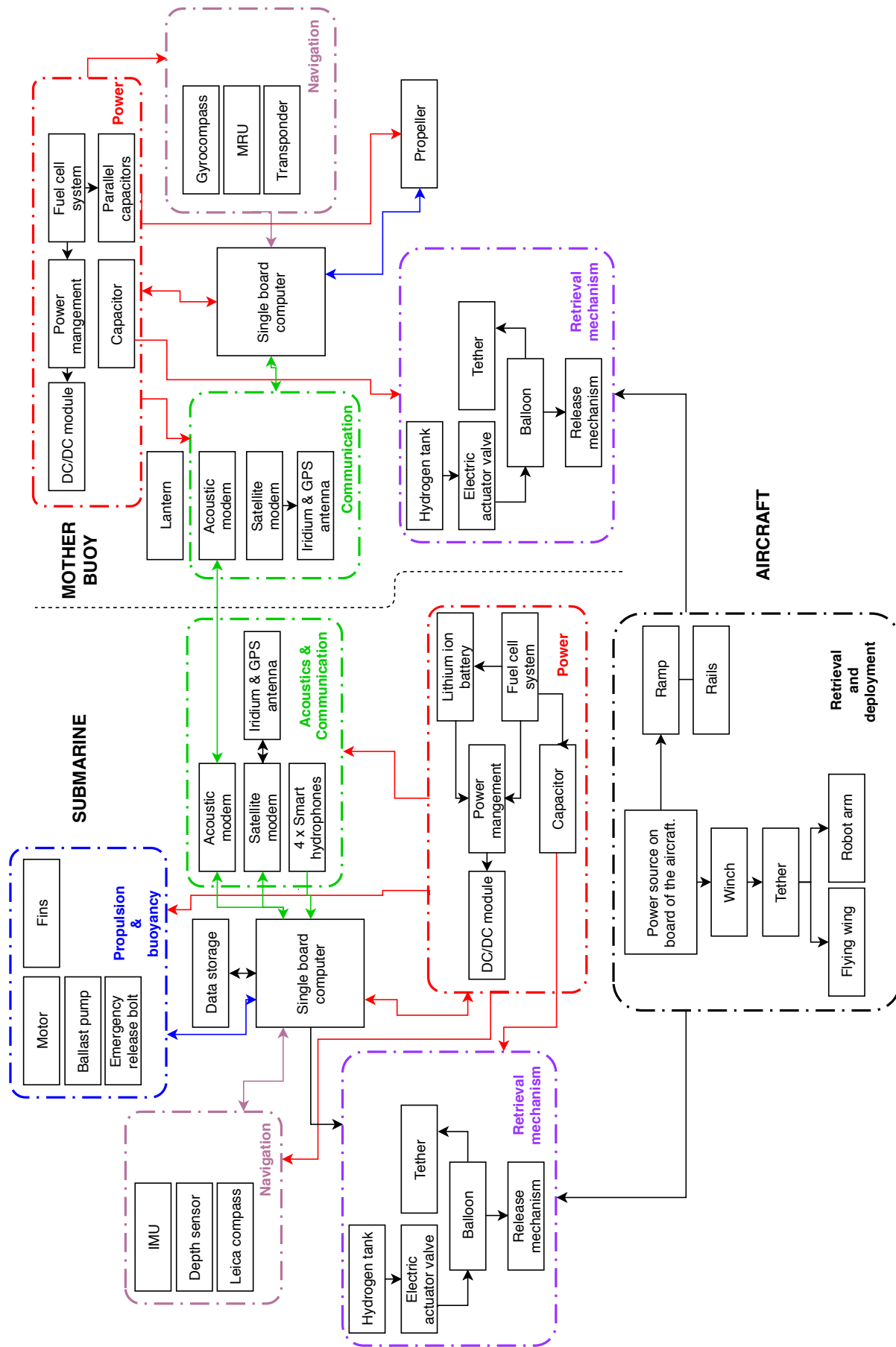


Figure 10.3: Hardware diagram of the different systems and subsystems.

Risk Assessment

This chapter describes the risks associated with the ULB project and proposes some mitigation strategies for these. First, in section 11.1 potential risks - both technical and operational - are identified. To reduce these risks, section 11.2 presents some risk mitigation strategies. Here, a description of the strategy is given, along with which risk events they affect.

11.1. Risk Identification

This section presents potential risk events that may occur during the development and operation of the mission. These risks are categorized into different system related risks and, for the risk events that do not belong to a system, external risks. For each risk event, the severity and probability of each risk is defined. This is illustrated through a risk map, wherein the impact is measured qualitatively where "Catastrophic" means mission failure and "Negligible" is inconvenient to mission success. The probability is also measured qualitatively, based on the "Words of Estimative Probability" used by the Central Intelligence Agency of the U.S. [132]. This section concludes with a risk map, which visualizes the extent of the identified risks.

Airborne System Risks

- AR01 **Damage of airborne vehicle** is not probable as it will only be used to deploy and retrieve the search system. This event is catastrophic, especially when the airborne system is in the deployment phase. From the simulation in section 9.2.2, the retrieval dynamics should pose no risk to the aircraft. However, this neglects waves, thus the presence of waves poses a risk to the aircraft should a wave hit the search system during retrieval.
- AR02 **Unavailability of airborne system** means that the system can not be put into action, this could be due to maintenance. This event is catastrophic. The probability of this to happen, however, is low as the chosen aircraft type is common in military, and thus many are available. Furthermore, the system is designed such that it can be implemented in military transport aircraft (such as the A400M and C-130J).
- AR03 **Malfunction of airborne vehicle** will almost certainly not occur as these aircraft have been rigorously tested to ensure that they operate as intended. However, incidents and accidents still occur, such as the A400M crash in Seville in 2015 [133]. The issue here was that some essential software was accidentally erased. This event would be catastrophic if it were to occur.

Operational Risks

- OR01 **Lack of training/experience for operational personnel** could incur some delays in mission operations. Therefore, trained personnel should be available at each station in the network who can use the aircraft, the deployment & retrieval system and the communication system. The probability of too few users with required knowledge available, is about even [132] - due to the wide network. However, impact is marginal as there will be travelling teams.
- OR02 **False positive signal detection** is critical on the mission as it may trigger Phase 2 and cause a relocation to the location of the false signal, causing delays. Even though the signals are screened on-board with cross-correlation, due to the noise at sea, false signals may be sent for analysis to the ground station. From reference missions where analysts are used, the probability of finding an acoustic signal that is not associated with the ULB is about even [134].
- OR03 **Inconsistent work** will almost certainly happen due to the low frequency of air crashes over the deep water, as such there is no reliable stream of income. Impact is marginal due to secondary missions, but these are not always guaranteed.

Deployment Risks

- DR01 **Damage to search system fins** may occur during the descent from the aircraft, the impact with water, or during the transportation of the search systems. Damages are improbable due to the simplicity and design of the deployment trajectory and fins. The consequences for deployment operations are significant due to time constraints. The impact is therefore catastrophic. Moreover, if a fin breaks during descent, then the trajectory may be altered - causing the damage of a search system.

DR02 **Altered trajectory due to aircraft wake** is critical for the search system as it may cause it to hit the water in the wrong orientation, potentially causing damages. This is more critical for the mother buoy as its hull is not made as strong as the submarine's. The search system will probably be deployed in the wake of the aircraft. However, it only feels the influence of this for a few seconds as it falls.

Search System Risks

SR01 **Damages to submarine** due to both internal factors (e.g. short circuit) and external factors (e.g. collision with undersea mountain or marine life). This event encompasses anything that may negatively affect the performance, such as structural failures, communication loss, leakages, and/or faulty subsystems.

- (a) For a single submarine, impact is critical as other search systems are still operational. However, this may induce some delays. The likelihood of this occurring is not probable.
- (b) For a significant¹ number of submarines, the impact is catastrophic, as the mission can no longer be performed. This will almost certainly not occur as it necessitates damages compromising multiple search systems.

SR02 **Damages to mother-buoy** due to both internal factors (e.g. thermal runaway of batteries) and external factors (e.g. rough water). This event encompasses anything that may negatively affect the performance, such as structural failures, communication loss, leakages, and/or faulty subsystems.

- (a) For a single mother buoy, impact is critical as accurately tracking the submarine's location is no longer possible, but the submarine can somewhat navigate with the on-board IMU. The likelihood of this occurring is not probable.
- (b) For a significant¹ number of mother buoys, the impact is catastrophic. Even though the mission can still be carried out, as the submarines may still be operational, the location data obtained may be highly inaccurate. This will almost certainly not occur as it necessitates damages compromising multiple mother buoys.

SR03 **Search system deployed on secondary missions when an airplane crashes** is probable as they should be serving a secondary purpose to remain cost effective. The impact is critical as the search system may need to be retrieved first, causing delays.

SR04 **Loss of communication between mother-buoy and submarine** would imply that the position of the submarine is no longer known. This event is not probable to happen as it is a system that is currently used by Kongsberg [135]. Therefore, this system is a proven technology. The impact of this event is critical as there are still other search systems which may continue the mission, albeit delayed. The submarine - if undamaged - will surface at the end of its search path, and thus can be retrieved.

SR05 **Submarine runs out of power**, this can be due either insufficient battery capacity or a power outage. This would have critical consequences for the submarine, as it cannot move or communicate without power, this would probably lead to losing the submarine. It is however not probable that this will happen.

SR06 **Malfunction of buoyancy system** is critical as it may entail the loss of a submarine, which would delay the mission. Although the mission can continue, the environment will be negatively affected due to the loss of the submarine. Moreover, a replacement would need to be made, incurring more costs. As such, from a sustainability standpoint, this event is very problematic. The loss of a submarine due to buoyancy failure will almost certainly not occur due to the presence of the emergency ballast - provided it too does not fail.

SR07 **Failure of the propulsion system** would mean that the search system would no longer be able to perform its function. The impact of this is critical as the search system can still be retrieved, but the mission will be delayed. However, this is not probable to occur.

Retrieval System Risks

RR01 **Damage to flying wing (drone)** will probably occur during operation only, and thus the probability of occurrence is low. This could happen due to external factors, such as wind or waves, destabilizing or outright damaging the drone. The impact would be critical, as without a working drone the mother-buoys/submarines cannot be retrieved, but this is not time critical and the systems can be retrieved by other means (e.g. boat) if necessary.

¹Here, significant refers to the number of submarines for which the mission can no longer be performed

- RR02 **The retrieval arm fails to grab/locate search system**, meaning it attempts to grab the search system but misses (by failing to navigate to search system or by failing to secure the tether). This could happen due to unfavorable weather conditions, or due to unpredictable movement of the search system/drone itself. The chances that this happens are about even. However, the impact is negligible, as the aircraft can turn around and try again.
- RR03 **Tether breaks off** as a result of not being able to withstand the loads. This would be critical, as the drone would be lost and the retrieval process will have failed. As the submarine is deployed via free fall, it will most likely survive the drop. However, the mission will have ended, and thus the lost systems may be readily replaced. The probability of this occurring is low, as the tether is designed to withstand the predicted loads. It will thus only happen if the predicted loads are lower than the actual loads on the tether, which will almost certainly not be the case.
- RR04 **Drone collides with search system** will almost certainly not occur since the retrieval process is designed to avoid this. However, with unpredictable weather and currents, it is still a possibility. The impact would be critical since the mission has failed. However, there would be a potential loss of drone and submarine, which is detrimental to future retrieval operations or missions.
- RR05 **Balloon on search system fails to release** is a critical event as would mean that the search system cannot be retrieved by the airborne vehicle. Due to the reliability of valves, it is a real possibility. Despite this, the search system may still be retrieved by boat if it needs to be.
- RR06 **High waves hit the search system/drone during retrieval** will probably not occur as the balloon should be taller than the waves. However, extreme cases exist. The impact of this event is marginal if the search system is hit, as it can still be retrieved and repaired. However, if the drone is hit, its performance may be compromised. Therefore, this event is critical.
- RR07 **Malfunction of drone control systems** entails the failure of the drone to actuate its control surfaces/air-brakes or if the control system fails to identify the search system. This event will probably not occur, and would be marginal as the aircraft can attempt the retrieval again or bring the drone back inside and to fix the problem. This event would incur some delays, but as retrieval is not time critical, it is not of primary importance.

External Risks

- ER01 **Telecommunication interference/losses due to range and attenuation (e.g. rain)** is certain as there will always be losses. The consequence depends on the level of interference/loss and attenuation, but these may lead to a complete loss in communication. As such, this event is critical².
- ER02 **Unfavorable weather conditions disallowing the use of the airborne system** has critical impact, due to delays. The probability of this event is low due to the airborne system chosen (military aircraft), only for very extreme storms will the system be unable to operate. Such storms are not probable.
- ER03 **Ship damage due to search systems** is not probable to happen, as most of the search mission is performed by submarines under water. However, if a search system damages a ship, impact may be marginal³ on cost.
- ER04 **Search system vandalism** (e.g. by pirates) may compromise the operations of the search system, depending on the severity of the vandalism. This event also encompasses possible theft. This event is more of a concern for the mother-buoys rather than the submarines, as they are permanently on the surface.
- (a) For a single search system, impact is critical⁴. The likelihood of this occurring is not probable.
 - (b) For a significant number of search systems, the impact is catastrophic⁴. This will almost certainly not occur as it necessitates the vandalism of multiple search systems. This type of vandalism is more probable in Phase 2 than in Phase 1 as the search systems will be located in close proximity.
- ER05 **Too strong currents causing deviations in planned path** is mainly an issue for the mother buoy as the currents are faster on the surface. This will most probably occur due to the nature of currents. However, as described in section 5.2, the search systems can account for most deviations. As such, the impact is negligible. Extreme scenarios may occur, which have critical impact on the mission as the communication between mother buoy and submarine may be lost (see SR04).

²Intentional interference (e.g. hacking) would be catastrophic as the transmitted data can be corrupted or changed.

³Depends on severity of crash; if a large boat sinks, impact is catastrophic. If it just scratches the boat, impact is negligible.

⁴Same reasoning as with M01.

ER06 **Missing sections of the search area due to depth variation** would occur due to the assumption that the search system moves along a constant depth from the surface. This depth is 500 meters above its initial landing point. Therefore, if the depth of the ocean increases, sections of the search area would not be covered. This event is not probable as the depth variation in deep ocean is not large [24]. However, the impact is catastrophic as the location of the crashed aircraft may be missed.

ER07 **Broken ULB** is not probable, as the ULBs are designed to survive crashes. Moreover, there are usually two ULBs aboard the aircraft to mitigate this risk. However, instances where both ULBs break, such as Air France flight 447 [134], are still a possibility. The impact of this is catastrophic as the aircraft cannot be found with the hydrophones.

Table 11.1: System Risk Map for ULB finder system, the different events are given below. Colors indicate the importance of each risk; red indicates high risk, yellow indicates medium risk, and green indicates low risk.

Probability	Almost Certain	OR03	OR01	ER01	AR01, AR02, DR01, ER06, ER07
	Probable	ER05		DR02, SR03	
	Chances About Even	RR02		OR02	
	Not Probable	RR07, ER03		SR01a, SR02a, SR04, SR05, SR07, RR01, RR03, RR05, RR06, ER02, ER04a	
	Almost Certainly Not		SR06, RR04	AR03, SR01b, SR02b, ER04b	
	Negligible	Marginal	Critical	Catastrophic	
Impact					

11.2. Risk Mitigation Strategies

This section will discuss possible risk mitigation strategies to reduce the risks presented in section 11.1. These are described below. Table 11.2 gives an overview of the possible strategies, and indicates which risk events they affect (both positively and negatively). Not all risks could be mitigated since some risks were based entirely on uncontrollable factors. As such, the consequences of these risk events will be accepted. These risks include ER02, ER05, and ER07 which have to do with poor weather, ocean currents and broken ULBs respectively. A posterior risk map is given by table 11.3.

RM-01 **Redundant submarines/buoys** mitigate risks associated with submarine/buoy losses and damages by reducing the impact of single failures. Moreover, the probability of failure of a significant number of search systems is decreased with redundancy. However, deployment times, transport space and both development and operational costs will increase. Additionally:

- (a) For the mother-buoys, an increase in number means that the likelihood of vandalism/ship strikes increases.
- (b) For submarines the risk of vandalism/ship strike does not increase significantly, as they mainly operate under water. However, they still surface for retrieval, and in the event of an emergency.

The redundant submarines/buoys can be implemented at the search location and/or stored as spares at the base station. These can be deployed if required. Furthermore, having spares mitigates risks associated with mass losses (e.g. from an extreme storm). This, however, incurs more costs.

RM-02 **Involve a ship in the mission** would mitigate the impact of risks associated with the failure or malfunction of the retrieval system. If the retrieval system is unable to operate (due to damages or otherwise), the ship may be used to pick-up the search systems. This will primarily serve as a back-up, especially since it would take time for the ship to arrive at the location. Furthermore, having a ship will allow for search system repairs/recharging to be done on-site. If successful, the search system may be quickly redeployed. An alternative would be to bring spares on the ship, which can replace non-operational search systems. When not repairing things, the ship may also be used to search for the ULB signal.

RM-03 **Multiple retrieval devices** mitigate the impact of damages, as the system can be replaced during the mission. This strategy can be implemented through redundancy or the use of "spares". An example of "spares" would be to keep some extra retrieval system parts on the aircraft itself (e.g. extra drones or retrieval arms), which can be replaced on-site. The probability of a component failure remains the same. The initial costs will increase.

- RM-04 **Experiments/Rigorous testing** can be run on prototypes of different components of the mission to obtain information about unknown parameters. For instance, the influence of the wake of the aircraft on the deployment of the search system can be obtained through experimental data. This would help design the control system for the deployment fins. Therefore, this mitigation method applies to any novel technology. Moreover, this strategy aims to reduce the risk event's probability of occurrence - by gaining a better understanding of the implemented technology.
- RM-05 **Employ a safety function which causes submarine to rise in case of emergency** lowers the probability of losing a submarine due to communication, power, or propulsive failures. Moreover, if this is used in combination with RM-02, then the impact may also be reduced as the submarine can be repaired on-board the ship. In the absence of the ship, the floating submarine is now more prone to vandalism and ship strikes until retrieved.
- RM-06 **Use of a streamline/sharp nose fairing or reinforced hull** addresses risks associated with impact damages from deployment. Streamline surfaces allow for greater penetration - such that the mother-buoy can dissipate its energy while travelling through the water. With this the probability of both external and internal (less severe shocks acting through the system) damages can be lowered. The reinforced hull not only helps to mitigate deployment damages, but will also provide some resistance to wave impacts during retrieval.
- RM-07 **Use of multiple (potentially different) airborne vehicles**, if planned correctly, ensures that at least one airborne vehicle is available for deployment at all times. This reduces the probability and impact of unavailability. Furthermore, a fleet of air vehicles may be used for more timely/efficient deployment or retrieval. As the system is compatible with both the A400M and C-130, the probability of an unavailable aircraft is further lowered. This compatibility also makes the system more attractive to prospective buyers. However, more vehicles will require more trained personnel and storage space, increasing operational costs.
- RM-08 **On-board data storage** will mitigate impact of communication failures. By having on-board storage, none of the information collected by the submarine will be lost. Moreover, in combination with RM-07, the submarine can rise and send a distress signal (if possible). Otherwise, along with RM-02, the ship can search for this lost submarine. The data can be reviewed once the submarine is retrieved.
- RM-09 **Encryption of transmitted data** will lower the probability of the data being intercepted and modified. The severity of this risk occurring remains the same. The disadvantages of this are that more computational power will be required to support encryption and decryption. Furthermore, the encryption is only possible on the mother buoy as the submarine has a extremely limited bit rate to use, as such, payload data takes a priority here.
- RM-10 **Program a "safe-mode" into the search system** which is able to run only on the power provided by the hydrogen fuel cell, in case the batteries fail. It would also be beneficial to split the power between batteries such that one battery failure does not result in a system failure. This safe-mode would keep only the essential functions of the search system running. This mitigation strategy reduces the impact of power outages.
- RM-11 **A visual alert object on the mother-buoys** can reduce the probability of ship strikes. However, this strategy will only work if the operators of the boat see the alert. To solve this problem, alert messages could be sent to all ships in the area, ensuring that operators are aware of the mother-buoys. The mother-buoy GPS coordinates could be broadcast to nearby ships, but this would increase the probability of vandalism.
- RM-12 **Use of reference mission data** to help distinguish between an actual ULB signal and a false positive. More advanced techniques would involve using machine learning to help with the process. However, trained professionals are also well equipped to aid with the identification process. In either case, the more data available, the better. This strategy reduces the probability of following a false positive signal.
- RM-13 **Design with current maintenance/operational/manufacturing practices in mind** minimizes personnel that needs additional training to operate the system effectively. This is mainly relevant for the airborne system - for example, using a civil aircraft with minimal modifications allows the use of typical civil aircraft maintenance engineers. The search system and deployment & retrieval system will probably require additional training but can be designed such that the processes involved reflect those commonly used in the industry. However, this requires designs to be as compatible as possible with current standards and may limit design options.
- RM-14 **Constantly deploy search system on secondary missions** ensures that there is a reliable revenue stream, lowering the probability of not making money due to infrequent work. However, this would mean that the system is almost always deployed on a secondary mission when a plane crashes. The constant use of the system increases the probability of damages. Due to negatively affecting more severe risks, this method's consequences have not been represented in table 11.2, as it will not be implemented. However, this mitigation strategy is kept for future use (in case revenue is low) and to indicate that more adaptive/scientifically

diverse payload instruments are of importance for versatile secondary missions. However, this risk mitigation strategy should be avoided without redundant mother-buoys.

RM-15 **Incorporate a safety release of the retrieval system** to abort the retrieval process, if it becomes too dangerous, mitigates the probability of damaging/crashing the aircraft. This strategy is more of a safety countermeasure to ensure the safety of the aircraft. Of course, this has several negative impacts for both the retrieval system and the search system as both may be damaged during this process.

Table 11.2: Table describing possible mitigation strategies and the risk events which they affect.

Method Identifier	Mitigation Strategy	Associated Events	
		Positively affected	Negatively affected
RM-01	Redundant submarines/mother-buoys	DR01, SR01-07	OR01, ER03, ER04
RM-02	Involve a ship in the mission	SR05, SR07, RR01-03, RR05, RR07, ER07	
RM-03	Multiple retrieval devices	RR01-03, RR07	
RM-04	Experiments/Rigorous testing	DR02, RR02, RR04, RR07	
RM-05	Employ a safety function to rise submarine	SR04-07	
RM-06	Use of a streamline/sharp nose fairing or reinforced hull	DR01, SR01, SR02	
RM-07	Use of multiple airborne vehicles	AR01-03	OR01
RM-08	On-board data storage	SR04, ER01	
RM-09	Encryption of data	ER01, ER04	
RM-10	Program a "safe-mode" into search system	SR05	
RM-11	A visual alert object on mother-buoys	ER03	ER04
RM-12	Use of reference mission data	OR02	
RM-13	Design with current practices in mind	OR01	
RM-14	Constantly deploy on secondary missions	OR03	
RM-15	Safety release of retrieval system	AR01	SR01, SR02, RR01, RR04

Table 11.3: Posterior Mission Risk Map for ULB finder system, the different events are given below. Colors indicate the importance of each risk; Red indicates high risk, Yellow indicates medium risk, and Green indicates low risk.

Probability	Almost Certain	ER05 OR03	SR03		
	Probable				
	Chances About Even		OR01,SR01a, SR02a, RR01, RR03, RR05, RR06, ER04a	ER01	
	Not Probable		SR04-07, RR02, RR07, ER03	DR02, ER06, OR02	ER07
	Almost Certainly Not			AR01-03, DR01, RR04*, ER02, ER04b	SR01b*, SR02b*
		Negligible	Marginal	Critical	Catastrophic
<i>Impact</i>					

*Note that these appear not to have moved, but the probability of these events have actually been lowered by the associated mitigation methods.

Product Evaluation

12.1. Requirement Compliance

In this section, the designed system is evaluated, specifically as to whether it complies with the requirements set in previous reports. In table 12.1, it can be seen that all requirements are met, except for *ULB-SYS-AIR-09*.

Table 12.1: Compliance matrix of the requirements.

Req. Code	Compliant	Comment	Req. Code	Compliant	Comment
ULB-USER-XX			<i>ULB-SYS-SMB-09</i>	Yes	
<i>ULB-USER-01</i>	Yes		<i>ULB-SYS-SMB-10</i>	Yes	
<i>ULB-USER-02</i>	Yes		<i>ULB-SYS-SMB-11</i>	Yes	
<i>ULB-USER-03</i>	Yes		<i>ULB-SYS-SMB-12</i>	Yes	
<i>ULB-USER-04</i>	Yes		<i>ULB-SYS-SMB-13</i>	Yes	
<i>ULB-USER-05</i>	Yes		<i>ULB-SYS-SMB-14</i>	Yes	
<i>ULB-USER-06</i>	Yes		<i>ULB-SYS-SMB-15</i>	Yes	
<i>ULB-USER-07</i>	Yes		<i>ULB-SYS-SMB-16</i>	Yes	
<i>ULB-USER-08</i>	Yes		<i>ULB-SYS-SMB-17</i>	Yes	
<i>ULB-USER-09</i>	Yes		<i>ULB-SYS-SMB-18</i>	Yes	
<i>ULB-USER-10</i>	Yes	Via mother buoy.	<i>ULB-SYS-SMB-19</i>	Yes	
ULB-SYS-AIR-XX			<i>ULB-SYS-SMB-20</i>	Yes	
<i>ULB-SYS-AIR-01</i>	Yes		<i>ULB-SYS-SMB-21</i>	Yes	
<i>ULB-SYS-AIR-02</i>	Yes	Via mother buoy.	<i>ULB-SYS-SMB-22</i>	Yes	
<i>ULB-SYS-AIR-03</i>	Yes		<i>ULB-SYS-SMB-23</i>	Yes	
<i>ULB-SYS-AIR-04</i>	Yes		<i>ULB-SYS-SMB-24</i>	N/A	Deleted.
<i>ULB-SYS-AIR-05</i>	Yes		ULB-SYS-DNR-XX	Yes	
<i>ULB-SYS-AIR-06</i>	Yes		<i>ULB-SYS-DNR-01</i>	Yes	
<i>ULB-SYS-AIR-07</i>	Yes		<i>ULB-SYS-DNR-02</i>	Yes	
<i>ULB-SYS-AIR-08</i>	Yes		<i>ULB-SYS-DNR-03</i>	Yes	
<i>ULB-SYS-AIR-09</i>	No	Range is 3300 km [25].	<i>ULB-SYS-DNR-04</i>	Yes	
<i>ULB-SYS-AIR-10</i>	Yes		<i>ULB-SYS-DNR-05</i>	Yes	
<i>ULB-SYS-AIR-11</i>	Yes		<i>ULB-SYS-DNR-06</i>	Yes	
<i>ULB-SYS-AIR-12</i>	Yes		<i>ULB-SYS-DNR-07</i>	Yes	
ULB-SYS-SMB-XX			<i>ULB-SYS-DNR-08</i>	Yes	
<i>ULB-SYS-SMB-01</i>	Yes		<i>ULB-SYS-DNR-09</i>	Yes	
<i>ULB-SYS-SMB-02</i>	Yes		<i>ULB-SYS-DNR-10</i>	Yes	
<i>ULB-SYS-SMB-03</i>	Yes		<i>ULB-SYS-DNR-11</i>	Yes	
<i>ULB-SYS-SMB-04</i>	Yes	With military equipment.	<i>ULB-SYS-DNR-12</i>	Yes	
<i>ULB-SYS-SMB-05</i>	Yes		<i>ULB-SYS-DNR-13</i>	Yes	
<i>ULB-SYS-SMB-06</i>	Yes		<i>ULB-SYS-DNR-14</i>	Yes	
<i>ULB-SYS-SMB-07</i>	Yes		<i>ULB-SYS-DNR-15</i>	N/A	Deleted.
<i>ULB-SYS-SMB-08</i>	Yes				

12.2. Sensitivity Analysis

To see how the full system reacts to changes in certain inputs, a sensitivity analysis is performed. Four scenarios are drawn up, and their impact on the total system is evaluated.

12.2.1. Sensitivity Analysis 1 - Different Shell Material

For the first sensitivity analysis the material of the submarine shell was changed from CFRP to aluminum. The main effect this has, is that it increases the mass of the submarine shell. However the new mass exceeds the maximum acceptable mass for buoyancy, so, using the original dimensions, the submarine would sink. To prevent this the diameter of the submarine is increased. The larger diameter further increases the structural mass. It also results in more power consumption by the buoyancy control and propulsion systems, therefore increasing the

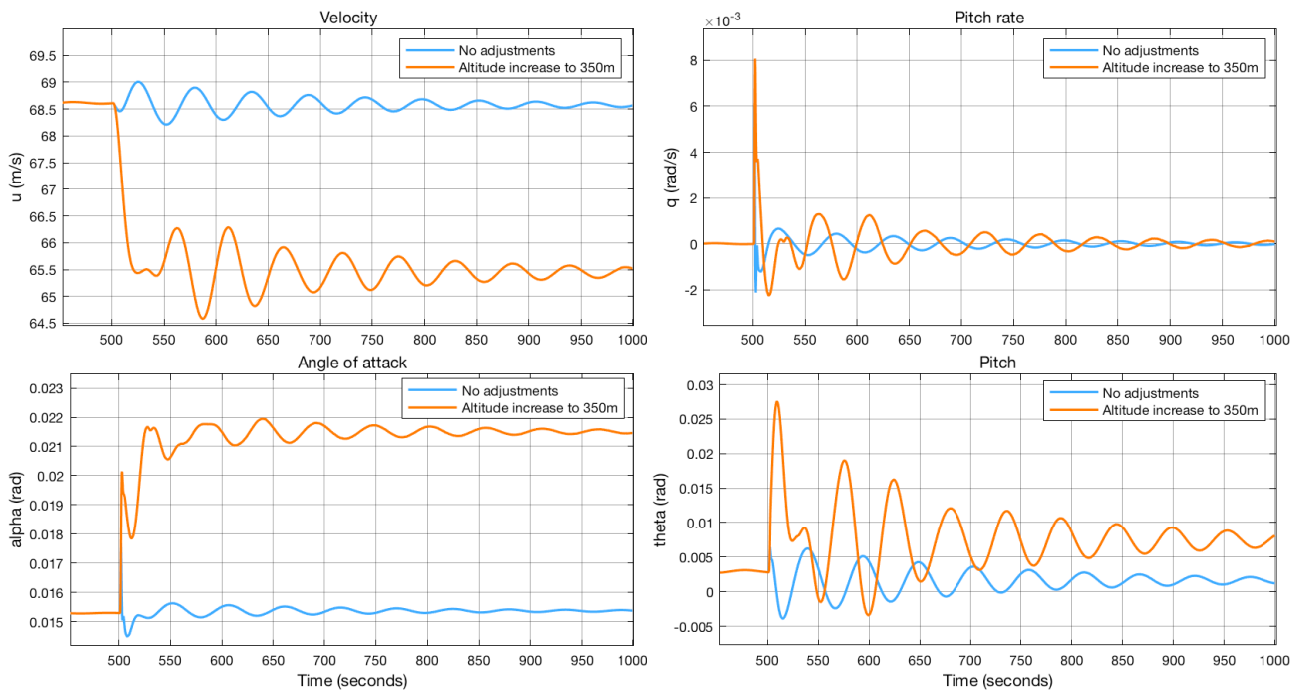


Figure 12.1: Graph comparing aircraft response with no change and with an increase in altitude for $m = 919$ kg.

mass of the power subsystem. Iterating through the submarine diameter, it is found that the minimal diameter for the submarine to satisfy the buoyancy constraint is 0.65 m. This corresponds to a length of 3.25 m. The changed mass and power budget breakdown can be found in table 12.2.

Since the total mass of the submarine has increased drastically, this also effects the other systems. The aircraft itself is still able to handle the oscillations due to retrieval (refer to fig. 12.1). However, the search system keeps hitting the water with the increased mass. To avoid this, the aircraft can fly at a higher altitude (from 100 to 350 meters), or the drone can produce more lift & drag to lift the search system above the water. However, this would increase the costs and complexity of the system.

Table 12.2: Differences in the submarine budget breakdown for sensitivity analysis 1.

Subsystem	Mass [kg]			Power [W]		
	Original	Sensitivity analysis 1	Difference	Original	Sensitivity analysis 1	Difference
Payload	4.0	4.0	0 %	4.8	4.8	0 %
Navigation	3.1	3.1	0 %	15.5	15.5	0 %
Structure	67.0	500.5	647 %	0	0	0 %
Communication	8.1	8.1	0 %	19.5	19.5	0 %
C&DH	2.5	2.5	0 %	0.3	0.3	0 %
Power	232.2	304.4	31 %	0.2	0.2	0 %
Propulsion	2.0	2.5	25 %	27.0	48.2	79 %
Buoyancy control	56.0	90.0	61 %	4021	5045	25 %
Retrieval mechanism	18.3	18.3	0 %	90.0	90.0	0
Total	393	919	135 %			

12.2.2. Sensitivity Analysis 2 - Larger search area

The system is designed to cover a search area with a 100 km radius, as specified in requirement **ULB-USER-04**. However there is no guarantee that the search area can always be narrowed down to this size. Therefore the second sensitivity analysis looks at the effects on the system if the given search area would have a 200 km radius.

There are two ways to compensate for this larger area. Either the original search systems would be used, meaning 22 search systems would be needed instead of 6. Mass and volume wise the A400M is still capable of carrying

and deploying 22 search systems.

The other solution is to keep the number of search systems to 6 and increase their velocity. The nominal velocity would have to increase from 1 to 4 m/s. Since the power needed by the propulsion system scales cubic with velocity, the power demand would increase from 27.0 W to 1829 W. For the mother buoy this increase would be even more drastic. These increases in power would in turn lead again to higher mass and therefore larger vessels.

If the search area would actually be increased a tradeoff would have to be performed to find the best compromise between increasing the number of search systems and their velocity. Increasing the number of search systems would likely be the better option since increasing velocity would significantly increase the power needed and make the retrieval more difficult.

12.2.3. Sensitivity Analysis 3 - Additional Payload

Currently the only payload on the submarines is the hydrophone array, therefore the system can only search for objects emitting an acoustic signal. This could be extended to include other objects by adding active sonar equipment to the submarine.

An active sonar would require 45 W of power [136], meaning a larger fuel cell would be needed. The full effects on the submarine can be found in table 12.3.

Table 12.3: Differences in the submarine budget breakdown for sensitivity analysis 3.

Subsystem	Mass [kg]			Power [W]		
	Original	Sensitivity analysis 3	Difference	Original	Sensitivity analysis 3	Difference
Payload	4.0	12.6.0	215 %	4.8	49.8	938 %
Navigation	3.1	3.1	0 %	15.5	15.5	0 %
Structure	67.0	114	70 %	0	0	0 %
Communication	8.1	8.1	0 %	19.5	19.5	0 %
C&DH	2.5	2.5	0 %	0.3	0.3	0 %
Power	232.2	453.3	95 %	0.2	0.2	0 %
Propulsion	2.0	2.0	0 %	27.0	41	52 %
Buoyancy control	56.0	62.8	12 %	4021	824	-80 %
Retrieval mechanism	18.3	18.3	0 %	90.0	90.0	0
Total	393	668	70 %			

The effect this increase in mass has on the aircraft dynamics can be seen in fig. 12.2. As expected the effects on the aircraft are larger, however they are still within the acceptable limits.

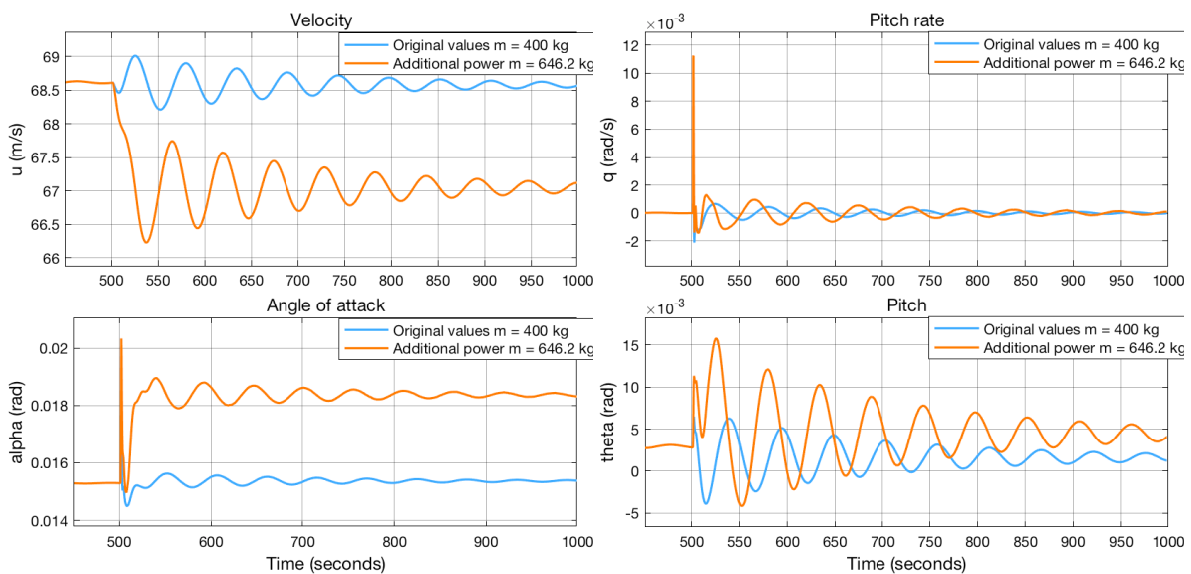


Figure 12.2: Effect of additional submarine payload on aircraft dynamics.

12.2.4. Sensitivity Analysis 4 - New ULB Signal

Since 2014 aircraft are equipped with ULBs with a frequency of 8.8 kHz in addition to of the original 37.5 kHz [38]. This lower frequency has a range of 8 km instead of 2 km [137]. This means that it is possible to detect the ULB from the ocean surface, so no submarines would be needed. Instead the mother buoys could be equipped with the hydrophone themselves. This would greatly reduce the complexity of the search system, because the mother buoys can constantly update their GPS position. Also less of a selection needs to be made in the data sent to the base station, because the bit rate limitations of the acoustic modem are being avoided. Using the same 1 m/s mother buoys as currently designed, only two would be needed to cover area within 30 days. Since the same mother buoys could be used, no changes have to be made to the deployment or retrieval systems.

12.3. Reliability, Availability, Maintainability and Safety Characteristics

This section discusses the reliability, availability, maintainability and safety of the final design of the ULB finder system. Analyzing these characteristics is useful in specifying important aspects of the system.

12.3.1. Reliability

"The quality of being trustworthy or of performing consistently well" [138]

Airborne system

The A400M has been a proven design and is already in use by different countries. The C-130 Hercules is as well proven to be a perfect candidate for dropping of cargo. However, accidents with airplanes still occur, that is why MARLIN is designing this ULB finder system and this is why the maintenance and inspection of the aircraft are very important prior to using them for the mission. The reliability of the aircraft are upon retrieving of the search systems from water is possible from the DSE design, if this is true in real life needs to be tested after the DSE phase.

Deployment

The deployment method is reliable as the dropping of cargo from the back door of the aircraft is easy and has been done for several years from different aircraft many times. However, this is almost always done with a parachute and this is not the case for the ULB finder system. From the DSE design it has been determined that the structure of the search systems can withstand the impact on water, what the impact is on the payload inside the search systems, needs to be tested after the DSE phase.

Search system with relocation

The search system, consisting of the submarines and mother buoys are based on proven designs, which makes them reliable. There are however some risks in the logistics and communication between the submarine and mother buoy. The mother buoy needs to follow the submarine, but there could be a loss of communication, resulting in a lost connection between the two, this can be mitigated by ensuring enough redundancy in the range of transmitting information.

Retrieval system

The retrieval system is a combination of actual designs proven in test, like the projects Fulton and Skyhook and picking up mail by means of a banner. This is a new design and on water, creating more degrees of freedom and difficulties. The reliability of the system is going to be determined by testing the system after the DSE phase in prototype and in real scale.

12.3.2. Availability

"The quality of being able to be used or obtained." [139]

Airborne system

Both the A400M and C-130 Hercules are military aircraft and have other purposes as well. The chance that the aircraft are not in use or in maintenance when it should be used for the finding an aircraft missing in deep water is low. This and the fact that aircraft crash once every 4 years in deep water makes the availability of the aircraft low. However, the aircraft are used for cargo transportation and a rescue mission could have a higher priority, making it more likely that the aircraft will be used for the ULB finder system.

Deployment

The search systems are deployed from the aircraft, when the aircraft is not available, the deployment is as well. The structures inside the cargo bay needed to deploy the search system will be only available for the ULB finder system, ensuring that if the aircraft is ready to be used, the deployment will happen.

Search system with relocation

The search system will be used mainly for the search of the ULB of aircraft crashed in deep water, however the system can also be used for secondary missions, such as ocean mapping or searching for other sunken vessels. This reduces the availability for the primary mission. This can be mitigated by renting the system for a limited period of time and producing more search systems than actual needed for the primary mission.

Retrieval system

The availability for the retrieval system is similar to that of the search system. It is produced for the primary mission, but due to the fact that aircraft crash only once every four year, the system will be rented for secondary missions.

12.3.3. Maintainability

"The probability that a failed equipment, machine, or system can be restored to its normal operable state within a given timeframe, using the prescribed practices and procedures." [140]

Airborne system

The A400M and C-130 Hercules have their own maintenance program with corresponding procedures. As they will be used for their primary purpose, transporting cargo, their maintainability is quite high. Most of the maintenance is performed within the given timeframe unless major components have been damaged.

Deployment

The structures needed for deployment are simple basic truss structures, they will not require much maintenance. Spare parts will be produced for redundancy.

Search system with relocation

The search system consists of 12 components, 6 mother buoys and 6 submarines. The submarine is quite small for a regular submarine and the payload integration is not that complicated. Due to the specific goal of the mission, the payload is smaller and different than that of an ordinary submarine. Maintenance of a submarine will be doable, only when the submarine is damaged, the time needed to repair will be more than the regular maintenance check. This is similar for the mother buoys. The only danger lies in the retrieving of the submarine or mother buoy when they need maintenance. The mother buoy and or submarine could be lost in the ocean or the retrieving could fail. This could lead to crossing the time limit for maintenance.

Retrieval system

The retrieval system is stored in the aircraft during the mission and its maintenance could be simultaneously with the aircraft. It consists of a control surface, rope, winch system and hook. These parts are integrated into one system and produced in such a way that the individual parts are easily separated to repair or restore the individual components rather than the whole system.

12.3.4. Safety

"Relative freedom from danger, risk, or threat of harm, injury, or loss to personnel and/or property, whether caused deliberately or by accident." [141]

Airborne system

The C-130 Hercules is an older aircraft than the A400M. The C-130 Hercules has more proven flights while dropping cargo, making the C-130 more safe than the A400M. In general, aerial cargo drops have strict procedures and rules to ensure safety of the load masters and cargo, making the aerial cargo drop safe.

Deployment

The deployment is safe when the dropping area is clear and provided for the cargo that is being dropped. When the rules and procedures are followed regarding aerial cargo drops, few can go wrong and the personnel and cargo is safe. The safety of the payload inside the search systems upon impact is not known yet and could be compromised. This can be determined when testing the aerial drop in water.

Search system with relocation

The submarines need to withstand the impact force upon deployment and the retrieval forces when retrieved. Between these activities it is beneath the surface at a depth of 4500 m. The submarine will have a map and will know approximately the path it follows and obstacles along its way. The mother buoy swims at the surface following the submarine and can be damaged by boats or stolen by pirates, which compromises the safety of the mother buoy and the mission consequently.

Retrieval system

The retrieval system is a novel design and its actual safety can be determined from tests after the DSE phase. From project Fulton and Skyhook it can be seen that it is possible to retrieve a person with an aircraft, however they stopped the project due to the fact that during a test, a person died using this retrieval method.

12.4. Safety Functions & Redundancy Philosophy

To aid the RAMS as discussed in section 12.3 the ULB finder system is equipped with several safety functions. These functions are designed to reduce the impact of failure of a subsystem. The following safety functions are incorporated in the design:

- i. **Emergency ballast** - As explained in section 7.4 the buoyancy system is backed up by an emergency ballast. This means that the submarine is still able to surface after a power outage or malfunction of the valves or pump in the VBS.
- ii. **Emergency release mechanism for tether** - In case the retrieval process jeopardizes the safety of the aircraft and its crew, the tether including drone can be released from the aircraft. This way the aircraft can safely return to the base.
- iii. **Emergency signal** - Both the mother buoys and submarines are programmed to continuously monitor their health status (including energy storage). If any critical malfunctions are found or energy is running very low, an emergency signal, including the location and health status, is sent to the base. In this case the airborne system can be deployed to retrieve the system and possibly replace it by a spare.

In addition to these safety functions, the completion of the mission is ensured by producing redundant systems and parts. The number of parts needed for the system is multiplied by 1.5 for the production, so spares are always at hand. This includes both parts and assembled systems, so a malfunctioning system can be replaced instantly. Having redundant part also aids in the ease of maintenance of the system.

Project Development and Manufacturing Plan

This chapter contains the project design and development logic, and the production plan which are represented in a set of flow block diagrams in section 13.1, a Gantt chart in section 13.2 and the production plan in section 13.3.

13.1. Project Development Planning

The project design and development logic can be seen in fig. 13.1. From this figure it can be seen which activities need to be performed after the DSE phase.

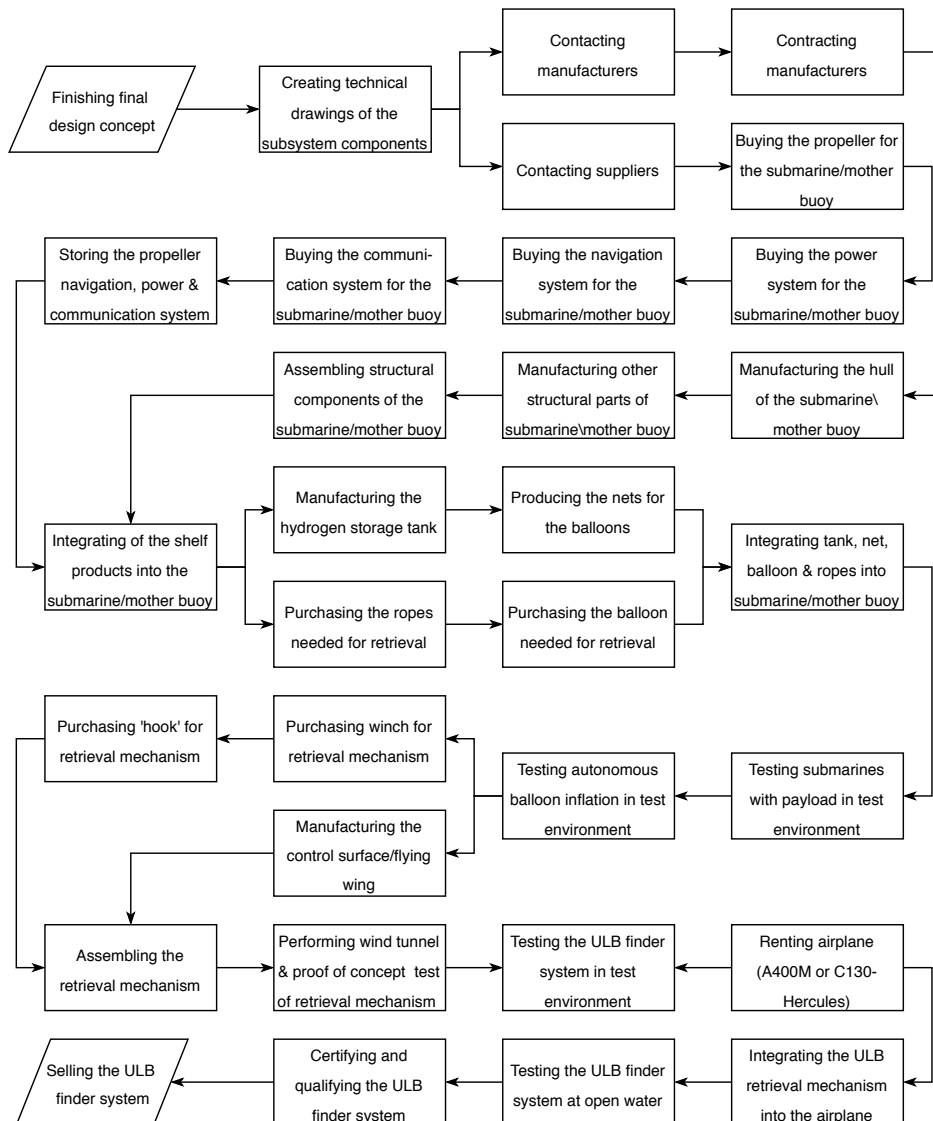


Figure 13.1: Project design and development logic.

13.2. Gantt Chart

The activities presented in the project design and development logic can be seen in Gantt chart format in fig. 13.3 and fig. 13.4. The color scheme used for the activities in the Gantt chart can be found in fig. 13.2.

Non-critical Activities
Critical Activities
Accountable to suppliers

Figure 13.2: Color scheme used to identify activities in the Gantt chart used for project development.

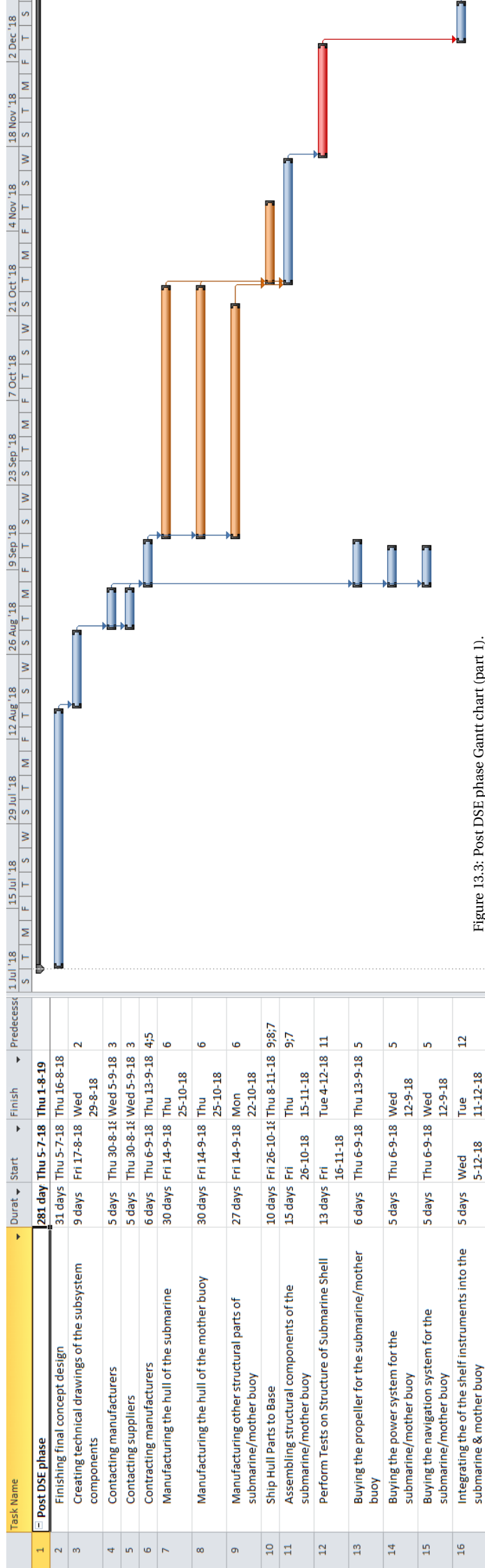


Figure 13.3: Post DSE phase Gantt chart (part 1).

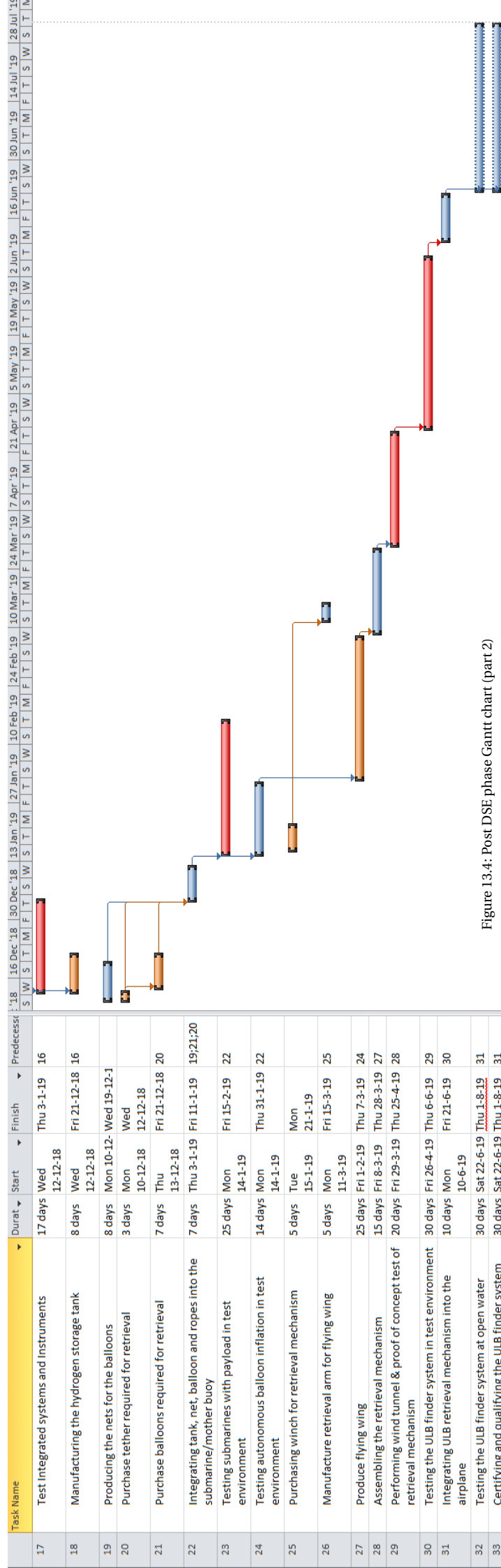


Figure 13.4: Post DSE phase Gantt chart (part 2)

13.3. Integration and Manufacturing Plan

This section outlines the necessary activities required to manufacture the different systems that are part of the ULB finder system. There is a slight overlap between the activities in the manufacturing plan and the project Gantt chart, nevertheless the difference between these is that the Gantt chart also presents activities regarding the logistics of the development.

13.3.1. Production Strategy

The ULB finder system can be characterized by the uniqueness of its operations. As presented in chapter 3, the final product is intended to enter a low demand market where it will be seldomly used. Consequently, the intended production strategy is a *chase demand strategy* in which the production rate is just satisfying the demand [142]. The fundamental idea of this strategy is that if demand increases, production increase; if demand decreases then the production decreases too. As presented in section 5.1.2 the optimal number of submarines used to cover the required area is 6. Noticeably, this is a low number which means the system will not be mass produced.

The ULB finder system involves careful integration between its elements in order to perform successfully; to do so a production plan is created to integrate these elements efficiently. The production plan for each system to be produced is presented below in section 13.3.2.

13.3.2. System Production Plan

This subsection addresses the production plan (or manufacturing plan) which outlines the activities to be performed to produce the parts and assemblies of the product. In addition, this section also implements the integration of systems into the production plan. Planning the production of a project of this complexity can be challenging and tedious. To tackle this situation, the manufacturing plan is broke down into each system, namely the airborne integration, deployment system, search systems and retrieval system.

The production plan activities are split into phases in order to have a better overview and control of the schedule. These phases are the following:

- i. **Parts Production/Purchase Phase (Identified with the second letter of activity name P)**: In this phase the necessary parts and products are manufactured, most of these are outsourced to partner companies since self-manufacturing would not be optimal.
- ii. **Assembly (Identified with the second letter of the activity name A)**: In this phase the outsourced and purchased parts arrive in the operations hub, then these are used to assemble components.
- iii. **Integration (Identified with the second letter of activity name I)**: This phase concerns the integration of the instruments, electronics and other components into a completed system. The integrated systems are also tested to verify correct functioning.

The box and color scheme description used in the production plan diagram for each system can be found in fig. 13.5.

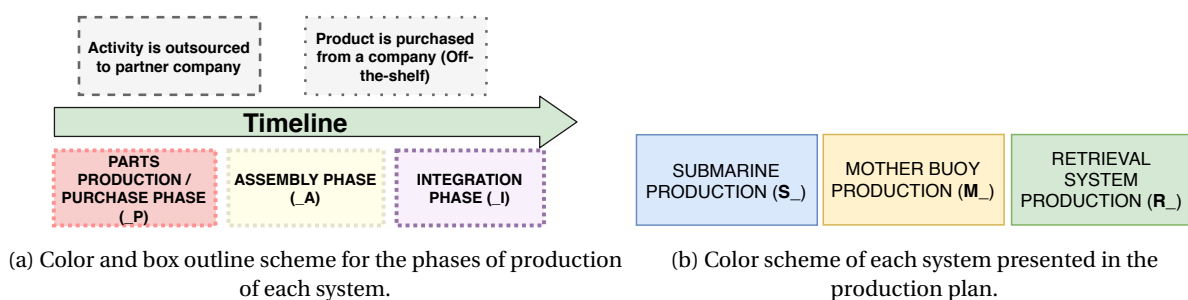


Figure 13.5: Color and box outline scheme used in production plan.

Finally, the parts that are outsourced are handled by expert companies in their respective industry and are summarized in table 13.1.

Aircraft & Deployment Production

As presented previously, the aircraft used to operate the ULB system is expected to be operated by a government organization (e.g. military), therefore, it is out of the scope of this project to design and produce such aircraft. In addition, it is expected that the aircraft has the necessary attachment points for enabling the deployment. To prove this, a visit to the Dutch Air Force was scheduled; two members of the ULB Project group discussed with experienced pilots and load masters regarding the adaptability of the aircraft to attach objects inside the cargo

bay. The cargo bay of the C-130 Hercules that was inspected during this visit can be found in section 5.4.2. The attachments points runs along the length of the fuselage. This led to the conclusion that the operator of the aircraft has the necessary equipment to deploy the search systems, hence, manufacturing this equipment is out of the scope of this project.

It is important to note that the airborne system that will be used is the Airbus A400M which is more modern than a C-130 Hercules. It is then assumed that the cargo bay of the A400M has the same, or improved cargo bay characteristics as the ones visible in section 5.4.2.

Submarine & Mother Buoy Production

As described in previous sections, the submarine and the mother buoy share similar characteristics such as the shape and structure. Consequently the manufacturing plan for these two systems are fairly similar. The plan for the submarine and the mother buoy can be found in fig. 13.6, fig. 13.7 and fig. 13.8.

Retrieval System Production

The production plan for the components of the retrieval system can be found in fig. 13.9. This system consists of various elements such as the flying wing, the tether and the retrieval arm that will be used to pierce the balloon.

Table 13.1: List of companies to which production or purchase or parts is outsourced to.

Part to Purchase / Manufacture	Company Name	Industry
Submarine Shell	<i>Tencate</i>	Composites
Mother Buoy Shell	<i>Tencate</i>	Composites
Submarine & Buoy motors	<i>Montevideo Technology</i>	Torque Systems
Flying wing instruments	<i>Opgal</i>	Camera Systems
Flying wing frame	<i>Skyeton</i>	UAV Systems
Flying wing hydraulics	<i>Ace</i>	Hydraulic Systems
Navigation Systems	<i>Kongsberg</i>	AUV systems

Timeline

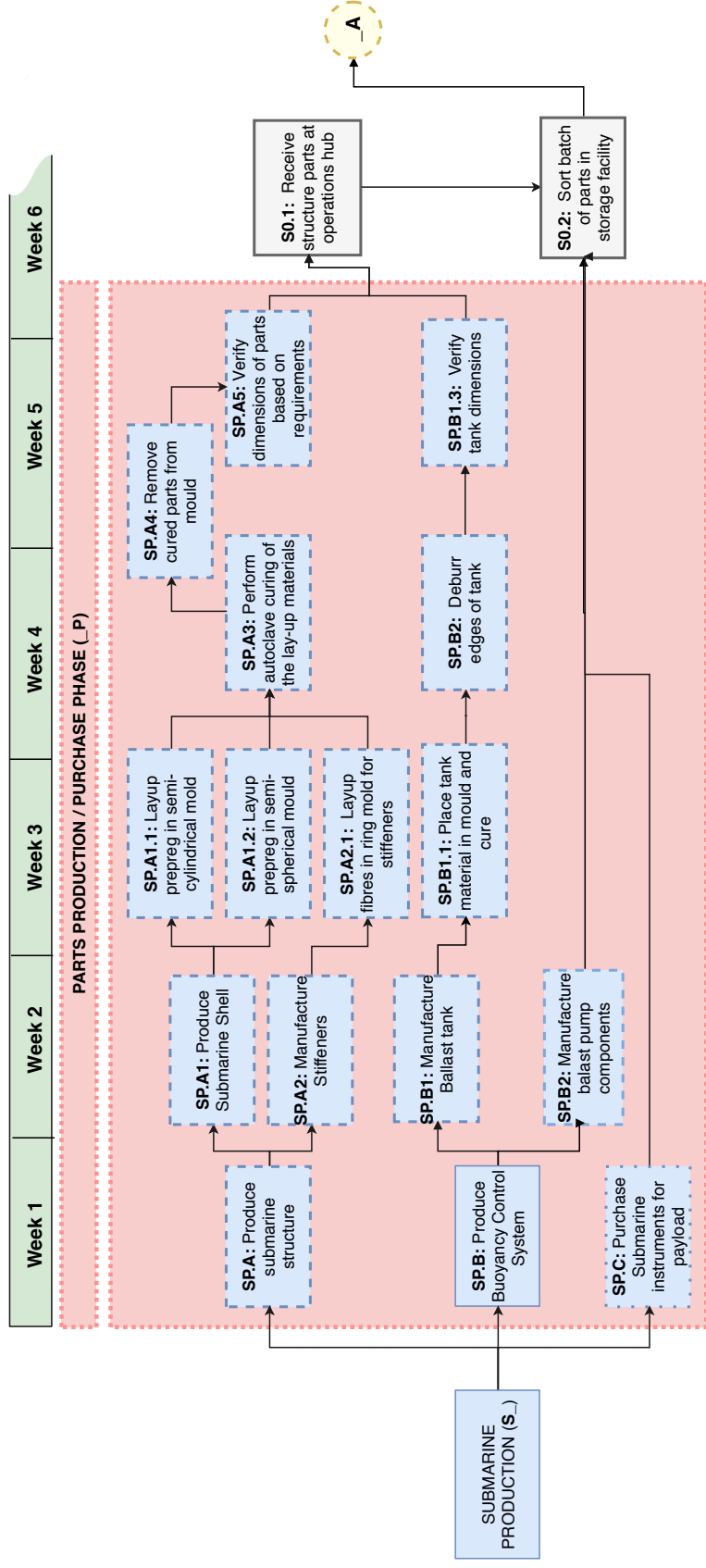


Figure 13.6: Production and purchasing parts phase of the submarine manufacturing.

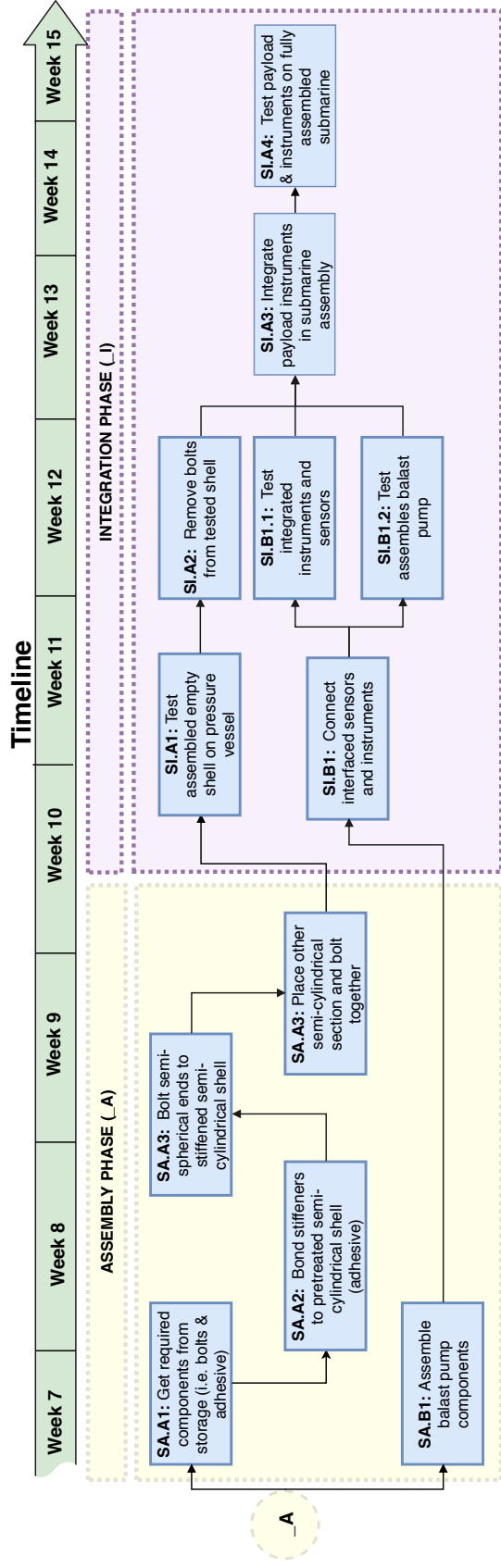
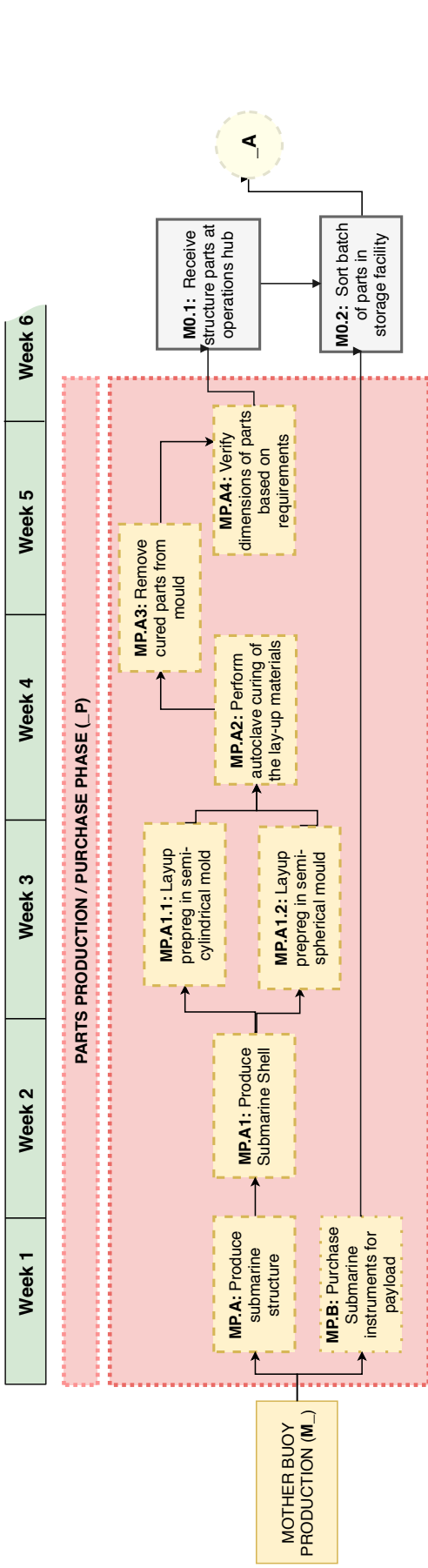


Figure 13.7: Assembly and integration phase of the submarine manufacturing.

Timeline



Timeline

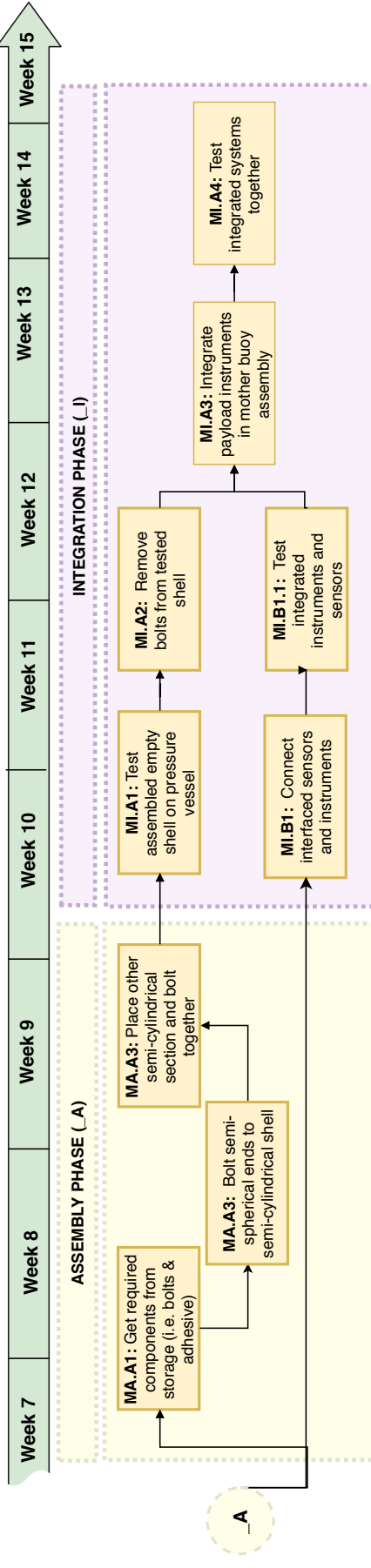


Figure 13.8: Production plan with estimated schedule of the mother buoy system.

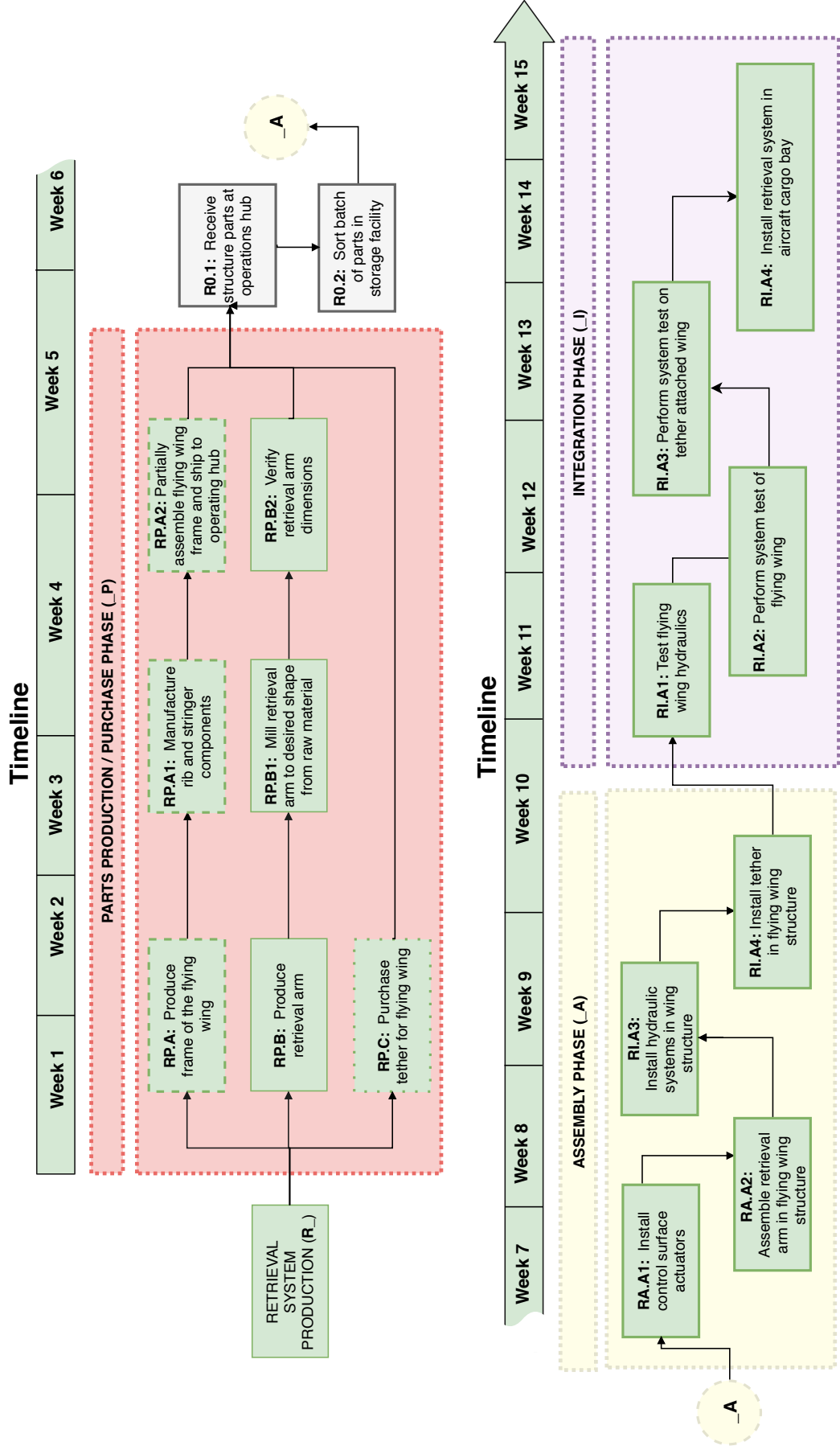


Figure 13.9: Production plan with estimated schedule of the retrieval system.

Financial Analysis

This chapter covers the financial part of the post DSE phase. A cost breakdown structure is given in section 14.1, which is followed by the return on investment and break-even in section 14.2.

14.1. Cost Breakdown

The available budget is €50 million. By means of the cost breakdown structure in fig. 14.1, the components from which the total cost will consist are shown.

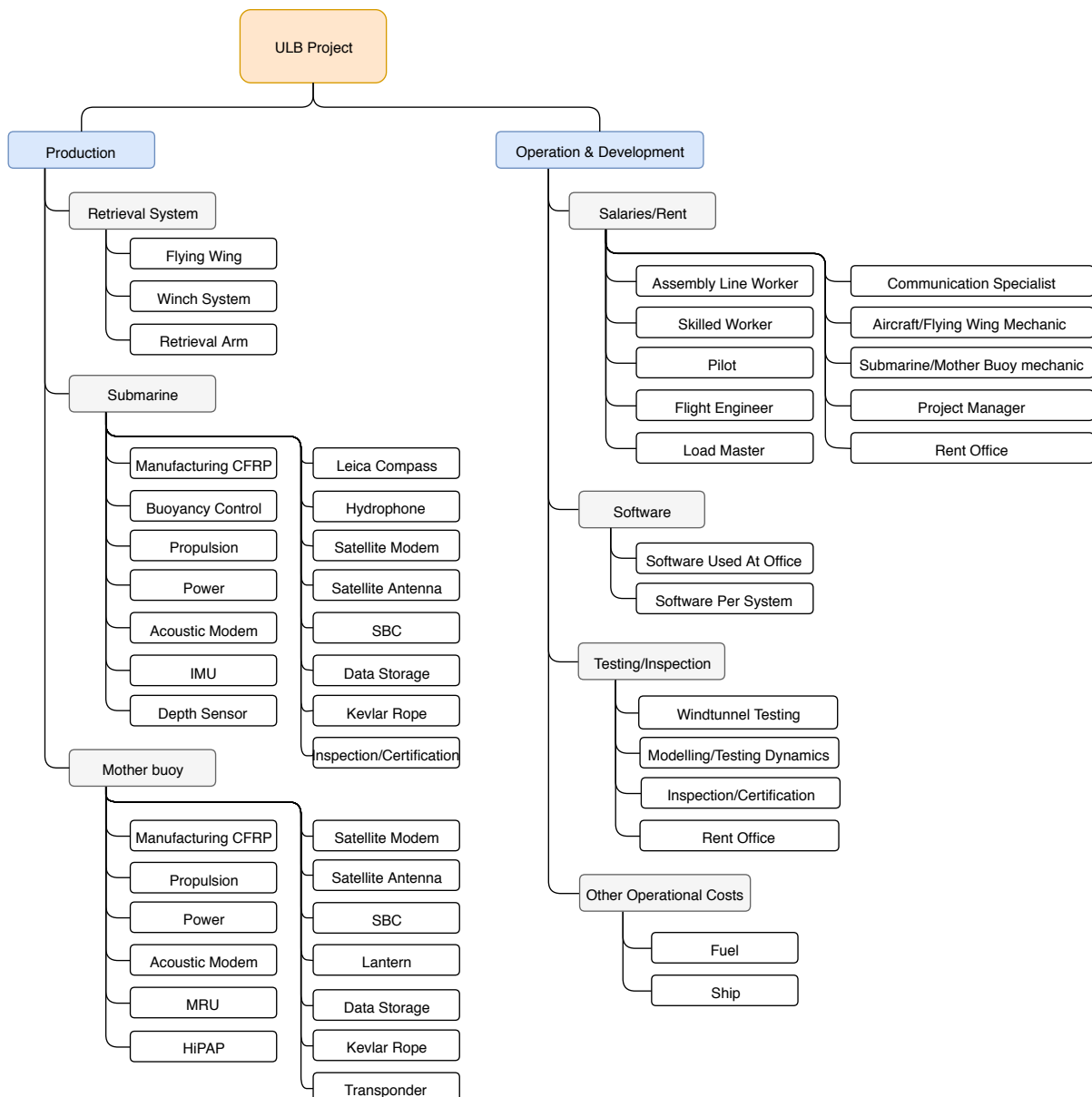


Figure 14.1: Cost breakdown structure of the post DSE phase.

The cost components are divided into 2 categories; production and operation & development. The production covers the retrieval system, mother buoy and submarine. The operation & development covers the salaries, software, testing & inspection and other operational costs.

14.2. Return on Investment

The return on investment (ROI) is the net profit divided by the cost of the investment [143]. It is mostly expressed as a percentage and used to see whether an investment is profitable. The ULB finder system is designed to improve current ULB finder search methods. Due to the humanitarian nature of the project, this project is not meant to make profit, resulting in an ROI of 0% by definition. Therefore, the ROI in the context of this project will be defined differently. As existing search methods are costly and time consuming, ROI will focus how much the search expenses are reduced by using this system. Therefore, the return on investment will be calculated as the difference in the current costs of search missions and the ULB finder system operational costs, over the operational costs of the ULB finder system. Equation (14.1) defines this relation.

$$\text{ROI} = \frac{\text{Operational Costs of Current Search Methods} - \text{ULB Finder System Operational Costs}}{\text{ULB Finder System Operational Costs}} \quad (14.1)$$

To establish the ROI as defined above, costs of previous search missions needed to be determined and analyzed. Following this, the cost estimates - both of development & production and operation - of the ULB finder system need to be defined. The development & production costs are also needed to calculate the break-even point of the initial investment for the ULB project.

Market Price

In order to determine the market price of the product, one should look at comparable products in the market. Since this is a system, it is hard to get an exact value for the market price. Therefore, research is done to similar locating lost aircraft missions to get a reference for the market price.

AF447 For the Air France flight AF447 [144], a sea search operation was conducted by the BEA and was divided into a surface search and 5 phases, see table 14.1.

Table 14.1: Cost and duration of sea search operation conducted by BEA for missing flight AF447 [144].

<i>Phase</i>	<i>Period</i>	<i>Duration</i>	<i>Cost</i>
Phase 01	June / July 2009	30 days	€ 9 million
Phase 02	August 2009	22 days	
Phase 03	April / May 2010	52 days	€ 12 million
Phase 04	March / April 2011	15 days	€ 4 million (estimate)
Phase 05	April / May 2011	31 days	€ 6 million
TOTAL phases 1-5		176 days	€ 31 million (estimate)

Phase 01 This was basically the search for the signals transmitted by the ULBs. Since the ULB only sends out a signal for 30 days, the duration of this phase was predetermined. In short, the search was performed by ships with a towed hydrophone and both manned and unmanned submarines.

Phase 02 Since the ULB signal stops working after 30 days, it was decided to use sonar for this search phase. A zone of 40 NM circle was covered via the Towed Acoustic Sonar (TAS) but without success.

Phase 03 In this phase, the reverse drift calculation was improved which led to a new limited search zone. Here, use was made of the REMUS 6000[8] and a ROV to scan the search zone.

Phase 04 Now drift buoys were used to improve the knowledge of surface currents and to evaluate the ability of reverse drift. This led to a new search strategy. Again, the REMUS 6000 was used but now with success.

Phase 05 This was the recovery phase which is not important for this market price analysis. The designed system is purely focused on locating the missing aircraft, not recovering.

As one can see in table 14.1, a total cost of € 31 million is reached for the complete sea search operation. With this, an estimate can be made for the market price. Please note that the system can only be compared with the first 30 days of the sea search operation, i.e. the search for the ULB (phase 01). During this sea search operation, however, it was noted that the ULBs in the missing aircraft malfunctioned. Therefore, the designed ULB locating system also wouldn't be able to locate the aircraft and is hard to compare to this sea search operation.

MH370 Another sea search operation was the search for the still missing MH370 flight. This operation, however, ended after 4 years of searching and has an extremely high cost. An estimation of the search costs, by Australian Government agencies up to 30th of June 2017, is given in table 14.2 from [145].

Table 14.2: Estimated search costs to 30 June 2017 by Australian Government agencies from [145].

<i>Phase</i>	<i>Cost area</i>	<i>Cost to 30 June 2017</i>
Underwater search - ATSB Lead program components	Underwater search	€ 108 million
	Bathymetry (Underwater mapping)	€ 13 million
	Program Management	€ 4.5 million
	Other sub-components	€ 0.6 million
Total		€ 126 million

Market Volume

"Market volume is the total amount of transactions observed in a specific marketplace over a specified time frame." [146]

The market volume is quite simple for the ULB system when it is sold. As there is only one ULB system produced, it can be sold for the exact amount of money it costs and results in one transaction.

When the ULB system is rented for search and rescue missions as well as for secondary purposes, the market volume will be larger. The use of the search and rescue mission is dependant on the amount of deep sea aircraft crashes. For the secondary purposes it has to be determined from the post DSE phase, when the system has been built and tested and is ready to be used.

Achievable Market Share

The market share is calculated by taking the sales of a company over a certain period and dividing it by the total sales of the industry in which the company is operating over the same period [147].

The market in which the ULB system finds itself operating in is quite specific and small. If the system is a success, it can achieve a relatively big share in this market. However, the retrieval technology is a novel design and needs to be tested thoroughly before it is considered a reliable option. Nevertheless, the system can be used without the retrieval option, and by being faster due to the airborne system, it has a major advantage than the deployment of search systems by boats.

Production Cost

In table tables B.1 and B.2 found in appendix B, all costs related to the production, development and operation of the ULB locating system are listed. The costs presented are off the shelf products or costs based on statistical data. As one can see, the total cost is lower compared to the set budget. A reason for this could be that most components/subsystems are outsourced and therefore cheaper. Also, since the system will most likely be sold to the government/military, no airborne system has to be bought. This significantly decreases the production/operational cost.

Table 14.3: Total cost estimation of ULB finder system.

	Cost [EUR]
Production/Development	
Manufacturing/Assembling structure	12.5 million
Office rental	0.12 million
Software architecture	0.25 million
Retrieval system	0.4 million
Search system	2.4 million
Modelling and testing	15 million
Operational	
Software	0.35 million
Salaries operating team	0.16 million
Fuel	0.16 million
Emergency ship*	7.2 million
Total (incl. 25 % contingency)	48 million

From table 14.3 the total costs of the ULB finder system are estimated to be around €48 million, with a 25% contingency (to account for uncertainties and inflation). Without the ship, the operational costs account for €0.8 million

of the total costs. If the ship is included, then the operational costs account for a total of €9.4 million of the total costs. The ROI will be calculated for both these scenarios.

From table 14.1, the operational cost of the first 30 days of Air France 447 amounted to around €85 million (surface search costs of €80 million and Phase 1 search costs of €5 million¹). For MH370, [81], the costs of the first 70 days is estimated to be €60.2 million. Again, assuming that the costs are distributed evenly among all days, then the cost of the MH370 search for the first 30 days amounts to €26 million. Taking the average of these costs yields an operational cost of €55.5 million.

Calculating the ROI with and without the ship for this operational costs gives an ROI of 6800% and 490% respectively. The reason these values seem quite high is because the reference missions are also based on estimates, and involve contributions of all involved countries. Furthermore, these estimates include surface searches, which are not considered by the ULB project. Therefore, another ROI can be performed which only considers the ULB segment of the mission. This would be a more realistic estimate. Up to this point, there are no definite costs for the ULB search phase of MH370. Thus, only the €5.5 million from Air France 447 will be used. Doing so, yields ROI values of 587% for a search without the ship and -45% for the search with the emergency ship. The latter ROI is undesirable since a higher operational cost than the current search methods is obtained. A summary of the different ROI scenarios is given in table 14.4.

14.2.1. Break-even

As the costs of the mission have been defined, the point at which the revenue of the product is equivalent to the costs must be determined. However, as the ULB finder system is not designed to generate profit or income, there is no break-even point as per the definition. Therefore, in the context of this project, the break-even point can be interpreted in two ways: 1) the price of the system itself, such that the development team can recuperate initial investments; and 2) for the buyer, the ROI may be used to determine how many searches are needed before the savings from using the finder system make up for the costs of the system.

As there is only "one" product, the break-even point under definition 1 will be reached if the finder system is sold at the price of the production and development costs (as the buyer will operate the system). In this case, to break-even, the price should be at least €38 million (production and development including contingencies). If profit is truly desired, then this can be increased. However, as this project is primarily for humanitarian purposes, the price will be kept at €38 million.

From the perspective of the buyer (definition 2), the number of searches needed to make up for the costs of the system depends on which ROI scenario is used. As the buyer will operate the system, the total costs of €48 million is used. For an ROI of 6800% the break-even point is after the first search, the same can be said for an ROI of 490% and 587%. The only ROI scenario which does not break-even is with an ROI of -45%. For this situation, the negative ROI is due to the operational costs of the emergency point. Hence, in this situation, it would be more expensive to operate the ULB finder system over existing methods. This is undesirable as this project aims to make searching cheaper and more effective. To mitigate this, a cheaper emergency ship may be employed. The different break-even point scenarios are summarized in table 14.4.

Table 14.4: Table summarizing the different possible ROI and Break-even results, based on different operational cost scenarios.

	Possible Cost Scenarios			
Reference Operational Cost [Millions EUR]	55.5	55.5	5.5	5.5
Operational Cost ULB Finder System [Millions EUR]	0.8	9.4	0.8	9.4
Return on Investment [%]	6800	490	587	-45
Number of Searches to Break-even [-]	1	1	1	N/A

¹To approximate the proportion of costs that was split between Phase 1 and 2, a simple ratio was used: $9 \cdot \frac{30}{30+22} = \text{€}5.2$ million, since the first phase took 30 days.

Conclusion & Recommendations

In order to satisfy the requirements and cohere to the mission and objective statement, the ULB Finder System has been designed to find missing aircraft in deep water. The mission statement is to "scan a predetermined ocean region in order to locate an aircraft which has crashed in deep water within 30 days." The objective statement is to "design an airborne system, within 10 weeks with 10 people, that can reach any location on Earth within 48 hours and is capable to locate the ULB signal of the missing aircraft in deep water". This report set out to analyze the feasibility of the ULB Project; the results of this report demonstrate that the ULB Project is achievable. This can be accomplished through search system units, consisting of a submarine and a mother buoy, that will follow a pre-determined coverage path of the search area to locate the ULB signal. The search systems will be deployed through controlled free fall and retrieving using a flying wing with a robot arm attached to the aircraft. The airborne system used is the Airbus A400M, but the system is also adaptable to C-130 Hercules.

The optimal coverage path results in the submarine travelling along parallel pathways. Since the ULB signal has a range of 2 km, the total coverage path was determined to be 9400 km. To confidently cover the search area and locate the ULB signal, the search system will take 20 days to cover the entire search area. This is known as search phase one. Each search system will look for the signal individually and together they will cover the total coverage distance. By combining the distance with the submarine velocity, 1 m/s, and a search time of 20 days, the total number of search systems was determined to be 6. Once one of these search systems receives the ULB signal, an approximate location of the aircraft, in the order of 1km, can be determined. Therefore, the total search area can be reduced. The reduction of the search area initiates the second search phase where all search systems will relocate to the smaller search area and a new search is started. However in the second search phase, the aircraft position will be determined with a minimum of three submarine - ensuring an accurate aircraft location via triangulation.

For the submarine, it was decided that a hydrophone array would be used with four omnidirectional hydrophones for detection of possible signals. For navigation, an INS is used to determine position along with location received from the mother buoy. Power is provided by a hybrid system using a 50 W fuel cell system, supported by a smaller lithium-ion battery. This enables the submarine to travel at 1 m/s. The design of the structure has a length of 2.5 m and a diameter of 0.5 m. The shell of the submarines will be made out of 0.0098 m thick CFRP and is reinforced by 8 ring stiffeners. The total mass of the submarine is 393 kg. The mother buoy has the same dimensions as the submarines. It is also powered by a propeller and will have a light mounted on the shell for visibility by other vessels. Each mother buoy weighs 414 kg.

For the retrieval, a drone-on-tether system is used. The tether is fixed to a winch, which reels the system once the search system is hooked. The drone is an autonomous flying wing with a small robot arm at the bottom that can pick up the search system. The search system will be picked up by releasing a hydrogen balloon, which rises to an altitude of 6 m. The balloon is pierced by the robot arm and is then reeled into the military aircraft via the tether. The retrieval process requires the airborne system to fly at an altitude of 100m and at a speed of 70 m/s.

The costs of the entire ULB Project have been estimated by considering the costs of development, production and operation. The total costs amount to €38 million. A contingency of %25 has been applied to these costs to account for inflation and uncertainties. This brings the total cost estimate of the system to €48 million, which is marginally lower than the budget of €50 million.

Due to the different possible sources of error, the designed system must be accurately verified and validated before bringing it out on the market. Due to the variety in subsystems and the scope of the project, this might result in complications, as well as high costs involved. However, if the design of the ULB finder system were to be further developed and more research was done, there are various recommendations that could be taken into account.

With regards to the deployment system, the use of PID controllers for the control surfaces should be investigated further. Moreover, interactions between a buoyancy control system and propulsion system could be looked into. More research on noise in deep water could be helpful as well. For the operational procedure, a change in search height was neglected and the submarine was assumed to travel in a horizontal straight line. However, currents can displace the submarines in vertical direction as well, which should be taken into account. Furthermore, the submarine could be designed to detect distance from the ocean floor, as to change its height accordingly and not risk collision or skipping parts of the search area.

A recommendation for the structural determination of the submarine could be to use a Finite Element Analysis. In this way, a more accurate estimation of stresses can be obtained. Since this would allow a structure with varying thickness, this could potentially reduce weight. Nevertheless, according to [92], a Finite Element Analysis shows that the actual buckling pressure is almost a half. It is then recommended to further investigate the structure design.

With regards to the retrieval process, an important recommendation is to perform the proposed validation experiments to validate the concept and simulation created. These will determine if the concept is truly feasible and if the assumptions made are reasonable. Furthermore, the simulation itself can be expanded upon by coupling the aircraft dynamics to the retrieval dynamics. This will directly show how the aircraft reacts to the retrieval dynamics and in turn how the aircraft response affects the retrieval dynamics. A PID controller may also be implemented to start the development of a control system which dampens the response of the aircraft. Furthermore, research may be done into possible flight maneuvers which make the retrieval process more efficient.

Bibliography

- [1] J. K. K. Ho. Formulation of a systemic pest analysis for strategic analysis. *European Academic Research*, 2(5):6478–6492, 2014.
- [2] Auburn University. Chapter macroeconomic variables. [Online; Accessed 21-05-2018].
- [3] T. Bush. Pestle analysis: Technological factors affecting business. *PESTLE Analysis*, Jul 2016.
- [4] M. E. Porter. How competitive forces shape strategy. 1979.
- [5] Ultra Electronics. Alfea sonobuoy active low frequency electro-acoustic sonobuoy type ssq 926. *Product Specification B047v4*, Ultra Electronics, Buckinghamshire, England, 2017.
- [6] Liquid Robotics. Boeing Sharc unmanned vehicle. <https://www.youtube.com/watch?v=7uZJ9wSx6Z0>. [Online; Accessed: 18-06-18].
- [7] L. D. Stone, C. M. Keller, T. M. Kratzke & J. P. Strumpfer. Search for the wreckage of air france flight af 447. *Statistical Science*, pages 69–80, 2014.
- [8] Kongsberg. REMUS 6000 Autonomous underwater vehicle. *Brochure*, Kongsberg Underwater Technology, Inc., Seattle, WA, 2017.
- [9] M. Yang, D. Vladimirova, et al. Creating and capturing value through sustainability. *Research-Technology Management*, Vol. 60(No. 6):pp. 30–39, Apr 2017. doi: 10.1080/08956308.2017.1301001.
- [10] S. Bonini. McKinsey on Sustainability & Resource Productivity. Sustainability Report 1, McKinsey & Company, 2012. [Accessed 18-06-18].
- [11] S. Bonini & S. Goerner. "The business of sustainability: Putting it into practice". Sustainability report, McKinsey & Company, 2011. [Accessed 18-06-18].
- [12] D. Partridge. Capturing the value of sustainability. Sustainability report, UK Green Building Council, Jan 2018. [Accessed 19-06-18].
- [13] S. Evans, D. Vladimirova et al. Business model innovation for sustainability: Towards a unified perspective for creation of sustainable business models. *Business Strategy and the Environment*, Vol. 26(No. 5):pp. 597–608, May 2017. doi: 10.1002/bse.1939.
- [14] J. Sinke. AE3211-II Production of Aerospace Systems: Chapter 10 Lean Manufacturing. Reader, March 2018.
- [15] P. C. Roling. *Airborne Underwater Locator Beacon (ULB) Finder System*. Delft University of Technology, 2018.
- [16] Hydro International. Deep-water Black-box Retrieval. <https://www.hydro-international.com/content/article/deep-water-black-box-retrieval?output=pdf>, 2018. [Online; Accessed 07-06-2018].
- [17] Egyptian Ministry of Civil Aviation. Factual Report of Investigation of Accident. <https://www.bea.aero/docspa/2004/su-f040103pa/pdf/su-f040103pa.pdf>, Jan. 2004. [Online; Accessed 18-05-18].
- [18] O. Ferrante & J. C. Vital. Underwater Recovery Operations off Sharm el-Sheikh. https://asasi.org/papers/2004/Ferrante%20et%20al_Underwater%20Recovery_ISASI04.pdf, May 2004. [Online; Accessed 23-05-18].
- [19] S. Y. Deen. "Autonomous Coverage Path Planning for AUVs Considering Location Uncertainty". Master thesis, TU Delft, Delft, the Netherlands, September 2017. [Accessed 07-06-18].
- [20] A. Lim. "Cruise Report 2017 No 1 Mid- Atlantic Ridge". Technical report, Trondheim, Norway, September 2017. [Accessed 13-06-18].
- [21] N. Wettmarshausen. Climate Memory. https://www.mpg.de/5861360/W005_Environment-climate_072-077.pdf. [Online; Accessed 08-06-2018].
- [22] Integrated Ocean Observing System. <https://www.ioos.us>, 2018. [Online; Accessed 07-06-2018].
- [23] National Ocean Service. The Global Conveyor Belt. https://oceanservice.noaa.gov/education/tutorial_currents/05conveyor2.html. [Online; Accessed 10-06-2018].
- [24] CSIR. National Institute of Oceanography. http://www.nio.org/index?option/com_nomenu/task/show/tid/85/sid/92/id/138.
- [25] Airbus. A400M - Delivery to the point of need. <http://www.airbus.com/defence/a400m.html>, 2018. [Online; Accessed 26-05-18].
- [26] D. Wevers. Electrical Engineer at the Dutch Royal Airforce, 2018.
- [27] Airbus. A400M (Future Large Aircraft) Military Transport Aircraft. <https://www.airforce-technology.com/projects/fla/>. [Online; Accessed 04-06-18].

- [28] HK Indian MBT. Airbus A400 M - Detailed Analysis Including Pilot Reports. <https://defence.pk/pdf/threads/airbus-a400-m-detailed-analysis-including-pilot-reports.273682/>, Aug 2013. [Online; Accessed 30-05-18].
- [29] J. A. Mulder, W. H. J. J. van Staveren, J.C. van der Vaart et al. *Flight Dynamics: Lecture Notes AE32023*. Control and Simulation division, Delft University of Technology, 2013.
- [30] A. S. Attallah, G. A. El-Sheikh et al. Modelling and simulation for free fall bomb dynamics in windy environment. *ASAT Conference*, Vol. 16, May 2015.
- [31] "The USAF Stability and Control DATCOM". Technical Report AFFDL-TR-79-3032, Flight Dynamics Laboratory, California, United States, December 1999.
- [32] J. E. Williams & S. R. Vukelich. "The USAF Stability and Control Digital DATCOM". Technical Report AFFDL-TR-79-3032, McDonnell Douglas Astronautics Company, Missouri, United States, April 1979.
- [33] C. Rosema, J. Doyle et al. "Missile DATCOM User's Manual - 2011 Revision". Technical Report AFRL-RB-WP-TR-2011-3071, U.S. Army Aviation & Missile Research, Alabama, United States, March 2011.
- [34] S. R. Vukelich. "Development Feasibility of Missile DATCOM". Technical Report AFWAL-TR-81-3130, McDonnell Douglas Astronautics Company, Missouri, United States, October 1981.
- [35] R. J. Arnold & J. B. Knight. "Weapon Delivery Analysis and Ballistic Flight Testing". Technical Report AGARD-AG-300 Vol.10, AGARD, Neuilly Sur Seine, France, July 1992.
- [36] A. L. Morris. Simulating new drop test vehicles and test techniques for the orion cev parachute assembly system. Technical Report 20110011397, AIAA, Houston, United States, Jan 2011.
- [37] E. S. Ray. Challenges of cpas flight testing. Technical Report 20110011550, AIAA, Houston, United States, May 2011.
- [38] BEA. "Interim Report n2 on the accident on 1st June 2009 to the Airbus A330-203 registered F-GZCP operated by Air France flight AF 447 Rio de Janeiro – Paris". Report 2, BEA, Le Bourget Cedex, France, Dec 2009. [Accessed 14-06-18].
- [39] Ocean Sonics. Products. <http://iclisten.com/product/>, 2018.
- [40] Ocean Sonics. Products - icListen Smart Hydrophone. <http://iclisten.com/product/>, 2013. [Online; Accessed 18-05-18].
- [41] Honeywell. Hg9900 imu. https://aerocontent.honeywell.com/aero/common/documents/myaerospacecatalog-documents/MilitaryAC/HG9900_IMU.pdf. [Online; Accessed 26-06-18].
- [42] Kongsberg. Hugin. https://www.kongsberg.com/ks/web/nokbg0397.nsf/AllWeb/76ABD1760DA9C064C1257B470029C7A5/\protect\T1\textdollarfile/382309_hugin_product_specification.pdf?OpenElement. [Online; Accessed 26-06-18].
- [43] L. Paull, M. Seto & H. Li. Area coverage planning that accounts for pose uncertainty with an auv seabed surveying application. pages 6592–6599, 09 2014.
- [44] Kongsberg. Hipap instruction manual. <https://www.kongsberg.com/ks/web/nokbg0397.nsf/AllWeb/22C73025B8AC53BDC1257C040031313B/\protect\T1\textdollarfile/164581-APOS-for-HiPAP-Instruction-Manual-complete.pdf>. [Online; Accessed 26-06-18].
- [45] M. Stojanovic & P. P. Beaujean. Acoustic Communication. <https://pdfs.semanticscholar.org/809e/d23d40944ec0b518a7739cd1242243968a46.pdf>, 2013. [Online; accessed 23-05-18].
- [46] M. Stojanovic. On the relationship between capacity and distance in an underwater acoustic communication channel. *WUWNet '06 Proceedings of the 1st ACM international workshop on Underwater networks*, pages 41–47, 2006.
- [47] T. Melodia, H. Kulhandjan et al. Advances in underwater acoustic networking. Technical report, State University of New York at Buffalo, 2012.
- [48] EvoLogics. S2CR 7/17 Product Information. https://www.evologics.de/files/DataSheets/EvoLogics_S2CR_717_Product_Information.pdf. [Online; Accessed 11-06-2018].
- [49] Iridium. Quake Q9612 Modem. <https://www.iridium.com/products/quake-q9612-modem/>. [Online; Accessed 08-06-2018].
- [50] Trident Sensors. Trident sensors' dual element active gps & passive iridium antenna. https://www.tridentsensors.com/images/Datasheets/Combined_GPS-Iridium_Feed-through.pdf. [Online; Accessed 02-06-18].
- [51] Invensense. Microphone array beamforming. <https://www.invensense.com/wp-content/uploads/2015/02/Microphone-Array-Beamforming.pdf>. [Online; Accessed 25-06-18].

- [52] Technology Systems. TS-4100. <https://www.embeddedarm.com/products/TS-4100>. [Online; Accessed 14-06-2018].
- [53] Western Digital. My book duo. https://www.wdc.com/content/dam/wdc/website/downloadable_assets/nld/product_overview/4178-707314.pdf. [Online; Accessed 22-06-18].
- [54] A. V. Medvadev, V. V. Kostenko & A. Y. Tolstonogov. Depth control methods of variable buoyancy auv. *Underwater Technology*, Feb. 2017. doi: 10.1109/UT.2017.7890333.
- [55] W. J. Kirkwood & D. E. Steele. Active variable buoyancy control system for mbari's roV. In *OCEANS '94, 'Oceans Engineering for Today's Technology and Tomorrow's Preservation.* Proceedings, volume 2, pages II/471-II/476 vol.2, Sep 1994.
- [56] Office of scientific research and development. "Methods of submarine buoyancy control". Technical report, National Defence Research Committee, Washington D.C., 1946.
- [57] B. K. Tiwari, R. Sharma & T. Asokan. A computer simulation model for design of variable buoyancy system for autonomous underwater vehicles/gliders. In *OCEANS 2016 - Shanghai*, pages 1-7, April 2016.
- [58] J. E. Poulin. Concept Design of a Long Range AUV Propulsion System with an Onboard Electrical Generator. Technical Report 815961818, Massachusetts Institute of Technology. Dept. of Mechanical Engineering, 2012. [Online; Accessed 22-05-18].
- [59] J. G. Bellingham, Y. Zhang, J. E. Kerwin et al. Efficient propulsion for the tethys long-range autonomous underwater vehicle. In *2010 IEEE/OES Autonomous Underwater Vehicles*, pages 1-7, Sept 2010.
- [60] Montevideo Technology Inc. BLOV-29-07-12P. <https://www.slmti.com/products/brushless-dc-motors/optimized-value/blow-series/motor/blow-29-07-12p/ismetric/1>. [Online; Accessed 19-06-18].
- [61] Battery University. Types of Lithium-ion. http://batteryuniversity.com/learn/article/types_of_lithium_ion. [Online; Accessed 08-06-2018].
- [62] G. Reid & J. Julve. Second life-batteries as flexible storage for renewable energies. <http://www.teledynemarine.com/blueview-3d-multibeam-scanning-sonar?ProductLineID=5>, April 2016. [Online; Accessed 18-06-18].
- [63] Y. S. Wong, L. L. Lai, S. Gao et al. Stationary and mobile battery energy storage systems for smart grids. *2011 4th International Conference on Electric Utility Deregulation and Restructuring and Power Technologies (DRPT)*, August 2011.
- [64] Epec. Battery Cell Comparison. <http://www.epectec.com/batteries/cell-comparison.html>, April 2014. [Online; Accessed 17-05-18].
- [65] D. Kushnir. Lithium ion battery recycling technology 2015. http://publications.lib.chalmers.se/records/fulltext/230991/local_230991.pdf, December 2015. [Online; Accessed 20-06-18].
- [66] Battery University. Battery recycling as a business. http://batteryuniversity.com/learn/article/battery_recycling_as_a_business. [Online; Accessed 21-06-18].
- [67] American Manganese Inc. Investment proposition. <https://americanmanganeseinc.com/investor-info-3/investment-proposition/>. [Online; Accessed 21-06-18].
- [68] ASaft. Lithium-ion battery life. <https://www.saftbatteries.com>, May 2014. [Online; Accessed 11-06-18].
- [69] J. Larminie & A. Dicks. *Fuel Cell Systems Explained*. Wiley, 2003.
- [70] I. Yamamoto, T. Aoki, S. Tsukioka et al. Fuel cell system of auv "urashima".
- [71] SWEP. B5t. <https://www.swep.net/products/b5t/>. [Online; Accessed 19-06-18].
- [72] Pragma Industries. PEM Fuel Cell Stacks. <https://www.pragma-industries.com/products/ocs/>. [Online; Accessed 11-06-2018].
- [73] A. Zuttel. Materials for hydrogen storage. *Materials Today*, September 2003.
- [74] BOC. Special products cylinder identification card. https://www.boconline.co.uk/internet.lg.lg.gbr/en/images/special-products-cylinder-identification410_39409.pdf?v=1.0. [Online; Accessed 14-06-18].
- [75] Applied Home Health Care Equipment. Oxygen cylinder sizes and info. <https://applied-inc.com/oxygen-cylinder-sizes-and-info>. [Online; Accessed 14-06-18].
- [76] K. L. Davis, R. M. Moore. Uuv fceps technology assessment and design process. Technical report, Hawaii Natural Energy Institute (HNEI), School of Ocean and Earth Science and Technology (SOEST), October 2006.
- [77] Pragma Industries. Metal hydride tanks. https://www.pragma-industries.com/wp-content/themes/default/images/MH_TANKS.pdf, 2018.

- [78] California Energy Commission. Assessment of time and cost needed to attain 100 hydrogen refueling stations in California. Technical report, December 2015.
- [79] Chemicool. Oxygen element facts. <https://www.chemicool.com/elements/oxygen.html>. [Online; Accessed 21-06-18].
- [80] Fuel Cell Store. Horizon 60w pem fuel cell. <http://www.fuelcellstore.com/fuel-cell-stacks/5w-100w-fuel-cell-stacks/horizon-30watt-fuel-cell-h-30>. [Online; Accessed 12-06-18].
- [81] Fuel Cell Store. Bl-20 metal hydride. <http://www.fuelcellstore.com/hydrogen-equipment/hydrogen-storage/metal-hydrides/bl-20-metal-hydride>. [Online; Accessed 19-06-18].
- [82] Dynautics. Spectre systems additional modules. https://www.dynautics.com/wp-content/uploads/2018/03/Datasheet_Flyer-SPECTRE-Add-ons.pdf. [Online; Accessed 21-06-18].
- [83] Power Integrations. 2SP0325x2Ax-CM2500DY-24S Preliminary Data Sheet. <https://nl.mouser.com/datasheet/2/328/2SP0325x2Ax-CM2500DY-24S-779348.pdf>, 2018. [Online; Accessed 22-06-18].
- [84] TDK Lambda. 9-40v input non-isolated dc-dc converter. <https://nl.mouser.com/datasheet/2/400/i6a-769886.pdf>. [Online; Accessed 22-06-18].
- [85] AVX. Scc series supercapacitors. <https://nl.mouser.com/datasheet/2/40/AVX-SCC-1018831.pdf>. [Online; Accessed 24-06-18].
- [86] J. Marsden, G. Levin., J. Eddison & D. Vigneswara. P6_3 bulletproof t-shirts. *Physics Special Topics*, Vol. 16(No. 1), Nov. 2017.
- [87] F. B. Brown. *Optimum Slenderness Ratio of a Stable Low-Drag Body*. A report on research conducted under contract with the Office of Naval Research of the Department of the Navy. Contract N6onr-24428. Report No. N-55.1., September 1949.
- [88] MatWeb. Material Property Data. <http://www.matweb.com/index.aspx>. [Online Database; Accessed 23-05-18].
- [89] G. B. V. Kumar, C. S. P. Rao, N. Selvaraj & M. S. Bhagyashekar. Studies on Al6061-SiC and Al7075-Al2O3 Metal Matrix Composites. *Journal of Minerals and Materials Characterization and Engineering*, Vol. 9(No. 01):43–55, 2010.
- [90] Aalco Metals Ltd. Aluminium Alloy Specifications. http://www.aalco.co.uk/datasheets/Aalco-Metals-Ltd_Aluminium-Alloy-6061-T6-Extrusions_145.pdf.ashx, Sept. 2017. [Online; Accessed 15-06-2018].
- [91] C. Felippa. Introduction to Aerospace Structure (ASEN 3112) - Thin Walled Pressure Vessel. Lecture 3 - Available at <https://www.colorado.edu/engineering/CAS/courses.d/Structures.d/IAST.Lect03.d/IAST.Lect03.pdf>, Sept. 2013. [Online Lecture Notes; accessed 23-05-18].
- [92] Carl T.F. Ross. *Pressure Vessels: External Pressure Technology, 2001*. Horwood Publishing Colophon, Chichester, 2001.
- [93] Somnath Chattopadhyay. *Pressure vessels: design and practice*. CRC press, 2004.
- [94] Dwight F Windenburg and Charles Trilling. Collapse by instability of thin cylindrical shells under external pressure.
- [95] J. R. MacKay and F. van Keulen. A review of external pressure testing techniques for shells including a novel volume-control method. *Experimental Mechanics*, 50(6):753–772, Jul 2010.
- [96] F. Oliviero. Ae3211-i systems engineering and aerospace design: Lecture 8 - risk management & reliability engineering. Lecture Slides, mar 2018. Slide 28.
- [97] Fondriest Environmental. Sl-15 solar marine lantern. <https://www.fondriest.com/sealite-sl15-1-2-nautical-mile-solar-marine-light.htm>. [Online; Accessed 21-06-18].
- [98] Kongsberg. MRU. https://www.ashtead-technology.com/datasheets/Kongsberg_Seatex_MRU5.pdf. [Online; Accessed 25-06-18].
- [99] Nate Seidle. GPS tutorial. <https://learn.sparkfun.com/tutorials/gps-basics>. [Online; Accessed 25-06-18].
- [100] Kongsberg. SPT and MPT 31x series. https://www.km.kongsberg.com/ks/web/nokbg0397.nsf/AllWeb/BB480C4CEE924F5CC12573630032ECA6/\protect\T1\textdollarfile/160820_SPT_MPT_31x_transponders_instruction_manual.pdf?OpenElement. [Online; Accessed 25-06-18].
- [101] Oceanflowenergy. 06. Markets/Ocean Currents. <http://www.oceanflowenergy.com/ocean-currents.html>. [Online; Accessed 22-06-18].
- [102] V. Bertram. *Practical Ship Hydrodynamics*. Butterworth-Heinemann, 2000.
- [103] E. O. Tuck. The wave resistance formula of j.h. michell (1898) and its significance to recent research in ship hydrodynamics. 30:365 – 377, 04 1989.

- [104] A. Papanikolaou. *Ship Design - Methodologies of Preliminary Design*. Springer, 09 2014.
- [105] Vishay. Power metal strip® resistors. <https://www.vishay.com/docs/30161/wsk0612.pdf>. [Online; Accessed 24-06-18].
- [106] F.M. White. *Fluid mechanics*. Engineering Series. McGraw-Hill, seventh edition, 2011.
- [107] Engineering Toolbox. Area moment of Inertia- Typical cross sections I. https://www.engineeringtoolbox.com/area-moment-inertia-d_1328.html, 2008. [Online; Accessed 11-06-18].
- [108] E. W. Weisstein. Spherical Segment. <http://mathworld.wolfram.com/SphericalSegment.html>, May 2018. [Online; Accessed 13-05-2018].
- [109] E. W. Weisstein. Circular Segment. <http://mathworld.wolfram.com/CircularSegment.html>, May 2018. [Online; Accessed 11-06-2018].
- [110] Hashimoto K. Kagami S. Kosuge K. Nammoto, T. High speed/accuracy visual servoing based on virtual visual servoing with stereo cameras. In *Intelligent Robots and Systems (IROS), 2013 IEEE/RSJ International Conference on*, pages 44–49. IEEE, 2013.
- [111] M. & Stewart H.B. Thompson, J. M. T. , Thompson. *Nonlinear Dynamics and Chaos*. Wiley, 2002.
- [112] Patrick T. Squire. Pendulum damping. *American Journal of Physics*, 54(11):984–991, 1986. doi:10.1119/1.14838.
- [113] Rafael M. Digilov, M. Reiner, and Z. Weizman. Damping in a variable mass on a spring pendulum. *American Journal of Physics*, 73(10):901–905, 2005. doi: 10.1119/1.1979498.
- [114] L. T. Bolton, J. N. Daniel, L. M. Hewin. "Fulton Air-to-Ground Pickup System for Caribou Aircraft". Technical Report Contract: DA 44-177-TC-804, Robert Fulton Company, Newtown, CT, Feb 1964. [Accessed 18-06-18].
- [115] M., Bruns T. et al Zastrau, D., Schlaak. The relation between storm risk and wind and wave forecast accuracy in the north atlantic ocean. 6:83–87, 02 2015.
- [116] P. T. M. M. Margarido. Flight dynamics and simulation of a generic aircraft for aeroservoelastic design.
- [117] Axces Spring. Compression Spring Rate. US.misumi-ec.com/vona2/detail/221000018138/?CategorySpec=00000030100%3a%3ae&Inch=0, June 2018. [Online; Accessed 18-05-2018].
- [118] Tribology-abc. Calculator for viscous fluid damping. <http://www.tribology-abc.com/calculators/damper.htm>, June 2018. [Online; Accessed 18-05-2018].
- [119] ASM Aerospace Specification Metals Inc. Aluminum 6061-T6; 6061-T651. <http://asm.matweb.com/search/SpecificMaterial.asp?bassnum=MA6061t6>. [Online; Accessed: 23-05-18].
- [120] Vumii. Sii AT/ML - Superior Thermal Security. Brochure, Vumii. [Accessed 20-06-18].
- [121] Airfoil Tools. Lift & drag polars. <http://airfoiltools.com/airfoil/details?r=polar/index/#xfoil>, 2018. [Online; Accessed 16-06-18].
- [122] Glenn Research Center. Shape Effects on Drag. <https://www.grc.nasa.gov/www/k-12/airplane/shaped.html>. [Online; Accessed 22-06-18].
- [123] US Netting. Kevlar™ Rope. <https://www.usnetting.com/rope/kevlar/>, April 2002. [Online; Accessed 13-05-18].
- [124] J. Hoekstra. Introduction to Aerospace Engineering - First Century of Flight: Ballooning. AE1111-I Lecture I - Handout at TU Delft, September 2015. [Online; Accessed 16-05-2018].
- [125] Engineering Toolbox. Aluminium Alloys- Mechanical Properties. https://www.engineeringtoolbox.com/properties-aluminum-pipe-d_1340.html, 2008. [Online; Accessed 18-06-18].
- [126] S. S. Makridis. Hydrogen storage and compression. <https://arxiv.org/ftp/arxiv/papers/1702/1702.06015.pdf>, Jun 2016. [Online; Accessed 18-06-18].
- [127] ASM Aerospace Specification Metal Inc. 2000 Series Aluminum Alloy. <http://asm.matweb.com/search/SpecificMaterial.asp?bassnum=MA2014T6>. [Online; Accessed 18-06-18].
- [128] Ingersoll Rand. Winches and high capacity hoists. *Winch Catalog*, (MHD55199), 2014. Japan, http://ingersollrand.jp/pdf/material/matehan_catalog_06.pdf, [Online; accessed 22-05-2018].
- [129] Vumii. Sii FG - Fog Vision System. Brochure BR-S-SIIFG, Opgal. [Accessed 20-06-18].
- [130] Forecast International. "The Market for Aviation APU Engines". Technical Report #F644, Forecast International, Newtown, CT, July 2010. [Accessed 19-06-18].
- [131] Valworx. "Industrial Electric Actuators". Product Specifications 5618.1117, Valworx, Cornelius, NC. [Accessed 19-06-18].

- [132] Central Intelligence Agency. Words of estimative probability. <https://www.cia.gov/library/center-for-the-study-of-intelligence/csi-publications/books-and-monographs/sherman-kent-and-the-board-of-national-estimates-collected-essays/6words.html>, Jul. 2007. [Online; Accessed 26-04-18].
- [133] L. Kelion. Fatal A400M crash linked to data-wipe mistake. <http://www.bbc.com/news/technology-33078767>, June 2015. [Online; Accessed 27-05-18].
- [134] Burea d'Enquêtes et d'Analyses. "Final Report - On the accident on 1st June 2009". Technical report, Burea d'Enquêtes et d'Analyses pour la sécurité de l'aviation civile, Paris, France, July 2012.
- [135] J. Laeret, J. K. & Radius. Inquiries about kongsberg, Jun 2018. Personal Interview with Kongsberg Employee (J. K. Laeret).
- [136] Teledyne Marine. 3d multibeam scanning sonar. <http://www.teledynemarine.com/blueview-3d-multibeam-scanning-sonar?ProductLineID=5>. [Online; Accessed 22-06-18].
- [137] P. São Thiago et al. R. Barmak, A. L. S. C. de Oliveira. Underwater Locator Beacon Signal Propagation on Tropical Waters. Jul. 2017. [Online; Accessed 10-06-2018].
- [138] English Oxford living Dictionaries. Reliability. <https://en.oxforddictionaries.com/definition/reliability>, 2018. [Online; Accessed 23-06-18].
- [139] English Oxford living Dictionaries. Availability. <https://en.oxforddictionaries.com/definition/availability>, 2018. [Online; Accessed 23-06-18].
- [140] Business Dictionary. Maintainability. <http://www.businessdictionary.com/definition/maintainability.html>, 2018. [Online; Accessed 23-06-18].
- [141] Business Dictionary. Safety. <http://www.businessdictionary.com/definition/safety.html>, 2018. [Online; Accessed 23-06-18].
- [142] W. E. Sasser. Match supply and demand in service industries. *Harvard Business Review*, 54(6):133–140, 1976.
- [143] Investing Answers. Return on Investment. <http://www.investinganswers.com/financial-dictionary/technical-analysis/return-investment-roi-1100>, 2018. [Online; Accessed 24-06-18].
- [144] BEA. Sea search operations. Technical report, Burea d'Enquêtes et d'Analyses pour la sécurité de l'aviation civile, Oct 2012.
- [145] Australian Transport Safety Bureau. The operational search for mh370. *Canberra, Australian Capital Territory, Commonwealth of Australia, Tech. Rep. AE-2014-054*, 2017.
- [146] Business Dictionary. Market Volume. <http://www.businessdictionary.com/definition/market-volume.html>, 2018. [Online; Accessed 24-06-18].
- [147] Investopedia. Market Share. <https://www.investopedia.com/terms/m/marketshare.asp>, 2018. [Online; Accessed 24-06-18].
- [148] Jacob Markish. Valuation Techniques for Commerical Aircraft Program Design. *Thesis*, Massachusetts Institute of Technology, Cambridge, MA, June 2002.
- [149] Right Price Chemicals. Ingersoll Rand FA5A Air Winch. <http://www.rightpricechemicals.com/ingersoll-rand-fa5a-air-winch.html>, Sept. 2017. [Online; Accessed 25-06-18].
- [150] N. Shama Rao, T. G. A. Simha, K. P. Rao & G. V. V. Ravi Kumar. "Carbon Composites are Becoming Competitive and Cost Effective". White paper, Infosys, 2018. [Accessed Online; 13-06-18].
- [151] Oceanvolt. Price Examples. <https://oceanvolt.com/price-examples/>, 2017. [Online; Accessed 25-06-18].
- [152] R. Kastner et al. B. Benson, Y. Li. Design of a low-cost, underwater acoustic modem for short-range sensor networks. In *OCEANS 2010 IEEE - Sydney*, pages 1–9, May 2010.
- [153] M. Chartier. Aerospace Engineering IMU System. Personal Communication (E-mail), June 2018. [Online; Accessed 11-06-18].
- [154] BlueRobotics. Bar100 High-Resolution 1000m Depth Pressure Sensor. <https://www.bluerobotics.com/store/electronics/bar100-sensor-r1/>, Dec. 2017. [Online; Accessed 25-06-18].
- [155] WaveINN. Thrane LT500 AHRS Electronic Compass With Heading Sensor. <https://www.waveinn.com/nautical-fishing/thrane-lt500-ahrs-electronic-compass-with-heading-sensor/136527019>. [Online; Accessed 25-06-18].
- [156] Audiosense. AMBIENT ASF-1 MKII. <https://www.audiosense.be/en/store/microphones/hydrophone/ambient-asf-1-mkii.html>, May 2018. [Online; Accessed 26-06-18].
- [157] SatphoneStore. Iridium 9602 SBD Modem. <http://www.satphonestore.com/tech-browsing/iridium-nav/iridium-sbd/equipment/iridium-9602-sbd-modem.html>, Dec 2017. [Online; Accessed 25-06-18].

- [158] SatphoneStore. Dual Mode Iridium GPS Antenna. <http://www.satphonestore.com/application-browsing/satellite-phones/satellite-phone-accessories/accessories-antennas/aero-at1621-162-dual-gps-iridium-antenna.html>, Sept. 2014. [Online; Accessed 25-06-18].
- [159] J. Hellendoorn. Comparative study of motion reference sensors (Offshore). http://www.dcsc.tudelft.nl/education/msc_program/systems_and_control/msc_thesis_topics/proposal-5754.html, 2017. [Online; Accessed 26-06-18].
- [160] Payscale. Salary Data & Career Research Center (United States). https://www.payscale.com/research/US/Country=United_States/Salary, 2018. [Online; Accessed 25-06-18].
- [161] Bureau of Labor Statistics. Professional, Scientific, and Technical Services: NAICS 54. <https://www.bls.gov/iag/tgs/iag54.htm>, June 2018. [Online; Accessed 25-06-18].
- [162] Skepp.nl. Kantoormuimte huren Amsterdam Noord, Distelweg 78-80. <https://www.sokanu.com/careers/software-engineer/salary/>, April 2016. [Online; Accessed 25-06-18].
- [163] R. Grabowski. What's the price of CATIA, really? <http://www.worldcadaccess.com/blog/2012/05/whats-the-price-of-catia.html>, May 2012. [Online; Accessed 26-06-18].
- [164] Sokanu. Software Eningeer Salary. <https://www.sokanu.com/careers/software-engineer/salary/>, April 2016. [Online; Accessed 25-06-18].
- [165] Kirsten Wind Tunnel. Services & Rates. <https://www.aa.washington.edu/AERL/KWT/rateguide>, Jan. 2015. [Online; Accessed 25-06-18].
- [166] O. Stroosma. Cost inquiry for DSE project. Personal Communication (E-mail), June 2018.
- [167] ASME. Boiler and Pressure Vessel (BPV) Certifications. <https://www.asme.org/shop/certification-accreditation/price-guide>, March 2017. [Online; Accessed 26-06-18].
- [168] International Air Transport Association. Jet Fuel Price Monitor. <http://www.iata.org/publications/economics/fuel-monitor/Pages/index.aspx>, June 2018. [Online; Accessed 25-06-18].
- [169] A. McNeilage T. Allard &. Most expensive aviation search: \$53 million to find flight MH370. <https://www.smh.com.au/national/most-expensive-aviation-search-53-million-to-find-flight-mh370-20140404-36463.html>, April 2014. [Online; Accessed 25-06-18].

Functional Flow and Breakdown Diagrams

This chapter covers the functional flow diagrams and functional breakdown structures and can be found in appendix A.1 and appendix A.2 respectively.

A.1. Functional flow

The functional flow diagrams are shown in this section. It starts with the top level functions and ends with the third level ones. It covers functions that must be executed during the search mission.

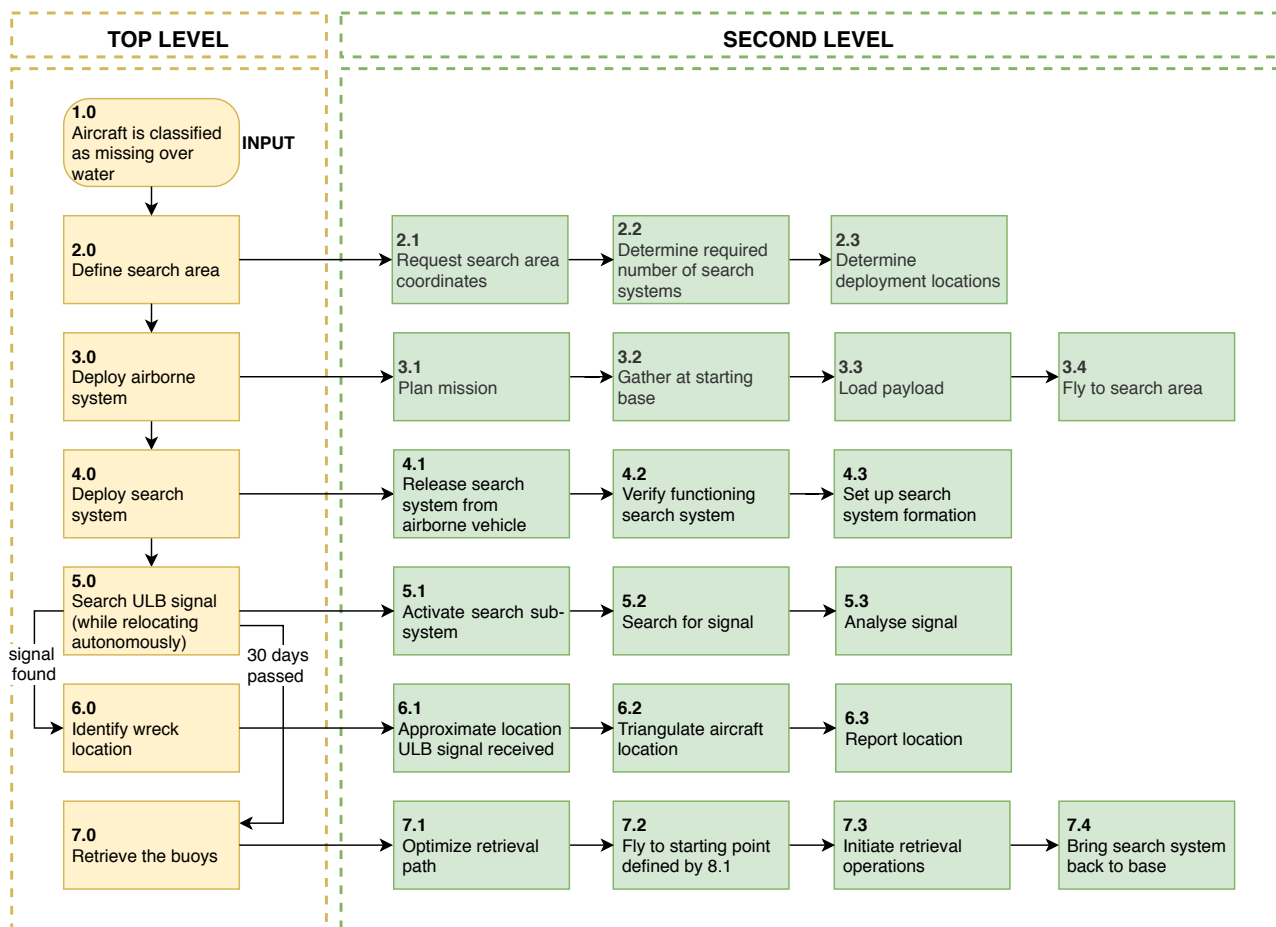


Figure A.1: Functional flow of the top and second level.

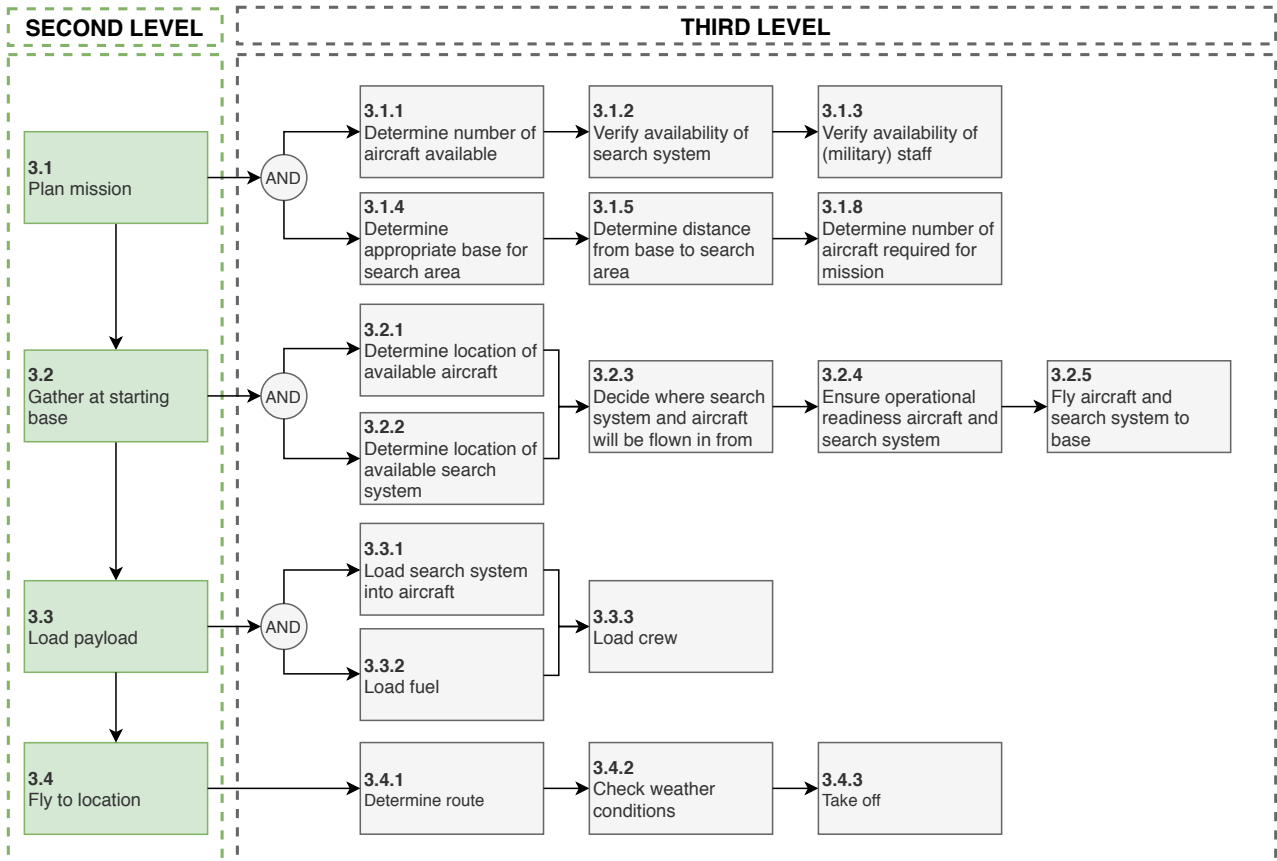


Figure A.2: Functional flow of the third level of the deployment of the airborne system.

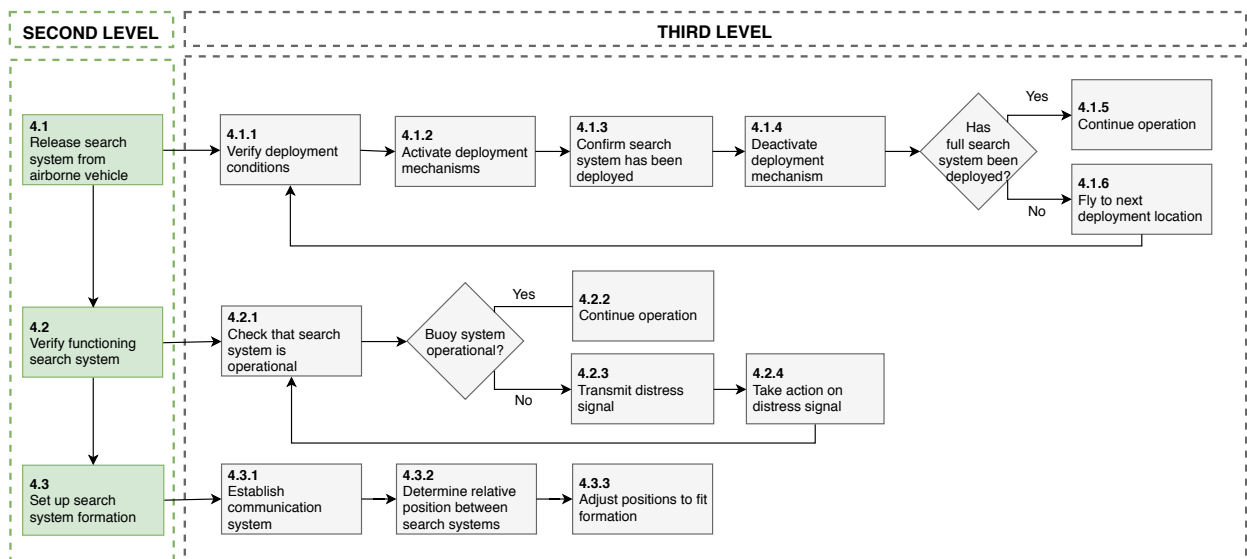


Figure A.3: Functional flow of the third level of the deployment of the search system.

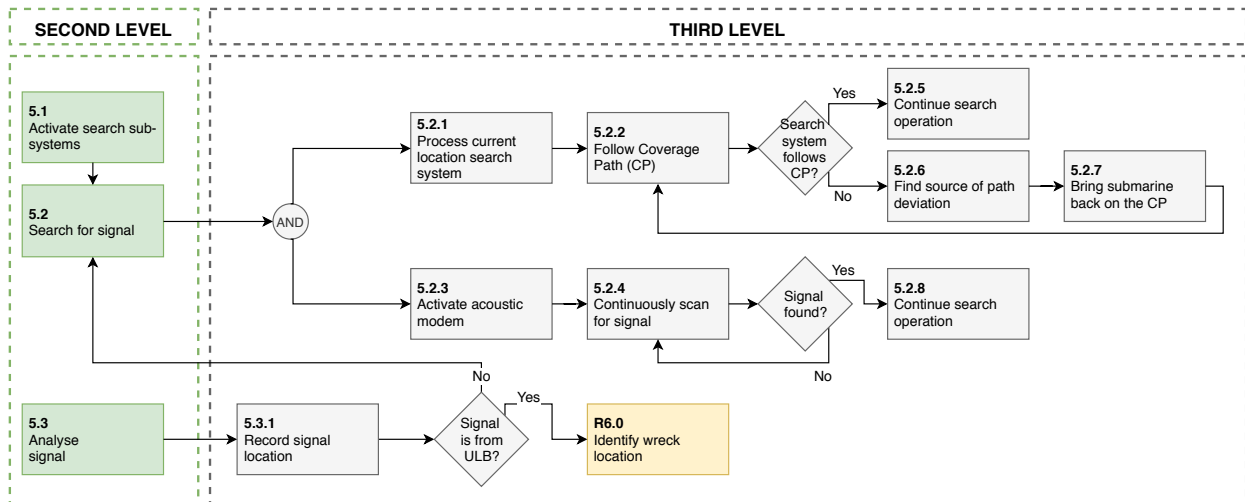


Figure A.4: Functional flow of the third level of the search phase.

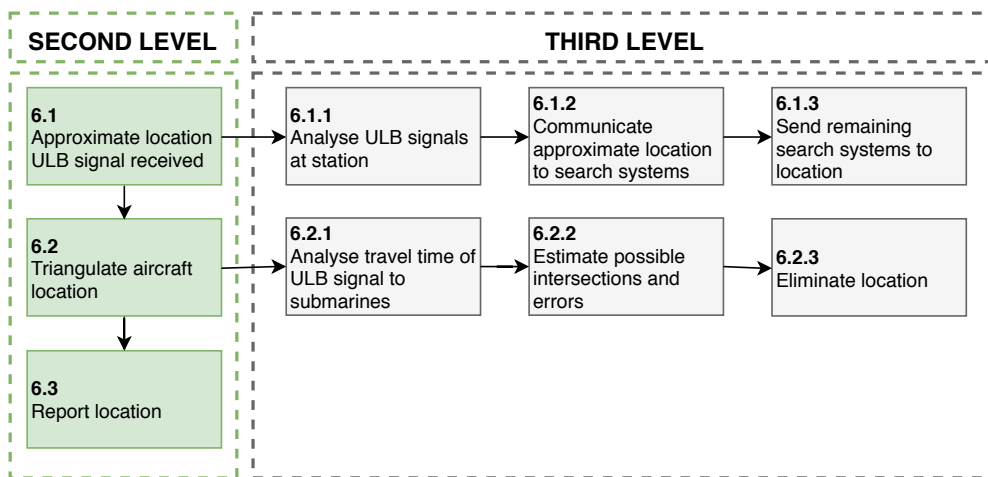


Figure A.5: Functional flow of the third level of the wreck location determination.

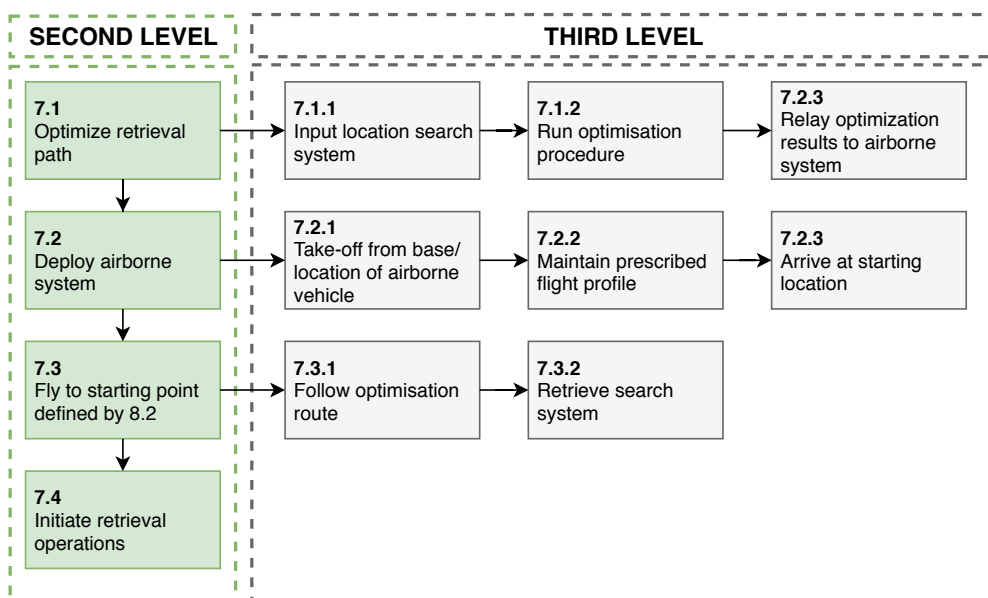
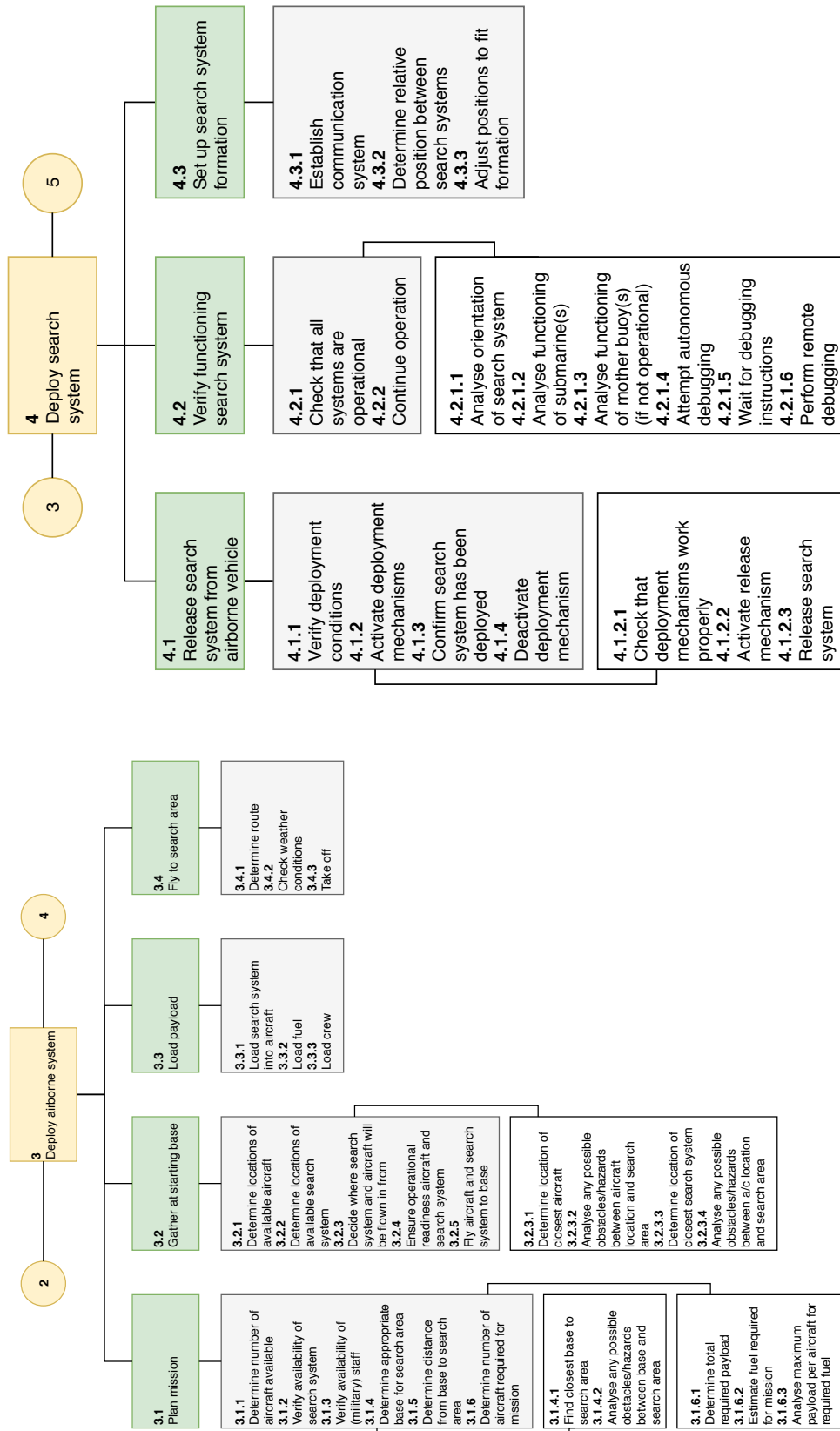


Figure A.6: Functional flow of the third level of the retrieval procedure.

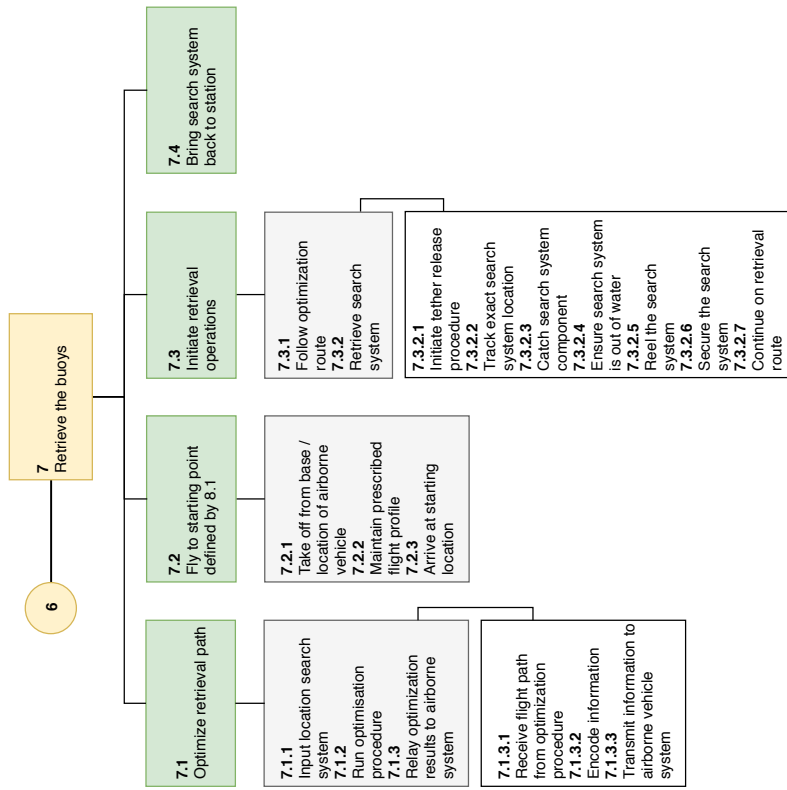
A.2. Functional breakdown structure

This section shows the functional breakdown structures. It shows fourth level functions and gives the functions needed to be performed for the entire duration of the mission.

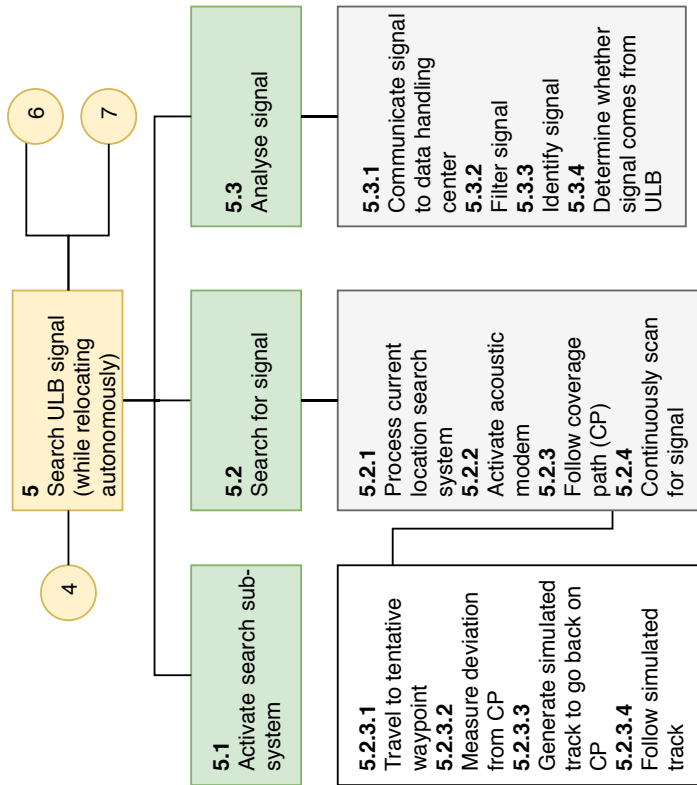


(a) Functional breakdown structure of the deployment of the airborne system.

(b) Functional breakdown structure of the deployment of the search system.



(b) Functional breakdown structure of the retrieval.



(a) Functional breakdown structure of the search phase.

Cost distribution

This appendix presents the distribution of costs of the ULB project, from development to production to operation. These costs are summarized in chapter 14, by table 14.3.

Table B.1: Production cost for different systems and corresponding components.

Production	Unit Cost [EUR]	Cost per system [EUR]
Retrieval System		
Flying wing [148]	85,000	255,000
Winch [149]	36,000	108,000
Retrieval arm [117]	1,100	3,300
Submarine		
Manufacturing CFRP [150]	19,650	120,000
Buoyancy control [55]	10,000	60,000
Propulsion [151]	7,500	45,000
Power (see section 7.7)	2,554.96	15,500
Acoustic modem [152]	6,868.13	41,500
IMU [153]	68,681	415,000
Depth sensor [154]	171.71	1,100
Leica compass [155]	858.52	5,200
Hydrophone [156]	8,000	48,000
Satellite modem [157]	214.63	1,300
Satellite antenna [158]	362.29	2,200
SBC [52]	177.72	1,100
Data storage [53]	400	2,400
Kevlar rope [123]	3260.55	19,600
Mother buoy		
Manufacturing CFRP [150]	19,650	120,000
Propulsion [151]	7,500	45,000
Power (see section 7.7)	2,554.95	15,500
Acoustic modem [152]	6,868.13	41,500
MRU [159]	51,480	310,000
HIPAP [44]	17,160	103,000
Satellite modem [157]	214.52	1,300
Satellite antenna [158]	362.11	2,200
SBC [52]	177.63	1,100
Lantern [97]	179.34	1,100
Data storage [53]	400	2,400
Kevlar rope [123]	3,260.55	19,600
Transponder [100]	12,000	72,000
Total (incl. 25% contingency)		2.8 million

Table B.2: Table summarizing the development and operational costs.

Operations & Development	Unit Cost [EUR]	Cost per system [EUR]
Salaries/Rent		
Assembly line worker (p. hour) [160]	11.18	1,788.8
Skilled worker (p.hour) [161]	35.26	12,524,352
Pilot (p. year) [160]	132,766	18,769.11
Flight engineer (p.year) [160]	100,484	7,102.70
Load master (p.year) [160]	74,192	10,488.51
Communications specialist (p.year) [160]	72,427	25,597.49
Aircraft/Flying wing mechanic (p.year) [160]	81,971	28,970.57
Submarine/Motherbuoy mechanic (p.year) [160]	66,803	18,887.86
Project manager (p.year) [160]	138,254	48,862.37
Rent office (p. month) [162]	5,000	120,000
Software		
Software used at office (p. person p. year) [163]	12,150	327,600
Software per system [164]	45,868.2	229,341.16
Testing/Inspection		
Windtunnel testing [p.hr] [165]	430	27,090
Modelling/Testing dynamics [166]	15 million	15 million
Inspection/Certification [167]	3,000	54,000
Other operational costs		
Fuel (EUR/L) [168]	0.64	162,560
Ship (p. day) [169]	380,000	7,233,000
Total (incl. 25% contingency)		44.7 million